MONASH University

CFD-DEM MODELLING AND ANALYSIS OF HYDRAULIC CONVEYING

By

Mengmeng Zhou

A THESIS SUBMITTED FOR THE DEGREE

OF

DOCTOR OF PHYLOSOPHY

AT THE LABORATORY OF SIMULATION AND MODELLING OF PARTICULATE SYSTEMS, DEPARTMENT OF CHEMICAL ENGINEERING, MONASH UNIVERSITY, CLAYTON, VIC 3800, AUSTRALIA

9 October 2020

To my family,

Love and Thanks.

Table of concent

LIST OF FIGURES

LIST OF TABLES

ABSTRACT

Hydraulic conveying generally transports solid bulk material from one position to another via a carrier liquid. It is widely encountered in many industries, such as chemical engineering, food, mining, oil and petroleum industries due to its low operation and maintenance cost, friendliness to the environment, and unlimited transporting distance. It can handle a wide variety of particles that can be either coarse or fine.

For the design and operation of a hydraulic conveying, the key performance parameters that should be considered are pressure drop, erosive wear, flow regimes and their transition. Most previous studies were focused on macro-mechanics information, such as pressure drop, pipe erosive wear and solid concentration distribution, which are essentially controlled by micro-mechanics information, such as forces, flow regimes and particle patterns. However, such micro-mechanics analysis of a hydraulic conveying has been rarely studied in literature. This project will focus on micro-mechanics analysis, especially flow behaviours in hydraulic conveying. A combined approach of computational fluid dynamics (CFD) for the liquid phase and discrete element method (DEM) for particles is applied to study the flow behaviours and features of coarse particles in vertical, horizontal and bend pipes, the main purposes include 1) developing and validating a CFD-DEM model to describe the complex liquid-solid flow and performance of hydraulic conveying; 2) understanding the fundamentals governing the flow and performance under various conditions in terms of particle-particle, particle-fluid and particle-wall interactions; and 3) investigating the flow regimes and their transition, solid pattern, and pipe wear under different geometrical, operational and material conditions.

COPYRIGHT NOTICE

I certify that I have made all reasonable efforts to secure copyright permissions for third-party content included in this thesis and have not knowingly added copyright content to my work without the owner's permission.

ORIGINALITY STATEMENT

I hereby declare that this thesis is my original work of research and contains no material which has been accepted for the award of any other degree or diploma at any university or equivalent institution, and this thesis contains no material previously published or written by another person, except where due reference is made in the text of the thesis. Any contribution made to the research by others, which whom I have worked at Monash University or elsewhere, is explicitly acknowledged in the thesis. I also declare that the intellectual content of this thesis is the product of my own work, except to the extent that assistance from other in the project's design and conception or in style, presentation and linguistic expression is acknowledged.

Signed:

Date:

ACKNOWLEDGEMENTS

I would like to thank my main supervisor, Prof Aibing Yu, for his suggestions, advice and support on the direction and key issues of my research throughout the whole process of my thesis. Also, I would like to thank my associate supervisors, Dr Shibo Kuang and Prof Kun Luo, for providing me with their expertise, advice and guidance for my PhD research. Thanks for Dr Kuang's and Prof Kun Luo's patience, especially when I had lots of difficulties during the research. This work would not be possible without their wise guidance and extraordinary inspiration. I also appreciate A/Prof Ruiping Zou for her suggestions and advice during my PhD research.

Thanks to my colleagues from SIMPAS, Monash University, and visitors to SIMPAS. This will remain to be special and beautiful memories of my life.

Thanks to the Australian Research Council for their financial support for this project and Monash University for the access to facilities and resources of research materials.

I would like to give my appreciations to my parents, my husband, my sister, my brother and relatives for their love and support. They always motivate me to be resilient and proactive towards any situations and setbacks in life. Especially, giving deeper appreciations to my dear Dad and Mom, who supported me to study overseas since I was nineteen. Thanks for always standing by my side and teaching me to never give up.

CHAPTER 1 INTRODUCTION

Hydraulic conveying generally transports solid bulk material from one position to another via a carrier liquid (Doron and Barnea, 1995). During the process of conveying, most of them belong to two-phase fluid, which is much more complicated than a one-phase fluid. In hydraulic conveying, it is quite easy to transfer small particles in horizontal or vertical pipelines, and the pressure losses could be predicted easily with sufficient accuracy. The hydraulic conveying of bulk particles in pipelines has been widely used and considered in chemical, coal and mining industries (Doron and Barnea, 1995, Ali and Yeung, 2014, Silva et al., 2015b, Asim and Mishra, 2016).

During the design and operation of hydraulic conveying, some key performance parameters must be carefully considered. Firstly, the pressure drop, which is a major parameter, needs to be carefully considered to obtain an expected throughput, avoid pipe blockage and so on. It is also tightly related to system energy efficiency. Secondly, the pipeline erosive wear is another important parameter in hydraulic conveying pipeline system. It not only increases operation and maintenance costs in the pipe section replacement, but also influences the flow behaviours as a result of the change in the inner shape of pipe caused by erosive wear. Thirdly, flow regimes and their transition, which are used to control the pressure drop and erosive wear, is incredibly important. Therefore, for better control of hydraulic conveying pipeline system, the understanding of flow regimes and their transition is quite important.

For the flow regimes and their transition, the most common types are classified by Doron et al., (1987). Firstly, the stationary bed flow, which would exist when the velocity is too low to have all particles being suspended, and so a stationary deposit would occur at the bottom of the pipeline, which may lead to partial blockage of the pipe and thereby reduce its efficiency. Secondly, a moving bed flow, which is defined as when the solids in the slurry are distributed in the bottom of the pipe, and the flow velocities are very low. Thirdly, the homogeneous

suspension flow exists when the mean mixture velocity is high, which leads to particles being suspended as the high mixture velocity could deter particle sedimentation. In the industry, the stationary bed flow is normally avoided as it tends to increase the risk of pipe blockage, so typically the velocities are higher than the stationary deposit (Miedema and Ramsdell, 2015). In addition, the full suspension is exhibited when the velocity is high enough, however, high energy would be consumed simultaneously (Pakzonka et al., 1981). Therefore, for hydraulic conveying, the conveying velocity zone between fully suspended and stationary deposit is widely used (Doron and Barnea, 1993, Doron and Barnea, 1996). Usually, in this velocity zone, a moving bed exists in the bottom of the pipeline, and the transition zone is above it so that the higher transposing velocity could convey the suspended particles. Nevertheless, although the concept of velocity zone is clear, predicting flow feature based on operating conditions is still the main conundrum (Uzi and Levy, 2018, Zhou et al., 2019, Zhou et al., 2020).

Through the flow features, some important information about liquid and solid dynamics could be obtained to predict many vital performances, such as the pressure drop, which determines the requirement of energy (Doron et al., 1987, Doron and Barnea, 1993, Gillies and Shook, 1994, Doron and Barnea, 1996, Gillies and Shook, 2000, Hong et al., 2002, Uzi and Levy, 2018, Zhou et al., 2019, Zhou et al., 2020). The minimum conveying velocity is determined by the stationary deposit velocity. The collision feature plays a decisive role in determining particle breakage calculations during the flow features, in which the collision velocity and collision frequency of particle-particle (p-p) and particle-wall (p-w) are included (Xu and Yu, 1997, Zhou et al., 2010). In addition, the collision velocity and collision frequency of particle-wall play an important role in predicting pipe erosive wear. Hence, predicting the hypothesis flow features and the collision features plays a vital role in determining the appropriate operational requirement.

In order to analyse the flow behaviours in hydraulic conveying, the first method is to use an expression, in which both the pressure gradient from experimental and the governing parameters, such as, solid concentration, fluid velocity and particle diameter, are associated (Miedema and Ramsdell, 2015). Lots of useful relations exist in the particular area of control parameters through this approach, however, for the hydraulic study, there is still a challenge in defining the general correlation.

A Two-layer model is the most common model used, which means only the upper and bottom layers exist in a pipeline (Gillies and Shook, 2000, Matoušek, 2005). This approach not only has a good tendency for matching the pressure drop from experimental results, but also matches the bed height from experimental results (Doron et al., 1987). Instead of changing velocity and concentration distribution of particles, an individual scalar is used to model each layer. Numerical simulation is quite an effective method, as the computational cost is low and it could effectively simulate the tendency of pressure drop or fluid velocity. However, due to the simplified hypothesis of two layers, this may cause difficulties in catching the intricate flow characteristic; therefore we do not suggest using this model to predict the erosion or attrition. Instead, a more intricate 3-dimentional model could be used to solve such problems.

With the developing computational technology, a 3D model is commonly applied to simulate and forecast multi-phase flows. There are two main methods: Firstly, continuum method has been studied by many researchers in the past few years (Messa et al., 2014, Messa and Malavasi, 2015, Peng and Cao, 2016, Wang et al., 2017a, Pei et al., 2018, Lospa et al., 2019, Singh et al., 2019a), where this method is widely used to model hydraulic conveying. In this method, Navier-Stokes equations are applied in liquid and solid phases as continuous phases, meanwhile the shear stress should be defined by the models of momentum equation for solid, and also the pressure that was produced by the collision. Secondly, discrete method has been studied by multiple researchers in the past decades (Xu and Yu, 1997, Lim, 2007, Zhu et al.,

2007, Zhu et al., 2008, Kuang et al., 2009, Zhou et al., 2010, Kuang and Yu, 2011, Zhang et al., 2012, Zhao et al., 2017, Uzi and Levy, 2018, Kuang et al., 2019a, Zhou et al., 2019, Uzi et al., 2020, Zhou et al., 2020), in which the liquid is modelled as the continuous phase, and the solid phase is simulated as the discrete phase. Individual particle's motion could be simulated through these methods so that the collisions of particle-particle and particle-wall could both be simulated. Discrete element method (DEM) is the most famous approach for the discrete method. The Newton 2nd law is applied to determine the particle motion, at the same time, all the main forces for different problems are needed to be included. This method could help us obtain more detailed information about the flow features.

For this PhD project, a CFD-DEM method is applied to study the flow features of coarse particles in vertical, horizontal and bend pipes. The specific aims of this project are listed as follows: Firstly, developing and validating a CFD-DEM model to describe the complex liquid-solid flow and performance of hydraulic conveying. Secondly, understanding the fundamentals governing the flow and performance under various conditions in terms of particle-particle, particle-fluid and particle-wall interactions. Thirdly, investigating the flow regimes and their transition, solid pattern, and pipe wear under different geometrical, operational and material conditions. This thesis is divided into seven chapters and the outline of each chapter is given below:

Chapter 1 introduces hydraulic conveying, including the classification, characteristics, key performance, influencing factors and the aims of present thesis work.

Chapter 2 reviews the previous studies on hydraulic conveying based on different research methods, namely experimental method and numerical method. For each method, the effects of geometrical, operational and material conditions on flow regimes, pressure drop and erosive wear are discussed in detail.

Chapter 3 proves the reasonability of applying the CFD-DEM method to simulate the flow behaviour of a hydraulic conveying in vertical pipe, where the lift force acting on a particle needs to be considered. The numerical results show that particles tend to concentrate in the middle of the vertical pipe. These results will shed light on the optimization of hydraulic conveying. The content of this chapter has been published in a peer-reviewed journal (Zhou et al., Powder Technology, 354 (2019) 893-905).

Chapter 4 successfully reproduces the typical flow regimes in a horizontal pipe for the first time by using the CFD-DEM model. The Effects of conveying speed and feed solid concentration on the pressure drop and the micromechanics information of the underlying mechanism are examined. Furthermore, the force analysis is also presented in detail, and a general prediction correlation of pressure drop is formulated in this chapter, which shows a good tendency with the measured results. The content of this chapter has been published in a peer-reviewed journal (Zhou et al., Powder Technology, 373 (2020) 543-554).

Chapter 5 studies the effects of pipe orientation and conveying speed on the flow behaviour and erosive wear. It is found that different pipe orientation will produce different impact angle, zone and erosive value in stationary and moving bend flow. When the conveying flow reaches a certain value, the pipe orientation has less effect on impact angle, zone and erosive value.

Chapter 6 extends the standard bend pipe to study the effect of bend shapes on the solid flow behaviour, erosive wear and pressure drop. The detailed analysis is presented here to show the importance of bend shapes on hydraulic conveying system.

Chapter 7 summarises the entire PhD project and points out the potential future studies in this field.

CHAPTER 2 LITERATURE REVIEW

2.1 Introduction

The presence of solid particles in the carrier liquid forms a mixture, called hydraulic conveying, which covers a wide range of applications and is of considerable interest in engineering research. The concept of hydraulic conveying has been used for a long time, and it has been widely used in many industries, such as minerals, chemicals, or coal industry. Pneumatic conveying is another method of conveying solid particles, which the gas is applied instead of liquid. However, because of its shortcomings such as high specific power consumption, potential particle breakage and degradation, high erosive wear rate of components and relatively limited distances (Dhodapkar and Jacob, 2006). On the other hand, because the advantages of hydraulic conveying are environmental friendliness, low operation and maintenance costs, and relatively simple infrastructure, it has aroused great interest and attention. Hydraulic conveying has become an advanced technology that can be used to transport a variety of solid materials in various sizes of pipes through different directions, such as sand, fine ash, with different densities, particle shapes (Abulnaga, 2002). It is very flexibly.as the conveyed pipe could be vertical, horizontal or bend.

During the design and operation of hydraulic conveying, some key performance parameters are necessary to be carefully considered. Firstly, the pressure drop, which is a major parameter needed to be carefully considered to obtain an expected throughput, avoid pipe blockage and so on. It is also tightly related to system energy efficiency. Secondly, the pipeline erosive wear, which is another important parameter in hydraulic conveying pipeline system. It not only increases operation and maintenance costs in the pipe section replacement, but also influences the flow behaviours as a result of the change in the inner shape of pipe caused by erosive wear. Thirdly, flow regimes and their transition, which are used to control the pressure drop and

erosive wear. Therefore, for better control of hydraulic conveying pipeline system, the understanding of flow regimes and their transition is quite important.

Since the 1950s, the key performance parameters of hydraulic conveying through pipes has been systematically studied (Matousek, 1996). Most works are mainly based on experimental research, that is, the use of various particles and pipe sizes to deal with pressure drop prediction and flow regime division at different conveying speeds, and then use the collected data to build an empirical model. Then the 1970s and 1980s marked the emergence of another method by which researchers focused more on basic principles or continuous methods based on rheology. Despite outstanding research work and progress in this area, our understanding of the basic and complex nature of the settled hydraulic conveying is still insufficient to meet engineering requirements. Because the engineers in hydraulic conveying need a viable and reliable method to adapt to all conditions met in the industry. Therefore, it is essential to investigate all relevant variables effects on the hydraulic conveying performances.

With the developing computer technology, the numerical method is more and more widely used, nowadays. In the past decade, more and more numerical researches, see Refs, (Peng and Cao, 2016, Xu et al., 2016, Wang et al., 2017a, Kannojiya et al., 2018, Pei et al., 2018, Lospa et al., 2019, Zhou et al., 2019, Xie et al., 2020, Uzi et al., 2020, Zhou et al., 2020), on hydraulic conveying have been informed in the literature with various operating, geometrical conditions and material property.

In this chapter, a comprehensive literature review on hydraulic conveying is provided here to show the previous highlighted works in both experimental and numerical fields. Finally, the research gaps and aims are summed up on the conclusion section.

2.2 Experimental studies on hydraulic conveying

2.2.1 Experiment set-up and measurement

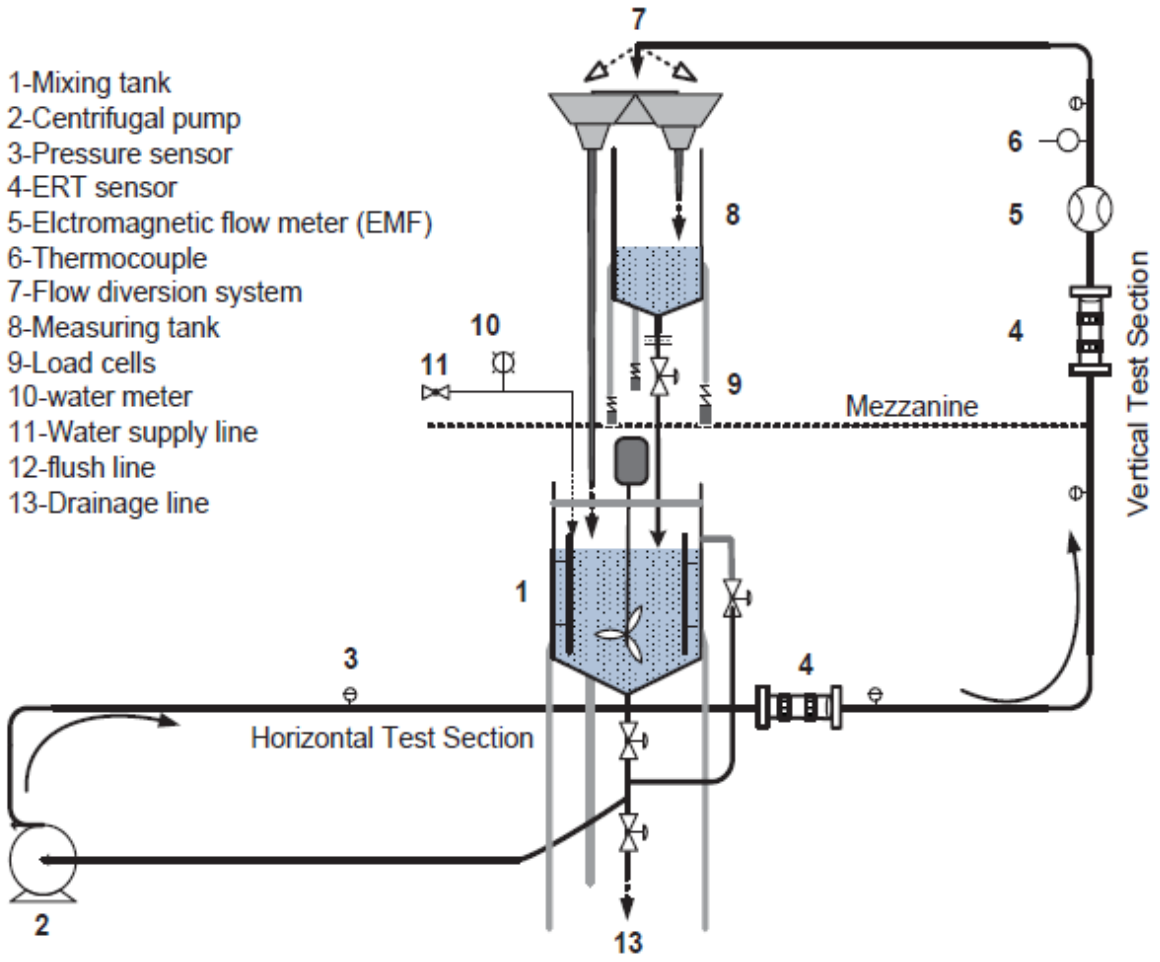

Figure 2-1 Sketch of test loop in hydraulic conveying (Faraj and Wang, 2012)

Before talking about the experimental researches on hydraulic conveying, the test loop used in hydraulic conveying system should be known. An example sketch of test loop in hydraulic conveying of Faraj and Wang, (2012) is presented on Figure 2-1, which the main sections are included the tank of mixing fluid, the centrifugal pump, both the horizontal and vertical test sections, the dual-plane Electrical Resistance Tomography (ERT) sensors, the flow diversion system, the Electromagnetic Flow meter (EMF), pressure sensors and a photo chamber. The mixing tank should have an enough capacity to hold the mixing fluid and it is connected to a

three-blade mixer in order to acquire a homogeneous mixing fluid before flowing it into the flow path. Thence, the mixing tank is applied here to mix and retain the mixture returned from the flow path before pumping it back to the flow path.

Some necessary measuring instruments are needed to obtain the flow parameters. Firstly, an electromagnetic flow meter (KROHNE Optiflux 2000) is applied to obtain value of the water flow rate, and using the transmission of the pump to adjust. And the solid flow rate is decided by a device designed and implemented by the laboratory. Optical measurement can also be obtained with a high-speed camera (Optronis CamRecord600). Generally, 1000 images with a resolution of 1280×1024 pixels are recorded at a frame rate of 500 Hz. To illuminate the flow backwards with Phlox's LED board, and the measurement of the pressure drop is used by two differential pressure sensors (VEGADIF65, VEGA, Germany).

A 15 KW centrifugal pump (2/1/2 AH WARMAN PUMP) is used to serve in the test loop, which is linked to a Digi-drive frequency converter (LEROY SOMER -15Kw) to control the average mixing speed. The test sections (horizontal and vertical) of the loop are placed on a straight line, thereby avoiding the effects of bending and flow interference (Matoušek, 1997). The mixture flow is turbid and opaque, it is very hard to capture the photographs of the mixture flowing. Therefore, a light box is used here to connect the observation part to make the solid particles flowing in the pipe part clearer.

Electrical resistance tomography (ERT) is one of the methods to measure the mixture flow through a pipeline, which has recently attracted great interest. The opaque nature of pipes and slurry leads it impossible to know what is happening inside the pipe, hence, using ERT is allowing the users to visualize the internal structure of the mixture flow by producing an image/tomogram that based on conductivity current (Dyakowski et al., 2000, Sharifi and Young, 2013). In addition, the velocity of multiphase flow could be measured by the Ultrasonic

Doppler Velocity Profiler (UDVP). As the UDVP through detecting and processing the Doppler shift frequency of the echo, which created by the reflected signal of the moving particles to measure the instantaneous velocity distribution in the flow field.

For the erosion problem, the scanning electron microscope (SEM; Phenom ProX, Phenom World, Eindhoven, Netherlands) normally is used to examine the microstructure and erosive wear surface morphology of the elbow pipe. During the SEM analysis, after the erosion test, a 10 mm square sample is needed to cut out from the both the entrance and exit of the test elbow pipe by the wire electrical discharge machining (WEDM) process.

With these instruments, researchers could acquire more detailed information, such as the pressure drop, and liquid or solid velocity (Zouaoui et al., 2016). The usage of these instruments help researchers to improve the knowledge of particle behaviours in hydraulic conveying. And it is necessary to highlight some important works in hydraulic conveying. Some typical results in experimental studies are shown below.

2.2.2 Flow regimes

Flow regimes play an important role in hydraulic conveying, which shows the microcosmic behaviour of the particles (Doron and Barnea, 1993), and could help us analyse particle-particle and particle-wall interactions, such performance characteristics could lead the industry to have an optimized design and decreased energy consumption.

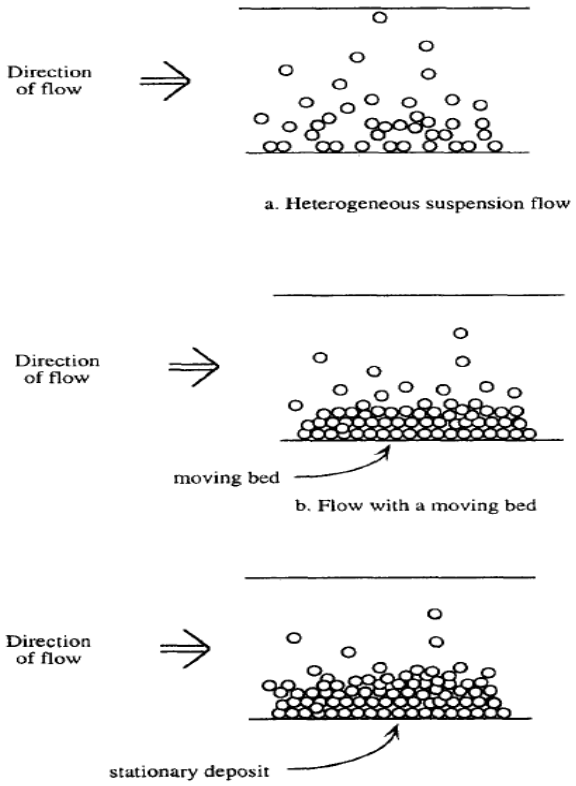

Figure 2-2 Different flow regimes (Doron and Barnea, 1996)

Doron and Barnea, (1996) observed some typical flow regimes and concluded the definitions: (i) suspended flow, at higher fluid velocity the carrier liquid may lead to all solid particles to be suspended. (ii) a moving bed flow, at lower fluid velocity a packed bed of rolling or moving particles would be formed, as the particles gathered at the bottom part of the pipe, few suspended particles might occupy the top of the pipe cross-section. (iii) stationary flow, when the fluid velocity is too low to allow any movement of all the soaked particles, at the bottom of

the pipe, a stationary settlement might be formed. With increasing flow rate, the stationary deposit would not decrease until its height decreases to zero. However, it begins moving when its height is several particle sizes.

2.2.2.1 Effect of conveying speed on flow regimes

Doron et al., (1987) studied hydraulic conveying of larger particles in the horizontal pipe. They found that a higher fluid velocity might lead the mixture flow to be suspended, and the liquid only pressure drop was smaller than mixture pressure drops. Reducing the mean velocity would result in a bed formation and led to a higher pressure drops than those of single liquid. Furthermore, the theoretical model has quite accurately predicted the influences on pressure drop and critical velocity. Engelmann, (1978) came up with empirical correlations on particle velocity and frictional element.

Doron and Barnea, (1996) indicated that the fluid velocity might play a vital role in the exchange from transition to fully suspended flow. In addition, for the larger particles, the scope of the presence of the moving bed flow increases, such phenomenon occurs because the larger particles produced higher settling velocities. The higher mixture flow rates could produce such phenomenon, and then it would cause the transition lines to divert.

Matousek, (2002) mentioned that fluid velocity had major effects on producing various flow regimes. For the shear layer, which is connected to the top of the bed and conveyed another particle with high velocities, the contact bed usually conveys a large proportion of particles.

Kumar et al., (2003) have shown that the particle diameter in the slurry would affect the deposition velocity and changed the flow regimes when other conditions except particle diameter was kept the same.

Garić-Grulović et al., (2004) studied the solid-liquid flow in a vertical pipe. When the particles moved vertically and also had some radial movement exited, that could be called turbulent flow,

which had smaller fluid and particle velocity characteristics and is quite similar to the reverse sedimentation of particle suspensions. Meanwhile, the flowing suspension is quite similar to a fluidized bed, which the tube walls would cause particles to suspend. However, the parallel flow led all particles to move vertically along a line. Such regime has higher fluid and particle velocity characteristics.

In addition, Vlasak et al., (2015) also indicated some typical flow regimes in horizontal pipe, which are shown in Figure 2-3, and also mentioned that increasing conveying velocity would lead to an increase in concentration, in which the conveying velocities increased from top to the bottom. It was clearly shown that increasing velocity would induce a suspended flow, as particles tended to be discrete and moving on the top of the pipe, as shown in the bottom of Figure 2-3.

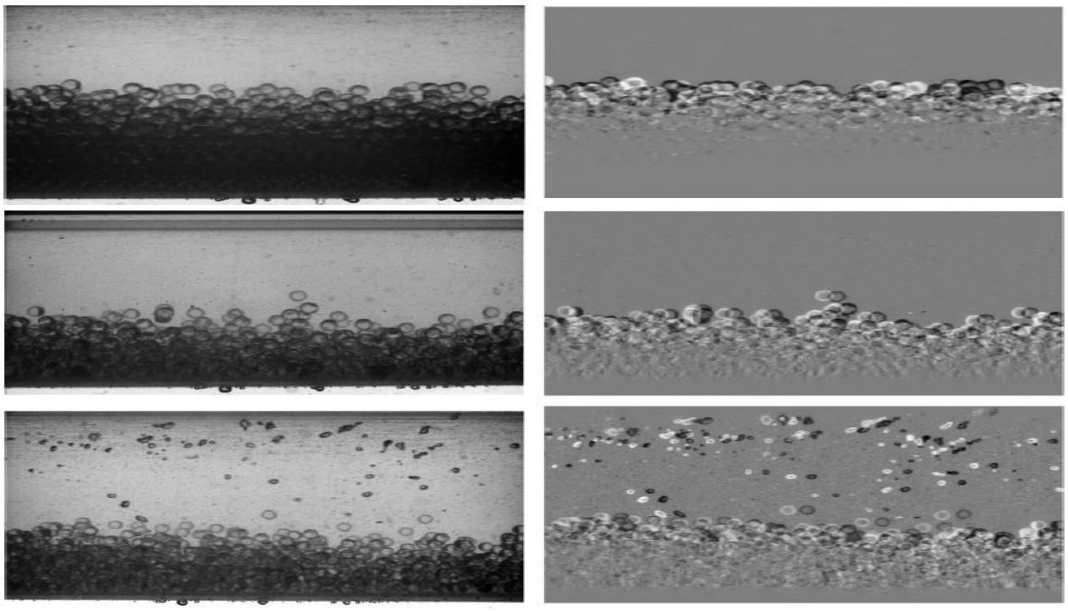

Figure 2-3 Different flow regimes are shown in horizontal pipe with different velocities (Vlasak et al., 2015)

2.2.2.2 Solid concentration influence on flow regimes

Nasr-El-Din et al., (1987) observed that the particle size has a major effect on concentration profiles with particles of relative density S = 1.05-1.06 and 2.65. The profile was not showing a sensitive head loss or flow rate, at least in the areas where the flow was completely suspended.

Gillies and Shook, (1994) indicated that in the flow of coarse particle at a high velocity, wall effect had an important influence on the solid concentration distribution at the bottom of the pipe. They also mentioned that, compared with previous studies, it is more complex in coarse particles to find the factors, which could be used to determine the concentration distribution. In addition, Gillies and Shook, (1994) also tested a horizontal pipe, which aimed to discover the concentration distributions in coarse sand slurries. A diffusion model was applied to forecast the concentration distributions. Some parameters, like mixture velocity, particle diameter, solid concentration and pipe diameter, were included in their experiments.

Doron and Barnea, (1995) indicated that the delivered concentration played a vital role in the process of transition to the suspension flow, as the solids content in the upper heterogeneous layer was affected. In order to observe the flow regimes, Doron and Barnea, (1995) presented the superficial velocity with delivered concentration. They found that the delivered concentration did not have any effects on transition from flow with a stationary bed. However, the higher concentrations would lead to the increased region of flow with a moving bed. The larger fluid velocity, which could cause particles to be fully suspended, was required for the additional quantity of particles in the fluid.

Peker and Helvaci, (2008) described the correlation between flow regimes and solid concentration. Figure 2-4 showed various flow regimes with different solid concentration distributions. For a suspension flow, the distribution of solid concentration was very stable, and all particles were suspended in the whole pipe. In addition, for the middle and bottom side, the

distribution of solid concentration in the lower layer was much larger than the top, which implied that there could be a moving bed on the bottom or all the particles were settling at the bottom.

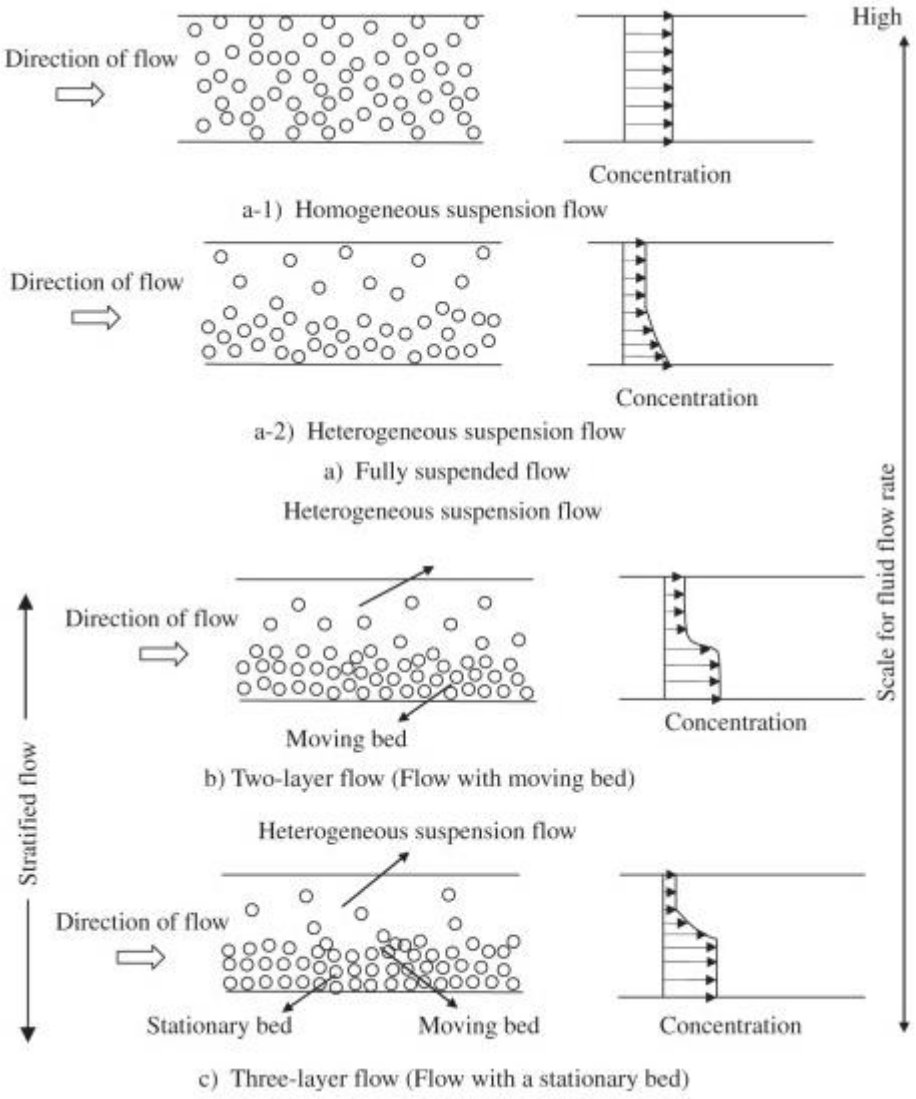

Figure 2-4 Different flow regimes with different solid concentration distributions (Peker and Helvaci, 2008)

Hill and Shook, (1998) pointed out that solid-liquid flow with coarse particle was highly stratified when water was used as the carrier fluid. For the two-layer model, pressure drop could be predicted by the particle concentration.

Hong et al., (2002) indicated that the volume concentration of slurry particle is usually measured by the mean velocity of solid particles, which is also a vital factor element for estimating flow regimes.

Ravelet et al., (2013) indicated that the increased delivered concentration might lead to a higher layer in the pipe. Nevertheless, the changed concentration only increased the critical velocity a very mildly.

2.2.2.3 Other parametric studies on flow regimes

Doron and Barnea, (1995) also tested the effect of different solid densities. It was clearly seen that a higher solid density would cause the transitions to occur at higher mixture flow rates. Such phenomenon was wise, as there existed a proportional action between the forces for moving the particles and suspending them and their weight.

Segregation phenomena would exist when mixing two or more particles, for the same density, particles with larger size might be conveyed on the top of the pipe, and the smaller particles might be conveyed on the bottom of the pipe. Such phenomenon was a big issue in most particle-fluid system. The reason for the consequence is not clear, and its effect on flow regimes is still not clear (Ravelet et al., 2013).

2.2.3 Pressure drop

For pipeline system, the most vital parameter is considering pressure drop, which is a major parameter needed to be carefully considered to acquire an expected throughput, avoid pipe blockage and so on. It is also tightly related to system energy efficiency. What's more, to study the changes of pressure drop in time or space of hydraulic conveying pipeline system could help researchers to obtained the dynamic behavior of fluid. In addition, pressure drop is a important parameter for the industry to better optimize the design. In solid-liquid flow, some helpful reference information on pressure drop and conveying concentration in vertical pipe for

different solid attributes are offered by Alajbegovi. et al., (1994). The shape influence of solid particles on the pressure gradient was performed by Chung et al., (1998). Engelmann Engelmann, (1978) accomplished experimental estimation of pressure drop, particle velocity and conveying concentration with various particle diameters and load ratios. More researches on pressure drop in hydraulic conveying are detailed discussed below.

2.2.3.1 Effect of conveying speed on pressure drop

Hydraulic or pressure gradient was another way of showing pressure drop (Toda et al., 1972, Engelmann, 1978, Chung et al., 1998, Aziz and Mohamed, 2013). Gillies and Shook, (2000) studied the effect of conveying speed on pressure drop, in which the particle size was 420 μm, and the pipe diameter was 264 mm. The results were shown in Figure 2-5. It was clearly seen that for a fixed feed solid concentration, the increasing conveying speed would produce a larger pressure drop.

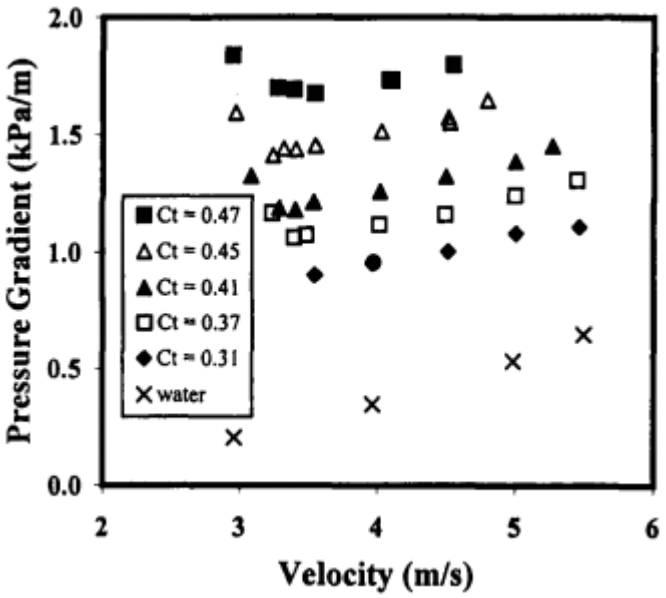

Figure 2-5 The effect of conveying speed and feed solid concentration on pressure drops at horizontal pipe (Gillies and Shook, 2000)

Kumar et al., (2003) stated that for lower velocity, the pressure drop increases slowly, while it would increase rapidly at higher velocities. Kaushal and Tomita, (2007) have also indicated that through their experiments, the pressure drop in the slurry would be affected by the deposition velocity.

Matoušek, (2009) showed the correlation between velocity and hydraulic gradient. For a fixed solid concentration, the hydraulic gradient might increase with increasing velocity. Similar results were also confirmed by Kaushal and Tomita, (2002).

Figure 2-6 shows the different pressure drops in horizontal and vertical pipes. Vlasak et al., (2015) observed that for the same pressure drop and same solid concentration, the velocity in vertical pipe was larger than that in horizontal pipe. In addition, for the same velocity and same concentration, the pressure drop was larger in horizontal pipe. However, the phenomenon in an inclined pipe is quite different and complex. They found that different velocities in ascending pipe would cause the pressure drop to grow up to a maximum point and then dropped down with different degrees of the inclined pipe.

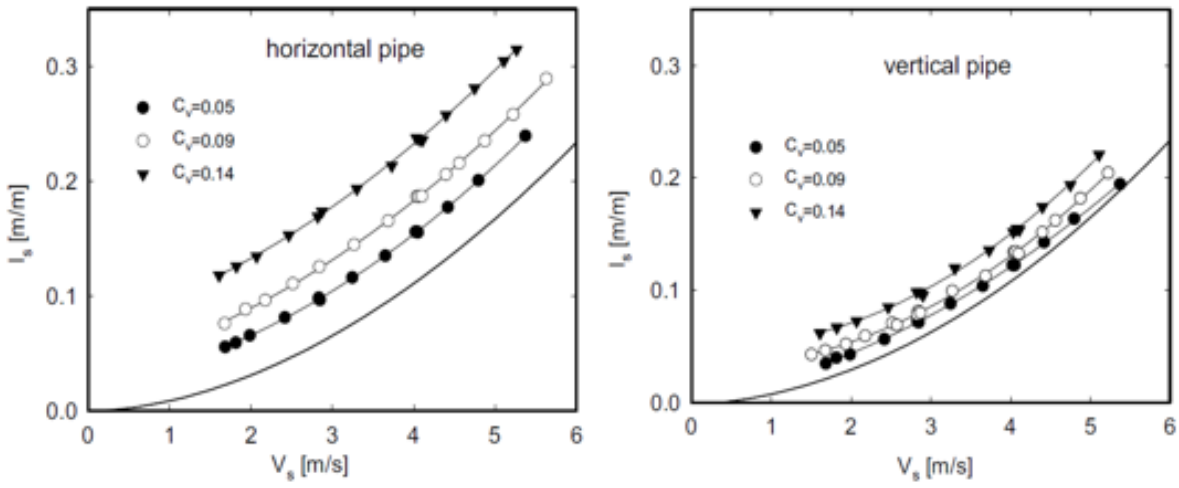

Figure 2-6 The effect of conveying speed and feed solid concentration on pressure drops at horizontal and vertical pipes (Vlasak et al., 2015)

2.2.3.2 Investigation of solid concentration influence on pressure drop

Hong et al., (2002) observed that both hydraulic gradient and volume concentration were influenced by Reynolds number, which relied on the mean water velocity. They also noticed that during the solid-water flow, load ratio played a vital role in the pressure drop. Due to the existence of solid particles, when the Reynolds number got higher, it tended to change the water velocity close to the pipe wall, therefore, the difference of hydraulic gradient for the solid-water flow and the water was larger.

Yoon et al., (2000) found that in the vertical pipe, the in-situ volume concentration of solid particles would play a major effect on the hydraulic gradient, the increased hydraulic gradient could be achieved with increasing in-situ volume concentration of solid particles. Furthermore, when the diameter of the pipe becomes larger and larger, there would be reductions of pressure drop. Vlasak et al., (2015) observed that at the same velocity, the pressure gradient would increase as there is an increasing in concentration. They also pointed out that the pressure gradient in vertical pipeline was lower than that in the horizontal pipe.

Hong et al., (2002) mentioned another important opinion, *i.e.*, load ratio, which played a vital impact on the solid concentration of particles, and ascertained the density of mixed solid-liquid flow and the static head loss in turn. When load ratio is a constant, the solid concentration will increase with the decreasing Reynolds number. Doron et al., (1987) explained that the increased input concentration led to higher pressure drops, while the critical velocity value was kept almost constant.

Aziz and Mohamed, (2013) pointed out that the input concentration played a vital role in the hydraulic conveying pipeline system. The increased input solid concentration would lead to an increase in pressure drop and a decrease in conveying efficiency, as the agglomeration and flocculation of solid particles occurred. They also mentioned that the specific gravity of solid

materials played a crucial effect in pressure gradient and conveying efficiency. With the increased specific gravity, the tendency of settling down was also increased, which would lead to an increase in pressure drop.

Zouaoui et al., (2016) indicated that in horizontal pipe, the increasing solid concentrations would have a higher pressure drop, in which the results are shown in Figure 2-7.

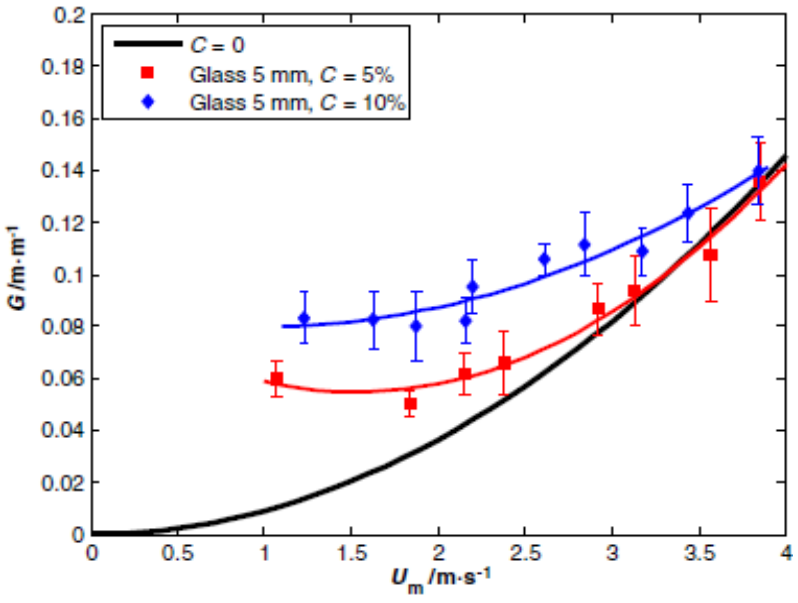

Figure 2-7 Pressure drops with different solid concentrations (Zouaoui et al., 2016)

2.2.3.3 Studies of particle size and shape on pressure drop

In horizontal pipe, Doron and Barnea, (1995) indicated that there are lots of cases for conveying slurries with small size particles, however, for the slurries of coal-water mixtures and sand could include larger size particles, which could be in the millimetres range. Doron and Barnea, (1995) also pointed out that such mixtures involving larger or smaller particles with high density are setting slurries. The mixture fluid would have an average density, the pressure drop for the mixture solid might be lower than the highest solid density itself (Ravelet et al., 2013).

Yoon et al., (2000) mentioned that for the same pipe diameter, the increasing particle size would lead to an increase of pressure drop in a vertical pipe. They noticed that for the smaller solid-

liquid velocity, the pressure drop data were dispersed, as the gain of the pressure vibration in lower velocity. Yoon et al., (2000) also tested different shapes of particles in vertical pipe, which are shown in Figure 2-8. They found that when the solid concentration was increased, the pressure drop of the spherical particles was a little higher than the non-spherical particles. As the non-spherical particles were easily destroyed, the non-Newtonian behaviour was easily observed. Chung et al., (1998) found that only for larger particles with higher solid concentrations, the pressure drop was affected by the different shapes of particles. Such opinion was evidenced by Yoon et al., (2000)

Figure 2-8 Different shapes of particles, left side is non-spherical particles and right side is spherical particles (Yoon et al., 2000)

Hong et al., (2002) used PTV method to observe a vertical flow, they determined that particle size plays a vital influence on both volume concentration and hydraulic gradients. The volume concentration is affected by particle size, which is controlled in lower Reynolds number, nevertheless, for the influence on pressure drop are the entire Reynolds number. Whereas, they also noticed that the impacts of particle sizes on pressure drop needed more experimental investigations. Vlasak and Chara, (2009) pointed out that the hydraulic gradients of coarse particles were higher than that in fine particle, furthermore, the difference could be decreased with a growth rate.

Kaushal and Tomita, (2007) stated that for 440 μm size particles, it was found that the pressure gradient of the equivalent fluid was larger at a lower velocity so that it could accelerate the bottom particles in the pipeline. However, for the higher velocity, pressure gradient was getting smaller as the near-wall lift exists. As a result, pipe economics for delivering coarser particles at a higher concentration and flow velocity would have a beneficial effect.

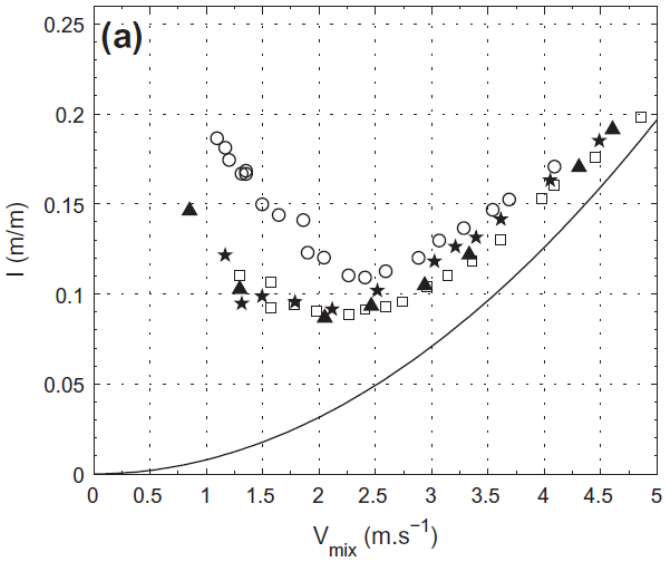

Figure 2-9 Pressure drops with different particle sizes,○: 6mm,□: 15mm (Ravelet et al., 2013)

Figure 2-9 shows the different pressure drops with different particle sizes in horizontal pipe. The experiment of Ravelet et al., (2013) was executed for the sake of better understanding the influence of particle size and density on the liquid velocity and the pressure drop, increasing particle sizes would let the pressure drop decrease when there were the fixed specific mass and delivered concentration. Comparing with a vertical pipe, it was found that the increased specific mass could increase both pressure drop and critical velocity. Furthermore, the increased specific mass would also lead to the increment of pressure drop and critical velocity.

2.2.4 Erosive wear

Pipeline erosive wear is another important consideration in the design of solid-liquid pipeline system. It not only increases operation and maintenance costs with regard to pipe section replacement and system failure, but also affects flow behaviours as a result of the change in the inner shape of pipe by wear. In some applications, the economic feasibility of the hydraulic hoisting system is even largely dependent on the life of the pipelines conveying the abrasive materials. More findings are discussed below.

2.2.4.1 Investigations of particle size and shape on erosive wear

The particle shape and size play an important role in erosive wear. The angular steel grits and spherical steel shots which are shown in Figure 2-10, were used to test the erosion wear by Levy and Chik, (1983). In their study, they found that the spherical steel shots could produce less erosive wear, when comparing with the angular steel grits that produced four times more erosion. The scanning electron microscope (SEM) was applied to examine the worn-out surfaces of the samples and indicated that the sharp craters which generated extruded platelets were formed by the angular steel grits, however, for the spherical steel shots, the more shallow and rounded craters were formed, and platelets were not developed.

Vittal and Tabakoff, (1984) stated that the collision efficiency, which is defined as the ratio of the number of particles per unit area of the impact surface per unit time and the number of particles contained in the suspension swept by the area per unit time, sharply decreased, resulted in the decreased particle size, so that the erosion rate was also decreased.

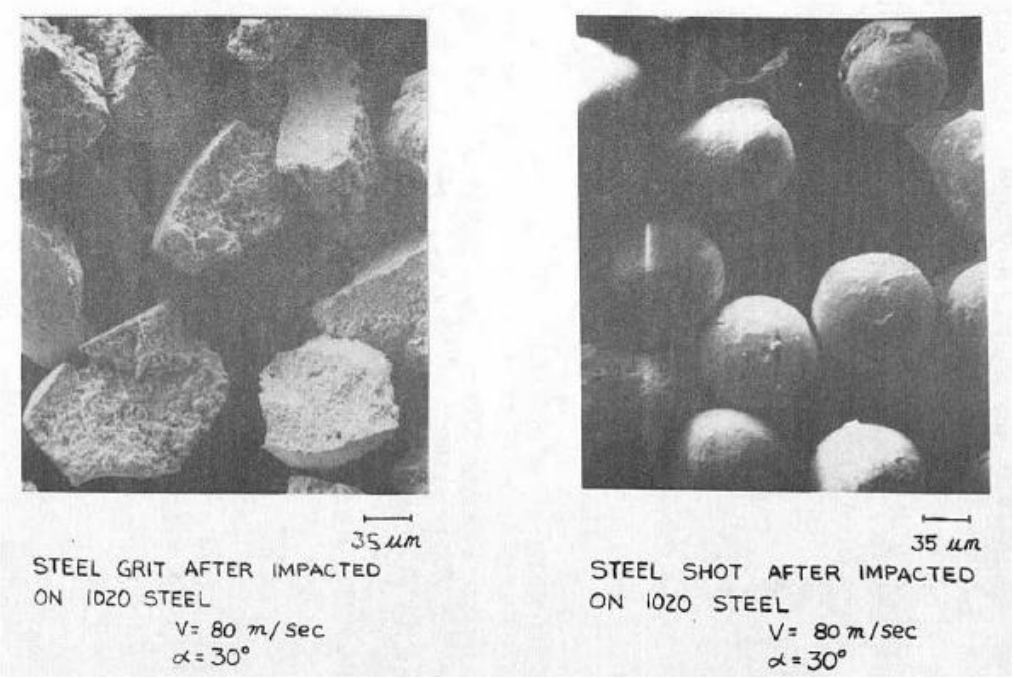

Figure 2-10 Steel particles, angular and spherical after impacted (Levy and Chik, 1983)

Gandhi and Borse, (2004) studied the effect of particle size, which was smaller than 75μm, on the erosive wear at two different impact angles of 30 ° and 75 °. The erosion rate increased with the increasing particle size.

Solid-liquid mixtures of three different natural erodent (quartz, alumina and silicon carbide) with similar particle sizes had been used to evaluate the mass loss of two targets at different orientation angles by Desale et al., (2006). The shape factor for each erodent was determined, and shown a decreasing value for the increase in angularity of the particle. It could be seen that the erosive wear increased with the decreasing shape factor and increasing density. Compared with blocky shape particles, the angular particles shown that its surface morphology had deeper craters and higher average surface roughness values. Therefore, compared with spherical particles, the erosive rate of angular particles was higher.

Desale et al., (2009) found in their experimental work that the erosive rate would be increased with the increasing average particle size, which the range of particle size was from 37.5 to 655

μm. They advised that there was a threshold kinetic energy that impacted the particles, which causes a change in the erosive rate at a specific particle size.

Huang et al., (2010) studied the effect of particle size on erosive wear rate in a horizontal pipe, in which the particle size was smaller than 500 μm, Figure 2-11 shows their results. The results of erosion rate on horizontal pipe was divided into three zones, top, middle and bottom, an averaged result was also shown in the figure. The results shown that the increased particle size would also lead to the erosion rate at the bottom and middle of the pipe to increase monotonically. However, the erosion rate at the top of the pipe was inversely proportional to the particle size, which meant that the erosion rate at the top of the pipe would be decreased when the particle size increased, except when the particle size was less than 150 μm, the erosion rate increased slightly. The average erosion rate of the entire periphery was close to the predicted value at the middle of the pipeline, which meant that the erosion rate measured at the middle section could approximately represent the average erosion rate.

Sinha et al., (2015) indicate that particle size was another important characteristic that affects the erosive rate. Several researchers analysed the effect of particle size on the erosion rate while keeping other operating conditions fixed. Compared with smaller particles, the larger particles have greater kinetic energy, even if they hit the target at the same speed. These large particles transferred more kinetic energy to the pipe wall that accelerated wear. Smaller particles were greatly affected by the flow turbulence, so they stay suspended in the flow and reduced impact on the surface.

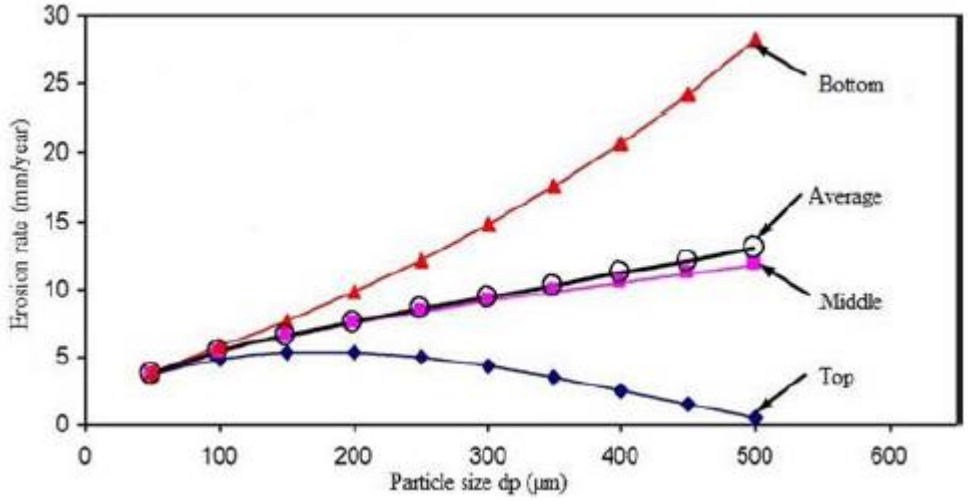

Figure 2-11 Effect of particle size on erosion rate (ER) at different locations of a pipe (Huang et al., 2010)

2.2.4.2 Studies of impact speed and angle on erosive wear

In hydraulic conveying pipe system, the impact speed and angle are another important parameter, which play an important role on erosive wear. Karabelas, (1978) studied the effect of impact speed on erosion rate, the range of conveying speed was from 2 to 4 m/s, the results are presented in Figure 2-12. It was shown that the increased conveying speed would produce a linearly increased erosion rate at three different position of the pipe.

Sinha et al., (2015) indicated that the erosion rate increased with the increasing conveying speed. It has a power law relationship with the conveying speed. It was assumed that there is no slip between the solid and the liquid phases so that the relative velocity between them disappeared. Therefore, the particles hit the wall at a speed equal to the solid-liquid conveying speed. They indicated that $\text{Wear rate} \propto (V_s)^n$, where V_s is the solid-liquid conveying speed. Various experiments were done in the past decades to establish the relationship between the conveying speed and the wear rate, the range of power index *n* was defined between 1.9 to 4.

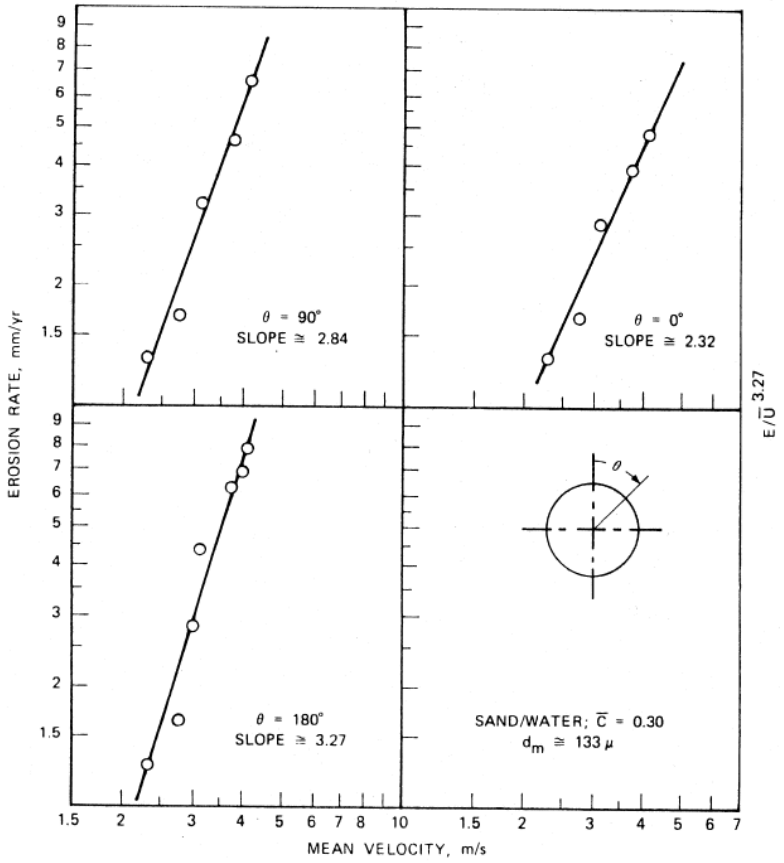

Figure 2-12 Effect of conveying speed on erosion rate (Karabelas, 1978)

Sinha et al., (2015) also pointed out that for the solid-liquid flow in horizontal pipe, as the inlet flow was parallel to the pipe wall. The particles trajectory was random so that a certain angle was produced when they collided with the pipe wall. Furthermore, the amount of erosion rate of the pipe wall would be depended on the colliding angle of these particles. Different investigations on the effect of impact angle on erosion wear were done in the past few years (Wellinger and Uetz., 1955, Tabakoff et al., 1979, Desale et al., 2011). Figure 2-13 shows the variation of erosion rate with orientation angle for different materials. The maximum erosion rate position changed with the increasing the impact angle.

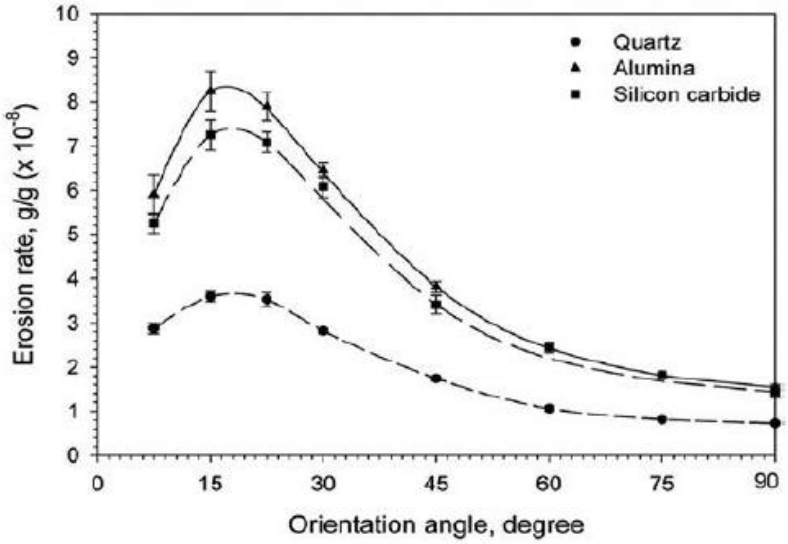

Figure 2-13 Variation of erosion rate with orientation angle for different materials (Desale et al., 2011)

2.2.4.3 Other factors affect erosive wear

The effect of mean curvature radius over pipe diameter (R/D) ratio on the erosion wear was investigated by Blanchard et al., (1984) through the circulating loop system. Bourgoyne, (1989) also studied the effect of R/D ratio on the erosion rate of an elbow pipe, and analysed the maximum erosion angle. Eventhough his experimental data on erosion was limited, many researchers still used his results as a database to develop erosion equations. An experimental loop was applied by Wood et al., (2004) to study the erosion rates for straight and bend pipes. In their study, they found that compared with the innermost side wall, the erosion wear of the outermost side wall of the bend was significantly higher, and the base of the bend had a significant erosion. The erosion-corrosion (EC) behaviour of the X65 pipe elbow was studied by Zeng et al., (2014) through the use of an array electrode technology. It was found that the erosion wear was mostly produced on the outside of the elbow pipe.

2.3 Numerical studies on hydraulic conveying

2.3.1 Numerical approach

As there is lacking reliable equations to predict pressure drop related to different flow regimes, a new approach is needed to study hydraulic conveying. Numerical approach is widely used nowadays (Xu and Yu, 1997, Zhou et al., 2010). Methods based on particle-fluid system including continuum method and discrete method. For the continuum method, normally Two Fluid Model (TFM) method was used, which was established on the average cells larger than particles but smaller than process equipment. The major assumptions in TFM model were constitutive relations for particle-particle interaction were needed, most of them were used for fine particles with diameter smaller than 1 mm, normally Computational Fluid Dynamics (CFD) was applied. For the discrete method (Xu and Yu, 1997, Zhou et al., 2010), normally Discrete Element Method (DEM) was applied, which was established on individual particles. In addition, DEM model had detailed information of forces, and least assumptions during simulating, it could be applied for predicting pipe wear and segregation phenomena, it was availably used for coarse particles with diameter larger than 1 mm.

2.3.1.1 Two Fluid Model (TFM) method

The basic concept of the two-fluid model is to treat each phase as a continuous medium that fills the entire flow field, and any point in the flow field is replaced by two components at the same time, that is, the particle phase is proposed to interpenetrate with the fluid phase. The view and basic method of establishing a two-phase flow equation using a two-fluid model is to first establish the transient, local conservation equation of each phase, and then use some average general form of the two-fluid flow equation is very complicated, use it directly to. There are still many difficulties in solving the specific flow problem. In order to use, it is

necessary to ignore the pulsation of the fluid phase density, the pulsation of the particle mass change rate and the unsteady correlation terms, and then to further simplify and gradually describe the constitutive equation of the fluid flow. For the particle phase, there is currently no universal reliability.

In the traditional two-fluid method, some empirical semi-theoretical models are often used to describe particle stress and stress-related physical quantities (Massoudi et al., 1992). Since the 1980s, particle dynamics theory has obtained the theoretical expression of particle corresponding force by considering particle collision. Therefore, this method has been more and more recognized by people.

2.3.1.2 Discrete method

Discrete element method is a direct simulation method developed from molecular dynamics theory to simulate particle flow. Its theoretical basis is that in the flow of particles, the energy dissipation is caused by inelastic collisions between particles, and the movement of particles is caused by external forces (such as gravity and fluid drag). Compared with the continuous method, the disadvantage of the discrete element method is that it can only simulate a certain number of particles. However, the discrete element method has many advantages: (1) it can give people insight into the microscopic motion characteristics of particles; (2) establish a general constitutive equation for the continuous method to provide particle microscopic flow information; (3) can consider the particle size and density distribution; (4) There is no problem that the equation of motion is not closed. With these advantages, the shortcomings of the discrete unit mentioned above are negligible. Generally, the discrete element method has a hard ball model and a soft ball model. The hard ball model believes that: (1) the particle-particle collision is very short compared to the particle free motion time, so the collision is completed

instantaneously, and the collision time is ignored; (2) at the same time, the particle can only collide with one particle; (3) The particles will not be deformed by the collision.

Obviously, the binary collision assumption of the hard sphere model is only suitable for systems with very low particle concentration. This problem does not exist in the soft ball model. The soft ball model believes that: (1) the particles may deform during the collision, so there is a small overlap in the particle volume; (2) the distance that the disturbance caused by the particle collision propagates in a time step must be less than a particle diameter; (3) At the same moment, the particles can collide with multiple balls at the same time; (4) The collision between the particles can continue.

In particle flow systems or multiphase flow systems dominated by particle flow, particle collisions are often multiple collisions. Therefore, the soft sphere model is currently one of the most effective tools for studying particles and particle-fluid systems (Zhu et al., 2007, Zhu et al., 2008). Generally, people call the soft-ball model DEM, but in some literatures, DEM is also used to represent both the hard-ball model and the soft-ball model. Since this whole project will use the ball model to study hydraulic conveying, for convenience, in the following content, unless otherwise specified, DEM stands for soft ball model.

2.3.2 CFD based researches

Brown, (2002) used a CFD based method to study the erosion problem in T pipe, in which the particle size was 150 μm. He suggested that a pivoting elbow pipe, which is shown in Figure 2-14, could be applied in solid-liquid system to replace the T pipe, as the erosion in the T pipe was high. This design had been successfully implemented in the industry.

Eesa and Marigo, (2009) used the same approach to model the hydraulic conveying in both the horizontal and vertical pipe for non-Newtonian carrier fluid, they observed that the increasing particle size would cause a decrease in maximum solids velocity, and the location where such

velocity was produced also moved up in the direction of the centre line. The higher solid concentrations would lead the solid and liquid velocities distributions to become flatter. Furthermore, the particle interactions result in the increase of friction losses, so the increasing concentration would also lead to an increase in pressure drop. In addition, for a single-phase flow, a remarkable tendency of rising in pressure drop would be obtained by the increased solid concentration.

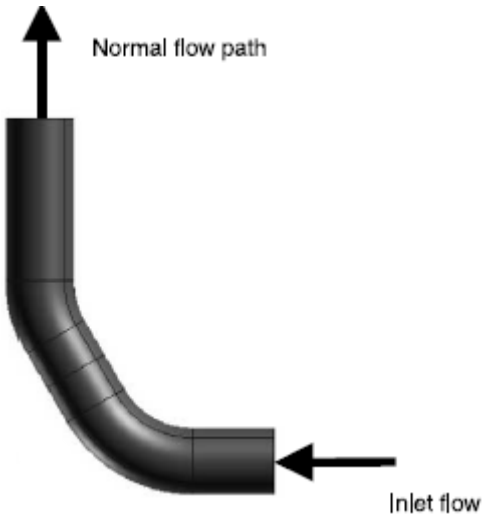

Figure 2-14 Schematic of pivoting elbow pipe (Brown, 2002)

Eesa and Marigo, (2009) also noticed that for the larger particles, the velocity distribution of the solid phase showed a remarkable level of asymmetry due to the raised tendency of the particles to settle, which increased with particle sizes. A remarkable blunting and asymmetry occur for the larger particles in the liquid-phase velocity distribution, and for the smaller particles the solid concentration distribution was closely uniform, which showed the pseudo-homogeneous flow. In addition, the increased particle sizes made the solid concentrations distribution to be deformed due to the improved sedimentation. The pressure drop would decrease when the particle diameter increases.

Kaushal et al., (2012) simulated hydraulic conveying in a horizontal pipe using a CFD-based method. They focused on multiphase fluid flow problems with Newtonian carrier fluid and particle size of 125 μm. They found that when the concentrations and flow velocity were high enough, lateral variation in solids concentration was more superior, as shown in Figure 2-15. For larger fluid velocity and concentrations, the larger solid concentration region was situated in the bottom half part of the pipe, away from the surrounded pipe boundaries. In addition, for larger fluid velocity and concentrations, the slip velocity at the pipe central caused most of the particles to move so that the concentrations at central was larger.

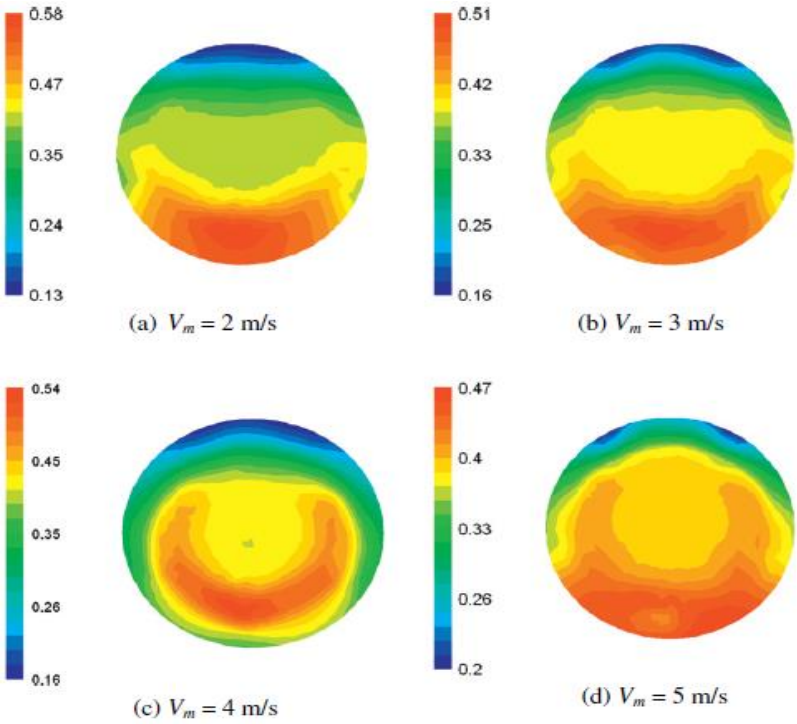

Figure 2-15 Different solid concentration profile with different velocities (Kaushal et al., 2012)

Azimian and Bart, (2014) applied CFD method to study different variables on erosion rate, such as, particle size, feed solid concentration, conveying speed and bend shape. During their study, the particle size was from 50 to 450 μm, and similar findings were obtained compared to other investigations. The difference was they compared different results on elbow pipe and

T pipe. They found that all the results on T pipe were larger than the elbow pipe in solid -liquid system, eventhough the T pipe was suggested to be used in gas-solid system. Figure 2-16 is shown here to show the contours of the effect of pipe geometries on erosion. It was obvious that the erosion position, value and impact zone for the two pipes were different. Figure 2-17 shows an example of the effect of sand concentration on maximum erosion rate with different pipe geometries. It could be easily seen that the maximum erosion rate for T pipe was always larger than elbows pipe. The pipe geometry plays an important role on erosion rate.

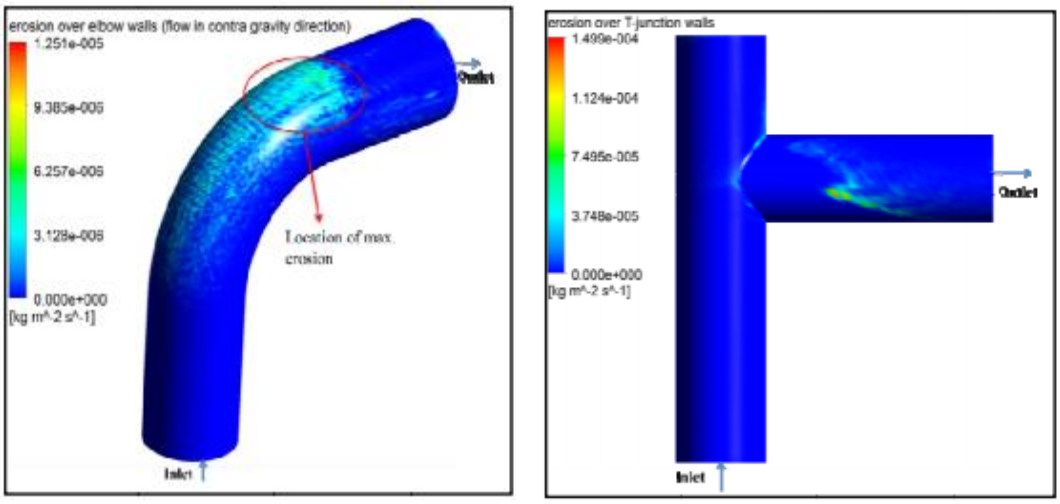

Figure 2-16 Contours of the effect of pipe geometries on erosion (Azimian and Bart, 2014)

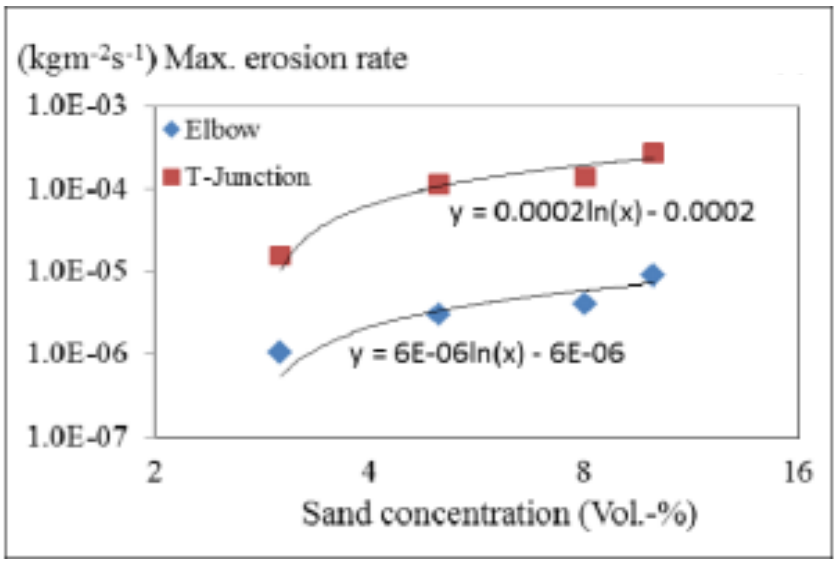

Figure 2-17 Shows the effect of sand concentration on maximum erosion rate with different pipe geometries (Azimian and Bart, 2014)

Messa et al., (2014) proposed a mathematical model based on CFD method to study the fully-suspended solid-liquid flow in horizontal pipe. In order to widely use such model, the capability of the model predictions of the main flow features, such as pressure drop, was validated with different researchers' experimental data, including a wide range of operating conditions, for example, the pipe diameter was from 50 to 150 mm, the solid material included sand and glass beads, the particle size was from 90 to 520 μm, and the conveying speed was from 1 to 7 m/s, and so on. Being compared to lots of experimental data, such model shown a good agreement and better performance.

Messa and Malavasi, (2015) applied a new two-fluid model based on CFD method in their research, in their simulation, the range of the particles size was between 280 to 640 μm, the delivered solid concentration was from 7 to 30%, and conveying velocity was 2 to 5 m/s, the results of one type of sand is shown in Figure 2-18. The simulation results shown a good agreement with experiment, the increased conveying speed would produce a higher pressure drop, and the larger the solid delivered concentration, the higher the pressure drop.

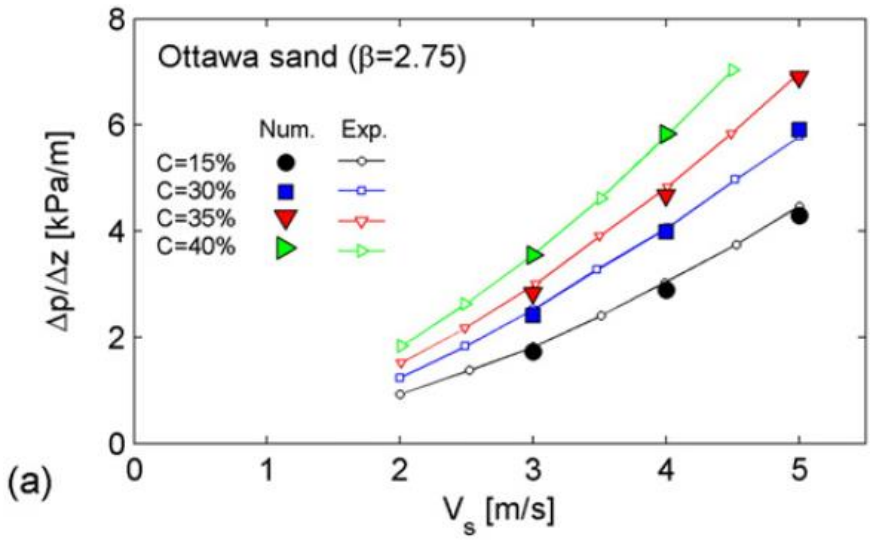

Figure 2-18 The effects of different solid delivered concentration and conveying speed on pressure drop (Messa and Malavasi, 2015)

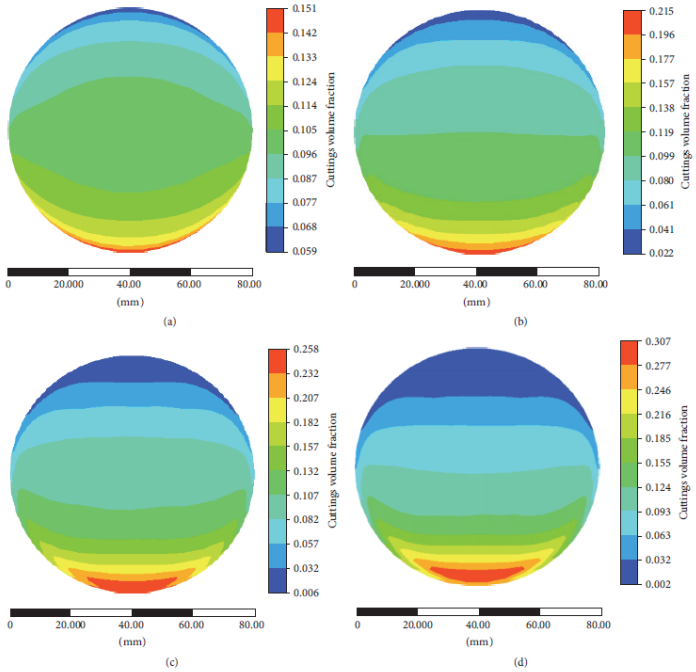

Figure 2-19 The effect of different particle size on solid volume fraction (Ofei and Ismail, 2016)

Ofei and Ismail, (2016) mentioned in their research, the Eulerian-Eulerian model was applied to predict the effect of particle size and feed solid concentration on the radial profile of solid volume fraction, velocity and pressure drop. An example of the effect of different particle size on solid volume fraction is shown in Figure 2-19. The increasing particle size would produce a larger solid volume fraction at the bottom of the pipe, however, , the solid volume fraction at the top was decreased.

Peng and Cao, (2016) studied the effects of different parameters, such as conveying speed, pipe diameter and bend angle on erosion rate through a CFD based method. The particle size used in their study was 200 μm. In their results, it was shown that the maximum erosion rate would be increased when the bend angle was increased, as shown in Figure 2-20(a). They also noticed

that as the angle of these three elbows were different, the impact angle of the particles for them were different so the maximum impact angle location changed with the increasing bend angle. In addition, Figure 2-20(b) shows the trends of erosion rate distribution for each bend angles, the larger bend angle would have multiple collision so that it produced more erosion rate peaks.

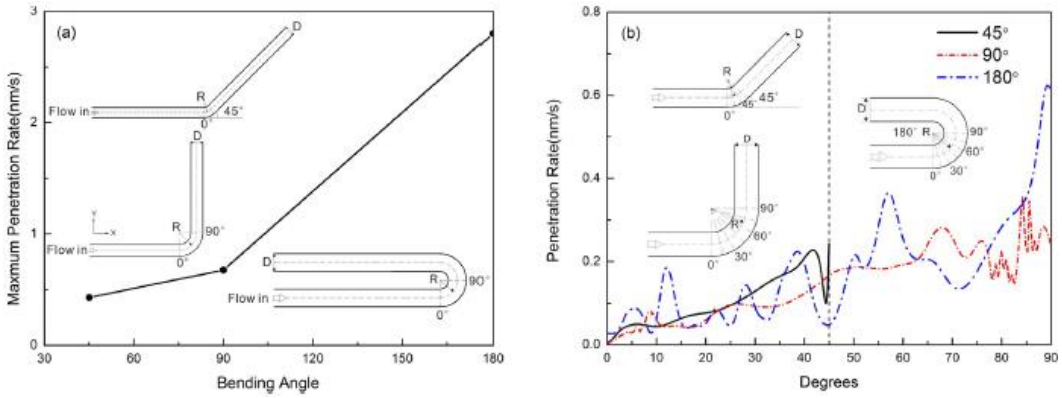

Figure 2-20 Effect of bend angle on predicted penetration rate: (a) penetration rate of the whole pipe bends; (b) penetration rate of the elbows (Peng and Cao, 2016)

A mathematical model combined with CFD method was established to predict the erosion rate in the elbows of oil pipelines by Wang et al., (2017a), in which the particle-fluid interaction was taken into account. The influences of bend orientation and particle size on the erosion wear were studied in detail. In addition, the correlation between particle trajectories and secondary flows was also investigated. The results shown that the erosion wear was mainly produced near the elbow outlet and the erosion behaviour depended on the forces acting on the particles, and the centrifugal effect of pipe flow. The complex coupled effects of the flow field and particle properties were quantified through an erosion pattern, which relied on the Stokes number was depicted in Figure 2-21.

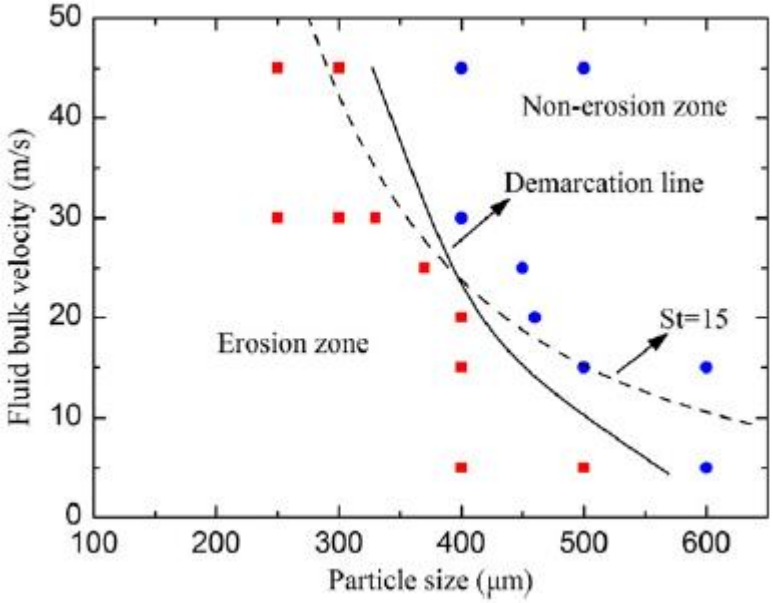

Figure 2-21 The erosion pattern based on stokes number (Wang et al., 2017a)

Pei et al., (2018) applied the CFD method to study the maximum erosion zone in elbow pipe, the range of particle size in their study was from 0.3 to 1.5 mm, and they found that there exists a direct relationship between the particle size and the erosion zone. The erosion zone would be changed when the particle size was increased. The conveying speed had less influence on the maximum erosion zone distribution, however, the value of maximum erosion would be increased when the conveying speed was increased.

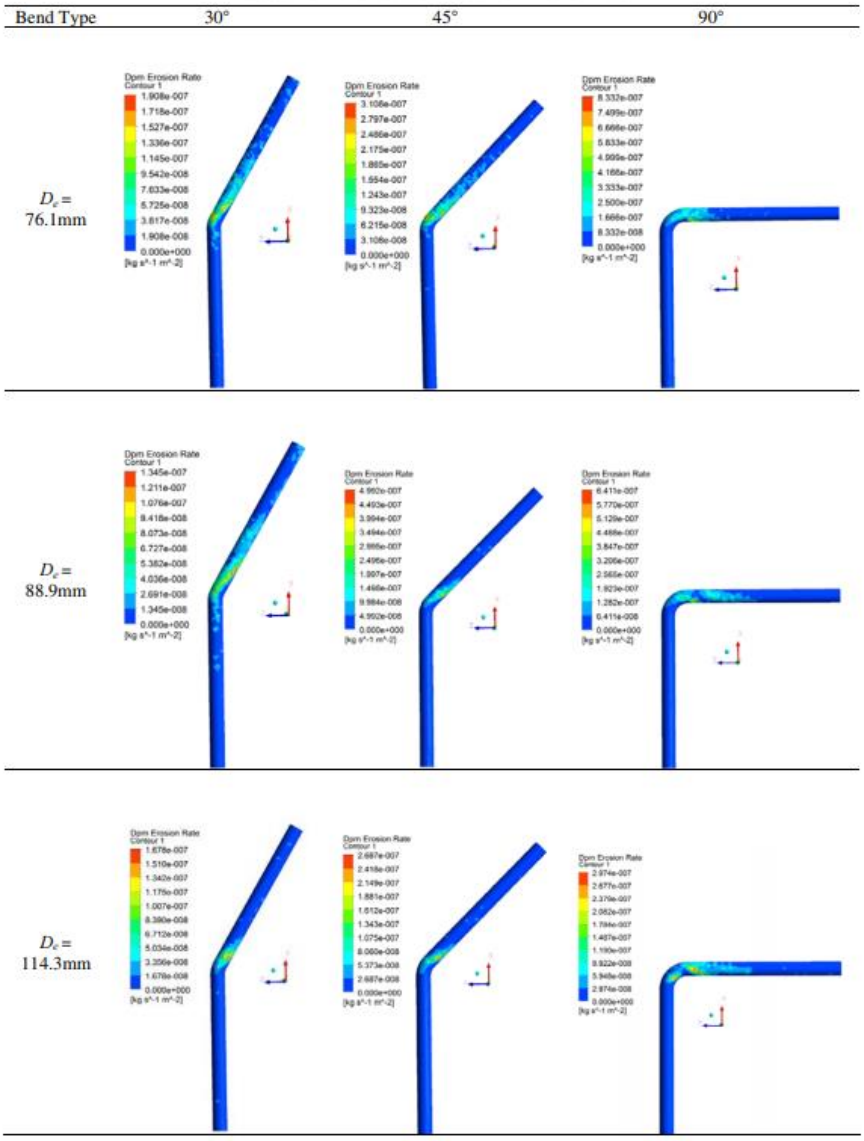

Figure 2-22 Contours of bend angle and pipe diameter on erosion rate (Lospa et al., 2019)

Lospa et al., (2019) investigated the effect of pipe diameter and bend angle on erosion rate, in which the particle size was 1 mm. The results of the effect of bend angle and pipe diameter on erosion rate is shown in Figure 2-22. The range of bend angle in their study was from 30 to 90 °, it was found that when other conditions were fixed, the increasing bend angle would produce a larger erosion rate, such result was in agreement with Peng and Cao, (2016), eventhough the particle size was increased to 1 mm. In addition, they found that for the 90

degree pipe, the increasing pipe diameter would produce a larger erosion rate, however results were not produced for the 30 degree or 45 degree bends.

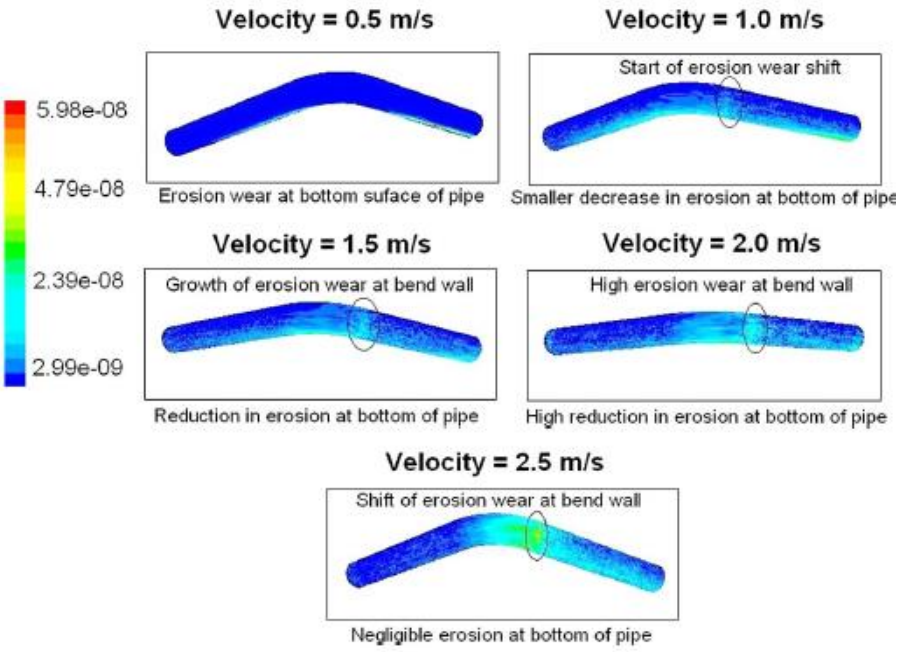

Figure 2-23 Contours of erosion wear distributions with different conveying velocities, which the dp =162μm, and Cv = 2.5% (Singh et al., 2019a)

Singh et al., (2019a) applied a CFD based method to study the different variables, such as, conveying speed, particle size and delivered solid concentration on erosion rate with a bend pipe. The particle sizes in their simulated case were 162 and 300 μm, the range of delivered solid concentration was from 2.5% to 10%. The increasing particle size and delivered solid concentration would produce a higher erosion rate. The results for the increasing conveying speed with erosion rate are presented in Figure 2-23. It indicated that the increasing conveying speed would also cause the erosion to increase, and the erosion at the bottom would be negligible. More investigations on hydraulic conveying based on CFD method are listed in Table 2-1.

Table 2-1 More CFD based investigations on hydraulic conveying

Reference	Variables	Finding
Ling et al., (2003)	Conveying speed	◆ Increasing conveying speed leads to decreased solid concentration
Wu et al., (2013)	(R/D	◆ The increased ratio of R/D has a lower secondary flow so that the lower erosion is examined.
Gopaliya and Kaushal, (2014)	Particles size	◆ Coarse particles have higher solids concentration.
Nabil et al., (2014)	Solid concentration	◆ Increasing solid concentration leads to increased pressure drop
Safaei et al., (2014)	Particle size	◆ When the conveying speed is high, for the micro size has a much larger maximum erosion rate, comparing with nano size.
Silva et al., (2015a)	Conveying speed	◆ The increasing conveying speed will produce a increased solid volume fraction at the top, and decreased at the bottom.
Khan et al., (2019)	Bend angles	◆ Erosion significantly occurs at the boundary walls of the flow pipeline near to the elbow exit. ◆ The increased bend angle leads a larger erosion rate.
Singh et al., (2019b)	Particle size, Solid concentration	◆ The particles size and solid concentrations have great effect on erosion wear in bend pipe. ◆ In bend pipe, the impacted zone and location of maximum erosion wear are more severe, comparing with the straight pipe.
Xie et al., (2020)	Pipe diameter, Bend angle	◆ The increased pipe diameter and bend angle produce a larger maximum erosion rate. ◆ The bend angle has the greatest influence on the maximum erosion rate of the bend pipe.

2.3.3 CFD-DEM based researches

Lim, (2007) studied the voidage waves in hydraulic conveying through vertical narrow pipes using a two-dimensional CFD-DEM model, in which a laminar flow was considered. Papista et al., (2011) coupled DEM with Direct Numerical Simulation (DNS) that was based on the finite element method other than the finite volume method in almost all other works, and studied the incipient sediment motion and the first stage of hydraulic conveying. They indicated that the highest particle velocities would appear in the particle-free layer above the particle bed, however, the particle velocities were nearly zero at the settlement near the bottom, the results are shown in Figure 2-24.

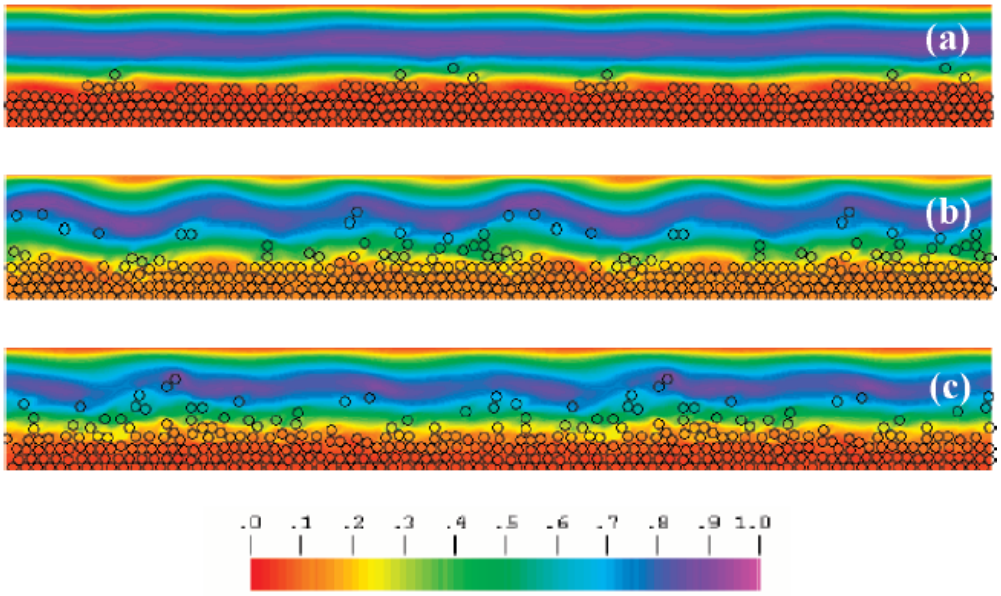

Figure 2-24 Instantaneous particle flow with different Reynold number, (a) Re= 4000, (b) Re = 6000 and (c) Re =8000 (Papista et al., 2011)

Zhang et al., (2012) studied the effect of conveying speed, bend orientation, bend angle on the maximum erosion zone and location in a standard bend pipe through CFD-DEM method, which the DEM was applied to track the particle trajectory and obtained the interaction force between particles. Figure 2-25 is presented here to show the effect of bend orientation on different flow

regimes. It was found that for the highly concentrated zone, it had low porosity, high drag force and high slip velocity, and the increasing conveying speed would cause a larger erosion. In addition, the bouncing tendency of the particle would be reduced by the gravitational force. The bend orientation played an important role on erosion.

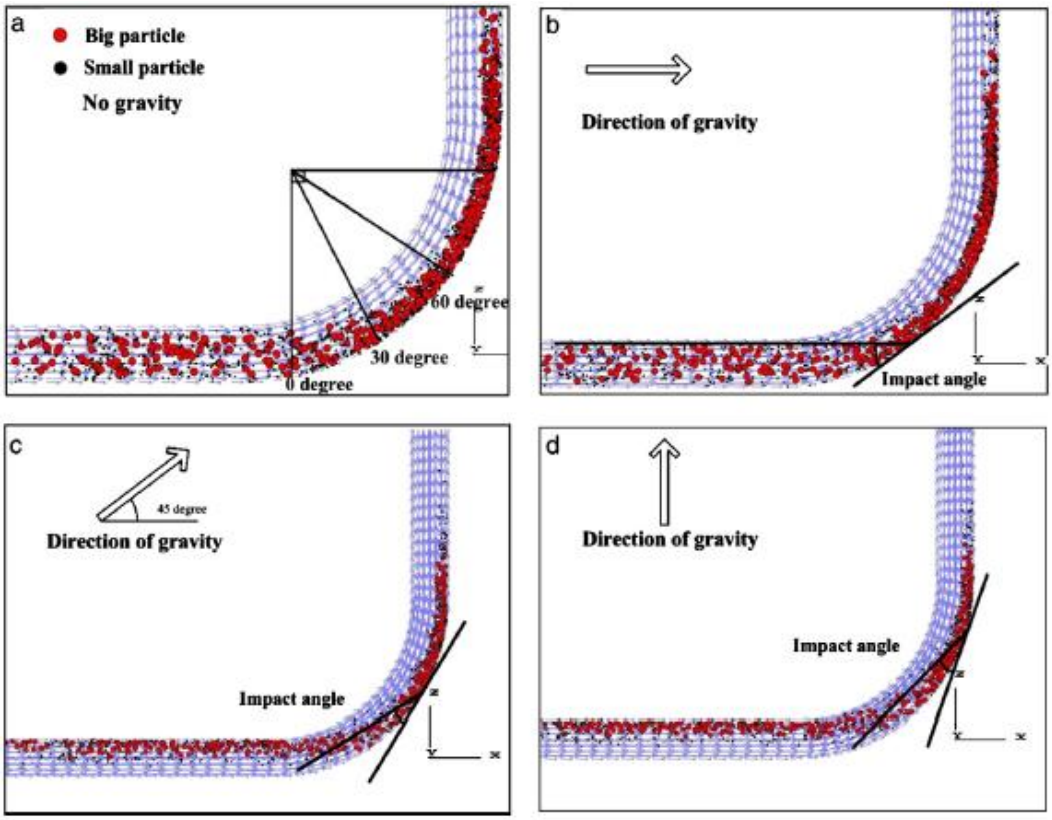

Figure 2-25 The effect of bend orientation on different flow regime: (a) no gravity considered pipe, (b) vertical to horizontally, (c) horizontal to vertically inclined; (d) horizontal to vertically (Zhang et al., 2012)

Capecelatro and Desjardins, (2013) developed the combined approach of DEM and Large Eddy Simulation (LES) for investigating the turbulent liquid-solid flow behaviours in horizontal hydraulic conveying of fine (mean size=165 μm) particles at two conveying speeds that were below and above the critical deposition velocity of particles, respectively.

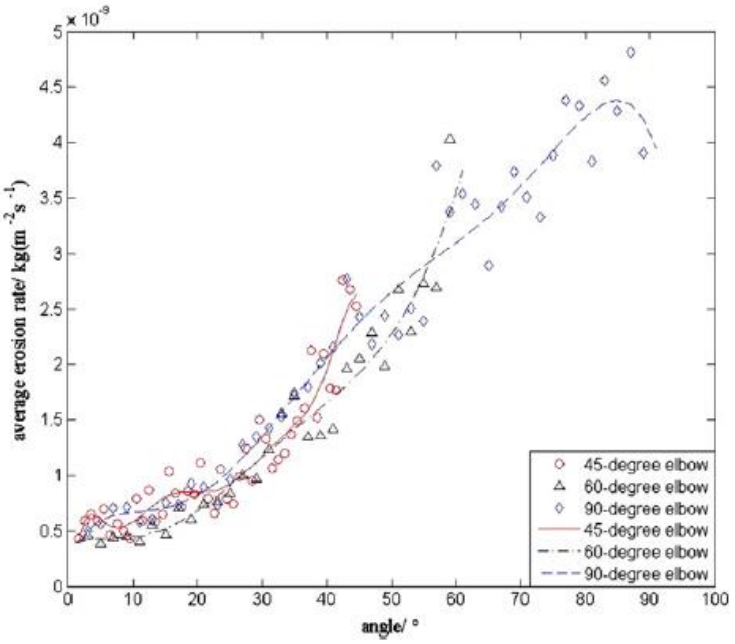

Figure 2-26 the effect of impact angle on erosion rate (Chen et al., 2015)

Chen et al., (2015) predicted the erosion law in the elbow pipe, and a CFD-DEM based model was used to simulate the different flow conditions in the elbow pipe. The liquid-particle, particle-particle and particle-wall interactions forces were taken into account in their new model. The particle size was 150 μm. The results indicated that the maximum erosive locations were near the outlet of the elbow, which was in agreement with other researchers. The bend angle has a great influence on the erosion. It not only affect the erosion, but also changed its magnitude, in which the results are presented in Figure 2-26.

Uzi and Levy, (2018) used CFD-DEM method to simulate the solid-liquid flow with coarse particles in the horizontal pipe, they found that increasing solid loading would increase the solid concentration at the same position, as shown in Figure 2-27. In addition, they stated that the increasing feed solid concentrations might increase the pressure drop. They also indicated that bottom concentration of particles was affected by the pipe size. The decreasing fluid velocity might allow the relative fluctuant turbulence to increase. Particles were compressed to the

bottom pipe wall through the particle-particle contact forces. Through CFD-DEM method, the flow regimes under different velocities could be described.

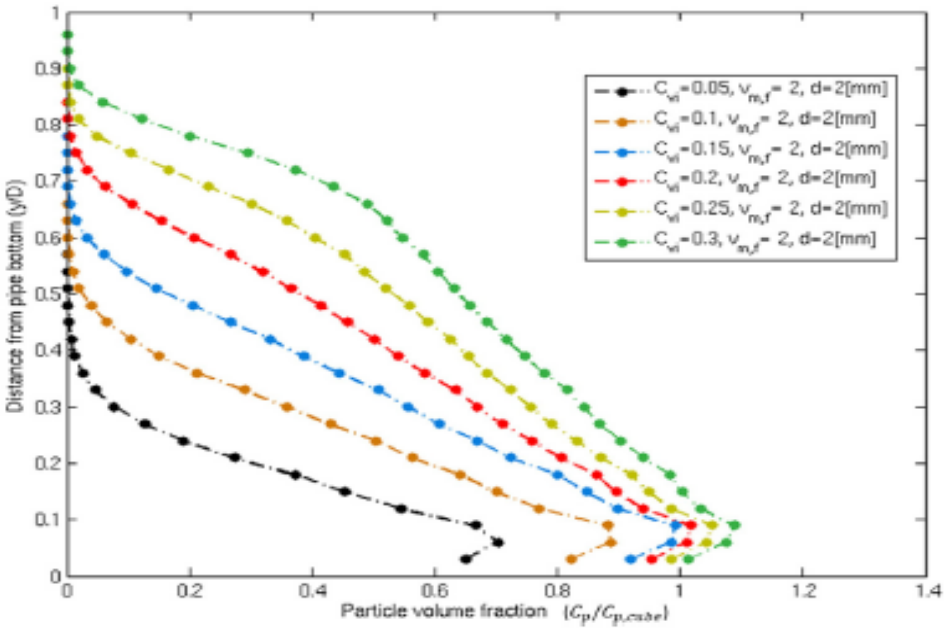

Figure 2-27 Radial solid concentration profile (Uzi and Levy, 2018)

Li et al., (2019) applied CFD-DEM models to study the erosion of hydraulic bends, in which the liquid flow was solved by the Reynolds-averaged Navier–Stokes equations (RANS) via a standard *k-ε* turbulence model. They compared experimental and simulated results, which is shown in Figure 2-28. It was indicated that for all operation conditions, the erosion of test sheet surface had similar pattern, however, the difference was the degree of erosion. Such results were consistent both in experiment and simulation. When the feed solid concentration was low, the amplitude of the erosion fringe was low. Conversely, it would be increased when the feed solid concentration was increased. However, when the feed solid concentration reached a level, the amplitude of the erosion fringe would not change too much.

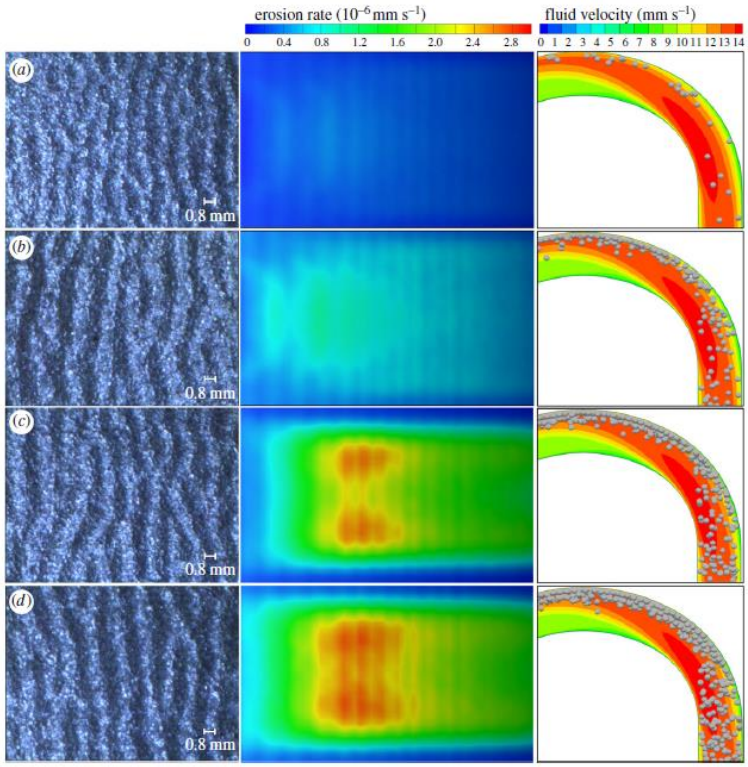

Figure 2-28 Comparing the experimental and simulated results, experiment (left), simulation (middle) and particle position (right), with different feed solid concentration. (a) 1%, (b) 6%, (c) 11% and (d) 15% (Li et al., 2019)

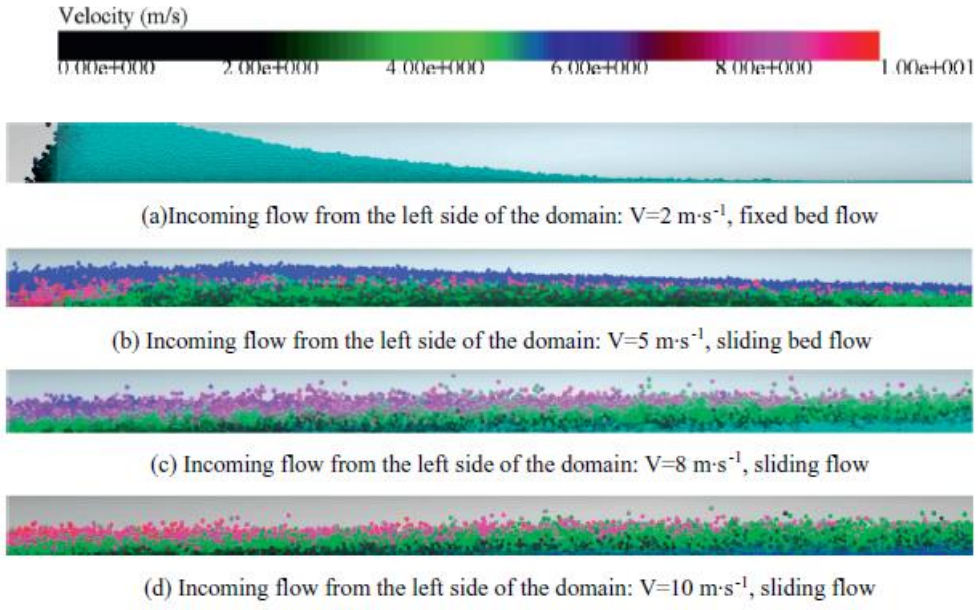

Figure 2-29 Instantaneous views of different flow regimes Ting et al., (2019)

The effect of conveying speed on flow regime is presented in Figure 2-29, which was obtained by Ting et al., (2019) who observed the pipe blockage in their CFD (RANS)-DEM simulations of the horizontal transport of coarse particle, in which the particle size was 10 mm with a low conveying speed. When the conveying speed increased, the flow regime changed, and particles tended to suspend more uniformly, and the solid velocity near the top tended to increase. In addition, they also analysed the solid volume fraction distribution for all flow regimes, and the effect of conveying speed on pressure drop. The increased conveying speed produced a larger pressure drop.

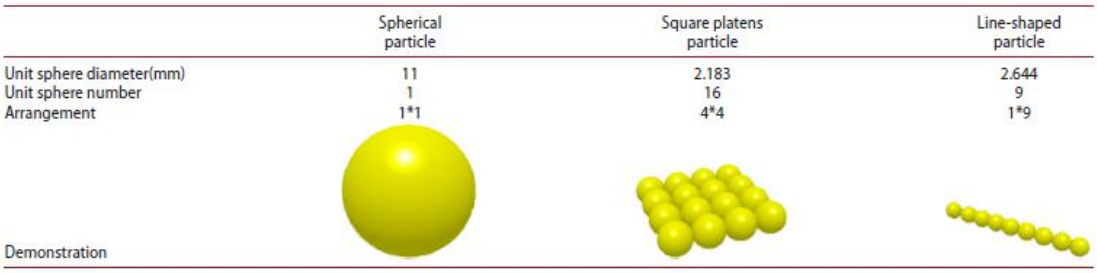

Figure 2-30 Schematic diagram of different particle shapes Chen et al., (2020)

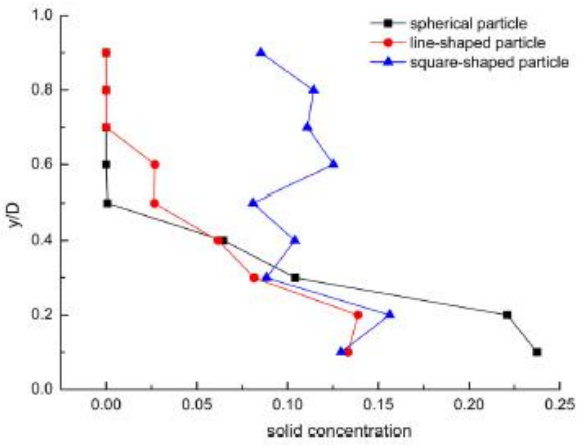

Figure 2-31 Solid concentration distribution with different particle shapes at moving-bed flow Chen et al., (2020)

Zhou et al., (2019) applied a LES-DEM model to study vertical hydraulic conveying of coarse particles. They identified the importance of lift force in hydraulic conveying system.

Via a similar method, Chen et al., (2020) studied the effect of particle sphericity on the horizontal hydraulic conveying in the form of moving-bed flow. The different particle shape is illustrated in Figure 2-30. The result for the solid concentration distribution with different particle shapes at moving-bed flow is presented in Figure 2-31. It was shown that the spherical particle had the largest solid concentration at the bottom of the pipe, and the solid concentration at the top was near to zero. For the square-shaped particle, the solid concentration was almost uniformly distributed in the vertical direction. A lot of particles settled at the top of the pipe that the blockage phenomenon has occurred. In addition, the fluctuation of solid concentration within the range of y/D = 0.3 to 0.9, indicating that the square-shaped particles were irregularly accumulated, which could easily cause blockage.

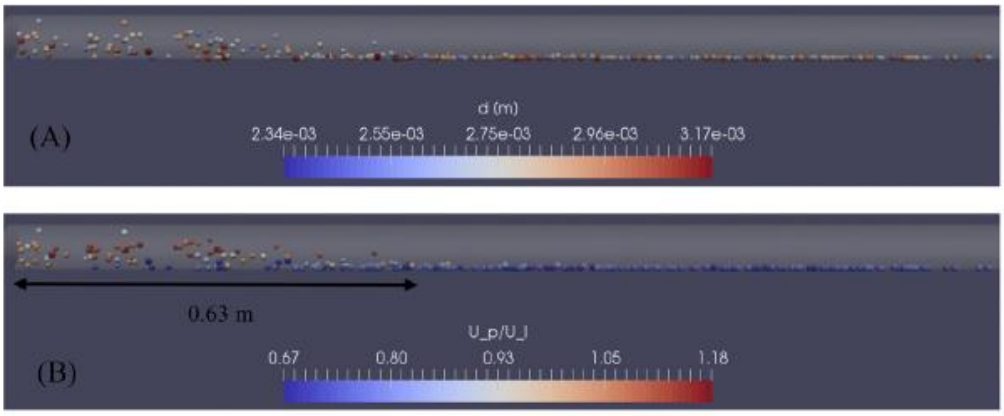

Figure 2-32 Instantaneous views of the particles at the inlet section, (a) particle size and (b) the axial solid velocity over the mean conveying speed (Uzi et al., 2020)

Uzi et al applied CFD-DEM method to study the flow, in which the model was also extended to the transport of salt particles Uzi et al., (2020). They noticed that after a short distance from the inlet position, there were lots of particles laying at the bottom of the pipe. For example, when the mean conveying speed was 1.218 m/s, this distance could be 0.63 m, which is presented in Figure 2-32. In addition, they summarized that the larger particles could settle down faster due to larger Archimedes number.

2.4 Conclusions

According to the literature review above, some research gaps are found here. Firstly, for the experimental researches, it is lack of reliable equations to predict pressure drop related to different flow regimes, and pipe erosive wear is difficult to predict and control, and particle behaviours were not analysed through such method. Secondly, for the numerical researches, the typical flow regimes were not reproduced successfully, and very few numerical studies on pipe erosive wear for hydraulic conveying, and most of them are only based on CFD method, which the particle behaviours are difficult to obtain. In addition, TFM modelling focuses on fine particles and the studies on the coarse particles through CFD-DEM method are quite rare.

Hence, a CFD-DEM method will be used here to study the coarse particles, the main aims of this projects are list below: Firstly, developing and validating a CFD-DEM model to describe the complex liquid-solid flow and performance of hydraulic conveying. Secondly, understanding the fundamentals governing the flow and performance under various geometrical, material properties and operational conditions in terms of particle-particle, particle-fluid and particle-wall interactions. Thirdly, investigating the flow regimes and their transition, solid pattern, and pipe erosive wear under different geometrical, operational and material conditions.

CHAPTER 3 CFD-DEM MODELLING OF HYDRAULIC CONVEYING OF SOLID PARTICLES IN A VERTICAL PIPE

3.1 Introduction

Hydraulic conveying transports bulk materials from one location to another by a closed pipeline system with the aid of carrier liquid. (Doron and Barnea, 1995) This transportation method is widely encountered in chemical, coal and mining industries (Ali and Yeung, 2014, Asim and Mishra, 2016, Silva et al., 2015b). With high demands on raw materials by modern industries, attention has also been paid to apply this technology to new source exploitation, for example, in the ocean industry (Oh et al., 2015, Oh et al., 2018). In applications of hydraulic conveying, critical velocity and solid concentration have been widely applied to determine different flow regimes. Several studies (Doron and Barnea, 1993, Doron and Barnea, 1996, Doron et al., 1997, Gillies and Shook, 2000) have demonstrated that these parameters may have a significant influence on pressure drop. However, the flow regimes occurring along hydraulic conveying pipelines are quite complicated and affected by a range of variables (e.g., conveying speed, solid concentration and particle diameter), which have hence attracted continuous interests among researchers and engineers, especially for operations at relatively high solid concentrations (Senapati et al., 2013).

During hydraulic transport, a low conveying velocity is often avoided to use, as it tends to form a stationary layer of particles on pipe bottom, causing the risk of pipe blockage drastically (Miedema, 2015). On the contrary, when the conveying velocity is high enough, a full suspension is exhibited while consuming high energy (Pakzonka et al., 1981). Therefore, the conveying velocity zone between full suspension and stationary deposit has been often used (Doron and Barnea, 1993, Doron and Barnea, 1996). Although the existence of the conveying zone is well recognized, reliably predicting flow features within this zone under different conditions still represents a main conundrum in applications of hydraulic conveying (Uzi and Levy, 2018).

Generally, particle and fluid dynamics, which can readily be extracted from the flows of fluid and solid phases, are necessary to predict many important fields. For example, the fluid pressure drop across a pipe defines energy requirements (Doron and Barnea, 1993, Doron and Barnea, 1996, Doron et al., 1997, Gillies and Shook, 2000). Also, deposit velocity is the key to determine the pump efficiency, minimum transporting velocity, and energy consumption efficiency. On the other hand, it is established that pipeline erosion (Jafari et al., 2014, Parsi et al., 2014, Mansouri et al., 2015, Sun et al., 2015, Vaezi and Kumar, 2015, Xu et al., 2016, Uzi et al., 2017, Zhao et al., 2017) and particle attrition (Vlasak and Chara, 2011, Chen et al., 2017, Kotzur et al., 2018) during the transport of particles may lower down product quality and even fail the pipeline system. The collision information plays a decisive role in the calculation of particle breakage, where the collision velocity and frequency of particle-particle/wall interactions are needed (Uzi et al., 2016, Zhao et al., 2017, Uzi and Levy, 2018). Also, for wear prediction, particle impact velocity and angle play an important role (Jafari et al., 2014, Parsi et al., 2014, Mansouri et al., 2015, Sun et al., 2015, Vaezi and Kumar, 2015, Ben-Ami et al., 2016, Xu et al., 2016, Uzi et al., 2017, Zhao et al., 2017). As such, the estimation of flow features as well as particle-particle/wall collisions are very necessary, which will ultimately be beneficial for determining suitable operating conditions for hydraulic transport systems.

In the past, various efforts have made to study flow features of hydraulic conveying (Turian and Yuan, 1977, Wilson et al., 2002, Matoušek, 2005, Rice et al., 2015, Hashemi et al., 2016). One of the general methods for analysing flow regimes in this process is by correlating pressure drop or other process parameters with operating parameters such as solid concentration, conveying speed and particle diameter based on experimental data, leading to a wide variety of correlations for process control (Matoušek, 2005, Miedema and Ramsdell, 2015, Silva et al., 2015b). However, such correlations are valid only under specific conditions and give large prediction errors when applying to the ranges beyond those covered originally. To date, it has

been a challenge to formulate general correlations for hydraulic conveying because of its complicated flow behaviours. Moreover, the correlations for predicting process parameters focus only on macroscopic information, and thus cannot provide insights into the liquid-solid flow along pipelines for achieving a full understanding of hydraulic transport to secure its reliable applications.

In line with the development of computational technology, numerical simulation has been becoming an effective and useful tool to predict the flow features in hydraulic conveying. The two-layer model is believed as the most common model, which simply divides the conveying into upper and bottom layers and models them separately (Gillies and Shook, 2000, Matoušek, 2005, Messa et al., 2014, Messa and Malavasi, 2015). This model can well predict not only the tendency of pressure drop but also the bed heights as measured (Doron et al., 1987, Messa and Malavasi, 2015, Uzi and Levy, 2018). However, the simplified hypothesis of two layers may lead to difficulties in obtaining complicated flow characteristics. Therefore, development and application of a more intricate model is imminently necessary for the practice of hydraulic conveying. For this purpose, two kinds of models can be used, namely, Euler-Euler method (Zhou et al., 2010, Kaushal et al., 2012, Messa and Malavasi, 2015), and Euler-Lagrange method (Zhou et al., 2010, Kuang and Yu, 2011, Kuang et al., 2013, Xu et al., 2016, Uzi and Levy, 2018). In the former method, both liquid and solid phases are treated as continuum media and described by Navier-Stokes equations. It is computationally convenient and widely adopted for applied research, though at present there are doubts about the general availability of constitutive relations for describing solid stresses reliably. Nevertheless, in the past few years, a few investigators (Doroodchi et al., 2005, Silva et al., 2015a, Ofei and Ismail, 2016) have employed the Euler-Euler method to study hydraulic conveying, leading to a better understanding of this process. However, such a method cannot obtain adequate information about particle-particle/wall collision, which is of vital importance to predicting various

important phenomena, as discussed above. In the Euler-Lagrange method, the liquid phase is modelled as a continuous phase, and the solid phase is simulated as a discrete phase. Through this method, the motion of an individual particle is simulated, and the particle-particle/wall collisions can readily be taken into account if needed (Xu and Yu, 1997, Zhou et al., 2010, Kuang and Yu, 2011, Kuang et al., 2013, Uzi and Levy, 2018). Discrete element method (DEM) is one of the most accepted methods for modeling particle-particle/wall interactions in the Lagrangian framework. In DEM, the Newton's second law is applied to describe the motion of individual particles with all the main forces included. Although this method has great potential for modelling different particle-fluid systems (Zhu et al., 2007, Zhu et al., 2008, Kuang et al., 2018, Kuang et al., 2019a), only a few efforts were reported in the past few years to use the coupled CFD-DEM method to study hydraulic conveying of solid particles (Lim, 2007, Capecelatro and Desjardins, 2013, Ren et al., 2017, Uzi and Levy, 2018). Moreover, most of those studies focused on horizontal pipes, where flow regimes are entirely different compared with those occurring in vertical pipes. To date, CFD-DEM studies on the influence of coarse particle diameter (>1 mm) on pressure drop, flow regimes, solid volume fraction distribution and so on have not been reported for vertical hydraulic conveying. Besides, none of the previous CFD-DEM studies tested the influence of lift force that may play an important role in vertical hydraulic conveying due to the relatively large ratio of fluid to particle densities and the absence of gravitational effect in the radial direction.

In this study, the CFD-DEM method is developed to study hydraulic conveying of coarse particles through a vertical pipe. This chapter is structured as follows. First, the governing equations for liquid flow and particle motion as well as their numerical implementation are given. Then, the CFD-DEM method is validated, and the effect of lift force is assessed. Finally, the influences of operating parameters including feed solid concentration, conveying speed,

and particle diameter on the instantaneous flow regimes and time-averaged variables are studied in detail.

3.2 Methodology

3.2.1 Fluid flow

The liquid flow is treated as a continuous phase and modelled in a similar way to the one in the conventional two-fluid modelling. Thus, its governing equations are the conservation of mass and momentum in terms of local mean variables over a computational cell, given respectively by

$$\frac{\partial}{\partial t}\left(\varepsilon_f \rho_f\right) + \nabla \cdot \left(\varepsilon_f \rho_f \mathbf{u}_f\right) = 0 \tag{1}$$

$$\frac{\partial}{\partial t}\left(\varepsilon_f \rho_f \mathbf{u}_f\right) + \nabla \cdot \left(\varepsilon_f \rho_f \mathbf{u}_f \mathbf{u}_f\right) = -\varepsilon_f \nabla p + \nabla(\varepsilon_f \mathbf{R}_f) + \varepsilon_f \rho_f \mathbf{g} + \mathbf{F}_{pf} \tag{2}$$

where ρ_f is the fluid density, $\mathbf{u}_f$ is the fluid velocity and ∇p is the fluid pressure gradient. $\mathbf{F}_{pf}$ is the volumetric fluid-solid interaction force. According to the work of Zhou *et al.*(Zhou et al., 2010), it is calculated by $\mathbf{F}_{pf} = -\frac{1}{V_{cell}} \sum_{i=1}^{k_c} \left(\mathbf{f}_{d,i} + \mathbf{f}_{lift,i} + \mathbf{f}_{add,i}\right)$, where k_c and V_{cell} are the number of particles in a considered computational cell and the volume of the computational cell, respectively. The stress tensor $\mathbf{R_f}$ includes two parts, that is, viscous stress and Reynolds stress, given by

$$\mathbf{R}_f = \eta \nabla \mathbf{u}_f + \rho_f \boldsymbol{\tau} \tag{3}$$

where η is the fluid viscosity. $\boldsymbol{\tau}$ represents the Reynolds stress, which is expressed as:

$$\tau = \frac{2}{\rho_f}\eta_t \mathbf{S} - \frac{2}{3}\frac{\eta}{\rho_f}\mathbf{I}, \quad \mathbf{S} = \frac{1}{2}\left(\nabla \mathbf{u}_f + \left(\nabla \mathbf{u}_f\right)^{\mathrm{T}}\right) \tag{4}$$

where η_t stands for the turbulent viscosity. A Smagorinsky model (Lilly, 1992) is used to calculate μ_t. Although the turbulence of fluid phase is included here, the turbulence modulation by particles is ignored. This treatment proves reasonable in modelling various two-phase flow systems by different investigators (Derksen et al., 2008, Gui et al., 2008, Kuang and Yu, 2011, Fox, 2012, Mallouppas and van Wachem, 2013, Wang et al., 2014, Sun and Xiao, 2016, Wang et al., 2017b).

3.2.2 Particle motion

The motion of each individual particle is described by the Newton's second law, formulated as follows:

$$m_i \frac{d\mathbf{v}_i}{dt} = m_i \mathbf{g} + \mathbf{f}_{fp,i} + \mathbf{f}_{p,i} + \sum\nolimits_{j=1,\, j\neq i}^{k} \mathbf{f}_{c,ij} \tag{5}$$

where m_i and v_i are, respectively, the particle mass and velocity, **g** is the gravitational acceleration, and $\mathbf{f}_{p,i}$ is the pressure gradient force. $\mathbf{f}_{c,ij}$ is the contact force exerting on particle i by particle j, which is solved by a soft-sphere contact model proposed originally by Cundall and Strack (Cundall and Strack, 1979) as follows:

$$\mathbf{f}_{c,ij} = \mathbf{f}_{cn,ij} + \mathbf{f}_{ct,ij} \tag{6}$$

$$\mathbf{f}_{cn,ij} = -k_{n,ij}\delta_{n,ij}\mathbf{n}_i - \gamma_{n,ij}(\mathbf{v}_r \cdot \mathbf{n}_i)\mathbf{n}_i \tag{7}$$

$$\mathbf{f}_{ct,ij} = -k_{t,ij}\delta_{t,ij}\mathbf{t}_i - \gamma_{t,ij}[(\mathbf{v}_r \cdot \mathbf{t}_i)\mathbf{t}_i + (\boldsymbol{\omega}_i \times \mathbf{r}_i - \boldsymbol{\omega}_j \times \mathbf{r}_j)] \tag{8}$$

where **n** and **t** stand for the normal and tangential unit vectors, respectively. ***r*** denotes the vector from the mass center of the current particle to the contacting point of the colliding pair.

$\mathbf{v}_r(=\mathbf{v}_i-\mathbf{v}_j)$ is the relative velocity vector of particle *i* and particle *j* in the colliding pair. *k*, γ and δ represent the spring constant, the damping coefficient and the displacement of a colliding pair, respectively. The equations for calculating the collision coefficients are listed in Table 3-1.

Table 3-1 Calculation of spring and damping coefficients

Normal spring constant $k_{n,ij}$ and normal damping coefficient $\gamma_{n,ij}$

$$k_{n,ij}=\frac{4}{3}Y^*\sqrt{R^*\delta_{n,ij}},\quad \gamma_{n,ij}=2\sqrt{\frac{5}{6}}\beta\sqrt{S_{n,ij}m^*}$$

Tangential spring constant $k_{n,ij}$ and tangential damping coefficient $\gamma_{t,ij}$

$$k_{t,ij}=8G^*\sqrt{R^*\delta_{n,ij}},\quad \gamma_{t,ij}=2\sqrt{\frac{5}{6}}\beta\sqrt{S_{t,ij}m^*}$$

where

$$\frac{1}{Y^*}=\frac{\left(1-\nu_i^2\right)}{Y_i}+\frac{\left(1-\nu_j^2\right)}{Y_j},\quad \frac{1}{R^*}=\frac{1}{R_i}+\frac{1}{R_j},\quad \frac{1}{m^*}=\frac{1}{m_i}+\frac{1}{m_j},\quad \beta=\frac{\ln(e)}{\sqrt{\ln^2(e)+\pi^2}}$$

$$\frac{1}{G^*}=\frac{2\left(2+\nu_i\right)\left(1-\nu_i\right)}{Y_i}-\frac{2\left(2+\nu_j\right)\left(1-\nu_j\right)}{Y_j},\quad S_{n,ij}=2Y^*\sqrt{R^*\delta_{n,ij}},\quad S_{t,ij}=8G^*\sqrt{R^*\delta_{t,ij}}$$

The Coulomb friction model is employed to calculate the tangential contact force when sliding friction occurs:

$$\mathbf{f}_{ct,ij}=-\mu_s\left|\mathbf{f}_{cn,ij}\right|\mathbf{t}_i \tag{9}$$

where μ_s is the sliding friction coefficient.

The rotational motion of a particle is expressed as:

$$I_i\frac{d\boldsymbol{\omega}_i}{dt}=\sum_{j=1}^{k}\mathbf{T}_{ij} \tag{10}$$

where $\boldsymbol{\omega}_i$ is the angular velocity of particle i. $\mathbf{T}_{ij}$ is the total torque between particle i and particle j.

3.2.3 Fluid-particle interaction

In the CFD-DEM method, the fluid phase and particles are coupled via the void fraction term (ε_f) and the fluid-particle interaction force term ($\mathbf{f}_{fp,i}$). The void fraction has been recognized as an important parameter affecting CFD-DEM simulations considerably. Its accurate evaluation in a cell is sometimes time-consuming, particularly when cells of irregular shape are involved. Numerical instability may occur because of the rapid temporal and spatial changes in porosity and associated properties. For these reasons, the following procedure is used to calculate void fraction.

First, the particle is divided into 48 elements to calculate the initial value of void fraction in a computational cell (Gui et al., 2008, Yang et al., 2014), which is expressed as:

$$\varepsilon_f = 1 - \frac{\sum_{i=1}^{n} V_{i,part}}{V_{cell}} \tag{11}$$

where $V_{i,part}$ and V_{cell} are, respectively, the total volume of elements of particle i and the cell volume, and n is the number of particles overlapped with the cell considered. Then, the diffusion-based averaging method (Sun and Xiao, 2015), which is equivalent to the statistical Gaussian kernel-based coarse graining method, is used to determine the porosity in the computational domain initiated with the values given by Eq. (11). To implement this method, a transient, homogeneous diffusion equation is solved over a period of pseudo-time τ_p. This volume-fraction calculation method is in principle applicable to different mesh sizes and easy for parallelism.

In dense gas-solid flows, the fluid-particle force mainly consists of drag force and pressure gradient force (Felice, 1994, Deen et al., 2007, Loth and Dorgan, 2009, Zhou et al., 2010,

Kuang et al., 2012, Wang et al., 2017b). From gas-solid flows to solid-liquid flows, the ratio of fluid to particle densities is increased by nearly 1000 times. The lift force, which has a close correlation with this ratio, is therefore expected to have a nontrivial effect on the simulation results (Zhu et al., 2007). However, to the best of our knowledge, the influence of lift force has not been assessed previously in the CFD-DEM simulations of solid-liquid flows through vertical pipes. Thus, the importance of lift force will be evaluated in the next section. In this work, the pressure gradient force is calculated by $\mathbf{f}_{p,i} = -V_i \nabla p_f$, where V_i is the particle volume. The drag force ($\mathbf{f}_{d,i}$) is calculated based on the Di Felice drag correlation (Felice, 1994):

$$\mathbf{f}_{d,i} = \frac{1}{2} C_D \frac{\pi d_i^2}{4} \rho_f \left|\mathbf{u}_f - \mathbf{v}_i\right| \left(\mathbf{u}_f - \mathbf{v}_i\right) \left(\varepsilon_f^{-\alpha}\right) \tag{12}$$

$$\alpha = 3.7 - 0.65 \exp\left[1 - \frac{\left(1.5 - \log_{10}\left(\mathrm{Re}_{p,i}\right)\right)^2}{2}\right] \tag{13}$$

where C_D is the drag coefficient for an isolated single particle. $\mathrm{Re}_{p,i}$ represents the particle Reynolds number, which is written as:

$$\mathrm{Re}_{p,i} = \frac{\rho_f \varepsilon_f d_i}{\eta} \left|\mathbf{u}_f - \mathbf{v}_i\right| \tag{14}$$

The lift force ($\mathbf{f}_{lift,i}$) is caused by the fluid pressure difference on opposite sides of a particle attributed to the fluid velocity difference resulting from the velocity shear gradient. The vorticity of fluid phase and particle rotation are two primary mechanisms for the lift force. According to the work of Loth et al.(Loth and Dorgan, 2009), the lift force is expressed as follows:

$$\mathbf{f}_{lift,i} = 0.125 \pi d_i^2 \rho_f C_L \left|\mathbf{u}_f - \mathbf{v}_i\right| \left[\left(\mathbf{u}_f - \mathbf{v}_i\right) \times \frac{\boldsymbol{\omega}_i}{\left|\boldsymbol{\omega}_i\right|}\right] \tag{15}$$

$$C_L = J^* \frac{12.92}{\pi} \sqrt{\frac{\omega^*}{\mathrm{Re}_p}} + \Omega_p^* C_{L,\Omega}^* \tag{16}$$

where ω^* and Ω_p^* are respectively related to the fluid vorticity and the particle angular velocity.

The added mass force $\mathbf{f}_{add,i,}$, also called as "virtual mass force", accounts for the "virtual mass" effect. This force is caused by the acceleration of fluid phase surrounding a particle *i*, and expressed as:

$$\mathbf{f}_{add,i} = \frac{1}{2}\rho_f V_i \frac{d}{dt}\left(\mathbf{u}_f - \mathbf{v}_i\right) \tag{17}$$

The viscous force is calculated by

$$\mathbf{f}_{\tau,i} = -\varepsilon_s \nabla \cdot \boldsymbol{\tau} \tag{18}$$

3.2.4 Coupling schemes between particle and fluid flows

The modelling of particle flow by DEM is at an individual particle scale, whereas the liquid flow by CFD is at a computational cell scale, which is supposed to be much larger than a particle. Their coupling can be numerically achieved as follows according to the work of Xu and Yu, (1997), and the coupling diagram is shown in Figure3-1. At each time step, the DEM provides information, such as the positions and velocities of individual particles, for the evaluation of porosity and volumetric particle-fluid force in each computational cell. The CFD model then uses this information to determine the liquid flow field, which is used to obtain the particle-fluid forces acting on individual particles. Incorporation of the resulting forces into the DEM enables the determination of the motion of individual particles for the next time step. The

particle-fluid forces acting on individual particles will react on the fluid phase so that Newton's third law of motion is satisfied.

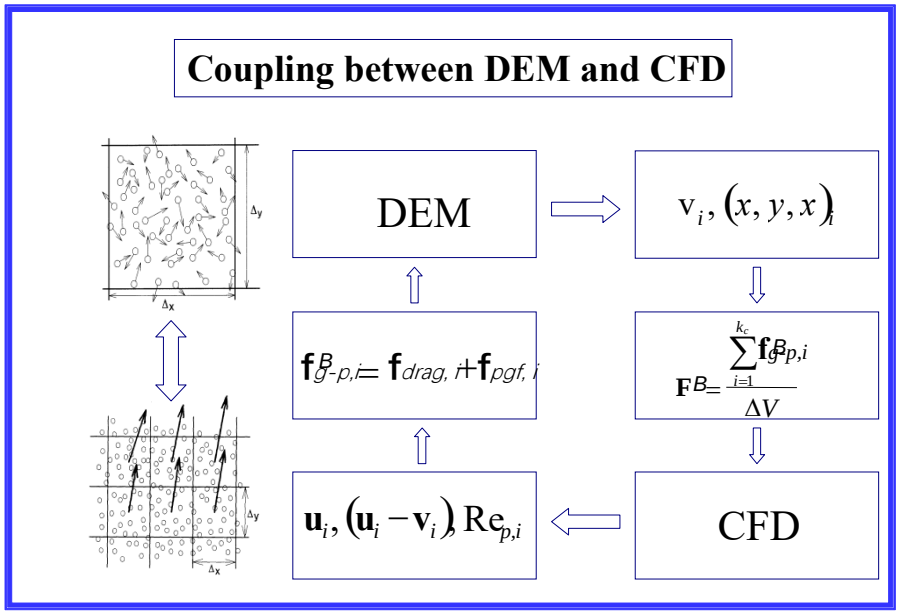

Figure 3-1 Schematic coupling between CFD and DEM (Xu and Yu, 1997)

3.3 Computational details

3.3.1 Numerical scheme

The governing equations are discretised by a finite volume method. A second-order Crank-Nicolson scheme is used for time integration (Moukalled et al., 2016). A second-order central differencing scheme is utilized for the discretization of convection and diffusion terms (Wen et al., 2015). The velocity-pressure coupling is handled with a Pressure-Implicit Split-Operators (PISO) algorithm (Issa, 1985). The equations for a particle are explicitly integrated, and then the position and velocity are updated for the next coupling procedure.

With respect to the CFD part, Coutant-Friedrich-Lewy (CFL) number is utilized to monitor the calculation procedure (J.H. Ferziger et al., 2002), which is written as:

$$CFL = \Delta t_{CFD} \max\left(\frac{|\mathbf{u}_f|}{\Delta x}\right) < 1 \tag{19}$$

where Δt_{CFD} is the time-step of liquid phase, Δx represents for the characteristic grid size. And the value of CFL should be smaller than 1.

In a CFD-DEM simulation, it is very important to set the appropriate time steps for both solid and liquid phases. The solid time step is limited by Rayleigh time Δt_R, which is calculated by:

$$\Delta t_R = \frac{\pi R_i}{0.1631\nu_i + 0.8766}\sqrt{\frac{2\rho_p(1+\nu_i)}{Y_i}} \tag{20}$$

where Y_i, ρ_p, R_i, υ_i are, respectively, the Young's modulus, density, radius and Poisson ratio of particle *i*. According to the particle properties used in the current work, the Δt_R (Raji and Favier, 2004, Li et al., 2005, Yang et al., 2014) is calculated as 2.0×10^{-4} s. The solid time step Δt_p is often smaller than the Rayleigh time Δt_R (Li et al., 2017). Thus, Δt_p is set to 1.0×10^{-5} s in the present study. According to the work of Tsuji et al. (Tsuji et al., 1993), the fluid time step could be 10 ~100 times of the solid time step. To reduce the simulation time, the time-step for the liquid phase is assigned as 1.0×10^{-4} s.

3.3.2 Simulation and boundary conditions

A 2.2 m pipe with a diameter of 0.0306 m, as used in the experimental work of Alajbegovi. et al., (1994), is simulated (see Figure 3-2(a)). Followed the experiment (Alajbegovi. et al., 1994), the results at the distance of 2.1 m away from inlet are considered for analysing radial profiles of flow properties, while the pressure drop and particle pattern are

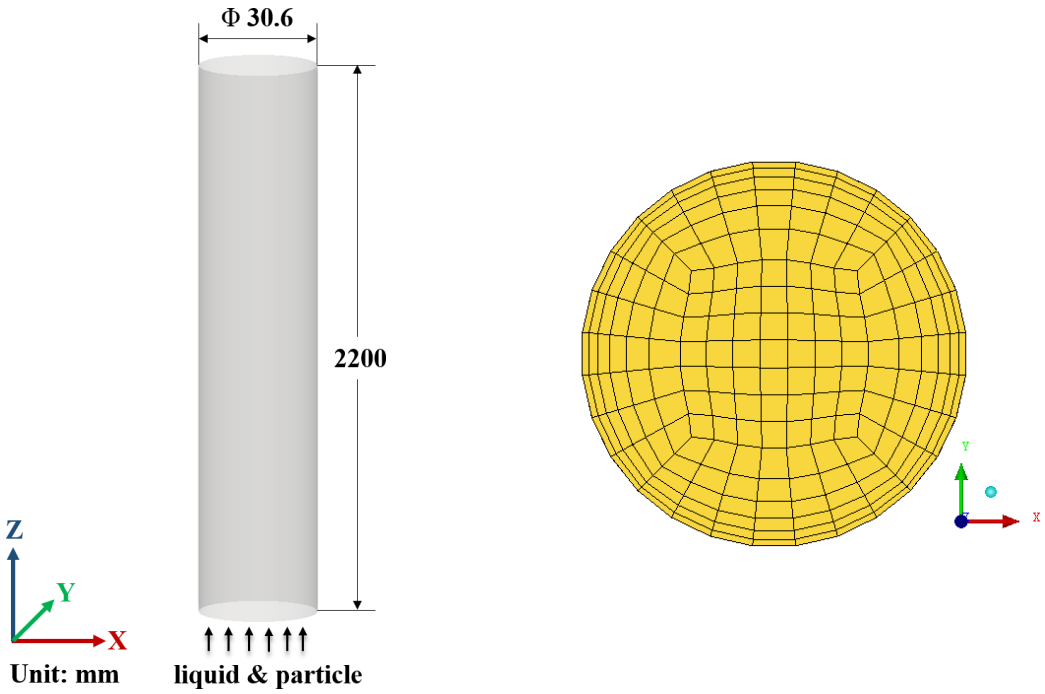

(a) (b)

Figure 3-2 Schematic representation of the vertical pipe simulated: (a) geometry configuration; (b) computational grids on a cross-section

taken from the section between z=1.5 m and z=2.0 m. This pipe is meshed with 30,000 hexahedra in the form of O-grid scheme using a commercial software package ANSYS ICEM^{TM}. With this mesh topology, the grids can be refined near the wall region for better predicting the liquid flow there, as shown in Figure 3-2(b). In each simulation, a uniform velocity liquid profile is specified at the inlet, while particles are injected from the cross-section at the same velocity as that of fluid. Note that fully developed flow is focused in this work, and thus these inlet boundary conditions do not affect results analysis. The number of particles injected is determined according to given feed solid concentration (by volume) and liquid flow rate. In each case, the injected particle number per second varies from 1500 to 71684, depending on flow conditions. A no-slip boundary condition is taken at the wall. The normal gradients of all variables at the outlet are set to zero for fluid phase assuming that the flow is fully developed there. Differently, particles are removed directly from the simulation when

flowing out of the pipe from the outlet. Table 3-2 lists the properties of liquid and particles considered.

Table 3-2 Simulation parameters used in the current simulations

Liquid property	
liquid density, (kg/m^3)	998
liquid flow rate, (kg/s)	1.612*
liquid temperature, (ºC)	25
liquid viscosity (kg/(m·s))	1.0×10^{-3}
Solid property	
Material	ceramic
Young's modular, (pa)	1×10^{7}
Poisson ratio	0.3
particle density, (kg/m^3)	2450
particle diameter, (mm)	2.32*
particle flow rate, (kg/s)	0.108*
particle-wall sliding friction coefficient	0.2
particle-particle sliding friction coefficient	0.1
Coefficient of restitution	0.85

Note: * represents the value for base case.

Table 3-3 summarizes the cases simulated, which are configured to specifically investigate the effects of particle diameter (d_p), conveying speed or velocity of liquid-solid mixture (U_f), and feed solid concentration (C_v). Correspondingly, the values of d_p are taken as 2.32 mm, 3.00 mm, and 3.82 mm following the physical experiments reported (Alajbegovi. et al., 1994). The

values of U_f are 3.7997 m/s, 4.3138 m/s, and 6.3699 m/s and those of C_v are 0.0273, 0.05, and 0.1. For the base case, the particle diameter is 2.32 mm, the conveying speed is 3.7997 m/s, and the feed solid concentration is 0.0273.

Table 3-3 Operating conditions used in the current simulations

Operating parameters	No.	Particle diameter, d_p (mm)	Conveying speed, U_f (m/s)	Feed solid concentration, C_v (by volume)
Effect of C_v	case 1	2.32	3.7997	0.0273
	case 2	2.32	3.7997	0.05
	case 3	2.32	3.7997	0.1
Effect of U_f	case 4	2.32	3.7997	0.0273
	case 5	2.32	4.3138	0.0273
	case 6	2.32	6.3699	0.0273
Effect of d_p	case 7	2.32	3.7997	0.0273
	case 8	3.00	3.7997	0.0273
	case 9	3.82	3.7997	0.0273

3.4 Results and discussion

3.4.1 Model validation

To examine the reasonability of the CFD-DEM method for simulating hydraulic conveying, the experimental setup of Alajbegovi. et al., (1994) is used. In the experiment, the pipe diameter is 30.6 mm, and the particle diameter is 2.32 mm.

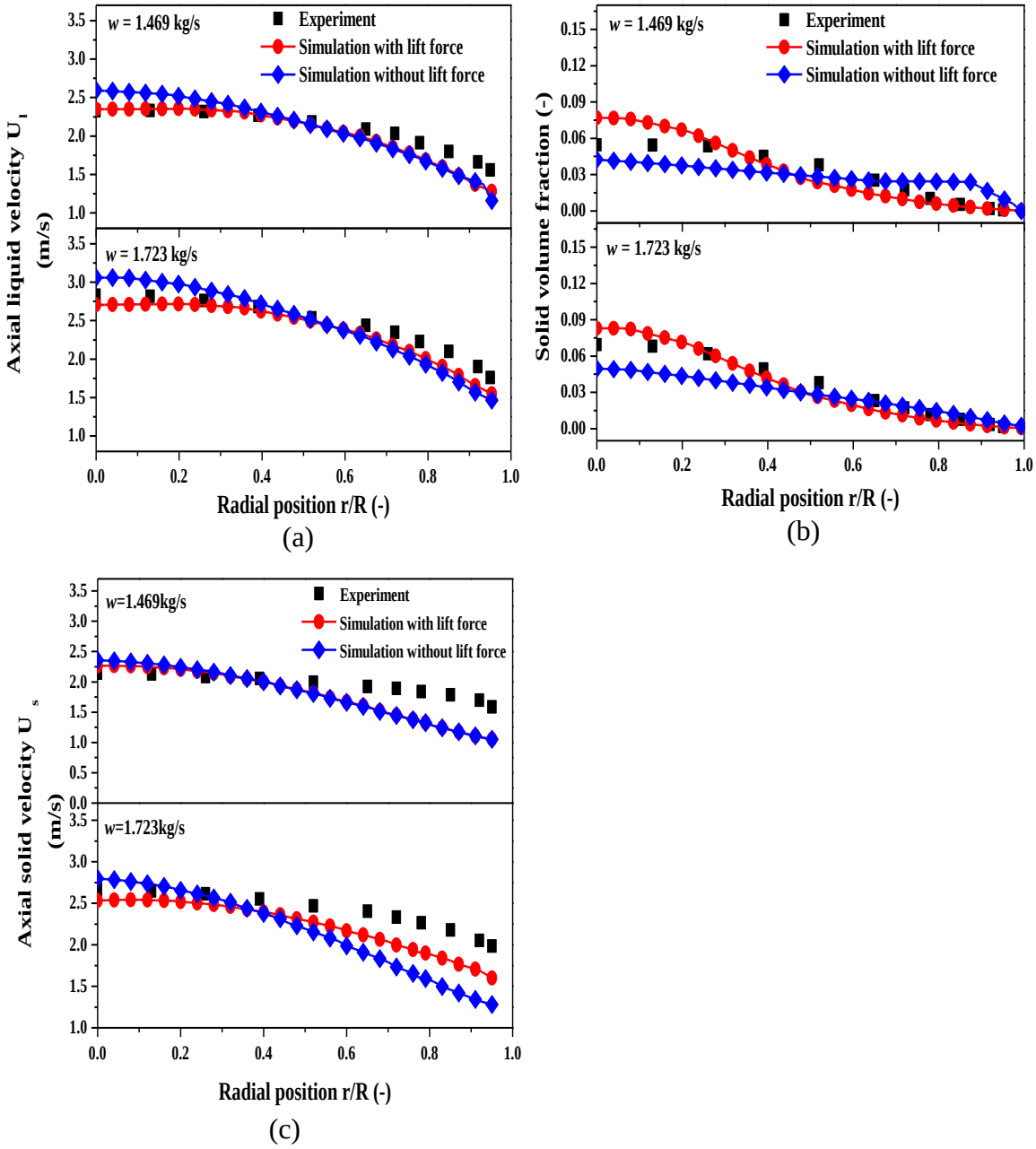

Figure 3-3 Predicted and measured (Alajbegovi. et al., 1994) (a) solid volume fraction (ε_s); (b) axial liquid velocity (U_l, m/s) at different total mass flow rates (w, kg/s); (c) axial solid velocity (U_s, m/s) at different total mass flow rates (w, kg/s)

Figure 3-3 compares the predicted solid volume fraction as well as axial liquid and solid velocities with the measurements at two total mass flow rates. Overall, the current model can well predict the trends measured. When simulations are conducted with lift force, prediction errors range from 0.8% to 17.9% for liquid velocity, from 2.0% to 41.0% solid concentration,

and from 5.0% to 35.9% for solid velocity. It is observed that particles concentrate in the central region with the largest axial liquid and solid velocities. These two velocities both decline in the radial direction toward the wall. In general, when the lift force is considered, numerical results are in better agreement with the experimental data compared with the predictions by the model without lift force. Notably, when the lift force is omitted, the tendency of the radial profile of solid volume fraction cannot be successfully reproduced. Specifically, at the total mass flow rate of 1.469 kg/s, a critical radical location (r/R = 0.9) is observed, from which the solid volume fraction experiences a drastic change for the simulations without lift force, which, however, is not observed experimentally (Figure 3(a)). This result highlights the importance of lift force in affecting flow regimes in vertical hydraulic conveying. The reasonable agreement between experimental and numerical results suggests that the present CFD-DEM method can be used to satisfactorily predict key flow features in vertical hydraulic conveying of solid particles.

In order to better understand the role of lift force, Figure 3-4 compares radial distributions of particle-fluid forces for a case used for model validation. Here, forces are normalized by particle gravity for comparison. It is observed that in the axial direction, all the forces are expectedly upward with positive values. The lift force is largely negligible, while the fluid drag force is much larger than others and thus plays a dominant role in the axial direction. On the contrast, the dominant force changes to the lift force in the radial direction. Its magnitude is the largest near the wall region, although it is overall much smaller than that of axial fluid drag force. As expected, the value of the lift force is mainly negative. Hereby, it is the lift force that drives particles away the wall.

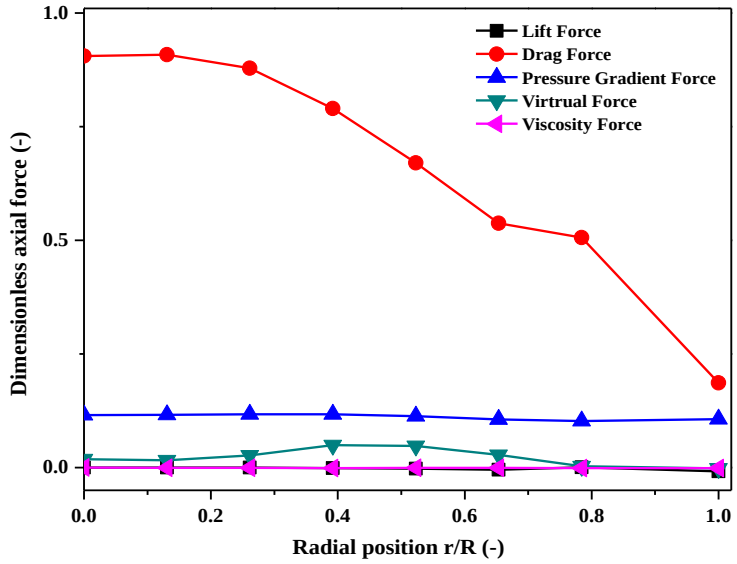

(a)

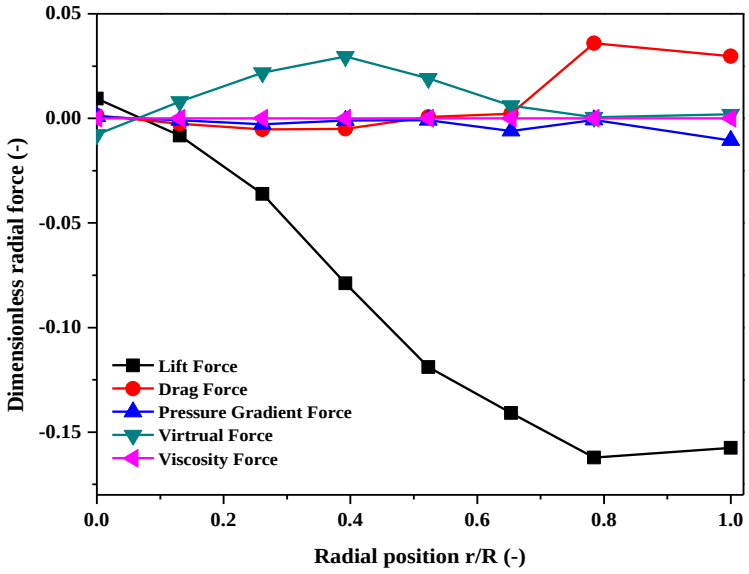

(b)

Figure 3-4 Distributions of particle-fluid forces in the radial direction for d_p = 2.32 mm, U_f = 2.2576 m/s and C_v=0.0273: (a) axial component and (b) radial component

3.4.2 Independence studies of grid resolution and calculation time

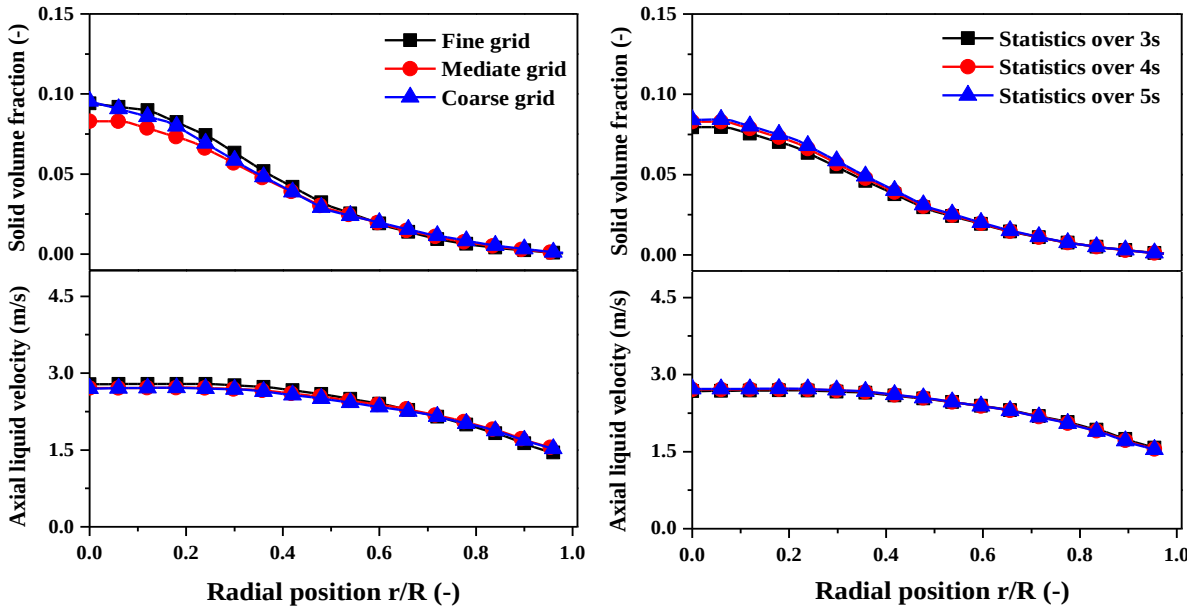

(a) (b)

Figure 3-5 Comparison of averaged solid volume fraction and axial liquid velocity in the radial direction at: (a) different grid resolutions; (b) different statistical times

Before our simulations, the independence of numerical results on grid resolution and calculation time has been examined. For this purpose, three grid solutions of the pipe are considered, corresponding to the cell number of 38,720 (fine grid), 29,645 (medium grid) and 21,780 (coarse grid), respectively. Figure 3-5(a) compares the radial profiles of time-averaged solid volume fraction and axial liquid velocity at different grid resolutions. It is of interest to note that the numerical results do not show a significant difference with respect to grid solution. Nonetheless, the medium grid scheme is taken in all our simulations considering the complicated flow behaviours involved. On the other hand, it is established particle-fluid flows somewhat fluctuate in time and space due to the discrete nature of particles and their intensive interactions with fluid and wall. Therefore, numerical results are often averaged over time and space to obtain their macroscopic trends. In this work, this averaging method is taken, and the effect of statistical time on averaged results is assessed. Figure 3-5(b) shows the profiles of

time-averaged solid volume fraction and axial liquid velocity over different statistical periods. Note that the physical time for each simulation case is 7 s, which is long enough for the flow to be established under all the conditions considered. To avoid the influence of startup process, the data after 3 s are used. Figure 4(b) shows that numerical results from different statistical periods are nearly the same. Therefore, in the following analysis, numerical results within the last 4 s of the total calculation time are representative.

3.4.3 Effect of feed solid concentration Cv

3.4.3.1 Effect of Cv on instantaneous flow regimes

Figure 3-6 shows with the increasing feed solid concentration, more particles prefer to accumulate within the pipe. Meanwhile, particles are more dispersed over the cross-section because the particle-particle contact frequencies increase remarkably with the increase of particle accumulation. Correspondingly, the solid-liquid flow is transmitted from a liquid-dominated pattern to a contact-dominated pattern. It is of interest to observe that particles always tend to concentrate in the middle of the pipe with a vigorous axial velocity, and the solid volume fraction augments with the increasing feed solid concentration. This is essentially due to that the flow system tends to minimize the energy consumption by migrating particle-wall interactions. Figure 3-6 also shows that the particle axial velocities decrease with the increase of feed solid concentration, because the kinematic energy of each particle is dissipated via the inter-particle interactions.

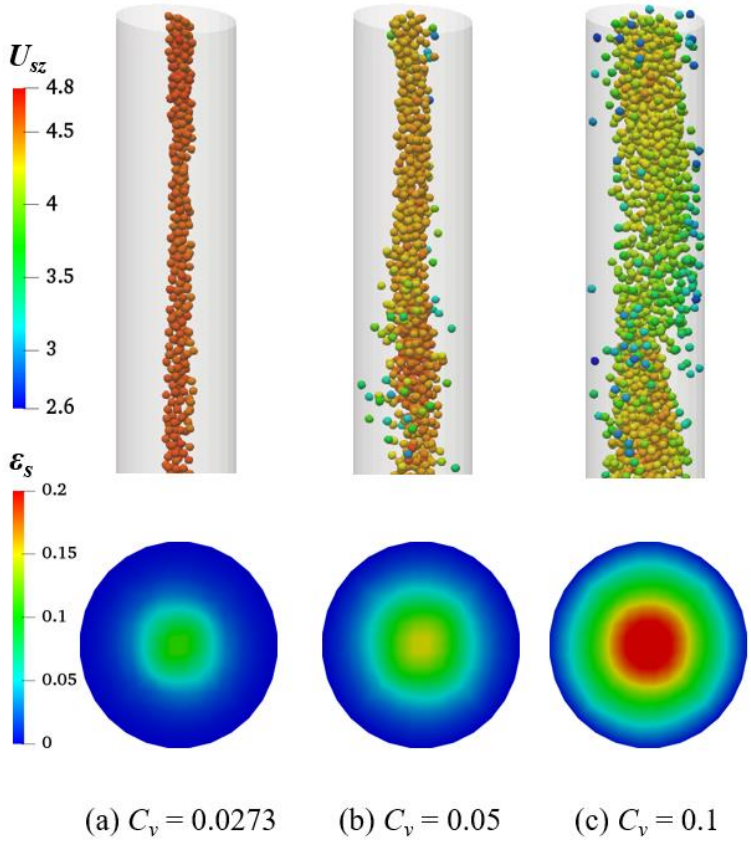

Figure 3-6 Contour plots of instantaneous flow regimes and time-averaged solid volume fraction at different feed solid concentrations for d_p = 2.32 mm and U_f = 3.7997 m/s: (a) C_v = 0.0273; (b) C_v = 0.05; (c) C_v = 0.1

3.4.3.2 Effect of Cv on time-averaged variables

Figure 3-7 shows the influence of feed solid concentration on the radial profiles of time-averaged solid volume fraction and axial liquid and solid velocities. Figure 3-7(a) reveals that under all feed solid concentrations considered, the value of solid volume fraction appears a peak in the middle of the pipe and then decreases gradually in the radial direction toward the wall, indicating that particles tend to be transported around the central region of the pipe. As the feed solid concentration increases, the solid volume fraction generally becomes larger, which is more evident in the central region. Because particles are more dispersed at a larger feed solid concentration, they tend to appear near the wall, leading to an increased solid volume

fraction there. These trends are in line with the experimental observations (Bartosik and Shook, 1995).

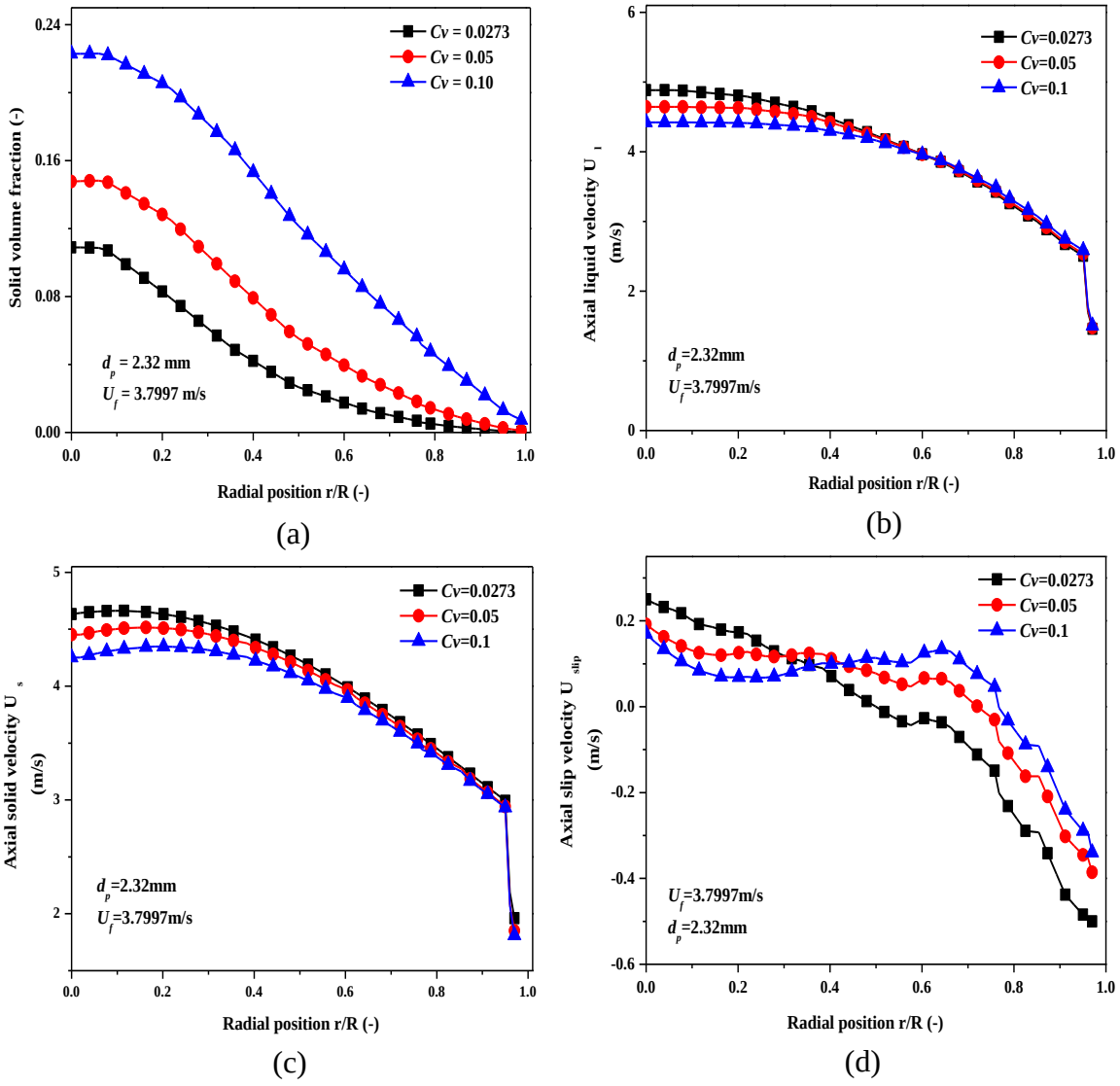

Figure 3-7 Effects of feed solid concentration on time-averaged variables for d_p = 2.32 mm, U_f = 3.7997 m/s: (a) solid volume fraction; (b) axial liquid velocity; (c) axial solid velocity; (d) axial slip velocity

Figure 3-7(b) and (c) shows that with the increasing feed solid concentration for a given mixture velocity, the axial solid and liquid velocities decrease in the central region, but this change becomes negligible near the wall. Expectedly, the velocity profiled of two phases are

similar due to the strong entrainment of liquid on particles. Here, the no-slip boundary condition accounts for the zero magnitude of liquid velocity at the wall.

Figure 3-7(d) shows how feed solid concentration affects slip velocity. Overall, particles are observed to move faster than fluid near the wall but slower in the central region. This result can be explained as follows. A non-slip velocity boundary condition is applied to the fluid phase at the wall leading to zero liquid velocity there. Conversely, particles can slide on the wall surface. These different boundary conditions of fluid and solid phases account for faster particles than fluid near the wall. As the radial distance from the wall to the center increases, the wall effect on fluid becomes less significant, the fluid flow driving particles upward becomes faster than particles. Also, it is shown that at a higher feed solid concentration, the magnitude of slip velocity between liquid and solid phases decreases. This is attributed to the more uniform solid distribution on pipe cross-section, which intensifies the momentum exchange between solid and fluid flows and thus reduces their difference.

3.4.3.3 Effect of Cv on pressure drop

Pressure drop is related to the energy consumption of hydraulic conveying, representing one of major industrial concerns in practical applications. It is contributed by particle-wall and fluid-wall friction as well as particle gravity for the fully developed flow through a vertical pipe [66]. Figure 3-8 plots pressure drop as a function of feed solid concentration. Here, the dimensionless pressure drop defined as $\mathrm{I} = \frac{\Delta p}{\Delta L} \cdot \frac{1}{\gamma_w}$ is considered as widely used in the application of hydraulic conveying, where γ_w is the specific weight of water (Ravelet et al., 2013). For given particle diameter and conveying speed, increasing feed solid concentration increases the pressure drop, which is consistent with the experimental observations and numerical predictions [75]. The larger the feed solid concentration is, more particles are transported in the pipe. This increases fluid drag forces and causes a more vigorous momentum transfer from the liquid phase to the

particle phase to overcome particle gravity. Consequently, more conveying energy is needed. However, a higher mass conveying is not the only reason for the increase of the pressure drop. In fact, when the feed solid concentration becomes larger, the friction losses resulting from particle-wall interaction increases, which can also contribute to the increase of pressure drop.

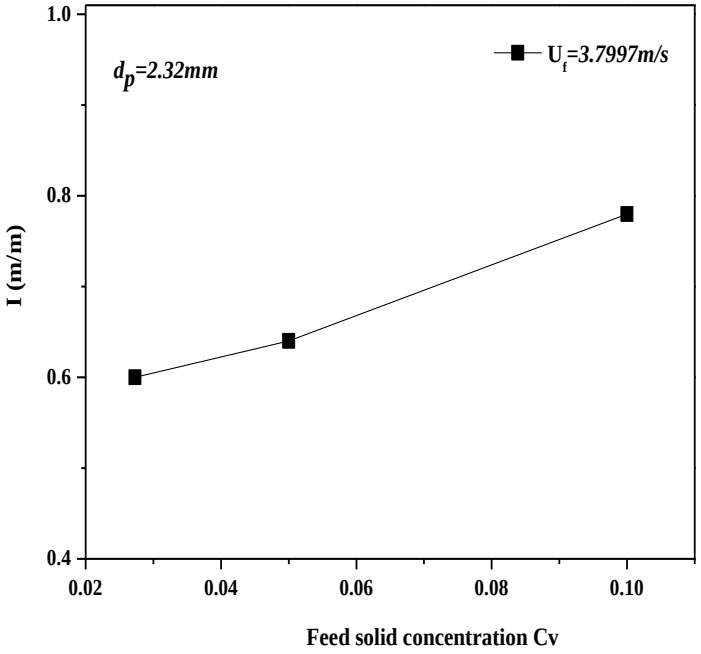

Figure 3-8 Effect of feed solid concentration on dimensionless pressure drop (I, m/m) at d_p = 2.32 mm and U_f = 3.7997 m/s

3.4.4 Effect of conveying speed U_f

Conveying speed U_f is another important parameter in hydraulic conveying system associated with system energy consumption, pump efficiency, and so on. In this section, the parametric study is conducted for conveying speed U_f, considering the values of 3.7997 m/s, 4.3138 m/s, and 6.3699 m/s as of, respectively, case 4, case 5, and case 6 in Table 3.

3.4.4.1 Effect of U_f on instantaneous flow regimes

Figure 3-9 presents the effect of conveying or conveying fluid speed on instantaneous flow regimes. As conveying speed increases, the axial solid velocity increases and particles are more

dispersed over the pipe cross-section. At a lower conveying fluid speed, particles tend to concentrate in the middle of the pipe, leading to an increased solid volume fraction there.

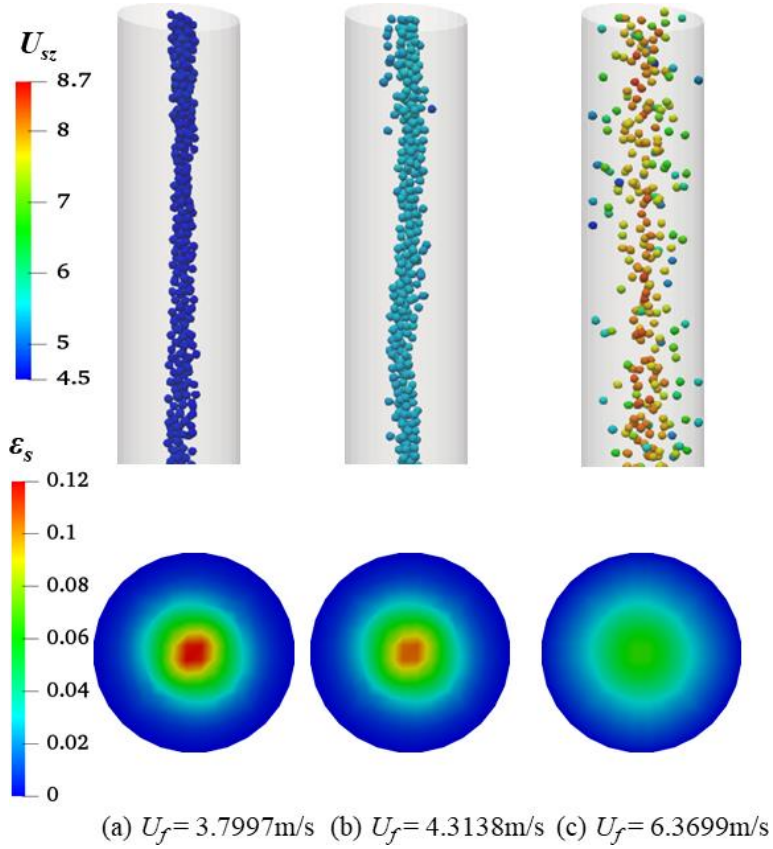

Figure 3-9 Contour plots of instantaneous flow regimes and average solid volume fraction at different conveying speeds for d_p = 2.32 mm and C_v = 0.0273: (a) U_f = 3.7997m/s; (b) U_f = 4.3138m/s; (c) U_f = 6.3669m/s

3.4.4.2 Effect of U_f on time-averaged variables

The effect of conveying speed on the time-averaged solid volume fraction is shown in Figure 3-10. When the conveying speed increases for given particle diameter and feed solid concentration, the solid volume fraction at the middle of pipe declines due to the intensified particle dispersion. Also, it is observed that the value of solid volume fraction has a peak in the middle of the pipe and then gradually decrease in the radial direction toward the wall. As the conveying speed increases, the solid volume fraction near the wall increases slightly.

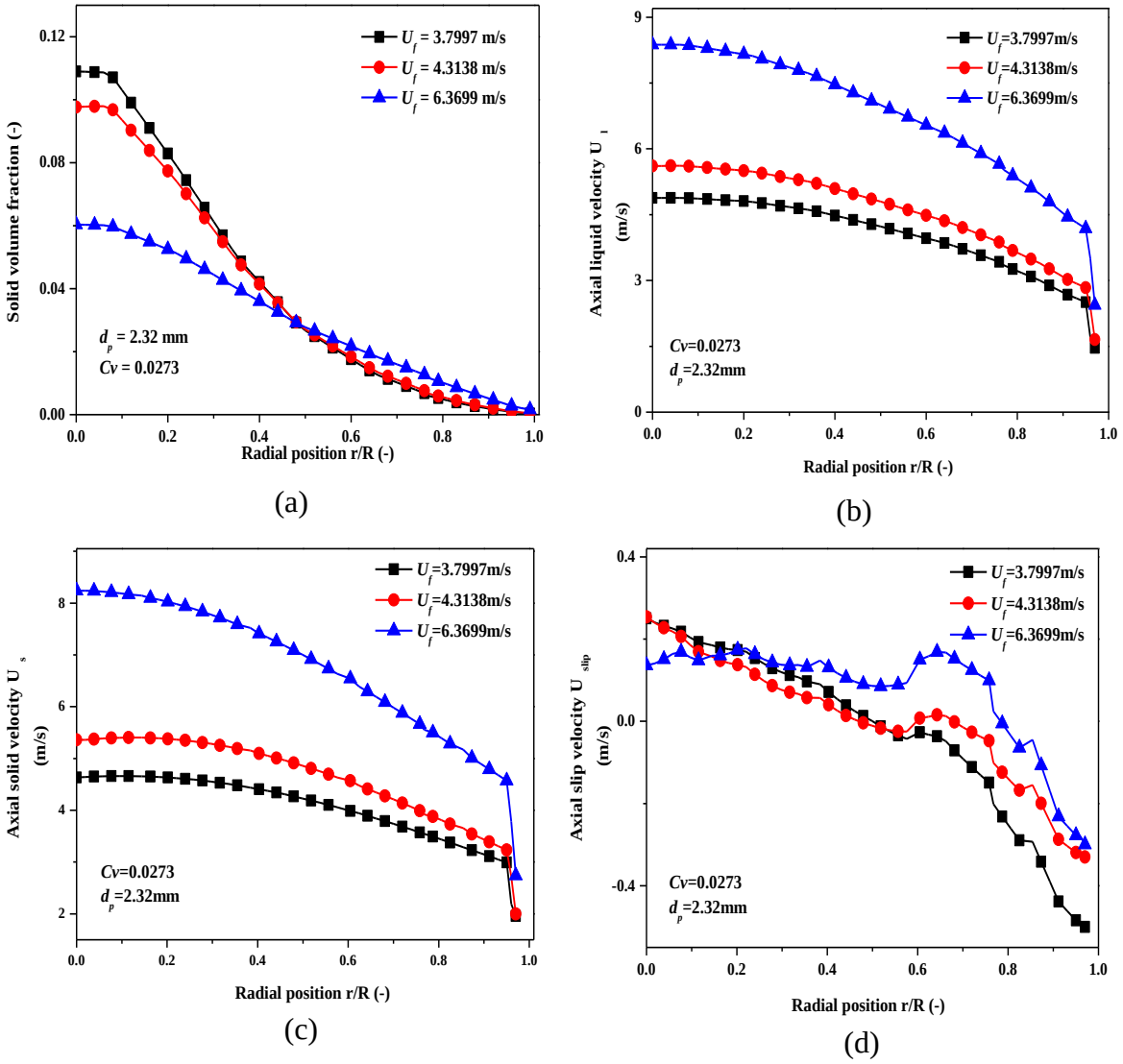

Figure 3-10 Effects of conveying speed on time-averaged variables at d_p = 2.32 mm and C_v = 0.0273: (a) solid volume fraction; (b) axial liquid velocity; (c) axial solid velocity; (d) axial slip velocity

Figure 3-10(b) and (c) shows the influences of conveying speed on the axial liquid and velocities. With the increasing conveying speed, the axial liquid or solid velocity at the middle of the pipe is also increased, which is consistent with the experimental observation (Bartosik and Shook, 1995). Figure 9(d) shows that increasing conveying speed reduces the magnitude of slip velocity, corresponding to more dispersed particles on pipe cross-section.

3.4.4.3 Effect of U_f on pressure drop

The effect of conveying speed on the pressure drop is shown in Figure 3-11. For given feed solid concentration and particle diameter, the increase of conveying speed increases the pressure drop. This trend well agrees with the experimental observations [75]. One may note that a higher conveying speed gives rise to more vigorous and frequent inter-particle interactions. As a result, more energy is dissipated in the current flow system, causing a larger pressure drop.

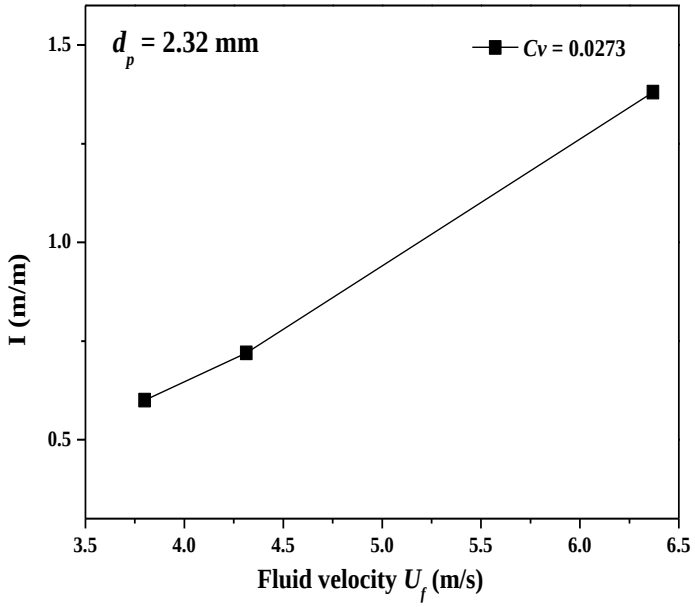

Figure 3-11 Effect of conveying speed on dimensionless pressure drop (I, m/m) at d_p = 2.32 mm and C_v = 0.0273

3.4.5 Effect of particle diameter d_p

Particles of different sizes are very common in industries. An understanding of the effect of particle diameter d_p can be useful to design and operate hydraulic conveying. Therefore, particle diameters of 2.32 mm, 3.00 mm, and 3.82 mm are simulated, respectively, through three cases (cases 7, 8, and 9) listed in Table 3.

3.4.5.1 Effect of d_p on instantaneous flow regimes

Figure 3-12 shows the representative flow regimes of solid-liquid flows in the vertical pipe at different particle diameters. With the increase of particle diameter, the total number of particles decreases. Nonetheless, particles always tend to concentrate in the middle of the pipe, and on average, the axial solid velocities are largely similar for the three diameters considered. It is noted that particles are slightly more dispersed in the case with a larger particle diameter. Accordingly, the solid volume fraction decreases with the increase of particle diameter.

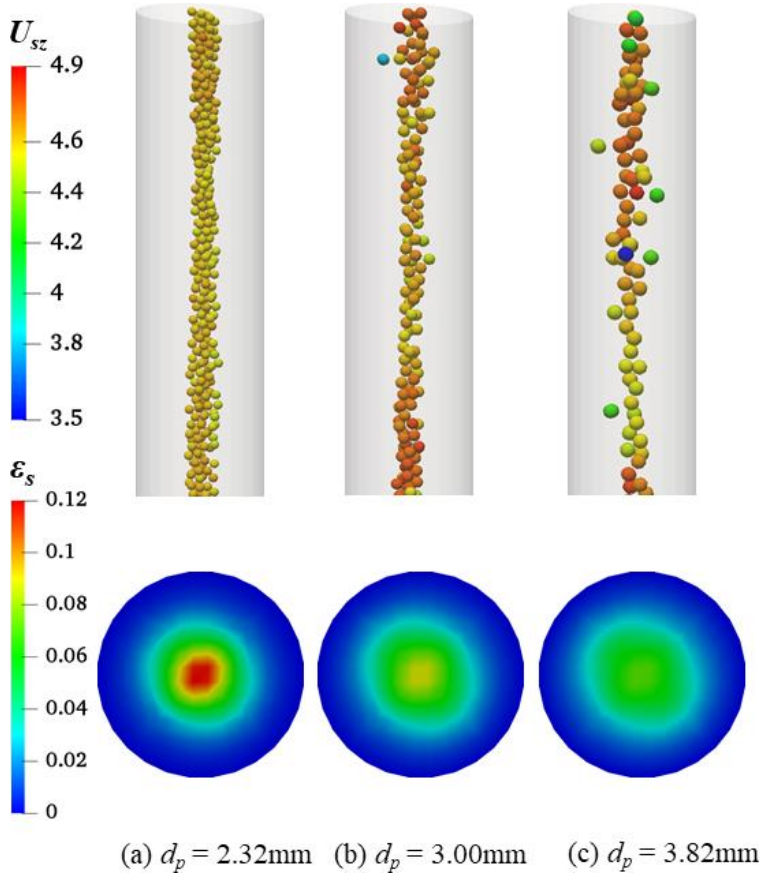

Figure 3-12 Contour plots of instantaneous flow regimes and solid volume fraction at different particle diameters for U_f = 3.7997 m/s and C_v = 0.0273: (a) d_p = 2.32 mm; (b) d_p = 3.0 mm; (c) d_p = 3.82 mm

3.4.5.2 Effect of d_p on time-averaged variables

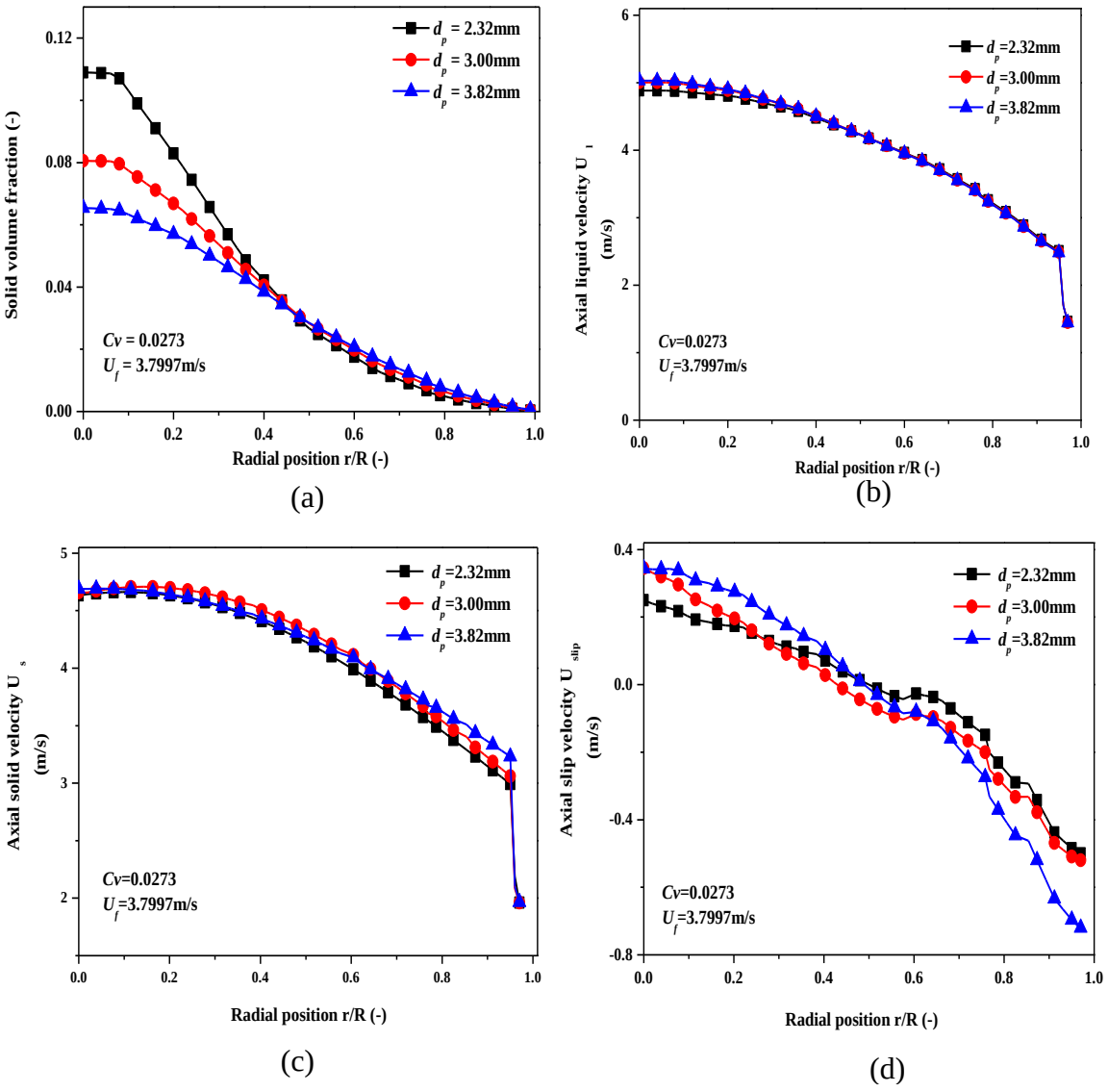

Figure 3-13 Effect of particle diameter on time-averaged variables at U_f = 3.7997 m/s and C_v = 0.0273: (a) solid volume fraction; (b) axial liquid velocity; (c) axial solid velocity; (d) axial slip velocity

Figure 3-13(a) shows the effect of particle diameter on time-averaged solid volume fraction. When the particle diameter increases while the conveying speed and feed solid concentration remain the same, the total number of particles decreases and the solid volume fraction is reduced at the middle of the pipe. Because of the hydrodynamic lift effect, particles are difficult

to move along the pipe wall, which accounts for the nearly zero solid volume fraction near the pipe wall.

As seen from Figure 3-13(b), all the radial profiles of axial liquid velocity have a peak in the middle of the pipe. Particle diameter has a negligible influence on the liquid velocity. This may be because the current flow system is a fluid-dominated system and thus the effect of solid phase on liquid phase is trivial. Figure 3-13(c) shows that particle diameter has a small influence on the axial solid velocity in the central region, and this influence becomes more obvious in the wall region. Figure 3-13(d) shows that the decrease of particle size reduces the magnitude of slip velocity because the entrainment effect of fluid on smaller particles becomes larger.

3.4.5.3 Effect of d_p on pressure drop

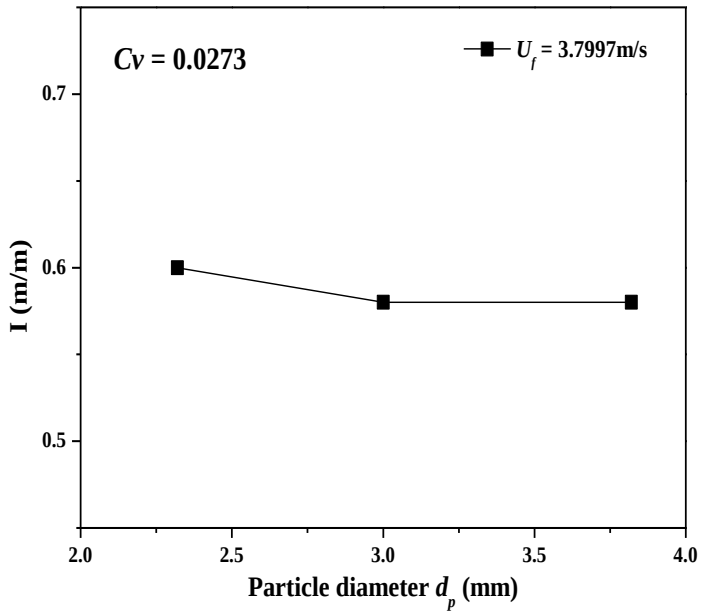

Figure 3-14 Effect of particle diameter on dimensionless pressure drop (I, m/m) at U_f = 3.7997 m/s and C_v = 0.0273

The effect of particle diameter on pressure drop is shown in Figure 3-14. With the increasing particle diameter, the pressure drop only changes slightly, which also means that particle

diameter has a small influence on the pressure drop, which has also been reported experimentally (Matousek, 2002).

3.5 Conclusions

In this work, the effects of feed solid concentration, conveying speed and particle diameter on vertical hydraulic pipe are evaluated via CFD-DEM simulations. The major conclusions are as follows:

i. Via the model validation, it demonstrates that the coupled CFD-DEM method is reasonable to use and the lift force can improve the numerical accuracy in the simulation of solid-liquid flow through a vertical pipe.

ii. Increasing feed solid concentration increases the time-averaged solid volume fraction while decreases the time-averaged axial liquid velocity and axial solid velocity in the central region of pipe. This influence becomes trivial near the wall region. Moreover, a larger feed solid concentration results in an increased pressure drop and particles become more dispersed over the cross-section of pipe.

iii. Increasing conveying speed decreases the time-averaged solid volume fraction but mainly in the central region of pipe. However, it overall increases the time-averaged axial liquid velocity and solid velocity in the radial direction. Moreover, as the conveying velocity increases, the pressure drop increases.

iv. Increasing particle diameter decreases the time-averaged solid volume fraction in the central region of pipe. The profiles of time-averaged axial liquid velocity nearly the same at different particle diameters. However, an increased axial solid velocity is observed near the wall for a larger particle diameter. In addition, particle diameter only has a minor effect on the pressure drop.

CHAPTER 4 MODELLING AND ANALYSIS OF FLOW REGIMES IN HYDRAULIC CONVEYING OF COARSE PARTICLES

4.1 Introduction

Hydraulic conveying is widely encountered in many industries, such as chemical engineering, food, mining, oil and petroleum industries due to its low operation and maintenance cost, friendliness to the environment, and unlimited transporting distance. It can handle a wide variety of particles that can be either coarse or fine. A key feature of this transportation is that different flow regimes occur along conveying pipelines. Generally, flow regimes are affected by a wide variety of variables related to material properties, operational conditions and pipe geometries. For example, vertical hydraulic conveying often runs in the form of suspension flow. Because the flow direction is perpendicular to the gravitational direction, horizontal transportation may experience the flow regime transition from the flow with a stationary bed, through the moving-bed flow, to the heterogeneous suspension flow, finally to the pseudohomogeneous suspension flow, as the conveying speed increases for a given feed solid concentration (Doron and Barnea, 1996). The characteristics of different flow regimes are very different, subsequently affecting the hydraulic conveying performance with regards to energy consumption, wall abrasion, particle degradation, and operation stability (Albunaga, 2002).

In the past decades, extensive experimental efforts have been made to explore the flow features of hydraulic conveying (see, e.g., Refs. (Turian and Yuan, 1977, Wilson et al., 2002, Matoušek, 2005, Parsi et al., 2014, Rice et al., 2015, Silva et al., 2015b, Hashemi et al., 2016)). Based on experimental data, the pressure drop and other process parameters have been correlated with a range of variables such as feed solid concentration, conveying speed, pipe diameter, particle diameter and density for facilitating applications (Matoušek, 2005, Silva et al., 2015b). Such empirical and semi-empirical correlations are often valid under specific conditions, and significant prediction errors may be observed when the application ranges are beyond the experimental data (Durand and Condolios, 1952). As pointed out by Crowe, (1998), the

accuracy of a model/correlation in predicting the flow characteristic of a liquid-solid suspension flow is intrinsically related to the capability of incorporating flow regime mechanisms by the model. Some early works in this respect were based on mechanistic models. For example, based on the concept of force balance, a two-layer model was developed by Wilson, (1976). This model assumed that the flow consists of two layers: the top layer in which the suspended particles linger, and the bottom layer in which the particles have settled. Also, each layer is assumed to have uniform concentration and phase-averaged velocity. The two-layer model fails to accurately predict the suspension behavior for low flowrates where a stationary bed is present. To overcome this problem, Doron et al., (1987) proposed a three-layer model, in which a heterogeneous flow in the top layer, a moving bed in the middle layer and a stationary bed in the bottom layer are considered.

Mechanistic models have improved empirical correlations considerably by incorporating some characteristics of flow regimes. However, such models cannot reliably capture the flow behavior between layers, rely heavily on experiments in the determination of model parameters, and introduce significant assumptions to the distributions of velocity and solid concentration in each layer. These problems bring limitations to model applications, as pointed out by Silva et al., (2015b). Therefore, it is necessary to look more insights into hydraulic conveying and better understand its flow regimes. This can, in principle, be realized via numerical simulation and modeling.

Generally, the numerical models that have been applied to hydraulic conveying can be continuum- or discrete-based according to different treatments of particles. They are represented by the Two-Fluid Model (TFM), and the combined approach of Computational Fluid Dynamics (CFD) and Discrete Element Method (DEM), respectively. The TFM approach treats both liquid and particles as continuous phases. It has been widely used to study hydraulic conveying of fine particles (Ling et al., 2003, Doroodchi et al., 2005, Eskin, 2005, Giguère et

al., 2008, Kaushal et al., 2012, Capecelatro and Desjardins, 2013, Messa et al., 2014, Vittorio Messa and Malavasi, 2014, Messa and Malavasi, 2015, Silva et al., 2015a, Ofei and Ismail, 2016, Messa and Matoušek, 2020, Uzi et al., 2020). However, the effective use of a TFM model depends on constitutive relations for the description of solid stresses, which have not been generally established (Jop et al., 2006). To date, a successful application of a TFM model to the hydraulic conveying of coarse particles cannot be found in the literature. On the other hand, in the CFD-DEM approach, the liquid is modelled as a continuous phase, while particles are simulated as a discrete phase (Zhou et al., 2010). It directly tracks the trajectories of and the forces acting on individual particles and thus does not need the complex constitutive relations between the stress and strain of particles. Therefore, the CFD-DEM approach is theoretically more rational than the TFM approach, and it is valid over a wide range of flow conditions (Zhu et al., 2007, Zhu et al., 2008, Kuang et al., 2018, Kuang et al., 2019b, Sakai et al., 2020a).

In recent years, some CFD-DEM studies have been reported for hydraulic conveying. Lim, (2007) studied the voidage waves in hydraulic conveying through narrow vertical pipes by a two-dimensional CFD-DEM model, in which a laminar flow was considered. Papista et al., (2011) coupled DEM with Direct Numerical Simulation (DNS) that was based on the finite element method other than the finite volume method used in almost all other works, and by use of it studied the incipient sediment motion and the first stage of hydraulic conveying. Zhang et al., (2012), Chen et al., (2015) and Li et al., (2019) applied CFD-DEM models for studying the erosion of hydraulic bends, in which the liquid flow was solved by the Reynolds-averaged Navier–Stokes equations (RANS) via a standard k-ε turbulence model. Capecelatro and Desjardins, (2013) developed the combined approach of DEM and Large Eddy Simulation (LES). Via this model, they studied the turbulent liquid-solid flow behaviors in horizontal hydraulic conveying of fine particles (mean size=165 μm) at two conveying speeds that are below and above the critical deposition velocity of particles, respectively. Zhou et al., (2019)

applied a LES-DEM model to study vertical hydraulic conveying of coarse particles. Via the CFD (RANS)-DEM approach, Uzi and Levy, (2018) simulated the horizontal conveying of coarse particles (mean size=2.4 mm), in which the moving-bed flow was focused. This model was also extended to study the transport of soluble salt particles (Uzi et al., 2020). The moving-bed flow regime was also obtained by Ting et al., (2019), who observed the pipe blockage in their CFD (RANS)-DEM simulations of the horizontal transport of 10 mm particles at a low conveying speed. Via a similar method, Chen et al., (2020) studied the effect of particle sphericity on the horizontal hydraulic conveying but focusing on the moving-bed flow.

To date, the previous CFD-DEM studies have not fully captured the flow regimes and their transition that are typically observed in horizontal hydraulic conveying. Additionally, during the flow regime transition, the pressure drop per unit pipe length may decrease initially to a minimum and then increase as the conveying speed increases (Doron et al., 1987, Ravelet et al., 2013). However, this trend has not been reported in the above discussed CFD-DEM studies. It has been obtained by Ren et al., (2017) in the CFD (RANS)-DEM study of the hydraulic conveying of fine (size=120.2 μm) particles but in narrow rectangular channels. Under their specific conditions, the wall effect becomes very significant, leading to the formation of dense clusters that are similar to the voidage wave in a vertical pipe (Lim, 2007). As such, at present, it is not clear if a CFD-DEM model can predict typical flow regimes and their transition and associated pressure characteristics in a horizontal pipe. Also, a better understanding of these phenomena is needed, so as to design and control hydraulic transport more reliably and efficiently.

In this chapter, the horizontal hydraulic conveying of coarse particles is studied by a recently reported CFD-DEM model (Zhou et al., 2019). The validity of the model is first verified. On this basis, it is used to predict typical flow regimes and the pressure characteristics in a horizontal pipe. Then, the simulation results are analyzed in detail in terms of particle patterns

as well as flow and force structures. A new phase diagram is also established using the forces that act on particles for identifying different flow regimes and their transition. Finally, based on the simulation data, correlations are formulated for predicting the pressure drop of the horizontal hydraulic conveying considered.

4.2 Simulation method

The current CFD-DEM model is the same as the one described in section 3.2 in Chapter 3. For more details please refer to section 3.2 in Chapter 3. The model is also outlined here for brevity. In this model, the motions of discrete particles are individually described using Newton's second law of motion and solved by DEM (Cundall and Strack, 1979) while the flow of the continuum liquid is described using Naiver-Stokes equations and solved by CFD based on the finite volume method (Ferziger and Peric, 2002). The coupling of CFD and DEM is realized according to Newton's Third law of motion, as detailed elsewhere (Xu and Yu, 1997).

4.3 Computational details

4.3.1 Numerical scheme

A finite volume method is used to discretize the governing equations (Ferziger and Peric, 2002), and a second-order Crank-Nicolson scheme (Moukalled et al., 2016) is used for the time integration. The discretization of convection and diffusion terms is based on a second-order central differencing scheme (Wen et al., 2015). A PISO algorithm is taken for the velocity-pressure coupling (Issa, 1985). The equations for a particle are explicitly integrated.

The Rayleigh time Δt_R is referred to select the DEM time step:

$$\Delta t_R = \frac{\pi R_i}{0.1631\nu_i + 0.8766}\sqrt{\frac{2\rho_p(1+\nu_i)}{Y_i}} \quad (1)$$

where R_i, υ_i, ρ_p, Y_i, are, respectively, the radius, Poisson ratio, density and Young's modulus of particle i. Based on the particle properties that are used in this study, the time step of the solid phase is calculated as 2.14×10^{-4} s. As the Rayleigh time Δt_R is often larger than the DEM time step Δt_p,(Issa, 1985) Δt_p is set as 1.0×10^{-5} s in the current study. Tsuji et al. (Tsuji et al., 1993) mentioned that the time step of the fluid could be 10 ~100 10 ~100 times larger than the time step of particles. Therefore, the CFD time-step is set as 1.0×10^{-4} s to decrease the simulation time.

4.3.2 Simulation conditions

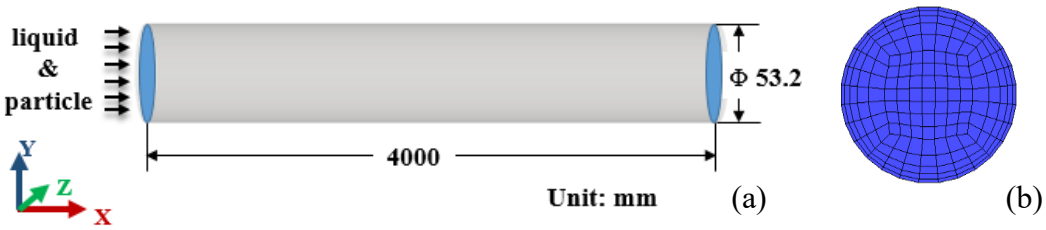

Figure 4-1 Schematic representation of the horizontal pipe simulated: (a) geometry configuration, and (b) computational grids on a cross-section

Figure 4-1(a) shows the simulated horizontal pipe that has a length of 4000 mm and a diameter of 53.2 mm, selected following the experimental work of Gillies and Shook, (1994). This pipe is meshed with hexahedra via an O-grid scheme (Figure 4-1(b)). With this mesh topology, the liquid flow near the wall can be better predicted by refining the grids. Table 2 lists the current simulation conditions. The conveying speed of liquid-solid mixture (U_f) is in the range between 0.65~10.0 m/s. The values of the solid concentration (C_v) in the slurry fed into the pipe, referred to as feed solid concentration, are 0.05, 0.1, 0.15 and 0.3, respectively. The particle density (ρ_{solid}) is 2650 kg/m^3. For each simulation, a uniform liquid velocity profile is specified at the

inlet, and particles are injected with the same velocity as the fluid. The number of particles that are injected into the pipe per second is calculated according to the liquid flow rate and feed solid concentration specified. At the outlet, the normal gradients of all variables are set to zero for the liquid phase, assuming that the flow is fully developed there. Differently, when particles are flowing out of the pipe outlet, they are removed directly from the simulation. A no-slip boundary condition is applied at the wall for the liquid flow. Facilitated with the above boundary conditions, the CFD-DEM model is solved using an in-house code. The results at the location of 3.5 m away from the inlet are chosen for analyzing the radial profiles of flow features, while the section between x = 2.5 m and x = 3.5 m is considered for obtaining the pressure drop and flow regimes.

Table 4-1 Simulation conditions in the current study.

Liquid flow	
Liquid density, (kg/m^3)	998
Liquid volume flow rate, (m^3/s)	0.00585
Liquid temperature, (ºC)	25
Liquid viscosity ($kg/(m \cdot s)$)	1.0×10^{-3}
Solid flow	
Material	Sand
Young's modular, (pa)	1×10^7
Poisson ratio	0.3
Particle density, (kg/m^3)	2650
Particle diameter, (mm)	2.4, 3.5

Conveying speed, (m^3/s)	0.65-10
Particle-wall sliding friction coefficient	0.3
Particle-particle sliding friction coefficient	0.1
Coefficient of restitution	0.65
Feed solid concentration (by volume)	0.05, 0.1, 0.15 0.3

4.4 Results and discussion

4.4.1 Independence tests of grid resolution and statistical time

The independence of numerical results on grid resolution and statistical time has been examined here. Thus, three grid schemes, as shown in Figure 4-2(a), are considered to mesh the pipe: fine (432,055 hexahedra and 1455 cells on a cross-section), medium (37,611 hexahedra and 189 cells on a cross-section) and coarse (21,492 hexahedra and 108 cells on a cross-section). Figure 4-2(a) shows the time-averaged solid volume fraction that is predicted via different grid schemes. The prediction with the coarse mesh significantly deviates from the measurement in the lower part of the pipe. This deviation becomes acceptable for the medium and fine meshes. To be computationally efficient, the medium grid scheme is chosen in all the simulations. The effect of statistical time on the time-averaged results is presented in Figure 4-2(b), in which the data after 3.0 s are used for statistics. Note that the physical time of 7 seconds is simulated to ensure that the liquid-solid flow has established for an adequately long time for conducting the statistical analysis in each simulation. This excludes the case of the conveying speed equaling 0.65 m/s, in which the simulated physical time is set to 15 s due to the complexity of this flow. The result in Figure 4-2(b) suggests that the effect of statistical time

on the solid volume fraction profile is trivial when the result in the last three seconds is considered in the analysis.

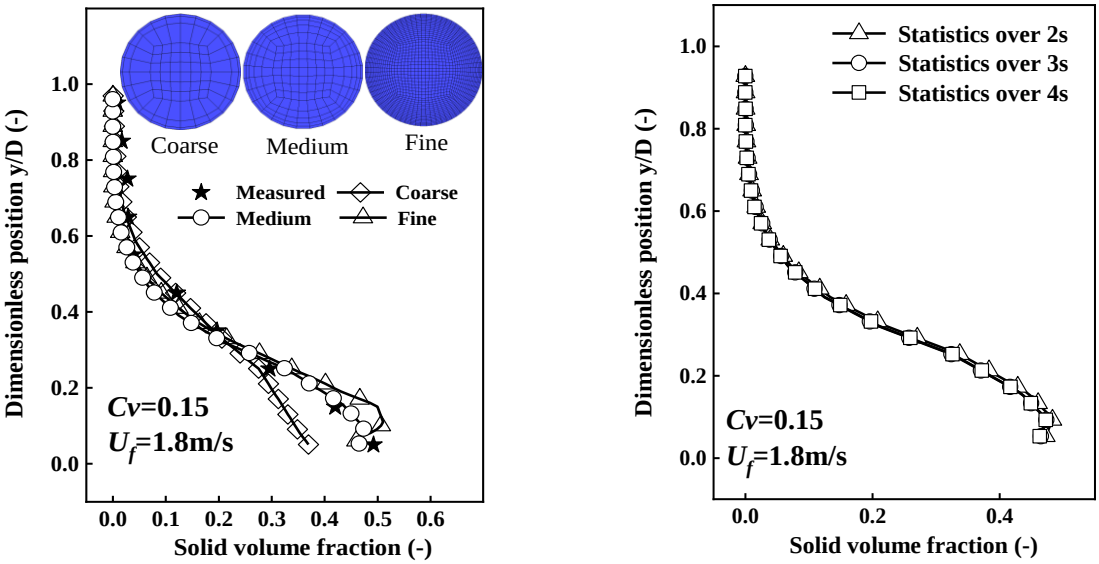

Figure 4-2 Comparison of variations of solid volume fraction along the vertical central line at the location x=3.5 m: (a) different grid resolutions; (b) different statistical times

4.4.2 Model application

To verify the validity of the current CFD-DEM model, the experimental data from two different applications have been considered. The first application focused on the vertical hydraulic conveying of coarse particles (Alajbegovi. et al., 1994). The predicted radial profiles of solid volume fraction, axial liquid velocity and axial solid velocity reasonably accord with the measurements (Zhou et al., 2019).

Further model validation is also conducted based on the experimental data of Gillies and Shook, (1994), who studied horizontal hydraulic conveying. Figure 4-3 compares the predicted solid volume fraction in the pipe with the measurements under four different conditions after the flow reaches the stable stage. In this comparison, the time-averaged data along the central vertical line (y-direction) on the cross-section of the pipe are considered. It can be seen from Figure 4-3 that the current model reasonably predicts the measured solid volume fraction.

When the feed solid concentration is relatively dense (C_v=0.3), the particles in the upper part of the pipe are more dilute in simulations compared to the experiments, especially at the relatively high conveying speed. This problem can also be observed in the work of Uzi and Levy, (2018), who studied horizontal hydraulic conveying by a CFD (RANS)-DEM model. One possible reason is the neglect of the influence of particles on turbulence, i.e., turbulent modulation. The modeling of turbulence modulation in particle-fluid systems has been an open topic and will be investigated via DNS-DEM simulations in the future. Nevertheless, all the results obtained thus far suggest that the current model is reliable for predicting the liquid-solid flow behavior in hydraulic conveying, at least qualitatively.

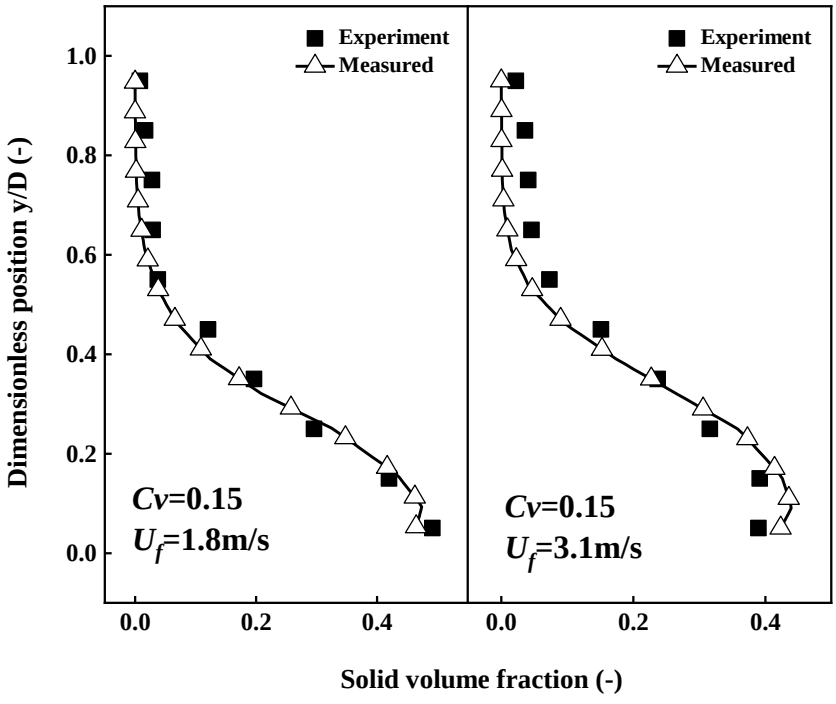

(a)

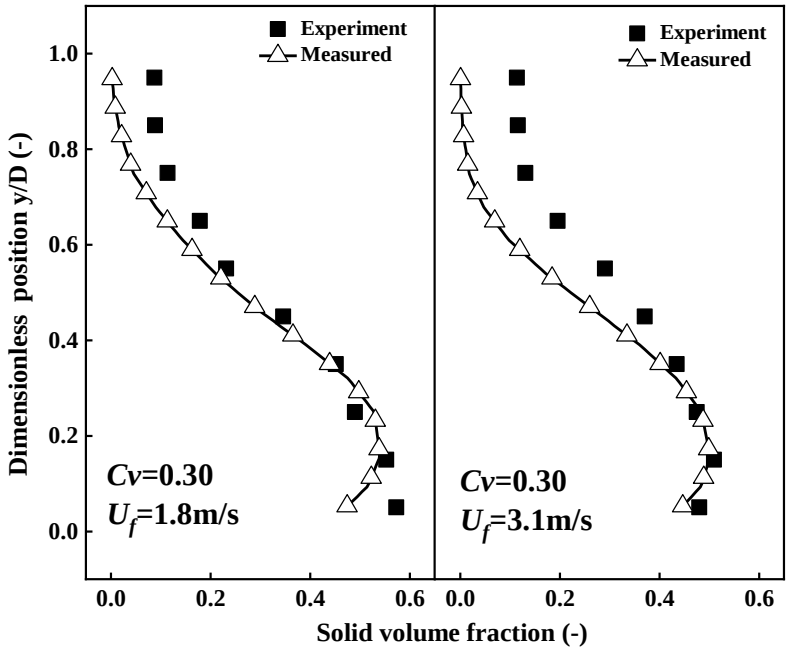

(b)

Figure 4-3 Comparison of predicted and measured (Gillies and Shook, 1994) profiles of solid volume fraction (=1-ε_f) at different conveying speeds for a feed solid concentration of (a) 0.15, and (b) 0.3

4.4.3 Flow regimes and their transition

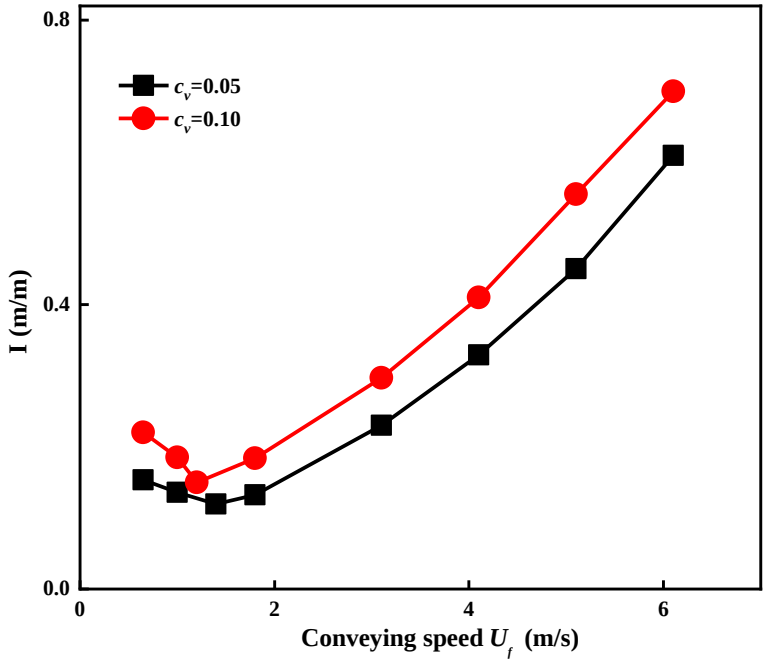

Figure 4-4 Phase diagram showing the variation of predicted pressure drop versus conveying speed at different feed solid concentrations

Via the validated CFD-DEM model, different flow regimes and the resulting pressure behavior are studied at the conveying speed (U_f) of 0.65 m/s - 10 m/s and the feed solid concentration of 0.05 - 0.1. Figure 4-4 is the predicted phase diagram that plots the time-averaged pressure drop across the pipe section between x=2.5 and 3.5 m versus the conveying speed while keeping a constant feed solid concentration. Here, the dimensionless pressure drop that is widely adopted to characterize hydraulic conveying is considered and calculated by $\mathrm{I} = \frac{\Delta p}{\Delta L} \cdot \frac{1}{\gamma_w}$, (Ravelet et al., 2013), where γ_w is the specific weight of water. As seen from Figure 4-4, with increasing conveying speed, the pressure drop decreases initially to a minimum and then increases. This trend can be observed at two feed solid concentrations. It is consistent with the experimental studies of the hydraulic conveying of coarse particles (Doron et al., 1987, Ravelet et al., 2013). However, this has not been obtained in the existing CFD-DEM studies of hydraulic conveying, as discussed previously. Figure 4-4 also shows that a higher feed solid concentration leads to a more significant pressure drop, similar to experimental observations (Doron et al., 1987, Ravelet et al., 2013).

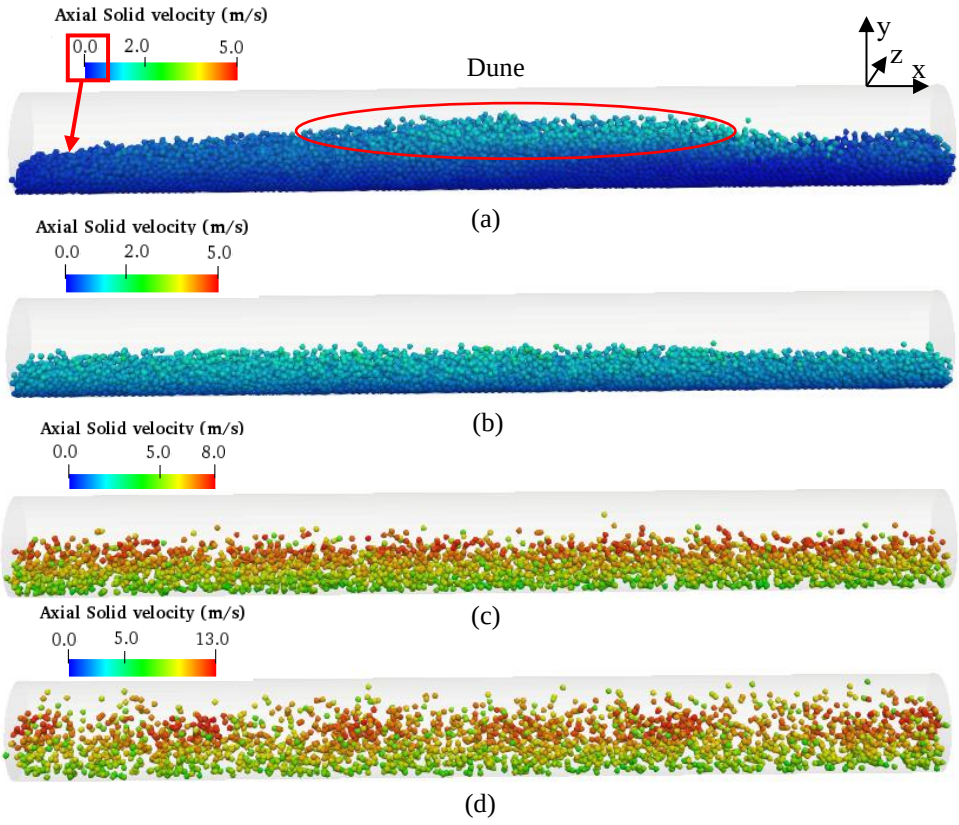

Figure 4-5 Snapshots showing solid flow patterns in the pipe section between x=3.0 and x=3.5 at different conveying speeds for d_p = 3.5 mm and C_v= 0.05: (a) U_f =1.0 m/s, (b) U_f = 1.8 m/s, (c) U_f = 6.1 m/s and (d) U_f = 10.0 m/s

Figure 4-5 shows the typical particle patterns that correspond to different flow regimes. In this figure, particles are coloured by axial solid velocities to show various particle behaviours better. When the conveying speed is low (U_f = 1.0 m/s), particles settle down in the bottom of the pipe forming a thick bed; the solid velocities are generally small and even close to zero near the bottom region of the pipe. This flow regime corresponds to the stationary-bed flow (Doron et al., 1987). Moreover, dunes are observed over the particle bed under the current condition, which has also been experimentally reported for the hydraulic conveying of coarse particles (Chara et al., 2015), but not for the transport of fine particles. With increasing conveying speed (e.g. U_f = 1.8 m/s), observable dunes do not form, and particles move forward in the form of moving bed, with only a few particles suspending over the bed. This flow regime is in the

moving-bed flow, in which the particle velocities in the vertical direction become much more uniform compared to those in the stationary-bed flow. When the conveying velocity continues to increase (e.g. U_f = 6.1 m/s), particles get more suspended and thus become more dispersed in the radial direction compared to the moving-bed flow. The particle velocities are much higher in the upper part of the pipe than in the lower part. This flow regime is in the heterogeneous-suspension flow. A further increase in conveying speed (U_f = 10.0 m/s) leads to more significant particle dispersion and less velocity heterogeneity in the vertical direction. Accordingly, the flow regime develops toward the pseudohomogeneous suspension flow.

To gain insights into the liquid-solid flow, the solid volume fraction together with the fluid velocity vectors, is examined corresponding to the particle patterns shown in Figure 4-6. In the stationary-bed flow, the particle bed is rather dense having a solid volume fraction of approximately 0.5, especially near the pipe bottom for a dune. It becomes much looser in the moving-bed flow, in which the solid volume fraction within the bed is approximately 0.35. In the heterogeneous-suspension flow, the maximum solid volume fraction drops below 0.13, and some particle clusters are observed. These clusters become smaller and move from the lower part of the pipe toward the centre as the conveying speed increases. Correspondingly, the liquid flows mainly over the particle bed in the stationary- and moving-bed flows, leading to the relatively high velocities for the particles near the bed surface. Thus, the parabolic liquid velocity profile of pure liquid flow is distorted substantially. This distortion is not apparent in the heterogeneous-suspension flow, where large liquid axial velocities appear near the central region of the pipe. When these large velocities, together with large velocity gradients, directly interact with multiple particles, this leads to intensive particle-fluid interactions and thus particle-particle collision. Consequently, particle clusters tend to form for counteracting the substantial energy loss resulting from particle-particle interactions, to some extent.

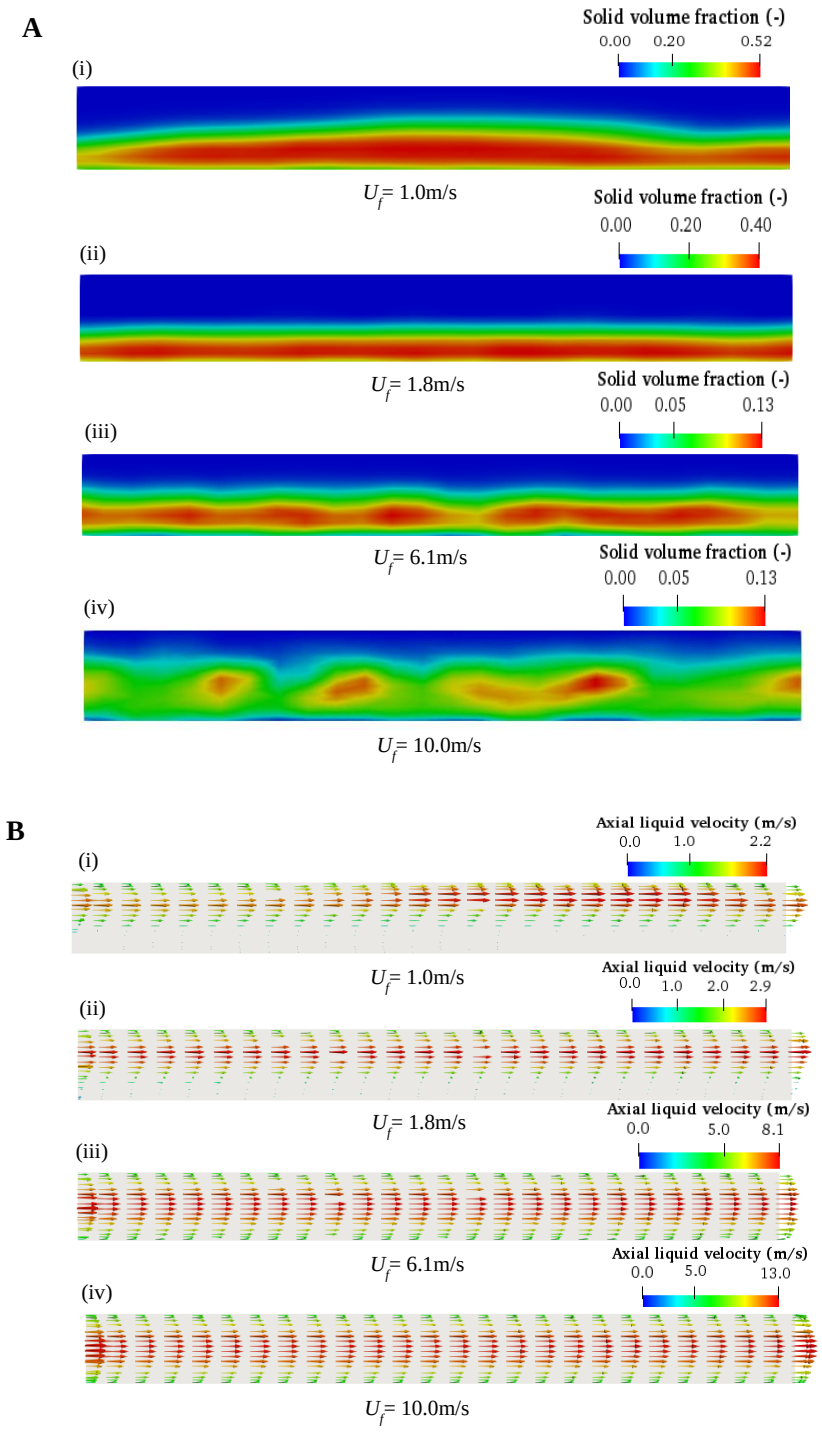

Figure 4-6 Contours of solid volume fraction (A) and fluid flow vectors (B) in the central vertical plane for different flow regimes: (i) stationary-bed flow, (ii) moving-bed flow, and (iii) and (iv) heterogeneous suspension flow

Figure 4-7 demonstrates the temporal variations of the solid volume fraction and pressure drop at the location x=3.5m. In this figure, the results are averaged over the cross-section. Expectedly, when the flow is in the stationary-bed flow, significant fluctuations are observed for both the solid volume fraction and pressure drop, which is attributed to the presence of dunes. Differently, the solid volume fraction does not fluctuate much in the moving-bed flow; this does not hold for the pressure. Here, the relatively significant pressure fluctuations are mainly caused by the heterogeneous variable structure of the moving bed other than the presence of dunes. For the heterogenous-suspension flow, the fluctuations in the solid volume fraction and pressure drop are relatively small. However, the former is slightly more significant at a higher conveying speed due to the formation of small clusters.

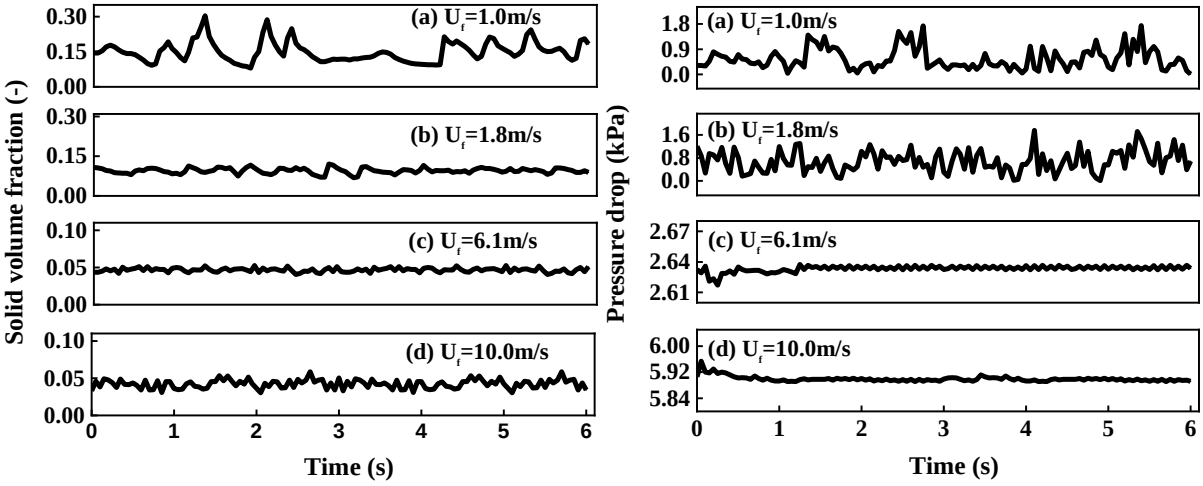

Figure 4-7 Temporal variations of solid volume fraction (left) and pressure drop (right) at the location x=3.5m for d_p = 3.5mm and C_v = 0.05 at different conveying speeds: (a) U_f = 1.0m/s, (b) U_f = 1.8m/s, (c) U_f = 6.1m/s and (d) U_f = 10.0m/s

Figure 4-8 shows how the conveying speed affects the time-averaged spatial distribution of solid volume fraction on the cross-section of the pipe. For all the flow regimes considered, the cross-section can largely be divided into three layers according to the values of solid volume fractions: a bottom layer, a middle layer, and a top layer. The solid volume fraction is relatively

uniform in the top and bottom layers but transits smoothly from the relatively high values in the bottom layer to the relatively low values in the top layer. Note that this three-layer characteristic does not accord well with the assumptions of the three-layer mechanistic model, (Doron et al., 1987) manifesting the complexity of the flow regimes.

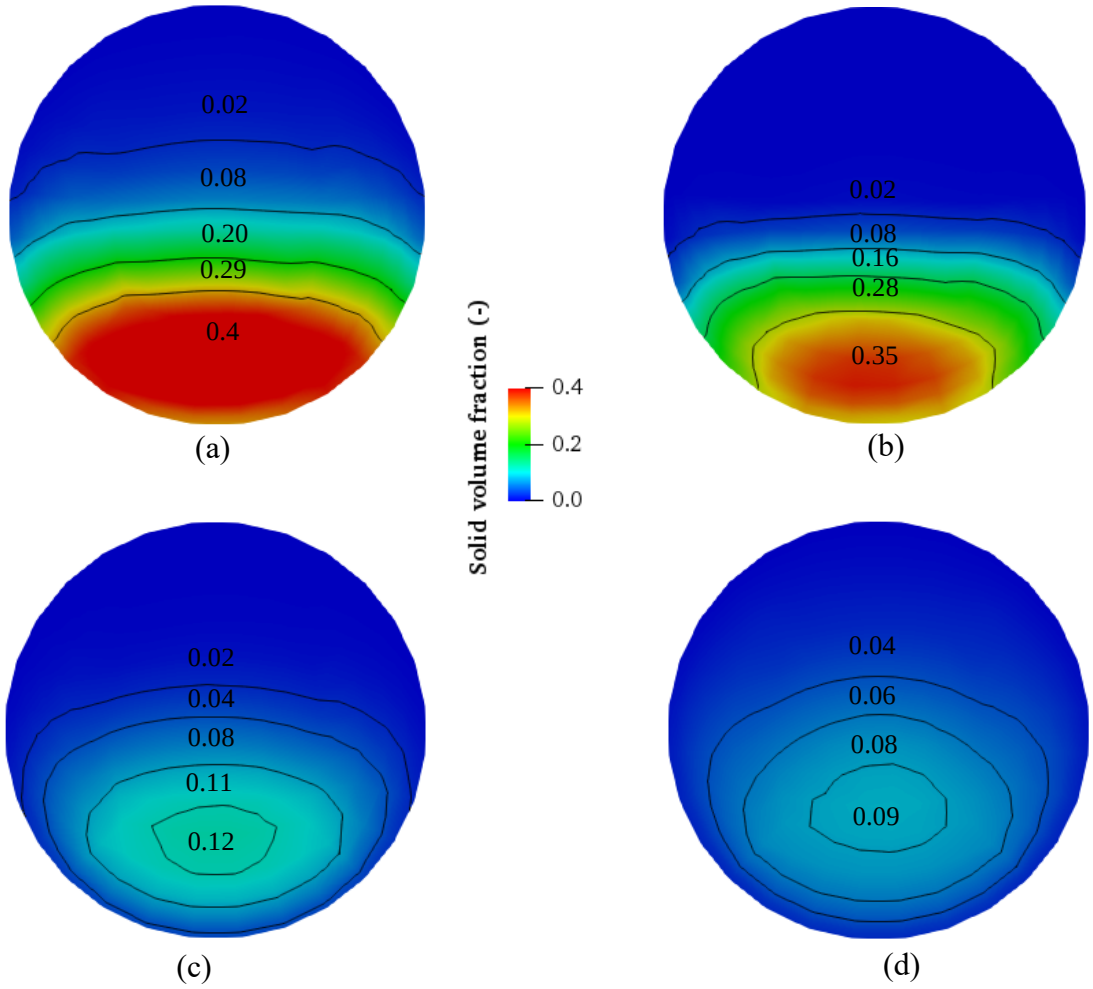

Figure 4-8 Effect of conveying speed on the contours of the solid volume fraction at the location x=3.5 m, d_p = 3.5 mm and C_v = 0.05: (a) U_f = 1.0 m/s, (b) U_f = 1.8 m/s, (c) U_f = 6.1 m/s and (d) U_f = 10.0 m/s

4.4.4 Force analysis

Essentially, particle flow regimes are governed by various forces, such as the particle-particle, particle-wall and particle-fluid forces and the gravity force (see Figure 4-9). Therefore, the

analysis of these forces helps gain insights into the behaviour of particles, thereby generating a better understanding of the flow regimes and their transition. This analysis is difficult to obtain experimentally, but it can readily be conducted based on CFD-DEM simulations.

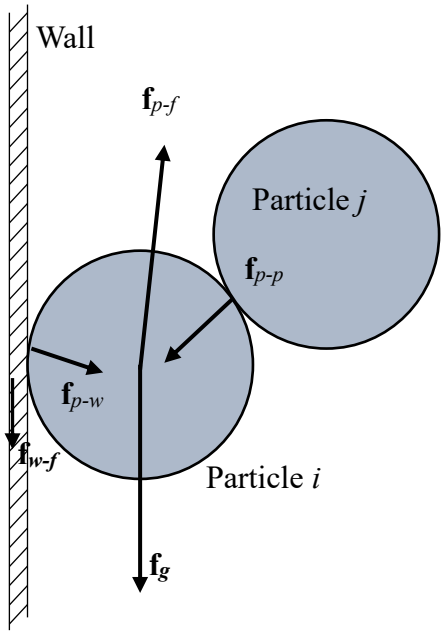

Figure 4-9 A schematic diagram for the force analysis at a particle scale

Following our studies of the pneumatic transport, (Kuang et al., 2009, Kuang and Yu, 2011) the volumetric particle-particle/wall force ($\left|\mathrm{F}\right|_{\mathrm{p\text{-}p/w}}$) and particle-fluid force ($\left|\mathrm{F}\right|_{\mathrm{p\text{-}f}}$) are analysed at a particle scale, which focuses on individual particles:

$$\left|\mathrm{F}\right|_{\mathrm{p\text{-}p/w}} = \frac{1}{\Delta t}\sum_{\Delta t}\left\{\frac{1}{V_{\mathrm{section}}}\left(\sum_{i=1}^{N_{\mathrm{p,section}}}\left(\sum_{j=1}^{k_i}\left|\mathrm{f}_{\mathrm{cn},ij}+\mathrm{f}_{\mathrm{ct},ij}\right|\right)\right)\right\} \tag{2}$$

$$\left|\mathrm{F}\right|_{\mathrm{p\text{-}f}} = \frac{1}{\Delta t}\sum_{\Delta t}\left\{\frac{1}{V_{\mathrm{section}}}\left(\sum_{i=1}^{N_{\mathrm{p,section}}}\left(\left|\mathrm{f}_{drag,i}+\mathrm{f}_{pgf,i}+\mathrm{f}_{\tau,i}+\mathrm{f}_{lift,i}+\mathrm{f}_{add,i}\right|\right)\right)\right\} \tag{3}$$

where $N_{\mathrm{p,section}}$ is the number particle in the pipe section that is considered for the analysis, and V_{section} is the volume of the pipe section.

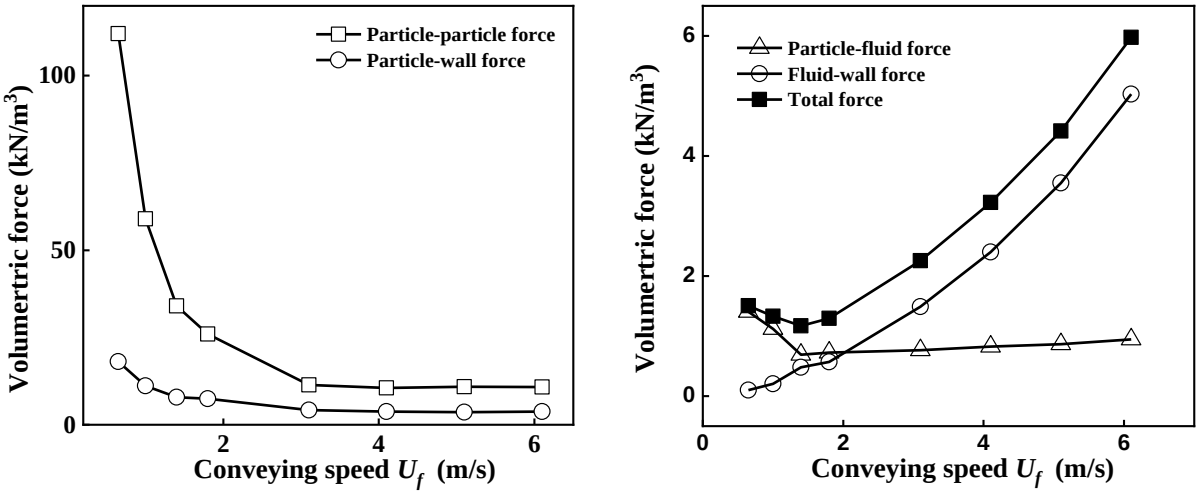

(a) **(b)**

Figure 4-10 Volumetric particle-particle/wall (a) and particle/wall–fluid (b) forces as a function of conveying velocity

Figure 4-10 plots the volumetric forces that are calculated using Eqs. (2) and (3) versus the conveying speed. Overall, the volumetric particle-particle and particle-wall forces have a similar trend. As the conveying speed increases, these two forces dramatically decrease and then remain nearly the same (Figure 4-10a). Note that particles are more likely to get suspended when the flow regime changes from stationary-bed flow, through moving-bed flow, and finally to heterogenous suspension flow. Also, with increasing conveying speed, the number of particles residing in the pipe section decreases for a given period. These two factors can both reduce the chance of the interactions between particles and between particle and wall, although these interactions should be more intense at a higher conveying speed. This explains why the particle-particle and particle-wall forces are nearly the same at relatively high conveying speeds. On the other hand, the volumetric particle-fluid force demonstrates a different trend (Figure 4-10b). With increasing conveying speed, it drastically decreases to a minimum initially and then increases gradually. Meanwhile, the volumetric wall-fluid force becomes larger substantially. Note that for a steady-state flow, both the particle-fluid and wall-fluid forces contribute directly to the pressure drop. (Kuang et al., 2012) The particle-fluid force is

much larger than the fluid-wall force at relatively low conveying speeds, which reverses at relatively high conveying speeds. As such, the sum of particle-fluid and fluid-wall forces decreases past a minimum and subsequently increases, which accounts for the variation of the pressure drop with the conveying speed.

The forces acting on a particle and a wall in a pipe section can be divided into three types according to their nature: the particle/wall-fluid force, which includes the fluid drag force, pressure gradient force, lift force, added mass force and viscous force on the particle and the fluid shear on the wall; the particle-particle and particle-wall forces, which have a similar property and thus are put together; and, the gravity force. Two dimensionless numbers, Π_1 and Π_2 can be obtained using these three types of forces, which is expressed as

$$\Pi_1 = \frac{\frac{1}{\Delta t}\sum_{\Delta t}\left\{\frac{1}{V_{\text{section}}}\left(\sum_{i=1}^{N_{\text{p,section}}}\left(\sum_{j=1}^{k_i+k_w}\left|\mathrm{f}_{\text{cn},ij}+\mathrm{f}_{\text{ct},ij}\right|\right)\right)\right\}}{\frac{1}{\Delta t}\sum_{\Delta t}\left[\frac{1}{V_{\text{section}}}\left(\sum_{i=1}^{N_{\text{p,section}}} m\mathrm{g}_{\text{i}}\right)\right]} \tag{4}$$

$$\Pi_2 = \frac{\frac{1}{\Delta t}\sum_{\Delta t}\left\{\frac{1}{V_{\text{section}}}\left(\sum_{i=1}^{N_{\text{p,section}}}\left|\mathrm{f}_{drag,i}+\mathrm{f}_{pgf,i}+\mathrm{f}_{\tau,i}+\mathrm{f}_{lift,i}+\mathrm{f}_{add,i}\right|+\sum_{i=1}^{N_{wc,\text{section}}}\left|\mathrm{f}_{f-w,i}\right|\right)\right\}}{\frac{1}{\Delta t}\sum_{\Delta t}\left[\frac{1}{V_{\text{section}}}\left(\sum_{i=1}^{N_{\text{p,section}}} m\mathrm{g}_{\text{i}}\right)\right]} \tag{5}$$

where $N_{\text{wc,section}}$ is the number of wall cells in the pipe section. The phase diagram in terms of these two dimensionless shows the distinct force characteristics of different flow regimes. It is therefore used to identify different flow regimes, their in-between boundaries and transition. The force characteristics represent the physical meaning behind two dimensionless numbers. Eqs. (4) and (5) suggest that Π_1 represents the mean particle-particle and particle forces per particle in the pipe section considered, while Π_2 denotes the mean particle-fluid force per

particle. These forces are expressed relative to the particle gravity to facilitate their comparison with the particle gravity.

Figure 4-11 demonstrates the relationship between Π_1 and Π_2 for the two feed solid concentrations (Cv). It indicates that the two different Cv have a similar trend for the different flow regimes with the increasing conveying speed. Three regions can be identified in this figure. In region I, Π_2 remains a small value while Π_1 varies within a large range. The flow regime is in the stationary-bed flow, in which vigorous particle-particle/wall interactions occur in the dense particle bed, and the particle-fluid force is small due to the overall small fluid velocities and the by-passing effect of the fluid over the particle bed for avoiding a significant pressure loss. In region II, Π_2 decreases with the increase of Π_1, and the flow region is in the moving-bed flow. Here, the particle-particle/wall interactions decrease as the particles get more suspended. This enhanced suspension also mitigates the by-passing effect of fluid and increases the particle-fluid interaction. In region III, Π_2 increases with the increase of Π_1, and the flow is in the heterogeneous suspension flow. This trend is attributed to the relatively high conveying speed, which makes it easier to suspend particles, leading to vigorous particle motion. Thus, both the particle-fluid and particle-particle/wall interactions are enhanced at a higher conveying speed.

Compared with the conventional pressure drop and conveying speed phase diagram (Figure 4-4), the new phase diagram (Figure 4-11) can better reflect the behaviors of different flow regimes and represents some fundamentals underlying different flow regimes in the aspect of various characteristics of forces acting on particles. These force characteristics accord well with particle flow patterns, as discussed above. Therefore, it helps identify the boundaries between flow regimes. This benefit cannot be achieved via the traditional phase diagram, in which the boundary between the moving-bed and heterogeneous suspension flows is difficult to determine visually. In particular, to date, it has been a challenge to identify the transition of

flow regimes from one to another. The proposed phase diagram promises to overcome this problem. However, further efforts are needed to test this diagram under different conditions.

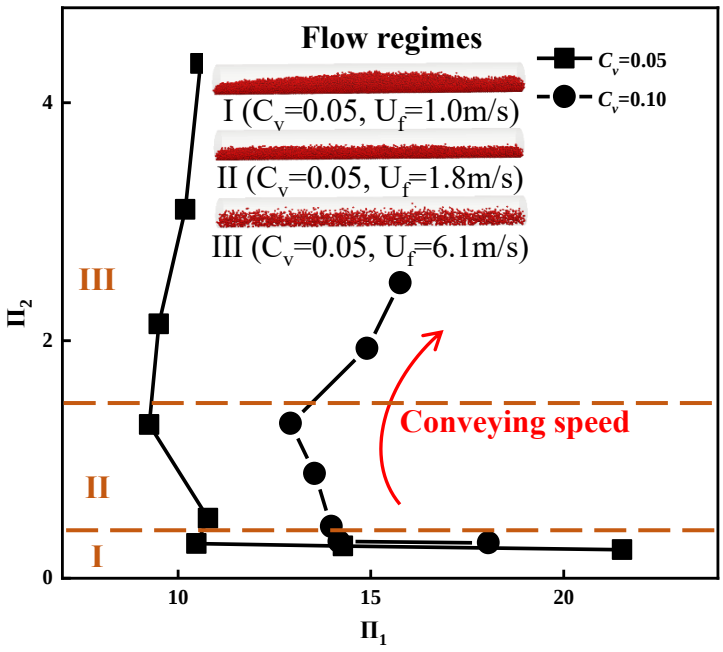

Figure 4-11 Phase diagram in terms of forces acting on particles and walls

4.4.5 Prediction correlation of pressure drop

The pressure loss along hydraulic conveying pipelines is a major industrial concern. Thus, an attempt is made in this section to develop correlations for predicting this process parameter based on current simulation results. The dimensionless pressure drop (I), as defined in Section 4.4.3, is considered to be a function of a few key variables,including the diameter of pipe d_{pipe}, the conveying speed U_{f}, the fluid viscosity η, the feed solid concentration C_{v}, the fluid density of liquid ρ_{l}, and the solid density ρ_{s}: (Matoušek, 2005, Silva et al., 2015b)

$$\mathrm{I} = \mathrm{F}(U_f, C_v, \rho_s, \rho_l, \eta, d_{pipe}) \tag{6}$$

It should be pointed out that the effect of particle diameter on the pressure drop is relatively small (Doron and Barnea, 1995, Uzi and Levy, 2018) and thus not considered. The

dimensionless analysis shows that I can be linked to three dimensionless quantities: $\mathrm{Re}_{\mathrm{mix}}, \frac{\rho_s}{\rho_l}, C_v$. In this study, it is expressed as:

$$\mathrm{I} = \alpha_1 \mathrm{Re}_{\mathrm{mix}}^{\alpha_2} \left(\frac{\rho_s}{\rho_l} \right)^{\alpha_3} C_v^{\alpha_4} \tag{7}$$

where $\mathrm{Re}_{\mathrm{mix}}$ is defined as $\mathrm{Re}_{\mathrm{mix}} = \frac{\rho_l U_f d_{\mathrm{pipe}}}{\eta}$, and α_i denotes the empirical parameters.

The values of these empirical parameters are determined by best fitting the simulation data. Note that Eq. (7) can only describe a monotonous trend, but it is not this case for the variation of the pressure drop shown in Figure 4-4. Thus, according to the critical conveying velocity, a curve of pressure drop is divided into two sections that have different trends. The correlation of Ravelet et al., (2013) can well predict the critical velocities in Figure 4 and thus is adopted here:

$$\mathrm{U}_{\mathrm{critical}} = 3.8 C_v^{2.4} \sqrt{3.03 d_p g \left(\frac{\rho_s}{\rho_l} - 1 \right)} \tag{8}$$

Based on the simulation data, curve fitting of Eq. (27) yields results in the following equation:

$$\mathrm{I} = \begin{cases} 6\mathrm{Re}_{\mathrm{mix}}^{-0.39} \left(\frac{\rho_s}{\rho_l} \right)^{1.09} C_v^{0.18} & U_f \le U_{critical} \\ 1.85 e^{-5} \mathrm{Re}_{\mathrm{mix}}^{1.16} \left(\frac{\rho_s}{\rho_l} \right)^{-3.5} C_v^{0.32} & U_f > U_{critical} \end{cases} \tag{9}$$

Figure 4-12 demonstrates that the predictions by Eqs. (8) and (9) are in good agreement with the results obtained by the CFD-DEM simulations. To examine the applicability of this correlation, the experimental data of Ravelet et al., (2013) are also considered, in which the

pipe diameter is 100 mm and the particles have a density of 3650 kg/m^3 and a size 6 mm. Figure 4-12 shows that Eqs. (8) and (9) can well predict the trend of the experimental data. However, over-prediction is observed, especially at high conveying speeds. This is because the effects of particle diameter and pipe diameter are not considered in the current study. Nevertheless, this result suggests that the CFD-DEM predictions under well-controlled conditions promise to help establish reliable correlations for predicting pressure drop in a cost-effective way. However, to fully achieve this, systematic studies are necessary for facilitating applications, as done elsewhere for other particle-fluid systems.(Ji et al., 2019)

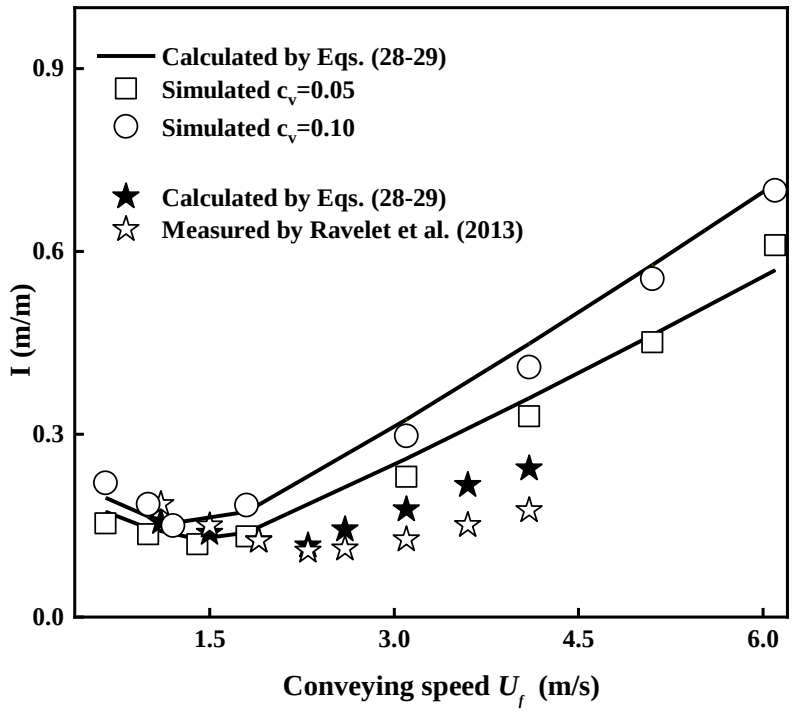

Figure 4-12 Prediction of pressure drops at different feed solid concentrations

4.5 Conclusions

The flow regimes and their transition in horizontal hydraulic conveying of coarse particles are numerically studied using a recently developed CFD-DEM model. The major findings of this study are summarized as follows:

i. The validity of the CFD-DEM model has been verified by the reasonable agreement between the predicted and measured profiles of solid volume fraction in a horizontal pipe at different feed solid concentrations and conveying speeds. Via this model, the transition from the stationary-bed flow, through the moving bed flow, finally to the heterogenous-suspension flow as the conveying speed increases while keeping a constant feed solid concentration is successfully reproduced. Corresponding to this transition, the predicted pressure drop decreases initially to a minimum and then increases. This phenomenon is consistent with the published experimental observations.

ii. The flow regimes and their transition are analyzed in the aspects of flow and force structures. It is shown that all the flow regimes can be divided into three layers according to the spatial distribution of solid volume fraction on the cross-section of the pipe, although the values in each layer are different for different flow regimes. The particle-particle and particle-wall forces decrease first and then remain nearly the same as the flow transits from the stationary-bed flow to the heterogenous-suspension flow. During this transition, the decrease in particle-fluid force accounts for the decrease in pressure drop, whereas the increase in wall-fluid shear plays a dominating role in the increase in pressure drop. Combining the simulation data and the dimensionless analysis, correlations are formulated for estimating the pressure drop. This correlation can well fit the current simulation results but needs to be improved via systematic studies of the effects of a range of key variables for general use.

iii. The forces governing the particle-fluid flow are used to establish a new phase diagram. This diagram can identify various flow regimes and the boundaries during the transition from one to another. This diagram shows that in the stationary-bed flow, the particle/wall-fluid forces remain a small value and the particle-particle/wall forces vary over a wide range; in the moving-bed flow, the particle/wall-fluid forces decrease with the increases of

the particle-particle/wall forces; in the heterogeneous-suspension flow, the particle/wall-fluid forces increase with the increases of the particle-particle/wall forces.

CHAPTER 5 CFD-DEM ANALYSIS OF HYDRAULIC BENDS

5.1 Introduction

Hydraulic conveying is a common operation in many industries, such as chemical engineering, food, mining, mineral processing, oil and petroleum industries. The advantages associated with this transportation method include low operation and maintenance costs, friendliness to the environment, and unlimited transporting distance. Also, it offers great layout flexibility via the use of bends that connect straight pipe sections in various manners. When the particle-fluid mixture enters the inlet of bend, it typically continues moving straight ahead to the first impact zone, and are then deflected at an angle towards the outlet of the elbow. The deflection angle is determined by the bend geometry, material properties and operating conditions involved. In many designs, the materials will hit one or more secondary impact zones before exiting the bend and re-accelerating to a fully developed status in a straight section or post-bend. In this process, additional pressure losses due to the impact and re-acceleration of particles are added to the system (resulting in more energy consumption), and severe bend erosion may be resulted. Due to the above phenomena, among all the components of a hydraulic conveying system, bends are probably the most potentially problematic and play a crucial role in affecting the overall performance of the system with regards to pressure loss, pipe wall erosion and conveying stability.

More and more studies were obtained in the past few years, most of them were focused on vertical or horizontal pipe (Doroodchi et al., 2005, Kaushal et al., 2012, Silva et al., 2015a, Ofei and Ismail, 2016, Zhou et al., 2019, Uzi et al., 2020), which are often connected by the bends. However, the studies on bends were least investigated and were not well understood although their simplicity. For better optimal operating and design of the solid-liquid system, the comprehensive two-phase flow must be studied, which could add pipe elements, such as,

bends to the pipeline that is a very common way, as the flow direction in bends will change along the pipeline route.

The bend element is a highly important and practical piping component for forming a pipeline layout. Comparing with vertical and horizontal pipes, the particle performance in bend pipe is harder to predict. In order to increase the overall bend design as well as to understand the complex particle performance, some factors could be used to describe it, such as the predictions of pressure drop and erosive wear. The pressure drop is related to the energy expenses, affected by fluid velocity, concentration and pipe orientation. The pipeline erosive wear is directly related to the equipment cost. Lots of studies in bend pipe have been done in gas-solid pipeline system in the past few years.(Chu and Yu, 2008, Kruggel-Emden and Oschmann, 2014, Xu et al., 2016, Uzi et al., 2017, Zhou et al., 2017, Zeng et al., 2018)

The pressure drops and erosive wear in hydraulic pipeline system could be affected by the flow regimes, particle diameter, conveying speed and pipe orientation. Current design of hydraulic pipeline system depends on two important sources: experimental data, empirical and theoretical correlations. For the former, a large quantity of experimental data, produced at various test institutions around the world (Sive, 1989), can be used as a check on the design calculations performed. For the latter, various analytical techniques are proposed. Since the 1950s, there has been an abundance of both empirical and theoretical correlations developed in an attempt to better describe multiphase flow systems (David et al., 2011, Wasp and Slatter, 2004).

Lots of efforts have been done in experimental studies, such as, Faddick, (1975) mentioned that erosive wear had a proportional relationship with the conveying speed and power, but it was inversely proportional to the cross-sectional area of the pipe. Archard, (1953) showed that the sliding distance, applied load and the material hardness could be used to represent erosive wear volume. Finnie, (1960) and Bitter, (1963) showed that the impact velocity and angle could

also use to describe the erosive wear. However, there is no single prediction equation or a limited set of equations for general and practical use (Meng and Ludema, 1995). More experimental studies have been done to examine the erosive wear in the past years (Levy and Hickey, 1987, Clark, 1995, Q. Fang et al., 1998, Li et al., 2019). But generally, they do suffer from a number of drawbacks such as downtime of monitoring the liners, taking a long time, usually over a year to yield results. Essentially, the pipeline erosive wear is caused by the surface erosion that is resulting from the dynamic action of moving particles on the pipe wall (Mazumder et al., 2008). Therefore, the quantification of particle-wall interaction plays an important role in solid-liquid system, which could be used to explain the formation of the surface erosive wear. To achieve this, micromechanical analysis on particle-wall collision at a particle scale is required.

In the past few years, some typical numerical researches on solid-liquid bend pipe are listed here, Chen et al., (2015) applied CFD-DEM method to study the bend pipe with different bend-angle on erosive wear with particle diameter 150 μm, Li et al., (2019) and Zhang et al., (2012) used CFD-DEM method to investigate the effect of coarse particle diameter on erosive wear, in which the particle diameter was larger than 1 mm. A new mathematical model was established by Wang et al., (2017a) to predict the bends erosion in oil pipelines with particle diameter of 150 μm. Kannojiya et al., (2018) studied the bend pipe with the CFD-CFX based method, and the particle diameter was 50 to 300 μm.

For better analysis of the particle performance in bend pipe, the promising method is CFD-DEM approach (Xu and Yu, 1997, Zhu et al., 2007, Zhu et al., 2008). In this approach, the motion of discrete particles is described by Newton's law of motion for every individual particle and the flow of continuum fluid is described by the local averaged Navier-Stokes equations that can be solved by the traditional CFD technique, and the coupling of the two models at different time and length scales is achieved by applying Newton's third law at a

computational cell level. It can generate detailed dynamic information such as particle trajectories and transient forces acting on individual particles that are extremely difficult, if not impossible, to obtain experimentally. Such information is important to depict the particle-particle and particle-fluid interactions and hence understanding the fundamentals of particle-fluid flow under different conditions.

To sum up, most researchers were studying fine particles, and only focused on erosive wear, not systemically describing the whole particle performance, and for the coarse particle, even less so. In this chapter, a hydraulic bend pipe, conveying of coarse particles is studied by a recently reported CFD-DEM model (Zhou et al., 2019, Zhou et al., 2020). The validity of the model is first verified. On this basis, it is used to predict typical flow regimes. Then, the simulation results are analysed in detail in terms of particle characteristic performance both in macro and micro view, such as, pressure drop, solid volume fraction distribution, solid velocity and erosive wear.

5.2 Simulation methods and conditions

The current CFD-DEM model is the same as the one described in section 3.2 in Chapter 3. For more details please refer to section 3.2 in Chapter 3. The model is also outlined here for brevity. In this model, the motions of discrete particles are individually described using Newton's second law of motion and solved by DEM (Cundall and Strack, 1979) while the flow of the continuum liquid is described using Naiver-Stokes equations and solved by CFD based on the finite volume method (Ferziger and Peric, 2002). The coupling of CFD and DEM is realized according to Newton's Third law of motion, as detailed elsewhere (Xu and Yu, 1997).

5.2.1 Erosive wear model

In view of its mechanism and many factors, it is indicated that particle erosion is a very complicated process. Though there is no model with general application as previously mentioned, many empirical formulas to predict erosion have been presented based on some specific application under different conditions. An erosion prediction model should take as many factors into account as possible to meet some given service requirement.

In this study, the erosion protection model is used by Ahlert, (1994), as following:

$$E_F = 1.559 \cdot e^{-6} \cdot B^{-0.59} \cdot v_p^{2.73} \cdot F_s \cdot f(\alpha) \quad (1)$$

$$f(\alpha) = 2.27\alpha - 3.84\alpha^2 \quad \text{for} \quad \alpha \le 15.3 \quad (2)$$

$$f(\alpha) = 3.147\cos^2\alpha \sin\alpha + \sin^2\alpha + 2.532 \quad \text{for} \quad \alpha > 15.3 \quad (3)$$

where E_F is the erosion wear with a unit of millimetre, α is the impact angle, B denotes the Brinell hardness of the wall material in kg/mm, v_p is the particle impact velocity and F_s is the particle shape factor.

5.3 Computational details

5.3.1 Numerical scheme

A finite volume method is used to discretise the governing equations, and a second-order Crank-Nicolson scheme (Moukalled et al., 2016) is used for the time integration. The discretization of convection and diffusion terms is based on a second-order central differencing scheme (Wen et al., 2015). A PISO algorithm is taken for the velocity-pressure coupling. (Issa, 1985) The equations for a particle are explicitly integrated, and then the position and velocity of the particle are updated for the next coupling procedure.

The Rayleigh time Δt_R is referred to select the DEM time step:

$$\Delta t_R = \frac{\pi R_i}{0.1631\nu_i + 0.8766}\sqrt{\frac{2\rho_p(1+\nu_i)}{Y_i}} \tag{4}$$

where R_i, υ_i, ρ_p, Y_i, are, respectively, the radius, Poisson ratio, density and Young's modulus of particle i. Based on the particle properties that are used in this study, the time step of the solid phase is calculated as 1.509×10^{-4} s. As the Rayleigh time Δt_R is often larger than the DEM time step Δt_p (Issa, 1985), Δt_p is set as 1.0×10^{-5} s in the present study. Tsuji et al. (Tsuji et al., 1993) mentioned that the time step of the fluid could be 10 ~100 times of the solid time step. Therefore, the CFD time-step is set as 1.0×10^{-4} s to reduce the computational time.

5.3.2 Configuration and boundary conditions

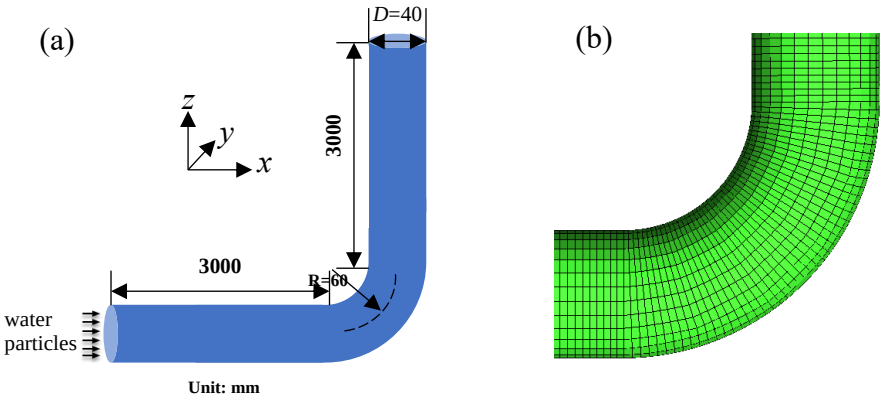

Figure 5-1 Schematic representation of the elbow pipe simulated: (a) geometry configuration, and (b) computational grids on a cross-section

Figure 5-1(a) shows the simulated elbow pipe that has a length of 3 m and a diameter of 40 mm. The pipe is meshed with hexahedra via an O-grid scheme, as shown in Figure 5-1(b). With this mesh topology, the liquid flow near the wall can be better predicted by refining the grids. Table 5-1 lists the current computational conditions. The conveying speed of liquid-solid mixture (U_f) is in the range between 1.2~4.0 m/s; the feed solid concentration (C_v) is 0.05, and the particle density (ρ_{solid}) is 2482 kg/m^3. For each case, a uniform liquid velocity profile is

specified at the inlet, and particles are injected with the same velocity as that of fluid. The number of particles injected into the pipe per second is calculated according to the given liquid flow rate and feed solid concentration (by volume). At the outlet, the normal gradients of all variables are set to zero for the liquid phase, assuming that the flow is fully developed there. Differently, when particles are flowing out of the pipe outlet, they are removed directly from the simulation. A no-slip boundary condition is applied at the wall for the liquid flow. The results at the location of 2.8 m away from the inlet are chosen for analysing the radial profiles of flow features, while the section between x = 2.9 m and z = 0.06 m is considered for obtaining the erosive wear.

Table 5-1 Simulation conditions in the current study.

Validation case	
Gas density, (kg/m^3)	1.205
Gas velocity (m/s)	12
Particle mass flowrate, (kg/s)	0.01, 0.017
Particle diameter, (mm)	0.25
Particle density, (kg/m^3)	2482
Liquid flow	
Liquid density, (kg/m^3)	998
Liquid volume flow rate, (m^3/s)	0.00585
Liquid temperature, (^oC)	25
Liquid viscosity (kg/(m·s))	1.0×10^{-3}
Solid flow	

Material	Sand
Young's modular, (pa)	1×10^7
Poisson ratio	0.3
Particle diameter, (mm)	3.5
Conveying speed, (m^3/s)	1.2-4.0
Particle-wall sliding friction coefficient	0.3
Particle-particle sliding friction coefficient	0.1
Coefficient of restitution	0.65
Feed solid concentration (by volume)	0.1

5.4 Results and discussions

5.4.1 Model validation

To validate the current CFD-DEM model, the experimental data from two different applications have been considered. The first application considered the vertical and horizontal hydraulic conveying of coarse particles.(Alajbegovi. et al., 1994, Gillies and Shook, 1994) where the measured and calculated radial profiles of solid volume fraction, axial liquid velocity and axial solid velocity are compared and reasonable agreement has been reported. (Zhou et al., 2019)

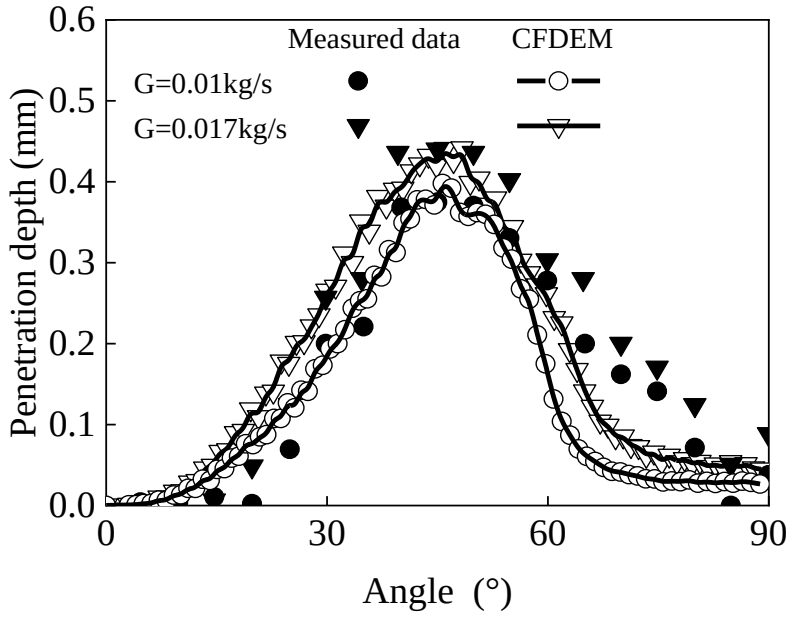

Figure 5-2 Comparison of predicted and measured (Zheng, 2016) penetration depth at different mass flowrate

The gas-solid experiment of Zheng, (2016) is used to further validate the erosion model and is presented in Table 5-1. Here the particle diameter is 0.25 mm with particle density of 2482 kg/m^3, and the injecting gas velocity is set to 12 m/s with two different particle mass flow rates. Figure 5-2 compares the predicted and measured penetration depth in the bend pipe with the measurements under two different mass flowrate conditions after reaching stable status. In this comparison, the time averaged data at the central line (y-direction) on the cross section of the pipe are considered at the bend section. It is evident that the current erosion model can well predict the measured trends under all the conditions. These validations give us more confidence in the analysis of the following results.

5.4.2 Flow regimes

First of all, to study the effect of the pipe orientation on the flow regimes and erosion position, the simulations are conducted by changing the direction of the gravity force while keeping the other parameters the same. For a better comparison, the results are drawn in this way that the

inlet pipe was always at the bottom-left corner of the figure, as shown in Figure 5-3. The vertical pipe is defined as the flow direction is the same as the gravity force, while the horizontal pipe is defined as the flow direction that is perpendicular to the gravity force.

For comparison, the flow direction is always at the left-side corner of the scheme, the direction of pipe parallel to the gravity force is considered as the vertical pipe, while the horizontal pipe is defined as its direction is perpendicular to the gravity force. Figure 5-3 shows the schematic representation of different elbow pipe orientation, θ=0° means the flow direction is from horizontal to vertically upward, θ=45° means the pipe is inclined to 45 degree to convey the mixed fluid, and when the degree is θ=90°, the flow direction is changed from vertical to horizontally upward.

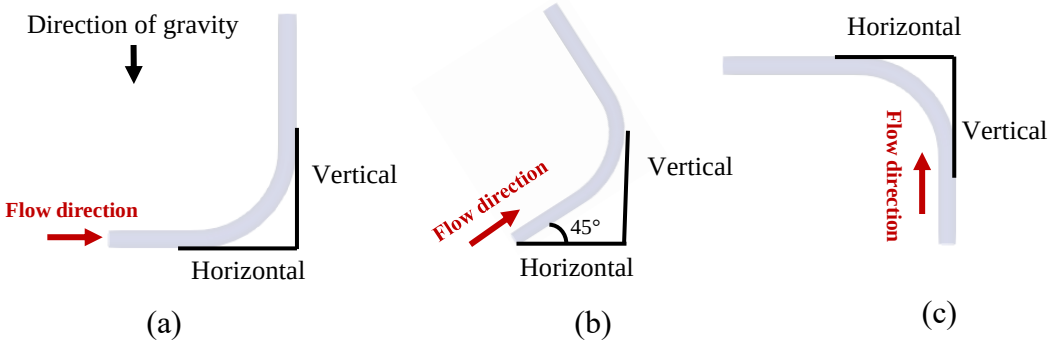

Figure 5-3 Schematic representation of different elbow pipe orientation: (a) θ=0° (b) θ=45°; (c) θ=90°

Generally speaking, the flow regimes have a great influence on the elbow pipe. Figures 5-4(a-c) indicates the particle movement with different conveying speeds in the pipe with different orientations. Here particles are coloured by magnitude solid velocities to better show particle behaviours. When the flow is stationary flow (Figure 5-4 (a)), with the increase of the pipe angle, the particles tend to suspend before the bend, and form a clustered particle flow, as the conveying speed is too low to distribute a uniform particles flow. For the horizontal-vertically pipes, particles settle in the bottom of the pipe forming a particle bed due to the effect of the

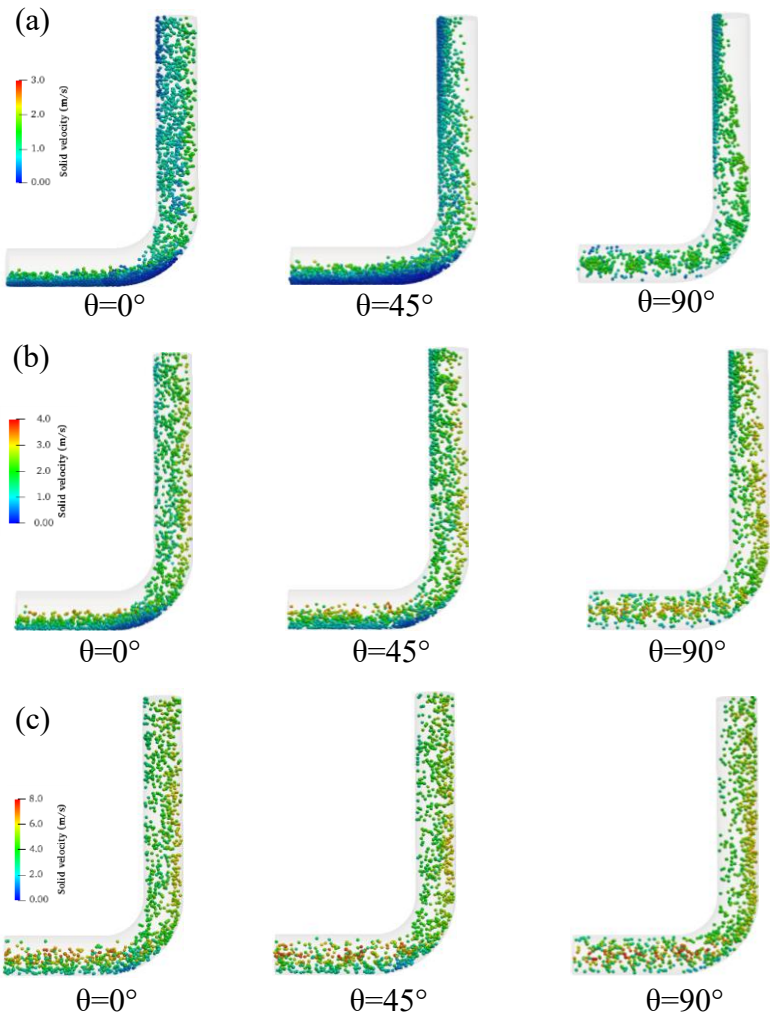

Figure 5-4 Snapshots showing solid flow regimes in the pipe section between x=2.8 and z=0.56 at different conveying speeds for d_p = 3.5 mm and C_v= 0.05: (a) U_f =1.2 m/s, (b) U_f = 2.0 m/s, (c) U_f = 4.0 m/s

conveying speed is too low to distribute a uniform particles flow. For the horizontal-vertically pipes, particles settle in the bottom of the pipe forming a particle bed due to the effect of the gravity force. In the elbow region, gravity force may cause most of the particles to move away from the central axis of the horizontal pipe. Due to the combined effect of gravity and drag force, the particle concentration area may also move deeper into the elbow. When the conveying speed is increased to 2.0 m/s as shown in Figure 5-4(b), the flow changes to be a moving-bed flow, in which the particles move forward in the form of a moving bed with only

a few suspended over the bed. The particle velocities become much more uniform compared to those in the stationary flow. Furthermore, the effect of pipe orientation on moving-bed flow is similar to those of the stationary flow. When the conveying velocity continues to 4.0 m/s (Figure 5-4(c)), it leads to more particle dispersion and the flow regime develops toward the pseudohomogeneous suspension flow. Comparing with other cases, as the conveying speed is high enough, the effect of pipe orientation on the flow regimes does not change too much.

5.4.3 Pressure drop

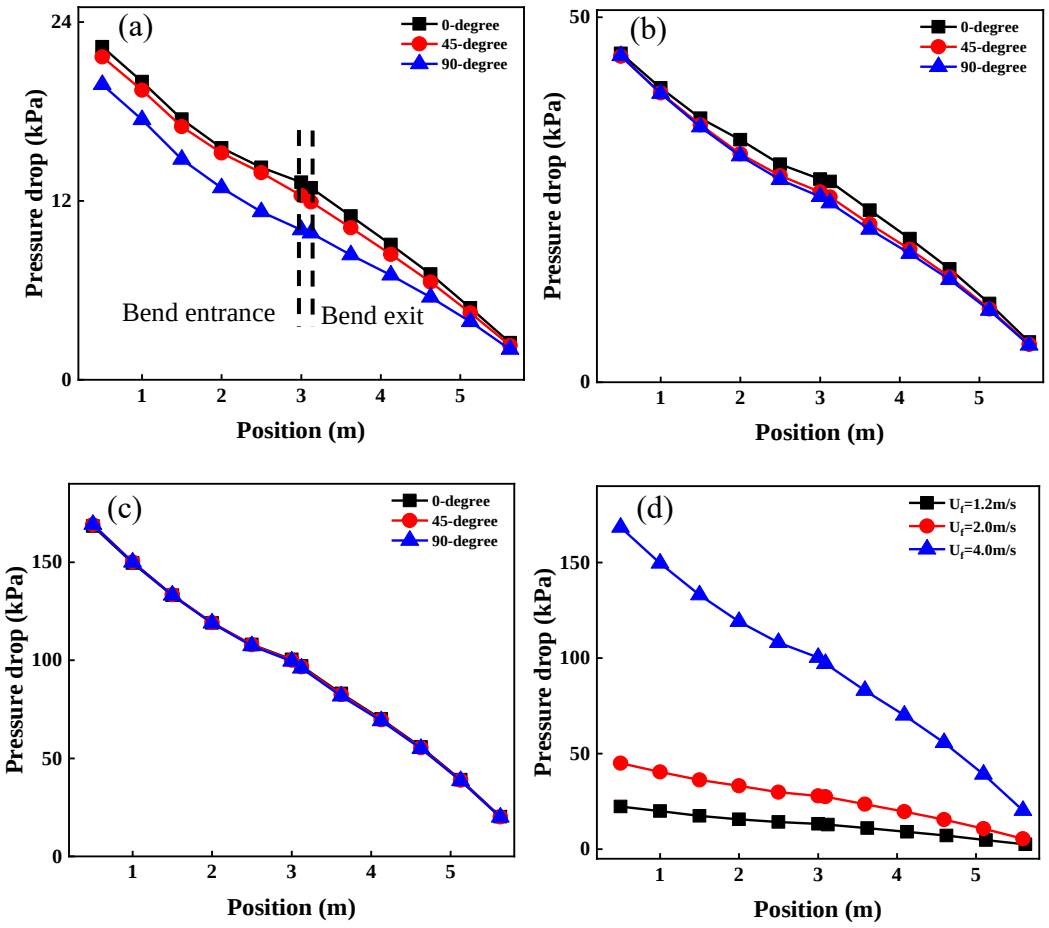

Figure 5-5 Phase diagram showing the variation of pressure drop versus pipe orientation at different conveying speed. (a) U_f =1.2 m/s; (b) U_f = 2.0 m/s; (c) U_f = 4.0 m/s; (d) θ=0°

Pressure drop is another important performance in solid-liquid system. Figure 5-5 shows the predicted phase diagram that plots the time-averaged pressure drop across the whole pipe

section against the conveying speed while keeping a constant feed solid concentration. When the conveying speed is 1.2 m/s, as the pipe degree increases, the pressure drop of bend entrance for the 0-degree and 45-degree show a similar trend, as they produce similar flow regimes. However, when the conveying speed is very high, the effect of pipe orientation on pressure drop is less. For a constant degree, the increased conveying speed produce a larger pressure drop.

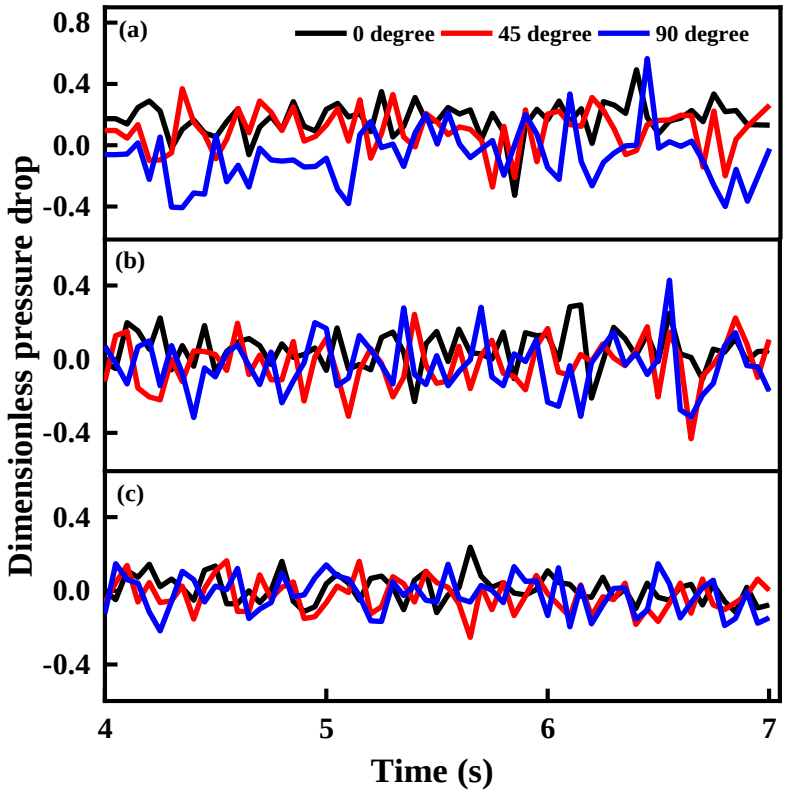

Figure 5-6 Temporal variations of pressure drop at the position p=5.13m for d_p = 3.5mm and C_v = 0.05 at different conveying speeds: (a) U_f = 1.2m/s; (b) U_f = 2.0m/s; (c) U_f = 4.0m/s

Figure 5-6 shows the variations of the pressure drop at the position p=5.13 m with time. Here the results are averaged over the cross-section when flow is statistically stable. As expected, when the flow is in the regime of stationary flow, the pipe orientation has significant effect on pressure drop, especially for the 90-degree in which strong fluctuations are observed. When

the flow turns to pseudohomogeneous suspension flow, it could be seen that the effect of pipe orientation on the fluctuation of pressure drop is less.

5.4.4 Solid volume fraction

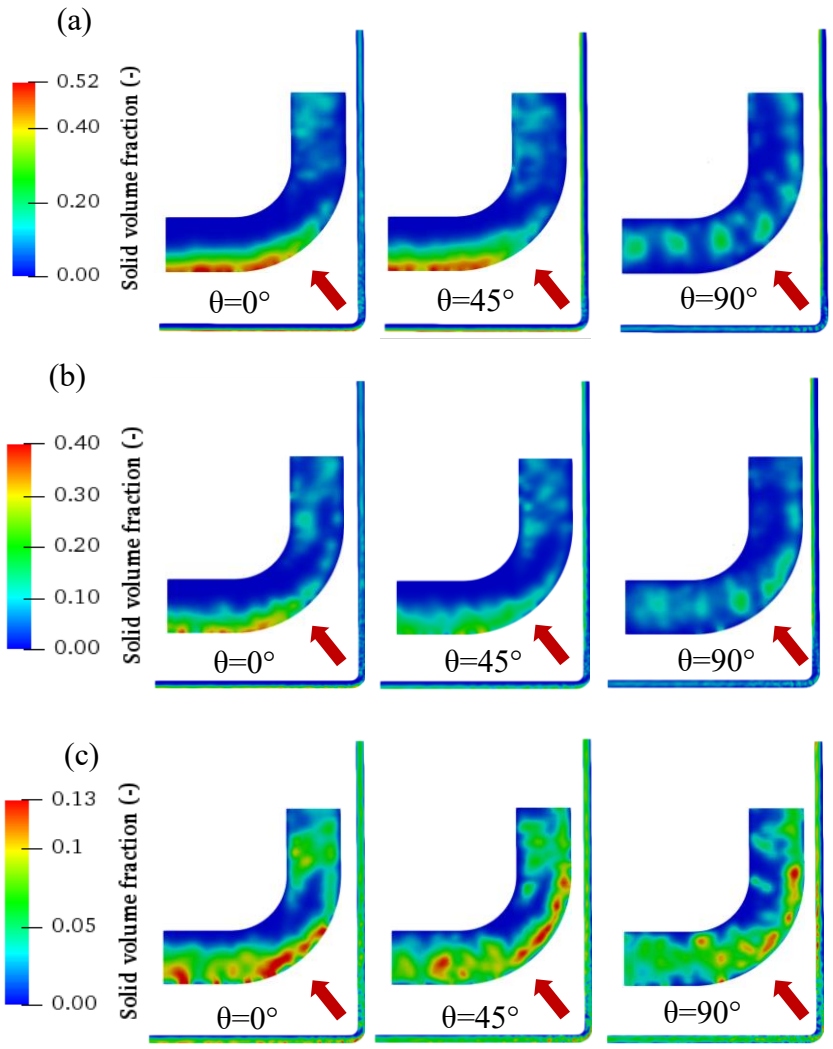

Figure 5-7 Contours of solid volume fraction in a central vertical plane for different flow regimes corresponding to Figure 3: (a) stationary-bed flow, (b) moving-bed flow, (c) pseudohomogeneous suspension flow

The contours of solid volume fraction in a central vertical plane for different flow regimes are presented in Figure 5-7. The position is x=2.8 m and z=0.06 m. For the 0-degree, it forms a particle bed and has a solid volume fraction of approximately 0.5, especially near the bottom

of the bend, as shown in Figure 5-7(a). When the pipe degree increases to 45-degree, the particle bed is thicker, and the maximum position of the solid volume fraction is changed. However, when the pipe degree turns to 90-degree, the particles becomes much looser and the solid volume fraction is decreased to 0.18. The reason is that for the 90-degree case, the inlet flow is in the vertical direction, which caused the particles to be more dispersed. Together with the lower conveying speed, particle clusters are finally observed. In Figure 5-7(b), flows here become much looser in all cases, as they are showing a moving-bed flow. For the 0-degree, the maximum solid volume fraction is 0.3. Similar phenomenon is also found here. With the increase of the pipe degree, the particle bed will firstly increase, then disperse, instated by the small clustered particles. It is worth noting that the increased conveying speed will decrease the clustered particles, and caused them to be distributed more uniformly. The results for the higher conveying speed are shown in Figure 5-7(c). As the conveying speed is high enough, the increased pipe degree did not change the particle bed too much, but the maximum position of the solid volume fraction is changed. In addition, the clusters become more dispersed, instated by uniform particle distribution, as the conveying speed increases.

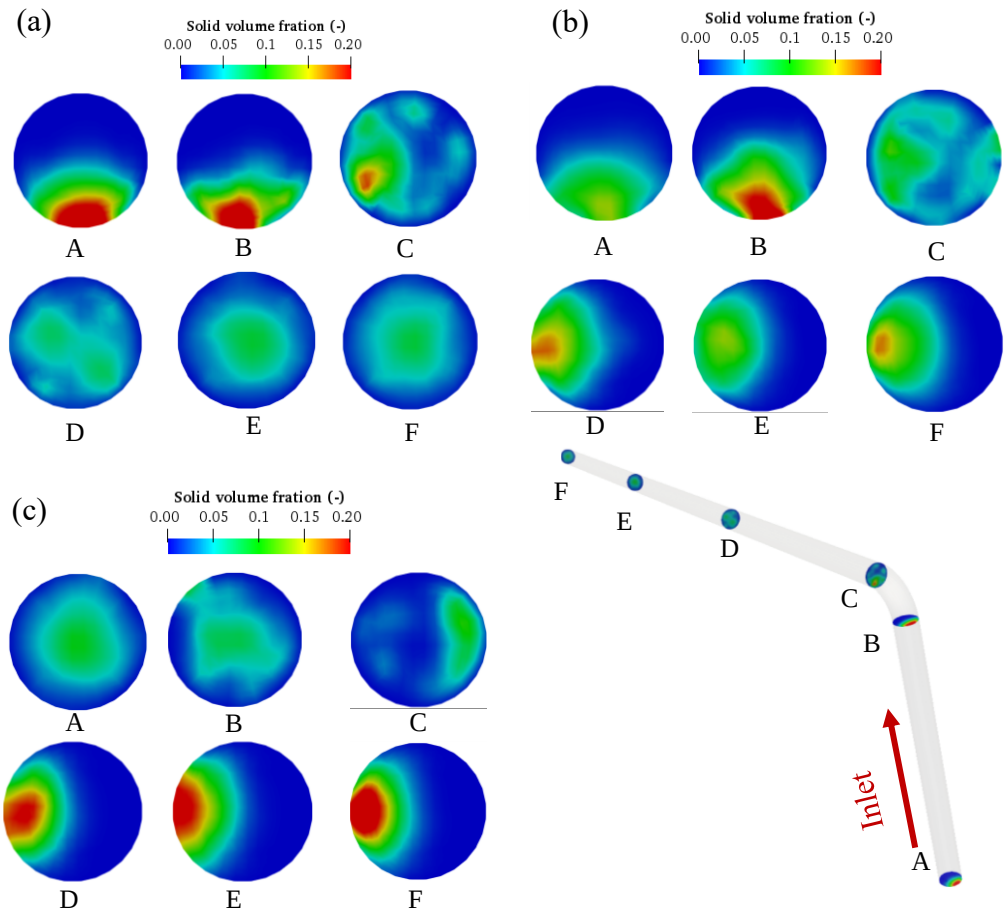

Figure 5-8 Effects of pipe orientation on mid cross-sectional contours of the temporal solid volume fraction spatial distribution at the locations between x=2.5 m and z=1.56m, d_p = 3.5 mm, C_v = 0.05, U_f = 2.0 m/s and t=7s: (a) θ=0°, (b) θ=45°, (c) θ=90°

Figure 5-8 demonstrates the effect of pipe orientation on the spatial distribution of the temporal solid volume fraction over the cross-section of the pipe at the locations between x=2.5 m and z=1.56 m at U_f = 2.0 m/s. For the case of θ=0°, the flow direction is from horizontal to vertical, and the solid volume fraction shows different distributions at different positions. From the inlet to the location before the bend, there is a higher solid volume fraction, as most particles are settled down at the bottom of the pipe. When the flow travels after the bend, the flow direction is parallel to the gravity. Particles tend to distribute more and more uniformly along the pipe, and most particles concentrate at the middle of the pipe, which is consistent with the previous

study in a vertical pipe [28], as shown in sections D-F. The results for the θ=45° at U_f = 2.0 m/s are presented in Figure 5-8(b). It is found that the spatial distribution of the solid volume fraction does not change too much between the front bend and the after-bend regions. Figure 5-8(c) shows the results for θ=90° at U_f = 2.0 m/s. Here the flow direction is from the vertical to horizontal direction. As the inlet flow is in the vertical direction, the inertia is larger so that the particles could move along the bend, and then settle down as the flow tends to be horizontal, as shown in sections D-F. These results are quite different from those of the case of θ=0°.

To deeply understand the effect of pipe orientation on solid volume fraction, Figure 5-9 shows the effects of pipe orientation on time-averaged solid volume fraction distribution at the whole pipe position with different conveying speeds. The result for stationary flow is shown in Figure 5-9(a), before the bend, when the pipe degree is increased to 45, the averaged solid volume fraction did not change too much, as the conveying speed is low, most particles are settled down at the bottom, however, when the pipe degree increases to 90, the averaged solid volume fraction is sharply descended, as the particles at 90 degree, the particle's gravity is perpendicular to the flow direction, which cause the particles to uniformly distribute so that the averaged solid volume fraction is lower than other degrees. After the bend, it is clearly noticed that the averaged solid volume fraction for the θ=45° is not changed too much comparing to the results before the bend, similar results are also obtained in moving-bend flow and pseudohomogeneous suspension flow, which are shown in Figures 5-9(b-c). The averaged solid volume fraction for θ=0° are sharply declined as the particles after the bend, moving to the vertical pipe, which will more easily discrete the particles, and particles tend to be uniformly distributed so that the average solid averaged fraction is smaller. On the contrary, for the θ=90°, after the bend, particles are moving from vertical direction to horizontal direction, as the conveying speed is quite low, most particles are settled down and form a thick particle bed so that the averaged solid volume fraction is increased. For the moving bed, which is shown

in Figure 5-9(b), before the bend, the increasing degree will cause the averaged solid volume fraction to decreases, as with the increased degree, particles are more easily suspended. However, after the bend, the results are opposite to the one before the bend as the flow direction is changed. The results for pseudohomogeneous suspension flow are presented in Figure 5-9(c), the effect of pipe orientation on averaged solid

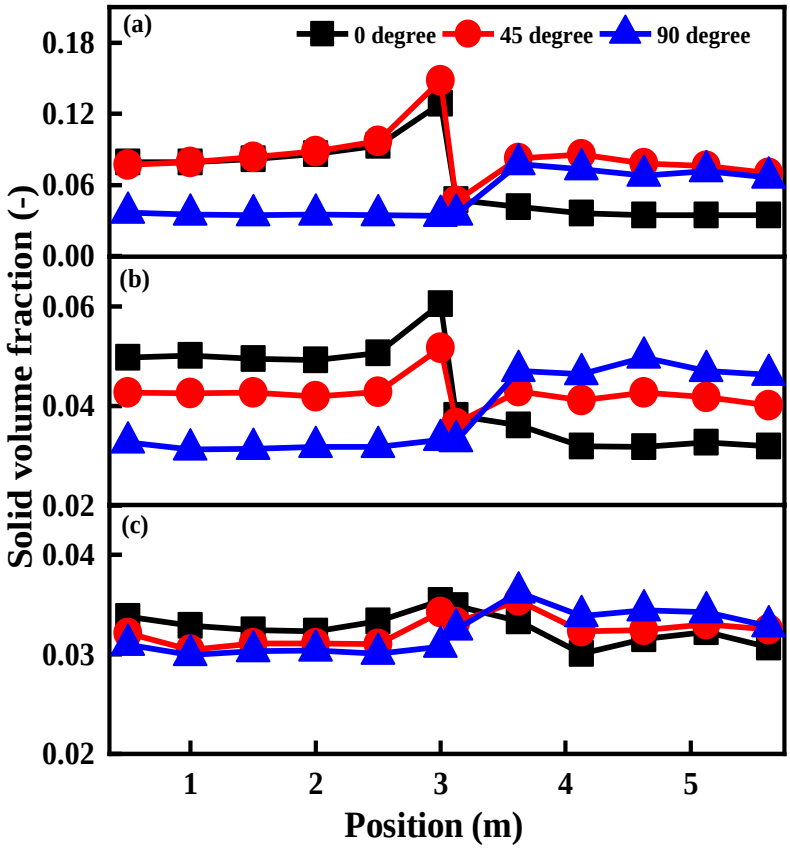

Figure 5-9 Effects of pipe orientation on time-averaged solid volume fraction distribution at the whole pipe position, d_p = 3.5 mm and C_v = 0.05: (a) U_f = 1.2 m/s, (b) U_f = 2.0 m/s, (c) U_f = 4.0 m/s

volume fraction is less comparing with other flows, as the conveying speed is high enough, it could easily cause particles to suspend in all different pipe orientations. Therefore, Figure 5-9 shows that the effect of pipe orientation on averaged solid volume fraction is dependent on different flow regimes.

5.4.5 Solid velocity

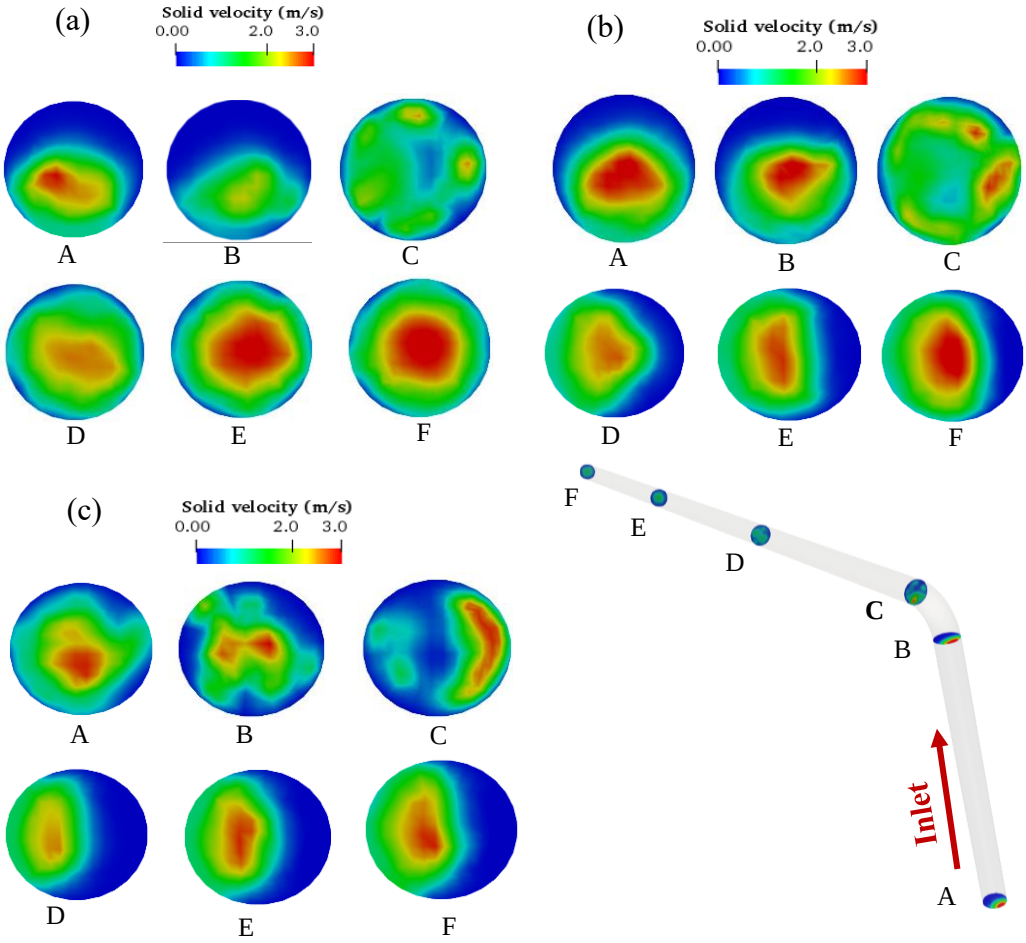

Figure 5-10 Effects of pipe orientation on mid cross-sectional contours of the temporal solid velocity spatial distribution at the locations between x=2.5 m and z=1.56m, d_p = 3.5 mm, C_v = 0.05, U_f = 2.0 m/s and t=7s: (a) θ=0°, (b) θ=45°, (c) θ=90°

In order to analyse how the pipe orientation affects the time-averaged spatial distribution of solid velocity on the cross-section of the pipe. Figure 5-10 is utilized here to illustrate. For the cross-sectional views A and B which are defined as before-bend, it is clearly seen that the increased pipe degree will produce a more uniform temporal solid velocity spatial distribution, and particles are easier to disperse. For the after-bend cross-sectional views D-F, the increasing pipe degree would cause the particles to settle down. As for the horizontal-vertically upward pipe (θ=0°), the direction of the gravity force is parallel to the flow direction so that the effect

is less, and particles are easier to distribute. However, for the horizontal-vertically upward inclined pipe (θ=45°) and vertical-horizontally upward pipe (θ=90°), due to the effect of the gravity force, particles are easier to be settled down. For the cross-sectional view C which is the sectional view of the bend exit, it shows that the maximum solid velocity is presented at the right side of the pipe for all cases, as when particles cross the bend due to the effect of inertia and centripetal force, particles are conveying along the outside of the bend so the velocity at the right side is higher.

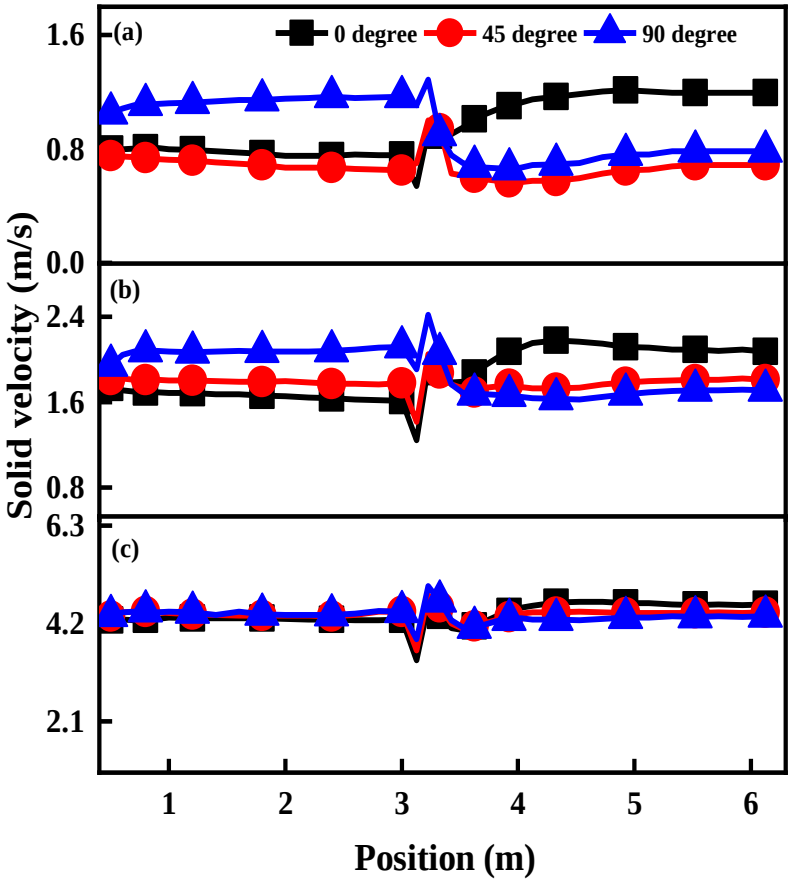

Figure 5-11 Effects of pipe orientation on time-averaged solid velocity at the whole pipe position, d_p = 3.5 mm and C_v = 0.05: (a) U_f = 1.2 m/s, (b) U_f = 2.0 m/s, (c) U_f = 4.0 m/s

To further analyse the effect of pipe orientation on different flow regimes, Figure 5-11 illustrates the time-averaged solid velocity at the whole pipe position with different conveying speeds and pipe orientations. For the stationary flow, when the degree θ=0°, the solid velocity

reaches stability at the position of 2 m, but suddenly decreases at the end of the bend, then sharply increases. It reaches stability again at the position of 4.5 m, as shown in Figure 9(a). However, for the horizontal-vertically upward inclined pipe (θ=45°), the situation after the bend is totally different from the case of horizontal-vertically upward pipe (θ=0°). It shows an increasing trend at the bend exit, then quickly decreases to reach stability at the position of 4.5 m. For the stable solid velocity, the solid velocity after the bend is similar to that before the bend. For the vertical- horizontally upward pipe (θ=90°), it shows an opposite trend to the horizontal-vertically upward pipe (θ=0°). As for these two cases, the direction is also opposite so that the results show an opposite trend. Before the bend, when the pipe degree increases, the averaged solid velocity firstly decreases then increases at the same position, corresponding to Figure 5-9(a). This is easily explained, as the lower solid velocity will show a higher solid volume fraction, since most particles are settled down at the bottom of the pipe. The increased pipe degree increases the particle bed, however as the conveying speed is so low that particles could not be able to suspend. As a result, most particles are still settled down to form a thick particle bed with quite low solid velocity. Such trend is changed oppositely after the bend. However, situations are totally different when the conveying speed is increased, in which a moving-bend-flow appears as shown in Figure 5-11(b) before the bend. It shows the increased pipe degrees will cause the averaged solid velocity increased, the trend is changed before the bend. The trend will not be changed too much when it conveys in a pseudohomogeneous suspension flow, which the result is presented in Figure 5-10(c). As the flow is already suspension, no matter the direction change, the flow regime will not be changed so that the results will show similarly. For the moving-bend and suspension flows, we notice that for all pipe orientation, after crossing the bend, it makes the particle solid velocity immediately increases then decreases to keep stable. The particle solid velocity will increase due to the effect of the inertia and gravity force.

5.4.6 Erosion wear

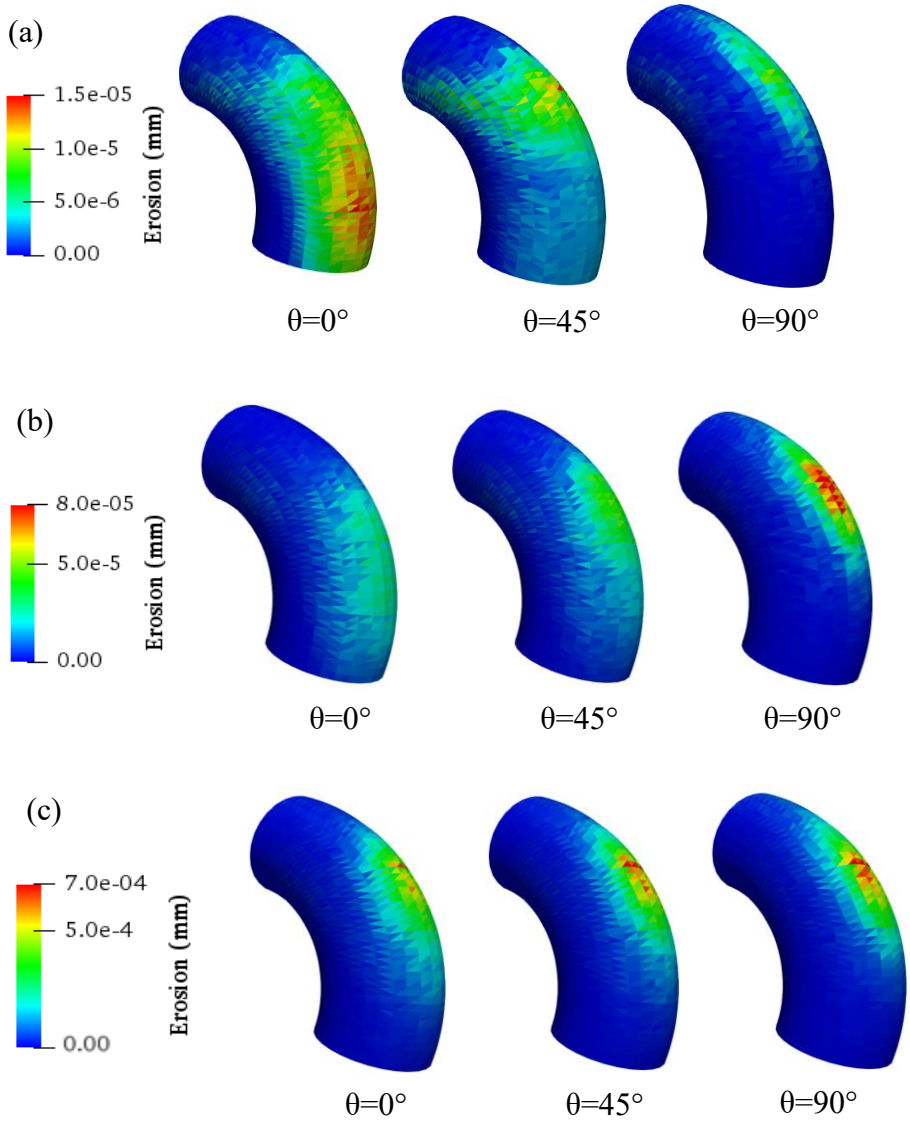

Figure 5-12 Effects of pipe orientation on whole bend sectional contours of the temporal erosion distribution at the bend locations between x=2.9 m and z=0.06m, d_p = 3.5 mm, C_v = 0.05,and t=7s: (a) U_f = 1.2 m/s, (b) U_f = 2.0 m/s, (c) U_f = 4.0 m/s

In this section, to analyze the effect of the pipe orientation on the erosion distribution for different flow regimes, simulations are conducted by changing the direction of the gravity force at each flow regimes. Generally, the flow regimes have a great effect on the erosion location. The temporal erosion distributions of the whole bend sectional contours with different

conveying speeds and pipe orientation are presented in Figure 5-12. The effect of conveying speed on the bend erosion position is firstly analysed with the pipe orientation fixed at horizontal-vertically upward pipe (θ=0°). The maximum flow speed is at the centerline of the pipe so that the corresponding impact velocity at the centerline of the pipe is also maximum. The maximum erosion location is shown at approximately an angle of 13° of the bend for U_f = 1.2 m/s (the angle is defined in Fig. 13(a)). When the conveying speed increases to 2.0 m/s, its maximum erosion location changes to be approximately 27° of the bend. The maximum erosion location is changed to 48° when the conveying speed is further increased to 4.0 m/s. Therefore, the conveying speed has significant effect on maximum erosion position. The reason for the position change is that the higher conveying speed will lead the particles to suspend and collide the bend with a higher velocity.

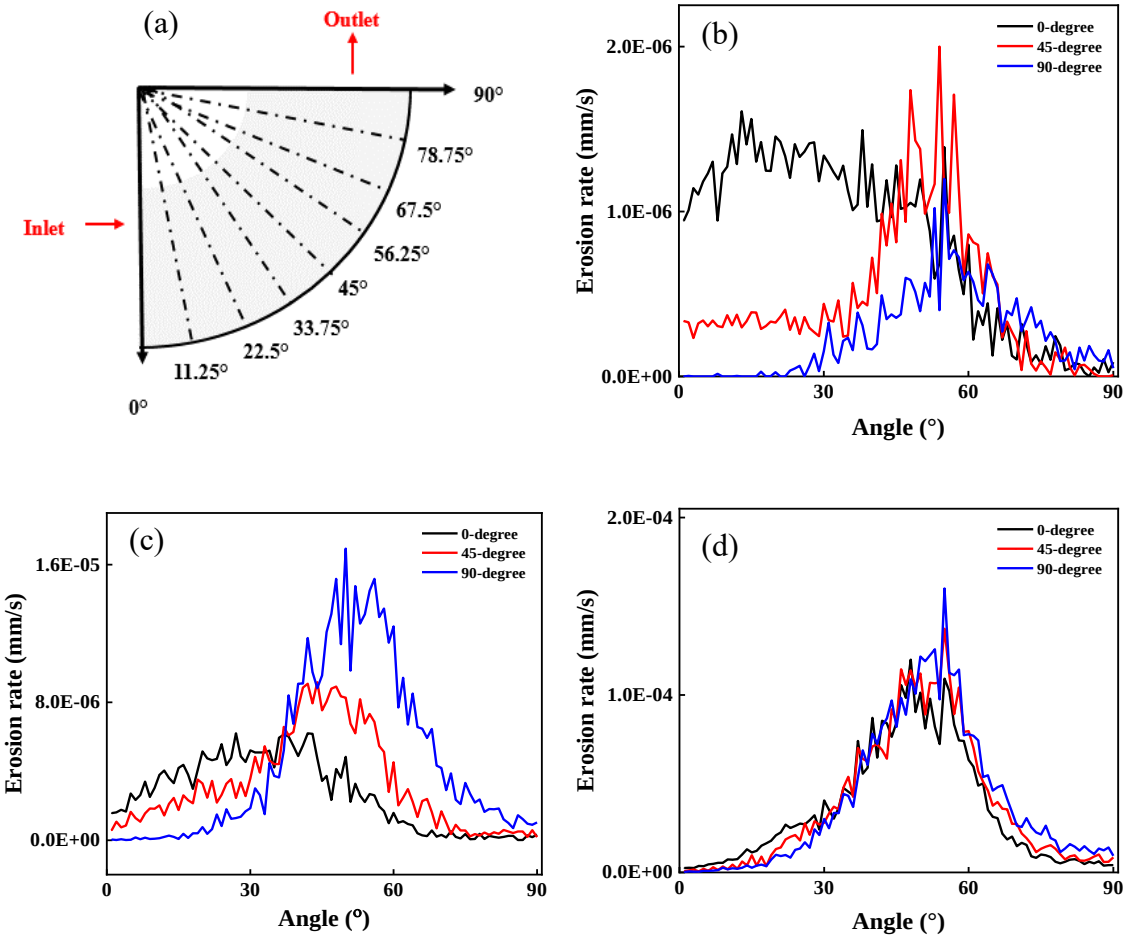

Figure 5-13 Effects of pipe orientation on time-averaged erosion rate distribution at different

conveying speeds, d_p = 3.5 mm and C_v = 0.05: (a)calculated angle defined, (b) U_f = 1.2 m/s, (c) U_f = 2.0 m/s, (d) U_f = 4.0 m/s

Figure 5-13 illustrates the time-averaged erosion rate distribution at different conveying speeds and pipe orientations versus the position in elbow. Firstly, it can be seen that the erosion rate is generally increased when the conveying speed is higher, for the pipe orientation is fixed. For deeper analyses, the pipe orientation is fixed at 0 degree, which means the flow direction is coming from horizontal pipe to vertical pipe. There are two observed peaks, for the U_f = 1.2 m/s, peaks are approximately 13° and 38° according to the trend of the lines, when the U_f = 2.0 m/s, peaks are approximately 38° and 54°, and when the U_f = 4.0 m/s, peaks are approximately 48° and 55°. The first peak is produced as the particles directly crash the bend from the horizontal pipe. The second peak is produced as the fluid–solid drag force, which lead the second peak moves to upstream as the conveying speed is increased, it means that from the inlet pipe, the lower layer particles directly crash on the elbow, which produces the first peak, and the second peak moves upstream, as the upper layer of particles is dragged deeper into the elbow, and also affected by the centripetal force.

Secondly, Figure 5-13 (b-d) shows the effect of pipe orientation on erosion rate distribution versus the position in the elbow at different flow regimes. It can be seen from that the maximum erosion rate in horizontal to vertically upward (θ=0°) is observed at approximately 27°, while the maximum erosion rate in horizontal to vertically upward (θ=45°) is observed at approximately 44°, and for the maximum erosion rate in the vertical to horizontally upward (θ=90°) is 50°. This indicates that the maximum erosion rate position in the elbows is indeed significantly affected by the pipe orientation, and the gravity force makes the maximum erosion rate position move deeper in a horizontal to vertically upward pipe. These phenomena are consistent with the experimental results of (Deng et al., 2005), who also indicated that the horizontal to vertically upward (θ=0°) pipe has the longest service life than other pipe

orientations. In horizontal to vertically upward (θ=0°) pipe, due to the effect of the gravity force, most particles are still conveyed at the bottom of the pipe. The particles crash the bend wall initially rather than conveying across the whole elbows so that the maximum erosion rate position is formed near the entrance of the elbows. However, for the vertical to horizontally upward (θ=90°) pipe, as the flow direction is parallel to the gravity force, particles are uniformly suspended within the whole pipe so that particle-particle collisions are less and the erosion rate distribution at the entrance of the bend is lower than that of the case of θ=0°. This suggests that high-frequency particle-particle collisions may decrease the particles directly crashing on the surface of pipe wall as mentioned by Andrews and Horsfield, (1983). However, when the conveying speed is high enough, pseudohomogeneous suspension flow appears as shown in Figure 5-13(d), it is found that the effect of pipe orientation on maximum erosion rate is lower. As when the flow regime already reaches a pseudohomogeneous suspension flow, particles are uniformly distributed and the effect of particle-particle collision is less so that the change in the pipe orientation may less affect the maximum erosion rate and position.

5.5 Conclusions

In this work, the influences of pipe orientation and conveying speed on bend hydraulic pipe are evaluated via CFD-DEM simulations. The main objective of this study is to investigate the flow characteristics and erosion phenomenon in bend hydraulic conveying pipe of coarse particles under varied pipe orientations. Through the analyses of the results, the major conclusions are shown as follows:

i. Wear model is successfully applied in the bend pipe, which shows a good agreement with experimental results.

ii. The different flow regimes in bend pipe determine the maximum erosion rate and the uniformity of wear. When the pipe orientation are 0º and 45º, for the stationary flow, most particles are concentrated at the bottom of the bend section, and the maximum erosion rate is produced at the lower position, when the flow changes to a moving bed flow, some particles tend to suspend, which caused the maximum erosion rate to move upward a little bit, when the flow changes to pseudohomogeneous suspension flow, all particles are uniformly discrete, and the maximum erosion rate moves upward again. However, when the pipe orientation is 90º, the flow regimes for three different conveying speed show similar behaviours, and position of the maximum erosion rate is not changed any more, only the value of maximum erosion rate is changed with the increasing conveying speed.

iii. Different pipe orientation would affect the maximum impact zones, erosion rate and pressure drop. When the conveying speed is not too high, the increasing pipe orientation would cause the particles to be uniformly discrete so that the position of maximum erosion rate is changed. However, if the particles show pseudohomogeneous suspension flow when the pipe orientation is 0º, then the increasing pipe orientation will not change the flow regimes, and the value and position of maximum erosion rate. For the same pipe orientation, the increasing conveying speed will cause the particles to be uniformly suspended along the pipe, and having a higher erosion rate.

CHAPTER 6 THE EFFECT OF BEND SHAPE ON HYDRAULIC BENDS

6.1 Introduction

Hydraulic conveying has been widely encountered in many industries, such as chemical engineering, food, mining, oil and petroleum industries due to its low operation and maintenance costs, friendliness to the environment, and unlimited transporting distance. It can handle a wide variety of particles that can be either coarse or fine. Also, it provides great layout flexibility by using bends to connect straight pipe sections in various ways. When the particle-fluid mixture enters the bend entrance, it generally continues to move straight ahead to the first impact zone, and then tilts towards the bend exit by an angle. The deflection angle depends on the bend shape, material properties and the operating conditions involved. In many designs, the material will hit one or more auxiliary impact zones before leaving the bend and reaccelerating to a fully suspended state after being straight or bent. During this process, additional pressure drop due to particle impact and reacceleration is added to the system (resulting in more energy consumption) and may cause severe bending erosion. Due to the above phenomena, bending is probably the most potential problem among all components of the hydraulic conveying system, and plays a vital role in affecting the overall performance of the system in terms of pressure drop, pipe wall erosion and conveying stability.

The importance of bend shape in pipeline system cannot be ignored. If they are not properly selected or designed, they will greatly affect the overall pressure drop and cause larger erosive wear, which will increase system maintenance cost (Dhodapkar et al., 2009). Some typical bend shapes are usually applied to study the flow regime, pressure drop and erosive wear. Firstly, the elbow bend pipe, the conveyed material may collide with the pipe wall multiple times, or it may slide along the outside radius, it will depend on the material properties or fluid velocity, and normally, the erosive wear occurs in the collision area. Secondly, the T pipe, it will be more specially, as the horizontal outlet is plugged it will allow the conveyed solids to

be accumulated. The advantages are it could decrease the incoming solids, and protect the horizontal outlet from erosion. However, the disadvantage is the T pipe needs lots of pressure drop to operate. Thirdly, the sharp pipe, which has a short turn radius, however, it will produce high particle attrition, as the particles directly impact on the pipe. For the solid-liquid system, as the flow regimes are totally different comparing with gas-solid system, therefore, the effect of bend shape on solid-liquid system should be analysed and discussed, and try to find an optimal bend design for solid-liquid system to decrease the pressure drop and erosive wear (Dhodapkar et al., 2009).

Some typical researches based on experiments are listed here: The effect of mean curvature radius over pipe diameter (R/D) ratio on the erosion wear was investigated by Blanchard et al., (1984) through the circulating loop system. Bourgoyne, (1989) also studied the effect of R/D ratio on the erosion rate of an elbow pipe, and analyses the maximum erosion angle. An experimental loop was applied by Wood et al., (2004) to study the erosion rates at straight and bend pipes. Giguère et al., (2009) characterized the effect of bend on flow regimes. Messa and Malavasi, (2014b), and Gupta et al., (1997) studied the solid distribution at the cross section of the bend and the distance required to achieve a developed flow.

The testing of erosion in experiments requires a very long time, however, the numerical method could quickly and effectively gain the erosion results. Generally, the numerical models that have been applied to hydraulic conveying can be continuum- or discrete-based according to different treatments of particles. They are represented by the Two-Fluid Model (TFM), and the combined approach of Computational Fluid Dynamics (CFD) and Discrete Element Method (DEM), respectively. The TFM approach treats both liquid and particles as continuous phases. It has been widely used to study hydraulic conveying of fine particles (Ling et al., 2003, Doroodchi et al., 2005, Eskin, 2005, Giguère et al., 2008, Kaushal et al., 2012, Capecelatro and Desjardins, 2013, Messa et al., 2014, Messa and Malavasi, 2014a, Messa and Malavasi, 2015,

Silva et al., 2015a, Ofei and Ismail, 2016, Messa and Matoušek, 2020). Some studies on bends are listed here: Wood et al., (2001) studied the effect of coarse particle on erosion wear through CFD method. Kannojiya et al., (2018) studied the effect of particle diameter on bend pipe with the CFD based method, in which the range of the particle diameter was 50 to 300 μm. Khan et al., (2019) applied the CFD method to study the effect of bend angle on erosion. Xie et al., (2020) investigated the effects of particle size and bend angle on bend pipe. Brown, (2002) used a CFD based method to study the erosion problem in T and pivoting elbow pipes, in which the particle size was 150 μm. Azimian and Bart, (2014) applied CFD method to study different variables on erosion rate through the elbow and T pipes.

However, the effective use of a TFM model depends on constitutive relations for the description of solid stresses, which have not been generally established (Jop et al., 2006). On the other hand, in the CFD-DEM approach, the liquid is modelled as the continuous phase, while particles are simulated as the discrete phase (Zhou et al., 2010). Correspondingly, it directly tracks the trajectories of the forces acting on individual particles and thus does not need the complex constitutive relations between the stress and strain of particles. Therefore, the CFD-DEM approach is theoretically more rational than the TFM approach, and it is valid over a wide range of flow conditions. (Kuang et al., 2019a, Kuang et al., 2018, Zhu et al., 2008, Zhu et al., 2007, Sakai et al., 2020b). Peretz and Levy, (2019) applied CFD-DEM method to study the effects of solid volume fraction and bend radius on bend pressure drop, and proposed a newly developed correlation equation for predicting pressure drop. Chen et al., (2015) applied CFD-DEM method to study the bend pipe with different bend angles on erosive wear with particle diameter of 150 μm. A new mathematical model based on CFD-DEM was established by Wang et al., (2017a) to predict the bends erosion in oil pipelines with the particle diameter of150 μm. Li et al., (2019) and Zhang et al., (2012) used CFD-DEM method to investigate the

effect of coarse particle diameter on erosive wear, in which the particle diameter was larger than 1 mm.

Among these studies, there was not much effort on studying the effect of bend shape on hydraulic bend. In this chapter, a hydraulic pipe conveying of coarse particles is studied by a recently reported CFD-DEM model (Zhou et al., 2019, Zhou et al., 2020). The validity of the erosive wear model is then verified. On this basis, the elbow pipe is defined as the standard pipe to be used to compare with other bend shapes, including sharp, sharp-135, T-90, T-135. Then, the simulation results for all bend shapes are analysed in detail in terms of particle characteristic performance both in macro and micro view, such as, pressure drop, solid volume fraction distribution, solid velocity and erosive wear.

6.2 Simulation methods and conditions

The current CFD-DEM model is the same as the one described in section 3.2 in Chapter 3. For more details please refer to section 3.2 in Chapter 3. The model is also outlined here for brevity. In this model, the motions of discrete particles are individually described using Newton's second law of motion and solved by DEM (Cundall and Strack, 1979) while the flow of the continuum liquid is described using Naiver-Stokes equations and solved by CFD based on the finite volume method (Ferziger and Peric, 2002). The coupling of CFD and DEM is realized according to Newton's Third law of motion, as detailed elsewhere (Xu and Yu, 1997).

6.3 Computational details

6.3.1 Numerical scheme

A finite volume method is used to discretise the governing equations, and a second-order Crank-Nicolson scheme (Moukalled et al., 2016) is used for the time integration. The

discretization of convection and diffusion terms is based on a second-order central differencing scheme (Wen et al., 2015). A PISO algorithm is taken for the velocity-pressure coupling. (Issa, 1985) The equations for a particle are explicitly integrated, and then the position and velocity of the particle are updated for the next coupling procedure.

The Rayleigh time Δt_R is referred to select the DEM time step:

$$\Delta t_R = \frac{\pi R_i}{0.1631\nu_i + 0.8766}\sqrt{\frac{2\rho_p(1+\nu_i)}{Y_i}} \quad (1)$$

where R_i, υ_i, ρ_p, Y_i, are, respectively, the radius, Poisson ratio, density and Young's modulus of particle i. Based on the particle properties that are used in this study, the time step of the solid phase is calculated as 1.509×10^{-4} s. As the Rayleigh time Δt_R is often larger than the DEM time step Δt_p (Issa, 1985), Δt_p is set as 1.0×10^{-5} s in the present study. Tsuji et al., (1993) mentioned that the time step of the fluid could be 10 ~100 times of the solid time step. Therefore, the CFD time-step is set as 1.0×10^{-4} s to reduce the computational time.

6.3.2 Configuration and boundary conditions

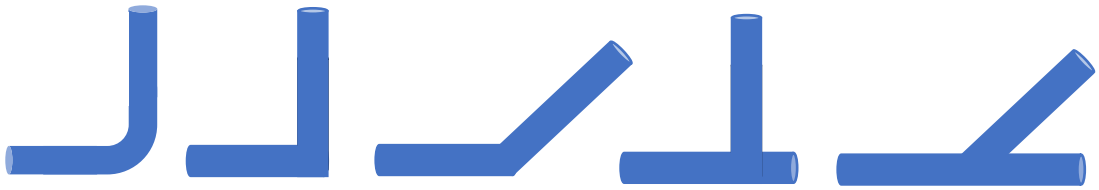

Figure 6-1 Schematic representation of varied bend geometries configuration: (a) standard, (b) sharp-90, (c) sharp-45, (d) T-90 and (e) T-45

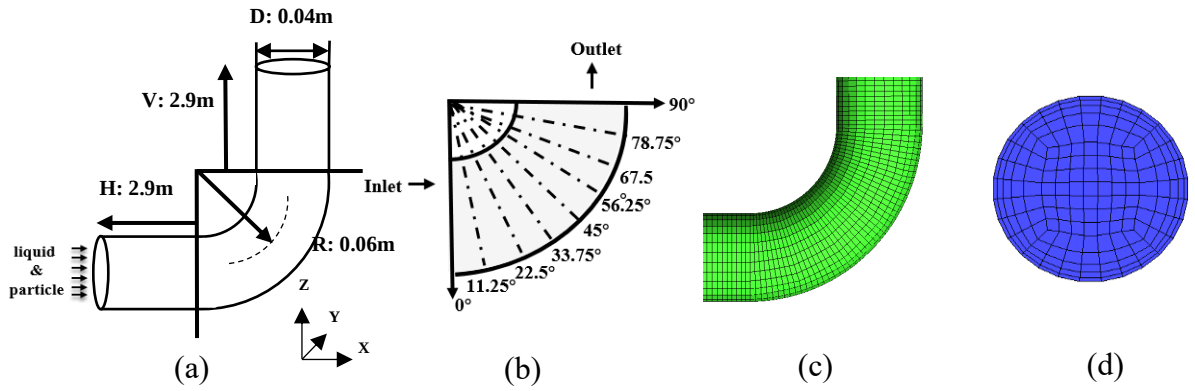

Figure 6-2 Schematic representation of the standard pipe simulated: (a) geometry configuration, (b) calculated angle defined, (c) computational grids on the bend, and (d) computational grids on a cross-section

In the current study, some typical bend geometries are chosen to be tested and discussed, all of them are widely used in gas-solid system. Figure 6-1 shows the various types of bend pipe, which include standard, sharp-90, sharp-45, T-90 and T-45 pipes. Figure 6-2 shows the schematic representation of the elbow pipe, which uses the standard pipe as an example. Figure 6-2(a) shows the simulated elbow pipe that has a length of 2.9 m both in horizontal and vertical direction, and a diameter of 40 mm. The calculated angle defined for the erosive wear is shown in Figure 6-2(b). The pipe is meshed with hexahedra via an O-grid scheme, as shown in Figure 6-2(c-d). With this mesh topology, the liquid flow near the wall can be better predicted by refining the grids. Table 6-1 lists the current computational conditions. The conveying speed of liquid-solid mixture (U_f) is 4.0 m/s; the feed solid concentration (C_v) is 0.05, and the particle density (ρ_{solid}) is 2482 kg/m^3. For each case, a uniform liquid velocity profile is specified at the inlet, and particles are injected with the same velocity as that of fluid. The number of particles injected into the pipe per second is calculated according to the given liquid flow rate and feed solid concentration (by volume). At the outlet, the normal gradients of all variables are set to zero for the liquid phase, assuming that the flow is fully developed there. Differently, when

particles are flowing out of the pipe outlet, they are removed directly from the simulation. A no-slip boundary condition is applied at the wall for the liquid flow. The results at the location of 2.8 m away from the inlet are chosen for analysing the radial profiles of flow features, while the section between x = 2.9 m and z = 0.06 m is considered for obtaining the erosive wear.

Table 6-1 Simulation conditions in the current study.

Validation case	
Gas density, (kg/m^3)	1.205
Gas velocity (m/s)	12
Particle mass flowrate, (kg/s)	0.01, 0.017
Particle diameter, (mm)	0.25
Particle density, (kg/m^3)	2482
Liquid flow	
Liquid density, (kg/m^3)	998
Liquid volume flow rate, (m^3/s)	0.00585
Liquid viscosity (kg/(m·s))	1.0×10^{-3}
Solid flow	
Material	Sand
Young's modular, (pa)	1×10^{7}
Poisson ratio	0.3
Particle diameter, (mm)	3.5
Conveying speed, (m^3/s)	1.2-4.0

Particle-wall sliding friction coefficient	0.3
Particle-particle sliding friction coefficient	0.1
Coefficient of restitution	0.65
Feed solid concentration (by volume)	0.1

6.4 Results and discussions

6.4.1 Model validation

To validate the current CFD-DEM model, the experimental data from two different applications have been considered. The first application considered the vertical and horizontal hydraulic conveying of coarse particles (Alajbegovi. et al., 1994, Gillies and Shook, 1994), where the measured and calculated radial profiles of solid volume fraction, axial liquid velocity and axial solid velocity are compared and reasonable agreement has been reported (Zhou et al., 2019, Zhou et al., 2020).

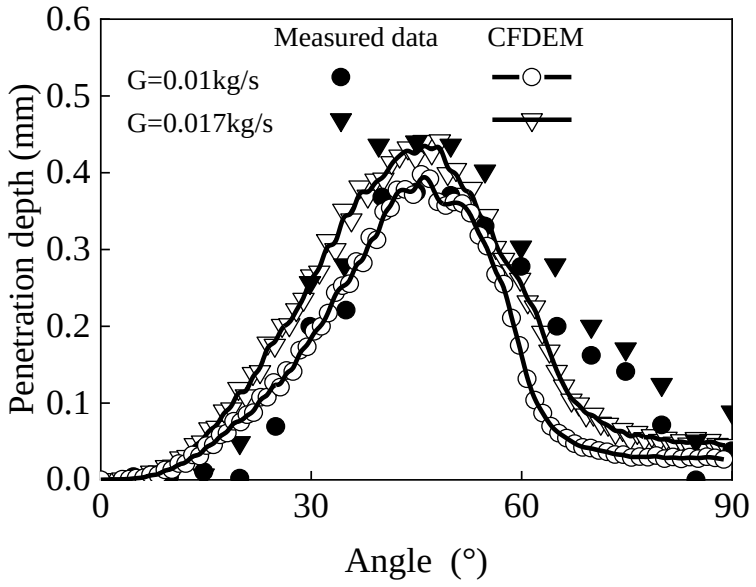

Figure 6-3 Comparison of predicted and measured (Zheng, 2016) penetration depth at different mass flowrate

The gas-solid experiment of Zheng, (2016) is used to further validate the erosion model and is presented in Table 6-1. Here the particle diameter is 0.25 mm with particle density of 2482 kg/m^3, and the injecting gas velocity is set to 12 m/s with two different particle mass flow rates. Figure 6-3 compares the predicted and measured penetration depth in the bend pipe with the

measurements under two different mass flowrate conditions after reaching stable status. In this comparison, the time averaged data at the central line (y-direction) on the cross section of the pipe are considered at the bend section. It is evident that the current erosion model can well predict the measured trends under all the conditions. These validations give us more confidence in the analysis of the following results.

6.4.2 Effect of bend geometry

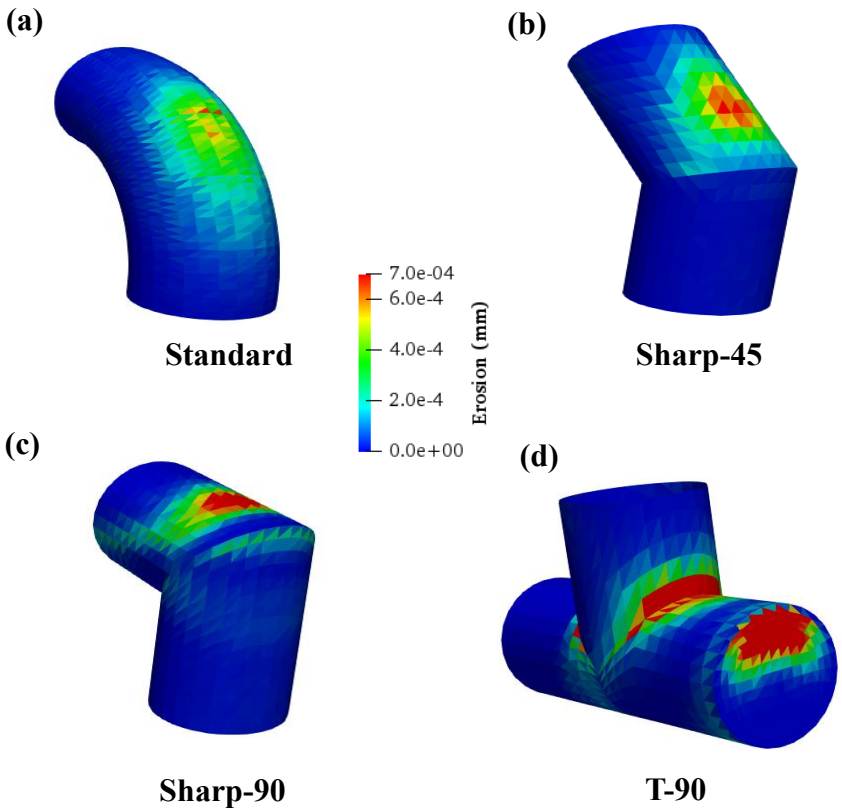

Figure 6-4 Effects of bend geometry on whole bend sectional contours of the temporal erosion distribution at the pipe locations between x=2.9 m and z=0.26m, d_p = 3.5 mm, C_v = 0.05, and t=7s: (a) standard, (b) sharp-45, (c)sharp-90, (d) T-90

Figure 6-4 shows the contour of erosion distribution for different bend geometry. It is clearly seen that the bend geometry plays an important role in erosive distribution, not only the

maximum erosive position is different, but also the erosive area. From the figure, it could be found that the erosion for the T-90 pipe is very high, which is converse with the results in gas-solid velocity. Similar results were also found by Azimian and Bart, (2014). For the T-90 pipe in solid-liquid system, the erosive wear at the blinded section is very high, comparing with other types, for deeper understanding, the quantitative analysis on erosive wear is needed.

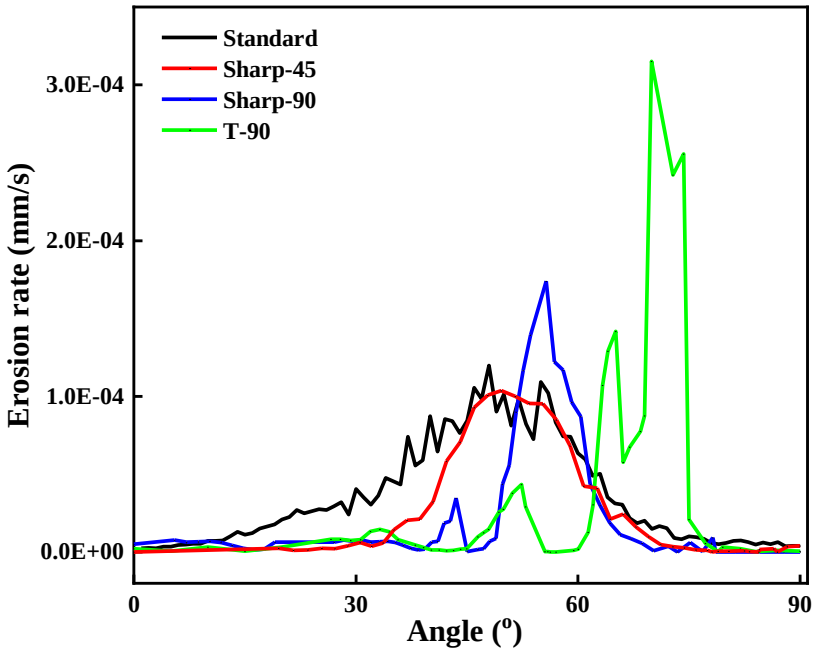

Figure 6-5 Effects of bend geometry on time-averaged erosion rate distribution at U_f =4.0m/s, d_p = 3.5 mm and C_v = 0.05

A quantitative analysis on erosive wear is presented in Figure 6-5, which clearly shows the effect of bend geometry on time-averaged erosion rate. Among these different bend geometries, the T-90 is the largest one, in which the maximum erosion rate is $3.15e^{-4}$ mm/s, and there are three peaks in T-90 pipe, as its geometry is more complex than others, they are 52°, 65°, 70°, separately. The sharp-90 pipe is the second one, in which the maximum erosion rate reaches $1.74\ e^{-4}$ mm/s, it has two peaks, they are 44°, 56°. The third one is the standard elbow pipe, in which the maximum erosion rate is $1.20\ e^{-4}$, and located at 48°, another peak is located at 55°. The maximum erosion rate for the sharp-45 pipe has the lowest value, which is $1.04e^{-4}$ mm/s,

and the location is at 50°. In addition, Figure 6-4 also shows the effect of bend geometry on the erosion rate zone is quite different, for the standard elbow pipe, most erosion rate is located between 13° to 74°, for the sharp-90 pipe, the location is changed to two zones, which are 40° to 45°, and 47° to 70°, for the sharp-45 pipe, the position is changed to 34° to 70°, and for the T-90 pipe, it also has two impacted zones, which are the 43° to 55°, and 60° to 74°. According to Figure 6-5, Table 6-2 is listed here to show the total erosion rate of various bend pipes. It shows that the standard elbow pipe has the largest total erosion rate, which is 3.20 e^{-3} mm/s, followed by the T-90 pipe, which the total erosion rate is 1.87 e^{-3} mm/s, the sharp-90 pipe is 1.41 e^{-3} mm/s, and the sharp-45 pipe has the lowest total erosion rate, which is 1.17 e^{-3} mm/s.

Table 6-2 Total erosion rate for varied bend geometries.

Type	Total erosion rate (mm/s)
Standard	$3.20e^{-3}$
Sharp-45	$1.17e^{-3}$
Sharp-90	$1.41e^{-3}$
T-90	$1.87e^{-3}$

Combining Figure 6-5 and Table 6-2, it is clearly shown that the effect of pipe angle plays an important role in solid-liquid system, and the sharp-45 has the lowest total erosion rate and the maximum erosion rate. The standard elbow pipe has the highest total erosion rate, but its maximum erosion rate is not too large, comparing with others. To consider a better bend pipe design, not only the erosion rate needs to be considered, but also the pressure drop, which plays an important role in whole pipeline system, as it would affect energy consumption.

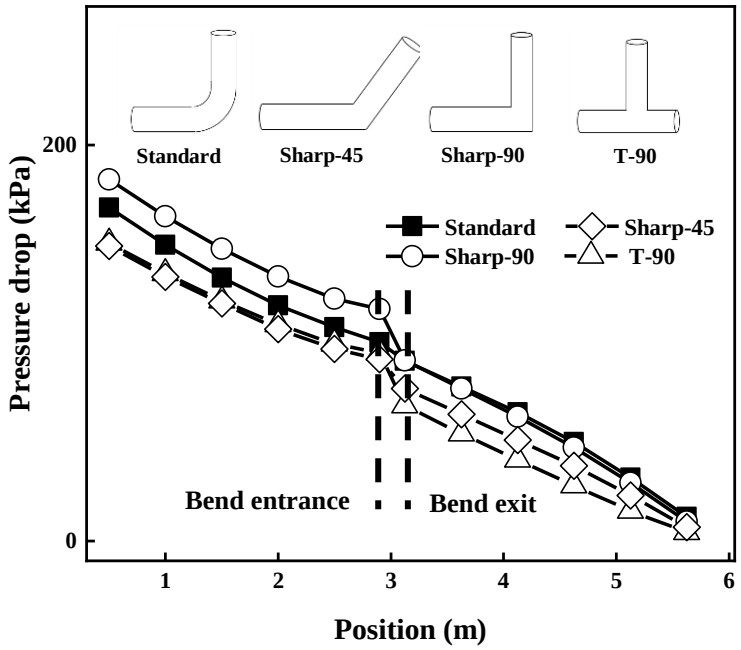

Figure 6-6 Phase diagram showing the variation of pressure drop versus varied bend geometry at same flow conditions

The phase diagram of the variation of pressure drop with varied bend geometries is presented in Figure 6-6. The trend of pressure drops for each bend geometry is quite different. Firstly, for the sharp-45 pipe, the pressure drop before the bend entrance, it has the lowest value, and shows a linearly decreasing trend, after the fluid conveys to the bend, it decreased down more slowly, comparing with sharp-90 pipe, then also shows a linearly decreasing trend, but the value for the pressure drop is still lower than standard and sharp-90 pipes. For the sharp-90 pipe, before the bend entrance, it has the highest value for all position, after the fluid conveys to the bend, the pressure drop is sharply decreased, and then turns to linearly decreased. It is interesting that, the T-90 pipe has the lowest pressure drop in both sections, before and after the bend. During the bend section, it shows a similar trend with sharp-90 pipe, the pressure drop is suddenly decreasing.

It is clearly seen that the effect of bend geometry plays an important role in erosion wear and pressure drop. To understand the formation of the erosion, and the peaks point, particle and fluid behaviours could be used to explain these phenomena, which will be discussed below.

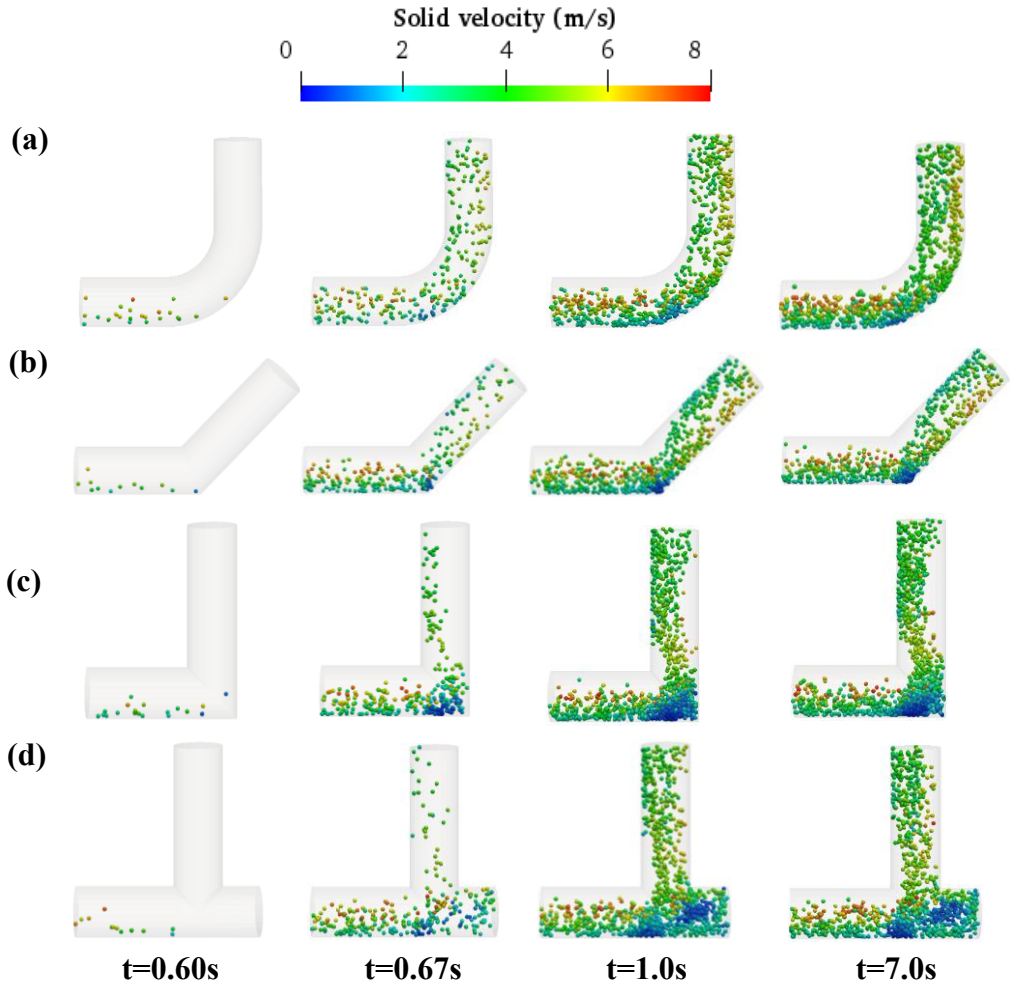

Figure 6-7 Snapshots showing the formation of the flow regimes for varied bend geometries in the pipe section between x=2.8 and z=0.26 at different times for d_p = 3.5 mm and C_v= 0.05: (a) standard, (b) sharp-45, (c) sharp-90, and (d) T-90

In solid-gas system, the T-90 pipe is normally used as it could plug the particles at the blind section so that the erosion rate at the blind section could be decreased, but the pressure drop is very high, as lots of particles are losing their momentum, and have to reaccelerate in the downstream of the bend. However, such results are inversed in solid-liquid system. In order to

understand the mechanism, the formation of flow regimes for varied bend geometries are shown in Figure 6-7. Figure 6-7 (b) presents the sharp-45 pipe, the degree of vertical pipe is changed to 45º, it shows there still has less particles convey with a very low velocity at the corner of the two pipes connected section. However, when particles move to the vertical section, they are quickly suspended to the whole pipe. From the figure, we could see that, for the sharp-90 pipe, which is indicated in Figure 6-7 (c), the particles will directly collide to the vertical pipe, leading to some of them slowing down, and forms a particle bed at the corner of the pipe, but the particles are not plugged so here are still lots of particles that are moving to upstream pipe. After the particles moved to the vertical pipe, the particles tend to move on the left side first, then turns to suspend across the whole pipe, this is due to the particle rebound effect, the particles convey with a very high velocity in horizontal pipe, then collide to the vertical pipe, the effects of higher velocity and inertia cause the particles to rebound to the other side. Comparing with the sharp-45 pipe, the decreased pipe degree causes the particles to move to the second pipe more softly, and not change the flow regime too much. The T-90 pipe is shown in Figure 6-7 (d), at the blind section, the plugged particles are not formed, there are only few particles having very low velocity. Similarly, with sharp-90 pipe, it has two normal peaks, the third peak is produced as the particles collide to the blind section. In Figure 6-7, for cases when the simulated time is after 1.0 s, the flow regimes for the bend section is not changed to much comparing with the snapshots at t=7.0 s. For deeper understanding of the flow behaviours, analysis of the solid and liquid velocities, as well as solid volume fraction will be discussed below.

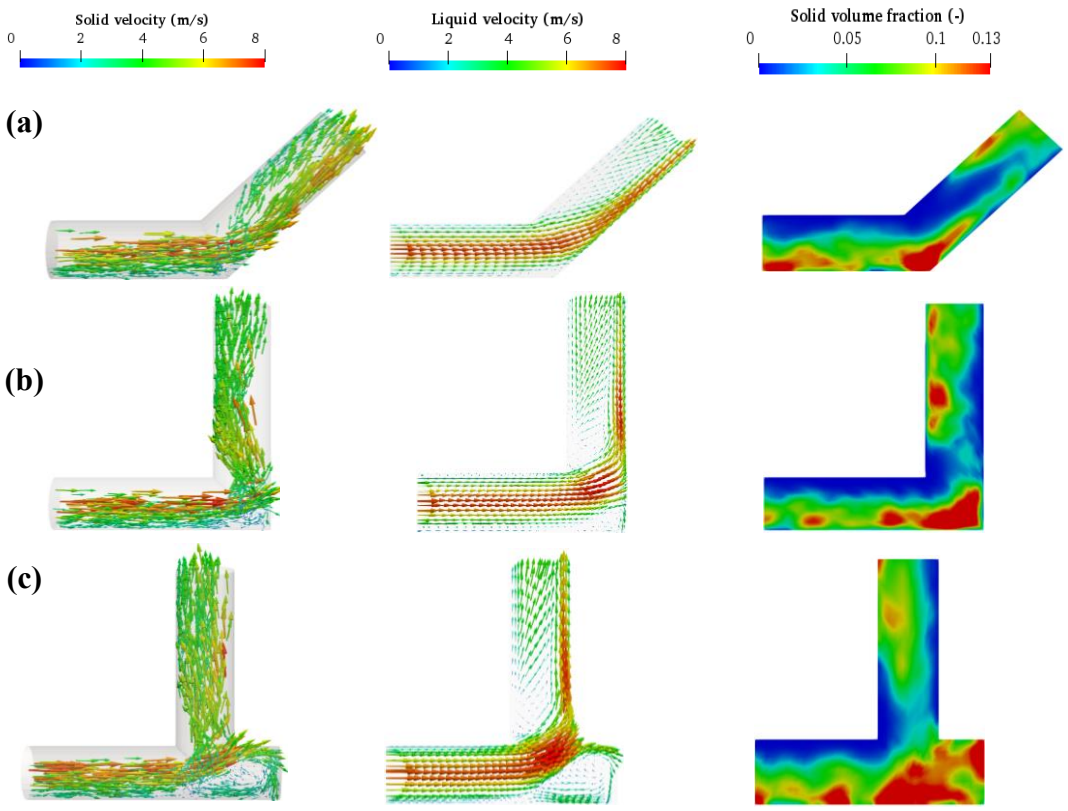

Figure 6-8 Contours of solid velocity (left), liquid velocity (middle) and solid volume fraction (right) in the central vertical plane at x=2.8m, z=0.26m for different bend geometries. (a) sharp-45, (b) sharp-90, and (c) T-90

Figure 6-8 presents the contours for solid and liquid velocities and solid volume fraction for different bend geometries. Firstly, Figure 6-8(a) shows the results of sharp-45 pipe, firstly, the particles will also collide the pipe directly, when they move to the next section, as the angle between the inclined pipe to the surface is decreased, the flow regime in the inclined section is not changed. The sharp-90 pipe is listed in Figure 6-8 (b), similarly with sharp-45 pipe, the conveyed fluid directly collides to the vertical pipe, then due to the effects of rebound and inertia, particles tend to move on the left side of the vertical pipe then uniformed discrete, and there are few particles existed at the corner of the pipe with a very low velocity, near to zero, and the solid volume fraction for the corner section is larger than 0.13, to link with Figure 6-5, it could be explained that why the sharp-90 has two peaks for the erosion. Comparing with

sharp-45 pipe, the decreased pipe degree causes the particle bed at the corner section to decrease. T-90 pipe is presented in Figure 6-8(c), both the results in solid and liquid velocities indicate that although the solid volume fraction at the blind section is significantly larger, and the distribution is also wider, there is no existing plugged particles at the blind section, instead, it produces a recycle flow, in which the particle conveys with a higher velocity to collide the pipe, then crosses to the blind section, the particle velocity is decreased and moves to the bottom, then moves to the vertical pipe. To link with Figure 6-5, as the flow at the blind section is recycle so that there will produce a higher erosion wear at the bottom of the pipe, and another one is located at the end section of the horizontal pipe, as the particles are directly colliding to it.

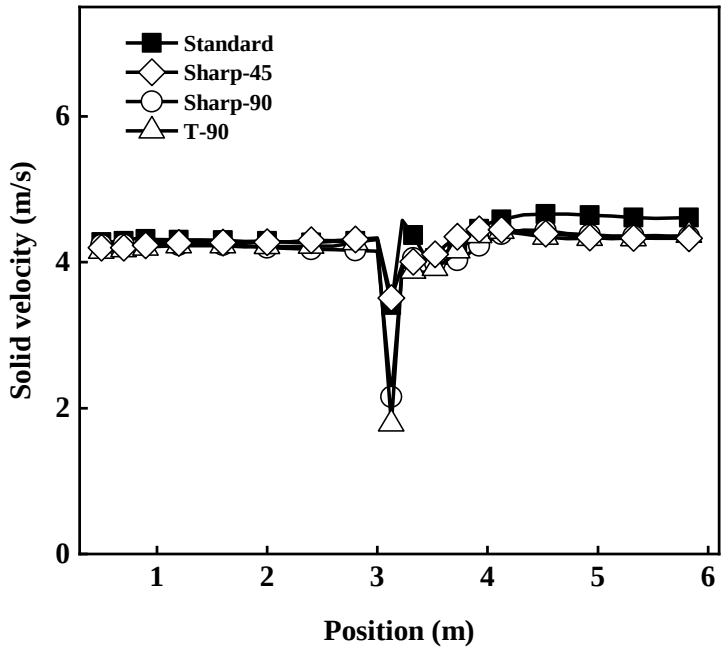

Figure 6-9 Effect of varied bend geometries on time-averaged solid velocity at the whole pipe position, d_p = 3.5 mm and C_v = 0.05

To further analyse the effect of bend geometries on solid-liquid system, Figure 6-9 illustrates the time-averaged solid velocity at the whole pipe position with different bend geometries. It is clearly seen that before the bend, the averaged solid velocity along the pipe is not changed

too much, and the system could quickly get a stable status, after crossing the bend, the solid velocity at the bend exit is quite different, the T-90 has the lowest averaged solid velocity, which is around 1.8 m/s, corresponding to Figure 6-8(c), it is not hard to understand, as there are some particles settled down at the bottom of the pipe, in which the solid velocity is nearly zero so that causes the averaged solid velocity to decrease. The sharp-90 also has a very low averaged solid velocity at the bend exit, similar to T-90 pipe. On the contrary, the averaged solid velocity at bend exit for the sharp-45 is not decreased too much. After crossing the bend, all of them will have an acceleration stage, and the system quickly reaches stable status at position 4 m, then the averaged solid velocity is kept the same, not changed anymore. After analysing the solid velocity distribution in different pipe position, the section after the bend is found to be quite important, the following results will focus on some typical position in after-bend section (vertical direction), they are the bend exit (z=0.06 m), the unstable section (z=0.56 m), and the stable section (z=1.56 m).

Figure 6-10 illustrates the mid cross-sectional contours of the temporal solid volume fraction spatial distribution at the locations i (z=1.56 m), ii (z=0.56 m) and iii (z=0.06m) with different bend geometries. For the sharp-90 pipe, which is presented in Figure 6-10(a), for the bend exit (iii), the solid volume fraction is higher near the inside wall, which is larger than 0.13, and from the contour, it could also be seen that most particles tends to move on the left side, this is due to the effect of the particles rebound, such results is corresponding to Figure 6-8(a). When the particles are moving upward, for the unstable section (ii), due to the effect of gravity force, particles tend to be discrete, but not uniformly distributed. When the particles continue moving upward, for the stable section (i), the particles are totally suspended across the whole pipe, as the spatial distribution of solid volume fraction is quite uniform. Most particles are concentrated at the middle of the pipe. For the sharp-45 pipe, which is presented in Figure 6-10(b), at the bend exit, most particles are concentrated at the inside wall, when the particles

continues to move upward, most particles tends to settle down, for this pipe, the vertical pipe has 45 degree from the surface, although its conveying speeds is quite high, due of the effect of gravity force, the particles still needs to overcome the gravity to move upward, so the particles could not be discrete uniformly. Such stage is not changed when the particles are moving to the stable section. The results for the T-90 pipe is demonstrated in Figure 6-10(c), for the bend exit, the distribution solid volume fraction is quite different comparing with the others, the maximum is also near the inside wall, but the distribution is more averaged, when particles are moving upward, particles are quickly suspended along the whole pipe. After analysing the solid volume fraction spatial distribution with three different position, the phenomenon on bend exit and stable section are quite different, therefore, the following results will only be focused on bend exit (z=0.06 m) and the stable section (z=1.56 m).

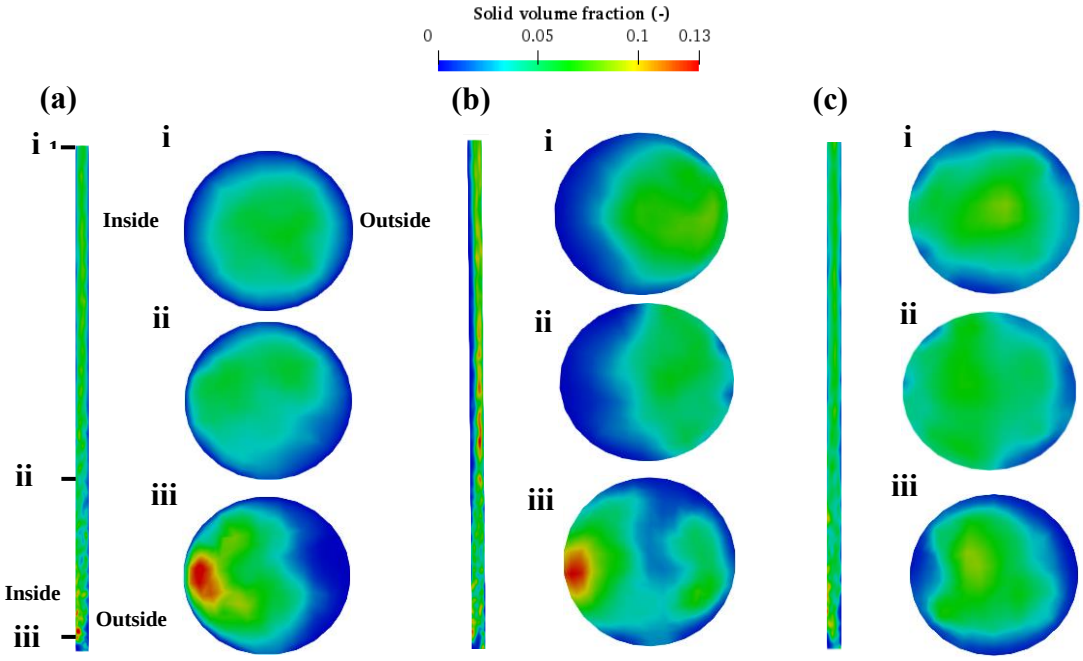

Figure 6-10 Effects of bend geometries on mid cross-sectional contours of the temporal solid volume fraction spatial distribution at the position i (z=1.56 m), ii (z=0.56 m) and iii (z=0.06m), d_p = 3.5 mm, C_v = 0.05, U_f = 4.0 m/s and t=7s: (a) sharp-90, (b) sharp-45, (c) T-90

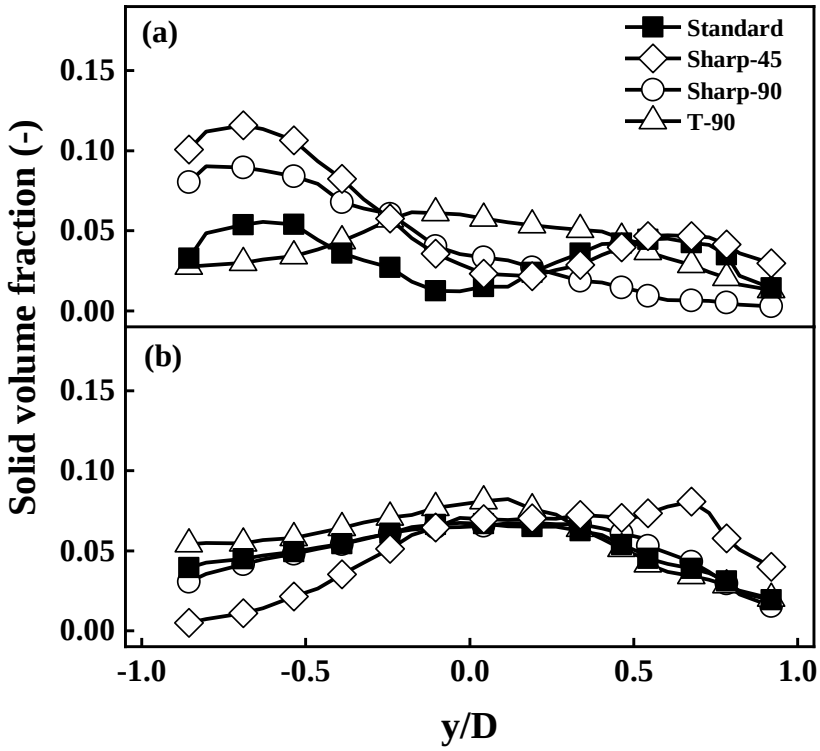

Figure 6-11 Effects of bend geometry on time-averaged solid volume fraction at U_f =4.0m/s, d_p = 3.5 mm and C_v = 0.05, (a) z=0.06m and (b) z=1.56m

In order to quantitatively analyse the solid volume fraction, Figure 6-11 is presented here to illustrate the solid volume fraction distribution at the radial position at two different locations. In Figure 6-11 (a), it is shown the position at z=0.06 m, for the sharp-45 and sharp-90 pipes, the highest solid volume fraction for both of them is located near the inside wall, and the value is 0.12 and 0.09, separately, this results is affected by the effect of the particles rebound when they directly collide to the vertical pipe, the difference is when the pipe degree decreased, there exists two peaks of the solid volume fraction, one near the inside wall, another one is near the outside wall. For the T-90 pipe, it has a blind section, the effect of particle rebound is a little decreased so the highest solid volume fraction is not located near the inside wall, and at the same time, the maximum value of solid volume fraction is decreased to 0.06, the trends turns to more uniform distribution, comparing with sharp pipes. Such results are corresponding to Figures 6-8 and 6-10. Figure 6-11(b) presents the solid volume fraction with radial position at

z=1.56 m, when the system reaches stable status, all pipes, except sharp-45 pipe, show a symmetry trend of solid volume fraction distribution at radial position, which is agreed with the analyses in vertical pipe in previous study. For the sharp-45, when the pipe degree decreased, the maximum solid volume fraction is located at y/D=0.68, which is near the bottom of the outside wall, and the value for the solid volume fraction is 0.08, as lots of particles are settled at the bottom of the pipe, the value for the solid volume fraction near the inside wall is decreased, such trend is quite similar with the results in horizontal pipe.

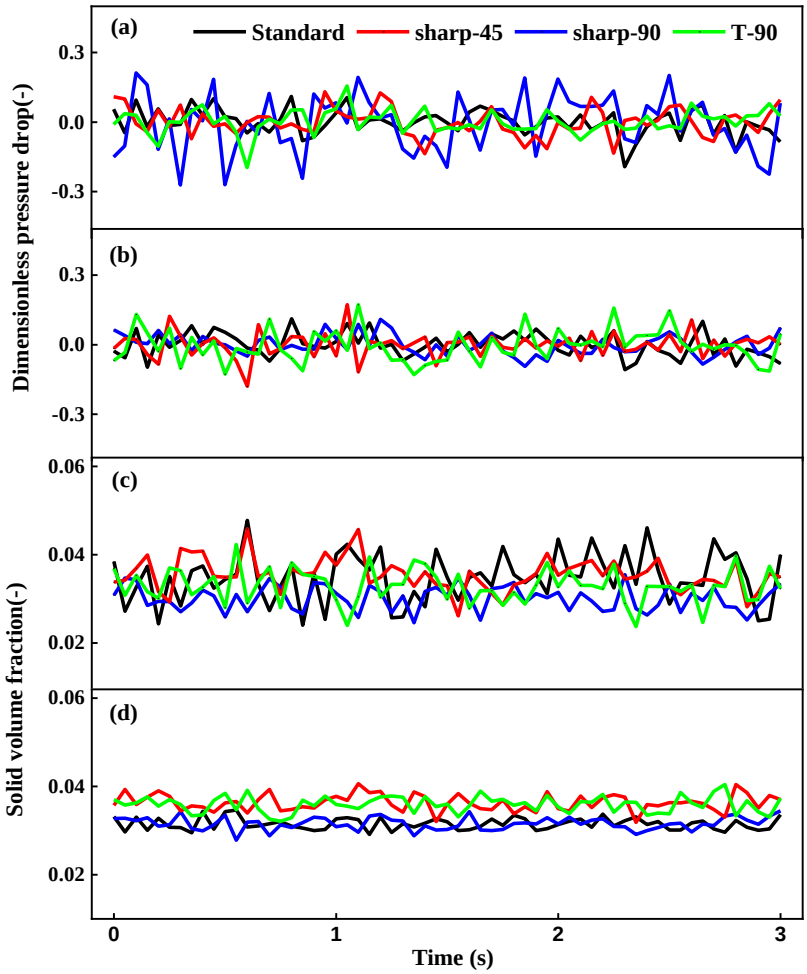

Figure 6-12 Temporal variations of dimensionless pressure drop (a-b) and solid volume fraction (c-d) for d_p = 3.5mm and C_v = 0.05 for different bend geometries: (a,c) z=0.06m, and (b, d) z=1.56m

Figure 6-12 shows the variations of the dimensionless pressure drop and solid volume fraction with different bend geometries at the locations z=0.06 m and z=1.56 m with time. In this figure, the results are averaged over the cross-section. Expectedly, when the flow at the bend exit, significant fluctuations are observed for both solid volume fraction and pressure drop, which is attributed to the presence of particles clusters. Differently, the dimensionless pressure drop and solid volume fraction do not fluctuate much in the stable section. Here, the relatively significant fluctuations are caused mainly by the varying flow structure at the bend exit. When particles move to the upward and get stable status, as the conveying speed is quite high, and particles are discrete relative uniformed so that the fluctuations in dimensionless pressure drop and the solid volume fraction are relatively small.

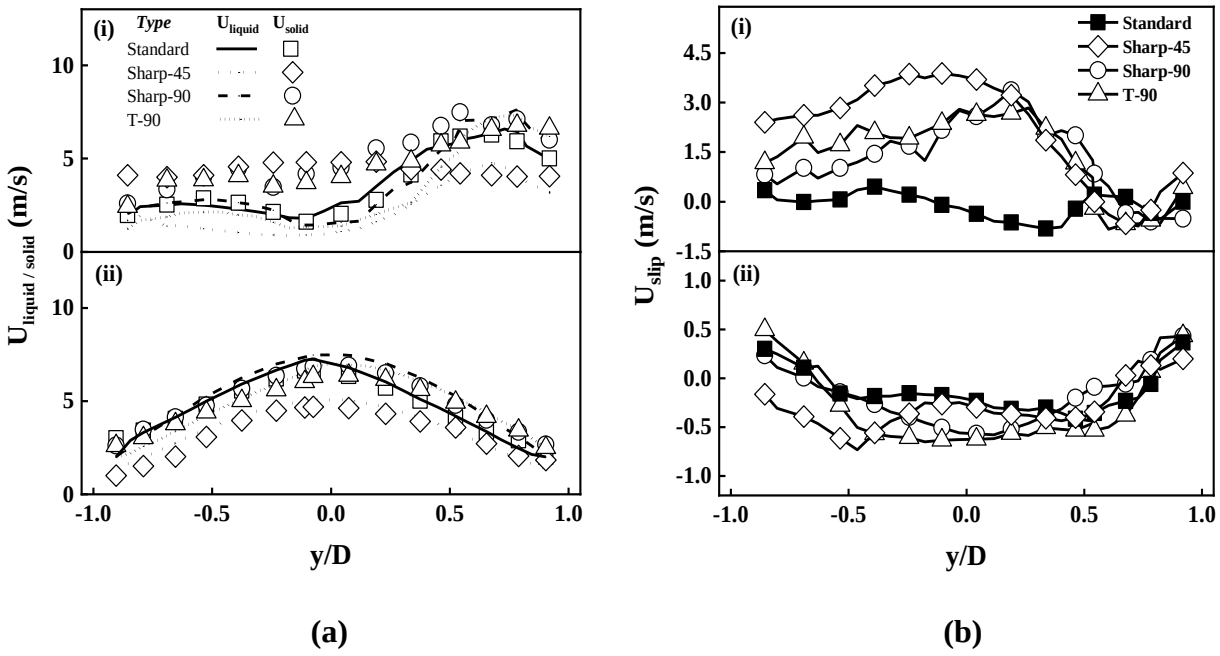

Figure 6-13 Effects of bend geometry on time-averaged liquid velocity, solid velocity and slip velocity distributions at different positions, i (z=0.06 m), and ii (z=1.56 m) with U_f =4.0m/s, d_p = 3.5 mm and C_v = 0.05. (a) liquid and solid velocities, and (b) slip velocity

Figure 6-13 (a) shows the liquid and solid velocities distribution at radial direction with different position, for the bend exit (i), after crossing the bend, the reaccelerated effect causes

the solid velocity to be higher than liquid velocity. For the stable section (ii), expectedly, the velocity profiled of two phases are similar due to the strong entrainment of liquid on particles. For the sharp-45 pipe, the maximum velocities for liquid and solid are not higher than other pipes, corresponding to Figure 6-11, the lower liquid velocity and solid velocity also leads to the decrease of solid volume fraction.

Figure 6-13(b) shows how bend geometry affects slip velocity. Firstly, for the bend exit (i), the trends of slip velocity distribution for all pipes are quite different, the solid velocity is higher than liquid velocity from the inside wall to the central region, except the standard pipe. The movement for the standard pipe is not changed too much as the elbow section in standard pipe plays an important role to decrease the effect of inertia, and it has enough length to cause the particles to reaccelerate and smoothly move to the vertical pipe. For the stable section (ii), overall, particles are observed to move faster than fluid near the wall but slower in the central region. This result can be explained as follows. A non-slip velocity boundary condition is applied to the fluid phase at the wall leading to zero liquid velocity there. Conversely, particles can slide on the wall surface. These different boundary conditions of fluid and solid phases account for faster particles than fluid near the wall. As the radial distance from the wall to the centre increases, the wall effect on fluid becomes less significant, the fluid flow driving particles upward becomes faster than particles. Also, except the sharp-45 pipe, the magnitude of slip velocity between liquid and solid phases decreases at the central region, corresponding to Figure 6-14(b), it is shown that the central region has a higher feed solid concentration. This is attributed to the more uniform solid distribution on pipe cross-section, which intensifies the momentum exchange between solid and fluid flows and thus reduces their difference. For the sharp-45 pipe, the liquid velocity is higher than the solid velocity at the inside wall, as in the inclined pipe, the effect of gravity still exited, particles are not uniformly distributed across the pipe so that the slip velocity for sharp-45 is not symmetry as other pipes.

6.4.3 Effect of pipe length and degree

In the current study, the effect of typical bend geometries on flow behaviours have been analysed and discussed in section 6.4.2. The results show that bend geometry plays an important role in liquid-solid system. In addition, for the T-90 pipe, there produces a recycle flow at the blind section, which is not found from the previous studies. Therefore, the effect of blind section length and pipe degree on T pipe will be analysed and discussed in section 6.4.3.

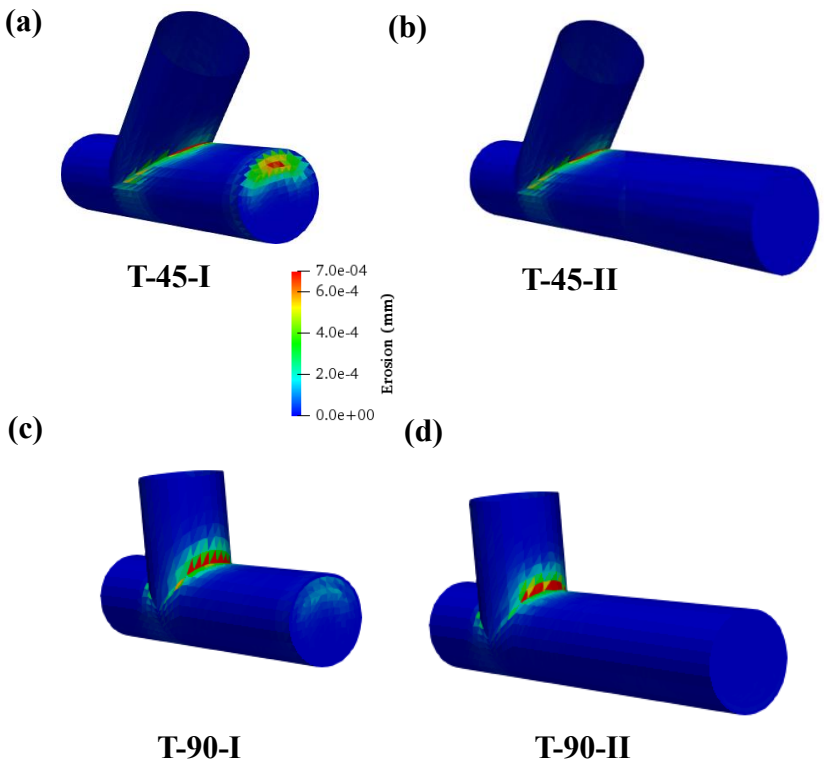

Figure 6-14 Effects of length and degree on whole bend sectional contours of the temporal erosion distribution at the pipe locations between x=2.9 m and z=0.26m, d_p = 3.5 mm, C_v = 0.05, and t=7s: (a) T-45-I, (b) T-45-II, (c) T-90-I, and (d) T-90-II

Figure 6-14 shows the contour of the effect of blind section length and pipe degree on erosion for the T pipes. From Figure 6-14, it is clearly seen that when the length of the blind section is increased, the erosion at the end of the horizontal pipe is also decreased. In addition, by comparing Figure 6-14 (b, d), when the length is fixed, the increasing pipe degree will have

smaller erosion area, and the erosion happened at the connected section for the horizontal and vertical pipes. The increasing pipe degree will decrease the erosion area in the inclined pipe. The blind section length and pipe degree play an important role in erosive distribution, not only the maximum erosive position is different, but also the erosive area, for deeper understanding, the quantitative analysis on erosive wear is needed.

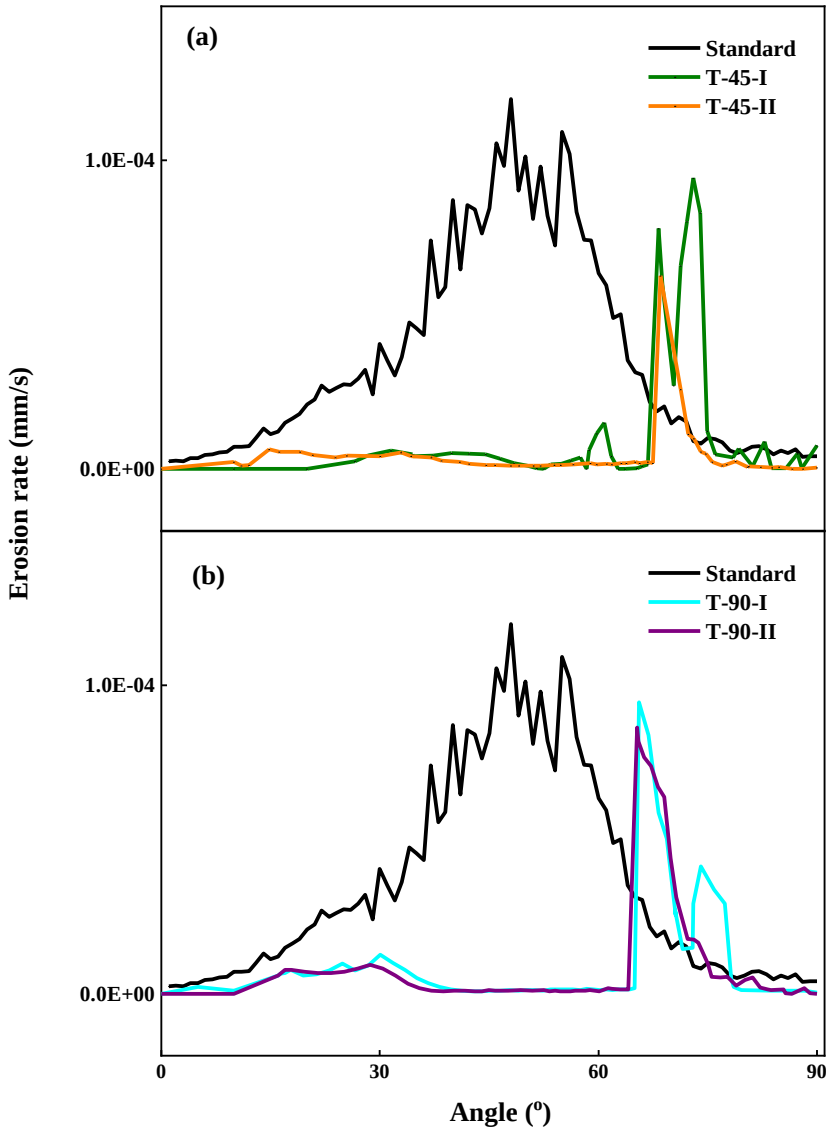

Figure 6-15 Effects of blind section length and pipe degree on time-averaged erosion rate distribution at U_f =4.0m/s, d_p = 3.5 mm and C_v = 0.05. (a) for T-45 pipes, and (b) for T-90 pipes

A quantitative analysis on erosive wear for different blind section length and pipe degree is presented in Figure 6-15, which clearly shows the effect of blind section length and pipe degree on time-averaged erosion rate. In figure 6-14(a), for the T-45-I pipe, there are two peaks, the positions are 68°, 74°, separately, in which the maximum erosion rate is $9.43e^{-5}$ mm/s, for the T-45-II pipe, the maximum erosion rate is 6.27 e^{-5} mm/s, and located at 68°. Figure 6-15(b) indicates that for the T-90-I pipe, there are two peaks, and the positions are 65°, 74°, separately, in which the maximum erosion rate is $9.45e^{-5}$ mm/s. And, for the T-90-II pipe, the maximum erosion rate is 8.63 e^{-5} mm/s, and located at 65°. The maximum erosion rate for all types of T are smaller than the standard elbow pipe, when the blind section length is increased, the maximum erosion rate will be decreased, and the decreasing pipe degree will also cause the maximum erosion rate to decrease, and the erosion at the end of the horizontal pipe will disappear so that the peaks are decreased to one point.

In addition, Figure.6-15 also shows that the blind section length and pipe degree have influence on the erosion area. The decreasing pipe degree causes the erosion area to become narrow, and the increasing blind section length causes the erosion area to decrease.

The phase diagram of the variation of pressure drop with varied blind section length and pipe degree is presented in Figure 6-16. For the T-90 pipes, before the bend entrance, they have a similar value on pressure drop with standard elbow pipe, when the particles convey cross the bend, after the bend exit, the pressure drop sharply decreases, then showing a linearly decreasing trend, and the pressure drop after bend exit is lower than standard elbow pipe. However, the decreasing pipe degree will lead to a lower value for the pressure drop distribution. Comparing with standard elbow pipe, when particles convey across the bend exit, the pressure drop is suddenly decreased, then linearly decreasing. For the T-90 and T-45 pipes, the increasing blind section length will not change the trend of the pressure drop distribution along the whole pipe.

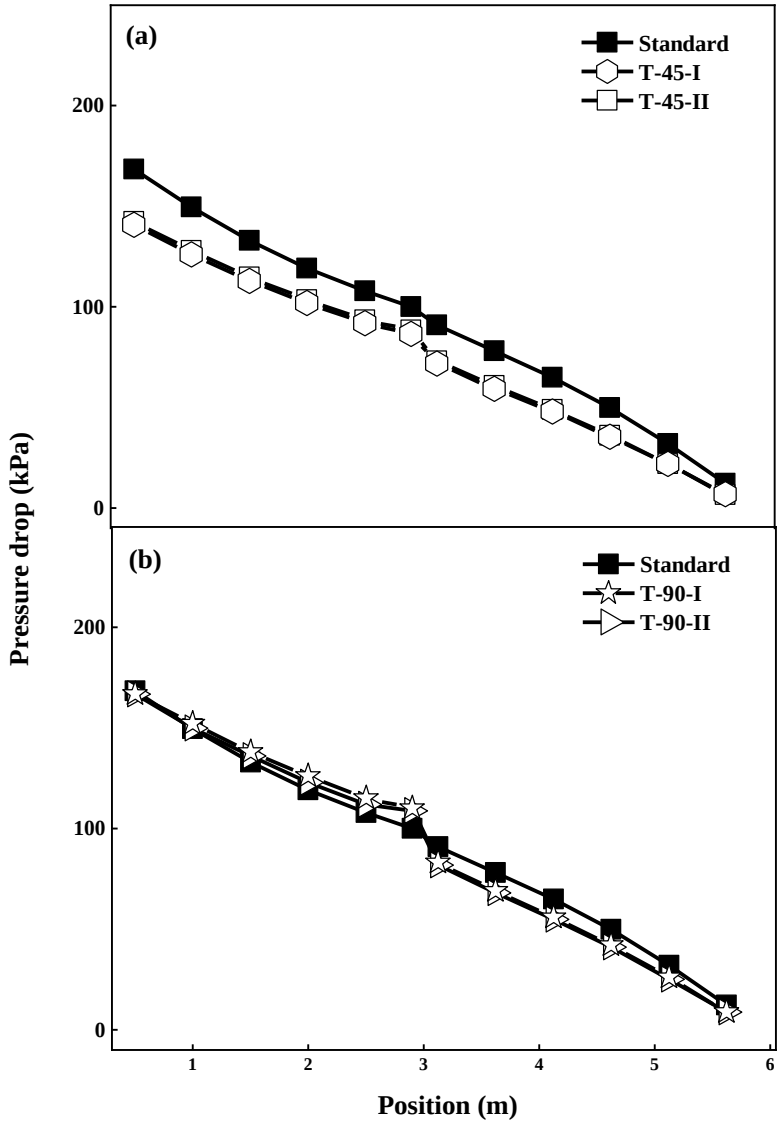

Figure 6-16 Phase diagram showing the variation of pressure drop versus varied blind section length and pipe degree at same flow conditions. (a) for T-45pipes, and (b) for T-90 pipes

It is clearly seen that the effect of blind section length and pipe degree play an important role in erosion wear and pressure drop. To understand the formation of the erosion, and the peaks point, particle and fluid behaviours could be used to explain these phenomena, which will be discussed below.

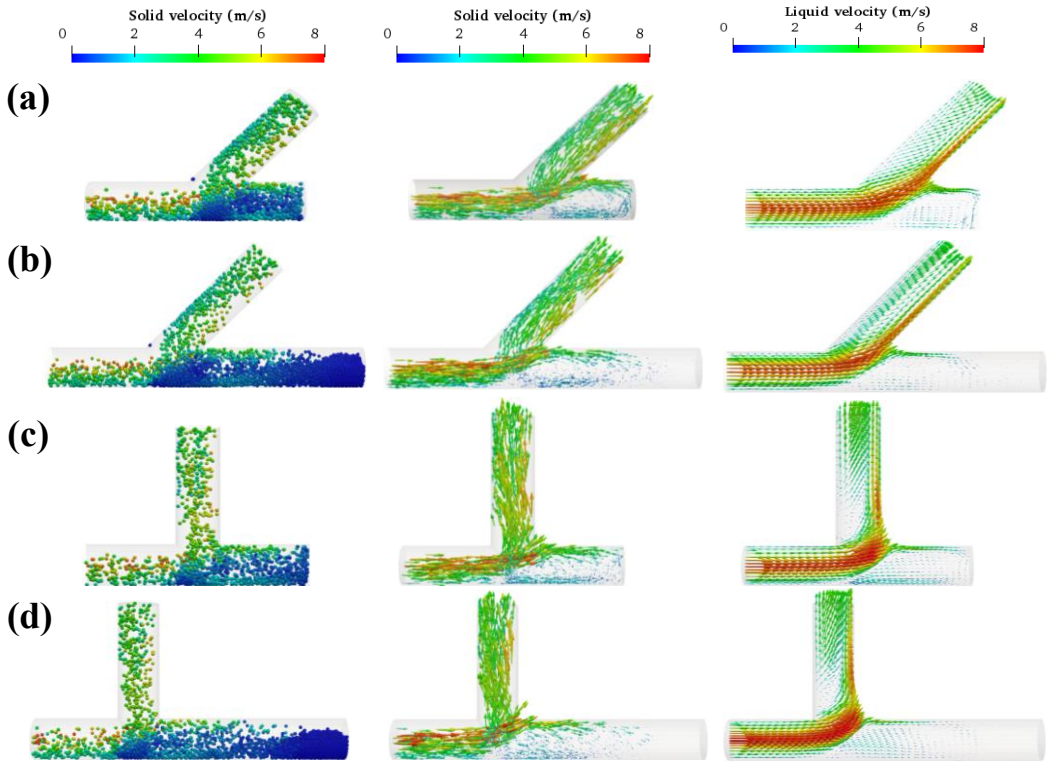

Figure 6-17 Contours of flow regime (left), solid velocity (middle), and liquid velocity (right) in the central vertical plane at x=2.8m, z=0.26m for different blind section length and pipe degree. (a) T-45-I, (b) T-45-II, (c) T-90-I, and (d) T-90-II

Figure 6-17 presents the contours for flow regimes, solid and liquid velocities for different blind section length and pipe degree. Firstly, results of T-45 pipes are presented in Figure 6-17 (a-b), when the pipe degree decreases, there will be more plugged particles at the blind section, as the angle between the inclined pipe to the surface is lower, the flow regime in the inclined section is not changed too much. The results of T-90-I and T-90-II pipes are listed in Figure 6-17 (c-d), for the T-90-I pipe, there is no existing plugged particles at the blind section, instead, it produces a recycle flow, in which the particle conveys with a higher velocity to collide the pipe, then crosses to the blind section, the particle velocity is decreased and moves to the bottom, then moves to the vertical pipe. For the T-90-II pipe, in which the blind section length is increased, Figure 6-17(d) clearly shows that there are more particles plugged at the end of blind section and the solid velocity of them are quite low, nearly zero, before the plugged

particles, the particles are still showing a recycle flow. To link with Figure 6-15, when the blind section length is increased, some particles are plugged at the end section of the horizontal pipe with a nearly zero solid velocity so the erosion rate peak at the end of the horizontal pipe is disappeared. There are still some particles in front of the plugged particles that are doing a recycle flow, which help to slow down the inlet particle velocity so that the erosion rate at the pipe connected part is also decreased. Similarly, same phenomenon is also found when the pipe degree decreased to 45.

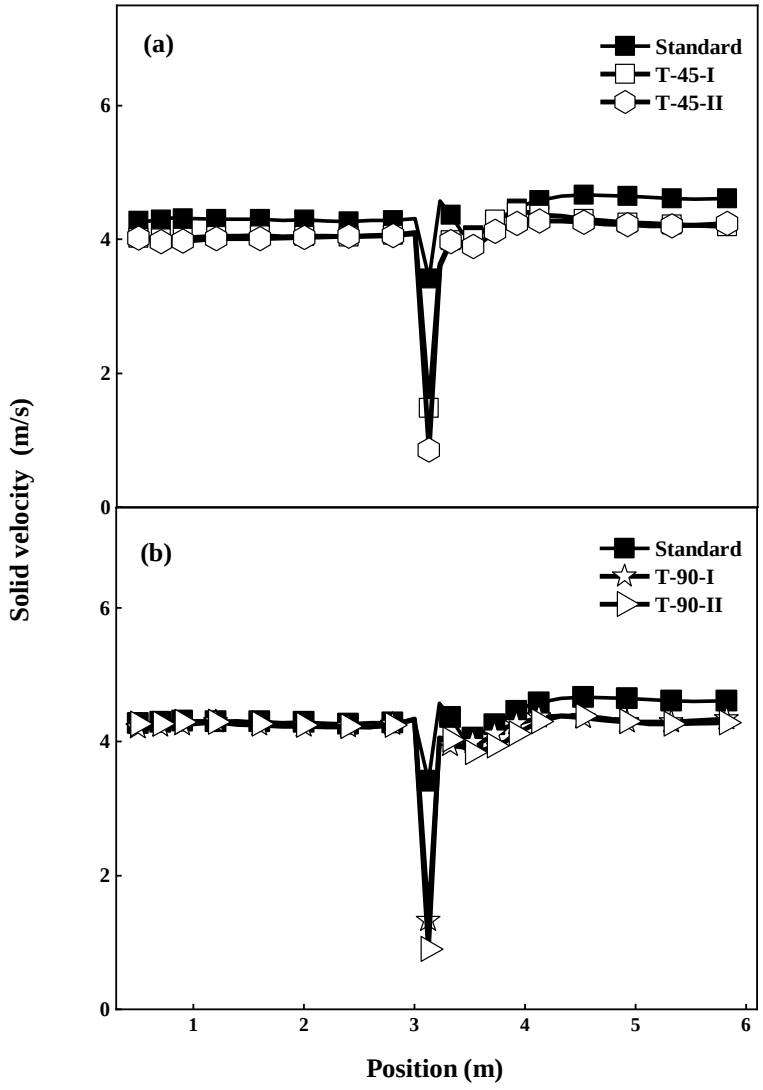

Figure 6-18 Effect of blind section length and pipe degree on time-averaged solid velocity at the whole pipe position, d_p = 3.5 mm and C_v = 0.05. (a) for T-45 pipes, and (b) for T-90 pipes

To further analyse the effect of blind section length and pipe degree on solid-liquid system, Figure 6-18 illustrates the time-averaged solid velocity at the whole pipe position. The T-45-II pipe has the lowest averaged solid velocity at the bend exit, which is around 0.85 m/s, as more particles are plugged at that pipes so that the averaged solid velocity will also be decreased, it is similar with T-90-II pipe. When the pipe degree increases, for the T-90-I and T-90-II pipes, it is indicated that before the bend, the averaged solid velocity along the pipe is not changed too much, and the system could quickly get a stable status, after crossing the bend, the solid velocity at the bend exit is quite different, the T-90-II has the lowest averaged solid velocity, which is around 0.90 m/s, corresponding to Figure 6-17(b), it is not hard to understand, as some particles plugged at the bottom of the pipe, in which the solid velocity is nearly zero so that causes the averaged solid velocity to decrease. After crossing the bend, all of them will have an acceleration stage, and the system quickly reaches stable status at position 4 m, then the averaged solid velocity is the same, and not changed anymore.

6.5 Conclusions

In this work, the influences of pipe geometry, blind section length and pipe degree on hydraulic pipe are evaluated via CFD-DEM simulations. The main objective of this study is to investigate the flow characteristics and erosion phenomenon in hydraulic conveying pipe of coarse particles under varied bend geometry, length and degree. Bending is a key aspect of any pipeline system layout, and the correct selection is a key aspect of system design and operation. The incorrect selection will produce excessive pressure drop, high erosion rate, which will bring additional maintenance, safety and environmental problems. Through the analyses of the results, the major conclusions are shown as follows:

i. For the pressure drop, comparing with standard, sharp-45, sharp-90, and T-90 pipes, the T-90 pipe has the lowest pressure drop. For the erosive wear analysis, the sharp-45

pipe has the lowest erosion rate. Based on these results, the sharp-45 pipe is the best design as it has the lowest erosion rate and the second lowest pressure drop among these pipes. Although T-90 pipe has the largest erosion rate, but it has the lowest pressure drop, and it is found that there exists a recycle flow at the blind section, which is not found in sharp or standard pipe.

ii. For deeper analysis of the T pipe, the various pipes of T-45 and T-90 are chosen here. Firstly, it is found that when the length of the blind section is increasing at a certain value, the pressure drop will not change too much, and the erosion rate at the end of the horizontal pipe is also disappeared as some particles are plugged there with a nearly zero solid velocity. The recycle flow is exists in both T-45 and T-90 pipes. Secondly, comparing with the T-90 pipe, when the pipe degree decreases to 45, the pressure drop will decrease, and there are more particles plugged at the end of the horizontal pipe, the decreasing pipe degree also leads to the decrease of maximum erosion rate, and the position is moving upward a little.

iii. After detailed analyses, the best design for hydraulic conveying is T-45-II pipe, which has the lowest erosion rate and pressure drop. It also indicated that the bend shapes, pipe degree and blind section length play an important role in hydraulic pipe system.

CHAPTER 7 CONCLUSIONS AND FUTURE STUDIES

7.1 Conclusions

In this work, the flow characteristic for hydraulic conveying pipe are investigated. It starts from the vertical pipe to validate the model capability, then the horizontal pipe is applied to study the different flow regimes, finally the bend pipe is used to investigate the erosion phenomenon. Both macroscopic and microscopic information are analysed, which include the flow regimes, force analysis, solid volume fraction distribution, and solid and liquid velocity distributions. The effects of material properties and geometry, operation conditions are also investigated comprehensively. For each chapter the major work is concluded as below:

i. Via the model validation in the vertical pipe in Chapter 3, it proves the reasonability of applying the CFD-DEM method in the simulation of a hydraulic conveying system flow system, where the lift force acting on a particle needs to be considered. Numerical results show that particles tend to concentrate in the middle of the vertical pipe. Increasing feed solid concentration and conveying speed gives a more dispersed distribution of particles and leads to an increase of pressure drop. In contrast, particle diameter has a negligible influence on instantaneous flow regimes and pressure drop. Under all the operating conditions considered, time-averaged variables including solid volume fraction, axial liquid velocity and axial solid velocity all present maximum values in the middle of the pipe, which decline gradually in the radial direction toward the wall. These results are expected to shed light on the optimization of hydraulic conveying.

ii. Different flow regimes may take place during hydraulic conveying but are not fully understood. The chapter 4 presents a numerical study of the **horizontal** hydraulic conveying of coarse particles by means of the combined approach of CFD for the liquid phase and DEM for particles. The applicability of the model is confirmed by comparing the measured and predicted profiles of solid volume fraction under different operational

conditions. It is shown that the flow regime transition from the stationary-bed flow, through the moving-bed flow, and finally to the heterogeneous-suspension flow as the conveying speed increases and associated pressure characteristics are successfully predicted. The numerical results are analysed in detail in terms of flow and force structures. A new phase diagram in terms of forces acting on particles is proposed to identify flow regimes and their transition. Also, based on the simulation data, correlations are formulated to predict the pressure drop.

iii. Bend pipe is generally used in pipeline system, and erosive wear is a common and important phenomenon in this type of pipeline system. A numerical study of the elbow hydraulic conveying of coarse particles by means of the combined approach of computational fluid dynamics (CFD) for the liquid phase and discrete element method (DEM) for particles is carried out, focused on the investigation into predicting the erosive wear distribution in elbow. In the chapter 5, the flow regimes are also presented and correspond to the wear pattern in the elbow. The numerical results are analysed in detail in terms of flow characteristic. Especially, the effects of pipe orientation and conveying speed on the solid volume fraction, flow regimes and erosion rate are discussed.

iv. The different bend shapes, including, elbow pipe, sharp pipe, sharp-135, T-pipe and T-135 pipe will produce different pressure drop, erosion rate, erosion zone and impacting location, which are mainly affected by the flow regimes and solid velocity. Among these bend designs, a recycle flow is produced in the T-90 and T-135 pipes. The numerical results in Chapter 6 are analysed in detail in terms of flow regimes, solid velocity, and erosion rate and erosion position. It is found that the T-45-II pipe has the lowest pressure drop and erosion rate.

7.2 Future studies

Through the work investigated in this thesis, several research gaps have been met, however, to obtain a comprehensive study, more research aspects are needed to be considered. The future work is suggested to be focused on the issues shown below:

i. The segregation phenomenon exists in hydraulic conveying system, with the small particle being transported at the bottom of the pipe while the large particle is transported on top, is indeed observed, and only few researches notice such phenomenon. This is quite complex. The reasons for that why this happen are not clear, and its effect on flow regimes is also unclear.

ii. The effects of different material properties, such as particle density, fluid density and particle size should also be investigated. In this thesis, only mono particle size and density are investigated, the effect of multi-size, and particle density on flow regimes, pressure drop, and pipe erosive wear are not clear.

iii. According to the literature review, the particle shape plays an important role in hydraulic conveying, especially for the erosive wear problem. Comparing with spherical particles, the non-spherical particles has lower pressure drop, but easily destroyed, and the non-Newtonian behaviour could be easily observed. The particle shapes could be considered as a key variable to comprehensive the study on the hydraulic conveying of coarse particles.

iv. In this thesis, only water is considered as the carrier liquid, the different types of fluid could also be considered in the future work, as its property plays important role in solid-liquid system.

v. A new phase diagram based on force analysis for the solid-liquid and gas-liquid pipe system is suggested to be obtained for deeper understanding of the flow behaviours of the whole pipeline system.

LIST OF REFERENCES

ABULNAGA, B. 2002. *Slurry Systems Handbook,* New York, McGraw-Hill.

AHLERT, K. 1994. *Effect of particle impingement angle and surface wetting on solid particle erosion of AISI 1018 steel.* Master, The University of Tulsa.

ALAJBEGOVI., A., ASSAD, A., BONETTO, F. & LAHEY JR, R. T. 1994. Phase distribution and turbulence structure for solid-fluid upflow in a pipe. *International Journal of Multiphase Flow,* 20**,** 453-479.

ALBUNAGA, B. E. 2002. *Slurry systems handbook,* McGraw-Hill.

ALI, S. F. & YEUNG, H. 2014. Two-phase flow patterns in large diameter vertical pipes. *Asia-Pacific Journal of Chemical Engineering,* 9**,** 105-116.

ANDREWS, D. R. & HORSFIELD, N. 1983. Particle collisions in the vicinity of an eroding surface. 16**,** 525-538.

ARCHARD, J. F. 1953. Contact and Rubbing of Flat Surfaces. *Journal of Applied Physics,* 24**,** 981-988.

ASIM, T. & MISHRA, R. 2016. Optimal design of hydraulic capsule pipelines transporting spherical capsules. *The Canadian Journal of Chemical Engineering,* 94**,** 966-979.

AZIMIAN, M. & BART, H.-J. 2014. Investigation of hydroabrasion in slurry pipeline elbows and t-junctions. *Energy and Power Engineering,* 8**,** 65-78.

AZIZ, A. & MOHAMED, H. 2013. A study of the factors affecting transporting solid—liquid suspension through pipelines. *Open Journal of Fluid Dynamics,* 03**,** 152-162.

BARTOSIK, A. S. & SHOOK, C. A. 1995. Prediction of vertical liquid solid pipe flow using measured concentration distribution. *Particulate Science and Technology,* 13**,** 85-104.

BEN-AMI, Y., UZI, A. & LEVY, A. 2016. Modelling the particles impingement angle to produce maximum erosion. *Powder Technology,* 301**,** 1032-1043.

BITTER, J. G. A. 1963. A study of erosion phenomena. *Wear,* 6**,** 5-21.

BLANCHARD, D. J., GRIFFITH, P. & RABINOWICZ, E. 1984. Erosion of a Pipe Bend by Solid Particles Entrained in Water. *Journal of Engineering for Industry,* 106**,** 213-217.

BOURGOYNE, A. T., JR. 1989. Experimental study of erosion in diverter systems due to sand production. *SPE/IADC Drilling Conference.* New Orleans, Louisiana: Society of Petroleum Engineers.

BROWN, G. J. 2002. Erosion prediction in slurry pipeline tee-junctions. *Applied Mathematical Modelling,* 26**,** 155-170.

CAPECELATRO, J. & DESJARDINS, O. 2013. Eulerian–Lagrangian modeling of turbulent liquid–solid slurries in horizontal pipes. *International Journal of Multiphase Flow,* 55**,** 64-79.

CHARA, Z., VLASAK, P., KONFRST, J. & KYSELA, B. 2015. Movement of dunes in a circular pipe.

CHEN, J., WANG, Y., LI, X., HE, R., HAN, S. & CHEN, Y. 2015. Erosion prediction of liquid-particle two-phase flow in pipeline elbows via CFD–DEM coupling method. *Powder Technology,* 275**,** 182-187.

CHEN, Q., XIONG, T., ZHANG, X. & JIANG, P. 2020. Study of the hydraulic transport of non-spherical particles in a pipeline based on the CFD-DEM. *Engineering Applications of Computational Fluid Mechanics,* 14**,** 53-69.

CHEN, W., ZHANG, J., DONOHUE, T., WILLIAMS, K., CHENG, R., JONES, M. & ZHOU, B. 2017. Effect of particle degradation on electrostatic sensor measurements and flow characteristics in dilute pneumatic conveying. *Particuology,* 33**,** 73-79.

CHU, K. W. & YU, A. B. 2008. Numerical simulation of the gas-solid flow in three-dimensional pneumatic conveying bends. *Ind. Eng. Chem. Res,* 47**,** 7058–7071.

CHUNG, J. S., YARIM, G. & SAVASCI, H. 1998. Shape effect of solids on pressure drop in a 2-phase vertically upward transport: silica sands and spherical beads. *The Eighth*

International Offshore and Polar Engineering Conference. Montreal, Canada: International Society of Offshore and Polar Engineers.

CLARK, H. M. 1995. A comparison of particle impact in gas-solid and liquid-solid erosion. *Wear,* 186-187**,** 465-472.

CROWE, C. T. On models for turbulence in fluid-particle flows. American Society of Mechanical Engineers, Fluids Engineering Division (Publication) FED, 1998.

CUNDALL, P. A. & STRACK, O. D. L. 1979. Discrete numerical-model for granular assemblies. *Geotechnique,* 29**,** 47-65.

DAVID, H., MICHAEL, F. & SIMON, B. 2011. The minimum transport velocity of colloidal silica suspensions. *Chemical Engineering Science,* 66**,** 2309-2316.

DEEN, N. G., VAN SINT ANNALAND, M., VAN DER HOEF, M. A. & KUIPERS, J. A. M. 2007. Review of discrete particle modeling of fluidized beds. *Chemical Engineering Science,* 62**,** 28-44.

DENG, T., PATEL, M., HUTCHINGS, I. & BRADLEY, M. S. A. 2005. Effect of bend orientation on life and puncture point location due to solid particle erosion of a high concentration flow in pneumatic conveyors. *Wear,* 258**,** 426-433.

DERKSEN, J. J., VAN DEN AKKER, H. E. A. & SUNDARESAN, S. 2008. Two-way coupled large-eddy simulations of the gas-solid flow in cyclone separators. *AIChE Journal,* 54**,** 872-885.

DESALE, G. R., GANDHI, B. K. & JAIN, S. C. 2006. Effect of erodent properties on erosion wear of ductile type materials. *Wear,* 261**,** 914-921.

DESALE, G. R., GANDHI, B. K. & JAIN, S. C. 2009. Particle size effects on the slurry erosion of aluminium alloy (AA 6063). *Wear,* 266**,** 1066-1071.

DESALE, G. R., GANDHI, B. K. & JAIN, S. C. 2011. Development of correlations for predicting the slurry erosion of ductile materials. *Journal of Tribology,* 133.

DHODAPKAR, S. & JACOB, K. 2006. *Multiphase flow handbook,* Taylor & Francis Group

DHODAPKAR, S., SOLT, P. & KLINZING, G. 2009. Understanding Bends In Pneumatic Conveying Systems. *Chemical Engineering,* 116**,** 53-60.

DORON, P. & BARNEA, D. 1993. A three-layer model for solid-liquid flow in horizontal pipes. *International Journal of Multiphase Flow,* 19**,** 1029-1043.

DORON, P. & BARNEA, D. 1995. Pressure drop and limit deposit velocity for solid-liquid flow in pipes. *Chemical Engineering Science,* 50**,** 1595-1604.

DORON, P. & BARNEA, D. 1996. Flow pattern maps for solid-liquid flow in pipes. *International Journal of Multiphase Flow,* 22**,** 273-283.

DORON, P., GRANICA, D. & BARNEA, D. 1987. Slurry flow in horizontal pipes—experimental and modeling. *International Journal of Multiphase Flow,* 13**,** 535-547.

DORON, P., SIMKHIS, M. & BARNEA, D. 1997. Flow of solid-liquid mixtures in inclined pipes. *International Journal of Multiphase Flow,* 23**,** 313-323.

DOROODCHI, E., GALVIN, K. P. & FLETCHER, D. F. 2005. The influence of inclined plates on expansion behaviour of solid suspensions in a liquid fluidised bed—a computational fluid dynamics study. *Powder Technology,* 156**,** 1-7.

DURAND, R. & CONDOLIOS, E. 1952. Hydraulic transportation of coal and solid material in pipes. . *London Colloquium of the National Coal Board.* London.

DYAKOWSKI, T., JEANMEURE, L. F. C. & JAWORSKI, A. J. 2000. Applications of electrical tomography for gas–solids and liquid–solids flows — a review. *Powder Technology,* 112**,** 174-192.

EESA, M. & MARIGO, M. 2009. CFD investigation of the pipe transport of coarse solids in laminar power law fluids. *Chemical Engineering Science - CHEM ENG SCI,* 64**,** 322-333.

ENGELMANN, H. E. 1978. Vertical hydraulic lifting of large-size particles - A contribution to marine mining. *Offshore Technology Conference*. Houston, Texas: Offshore Technology Conference.

ESKIN, D. 2005. An engineering model of solids diffusivity in hydraulic conveying. *Powder Technology,* 159**,** 78-86.

FADDICK, R. R. 1975. Pipeline wear from abrasive slurries. *First International Conference on the Internal and External Projection of pipelines.* BHRA, Durham.

FARAJ, Y. & WANG, M. 2012. ERT Investigation on Horizontal and Vertical Counter-gravity Slurry Flow in Pipelines. *Procedia Engineering,* 42**,** 588-606.

FELICE, R. D. 1994. The voidage function for fluid-particle interaction systems. *International Journal of Multiphase Flow,* 20**,** 153-159.

FERZIGER, J. & PERIC, M. 2002. *Computational methods for fluid dynamics,* New York, Springer.

FINNIE, I. 1960. Erosion of surfaces by solid particles. *Wear,* 3**,** 87-103.

FOX, R. O. 2012. Large-Eddy-Simulation tools for multiphase flows. *Annual Review of Fluid Mechanics,* 44**,** 47-76.

GANDHI, B. K. & BORSE, S. V. 2004. Nominal particle size of multi-sized particulate slurries for evaluation of erosion wear and effect of fine particles. *Wear,* 257**,** 73-79.

GARIĆ-GRULOVIĆ, R. V., GRBAVČIĆ, Ž. B. & ARSENIJEVIĆ, Z. L. 2004. Heat transfer and flow pattern in vertical liquid–solids flow. *Powder Technology,* 145**,** 163-171.

GIGUèRE, R., FRADETTE, L., MIGNON, D. & TANGUY, P. A. 2008. Characterization of slurry flow regime transitions by ERT. *Chemical Engineering Research and Design,* 86**,** 989-996.

GIGUèRE, R., FRADETTE, L., MIGNON, D. & TANGUY, P. A. 2009. Analysis of slurry flow regimes downstream of a pipe bend. *Chemical Engineering Research and Design,* 87**,** 943-950.

GILLIES, R. G. & SHOOK, C. A. 1994. Concentration distributions of sand slurries in horizontal pipe flow. *Particulate Science and Technology,* 12**,** 45-69.

GILLIES, R. G. & SHOOK, C. A. 2000. Modelling high concentration settling slurry flows. *The Canadian Journal of Chemical Engineering,* 78**,** 709-716.

GOPALIYA, M. K. & KAUSHAL, D. R. 2014. Analysis of effect of grain size on various parameters of slurry flow through pipeline using CFD. *Particulate Science and Technology,* 33**,** 369-384.

GUI, N., FAN, J. R. & LUO, K. 2008. DEM–LES study of 3-D bubbling fluidized bed with immersed tubes. *Chemical Engineering Science,* 63**,** 3654-3663.

GUPTA, R., SINGH, S. N. & SESHADRI, V. 1997. Migration of solid particles in the heterogeneous slurry flow through a 90 degree bend. *Indian Journal of Engineering & Materials Sciences,* 4**,** 10-20.

HASHEMI, S. A., SPELAY, R. B., ADANE, K. F. K. & SEAN SANDERS, R. 2016. Solids velocity fluctuations in concentrated slurries. *The Canadian Journal of Chemical Engineering,* 94**,** 1059-1065.

HILL, K. B. & SHOOK, C. A. 1998. Pipeline transport of coarse particles by water and by fluids with yield stresses. *Particulate Science and Technology,* 16**,** 163-183.

HONG, S., CHOI, J. & YANG, C.-K. 2002. Experimental study on solid-water slurry flow in vertical pipe. *The Twelfth (2002) International Offshore and Polar Engineering Conference.* Japan.

HUANG, C., MINEV, P., LUO, J. & NANDAKUMAR, K. 2010. A phenomenological model for erosion of material in a horizontal slurry pipeline flow. *Wear,* 269**,** 190-196.

ISSA, R. I. 1985. Solution of the implicitly discretised fluid flow equations by operator-splitting. *Journal of Computational Physics,* 62**,** 60-45.

J.H. FERZIGER, M. PERIĆ & STREET, R. L. 2002. *Computational methods for fluid dynamics,* Springer.

JAFARI, M., MANSOORI, Z., SAFFAR AVVAL, M., AHMADI, G. & EBADI, A. 2014. Modeling and numerical investigation of erosion rate for turbulent two-phase gas–solid flow in horizontal pipes. *Powder Technology,* 267**,** 362-370.

JI, L., CHEN, J., KUANG, S. B., QI, Z., CHU, K. W. & YU, A. B. 2019. Prediction of separation performance of hydrocyclones by a PC-based model. *Separation and Purification Technology,* 211**,** 141-150.

JOP, P., FORTERRE, Y. & POULIQUEN, O. 2006. A constitutive law for dense granular flows. *Nature,* 441**,** 727-730.

KANNOJIYA, V., DESHWAL, M. & DESHWAL, D. 2018. Numerical analysis of solid particle erosion in pipe elbow. *Materials Today: Proceedings,* 5**,** 5021-5030.

KARABELAS, A. 1978. An experimental study of pipe erosion by turbulent slurry flow. *Hydrotransport 5, 5th Intern. Conference of Hydraulic Transport of Solids in Pipes.*

KAUSHAL, D. R., THINGLAS, T., TOMITA, Y., KUCHII, S. & TSUKAMOTO, H. 2012. CFD modeling for pipeline flow of fine particles at high concentration. *International Journal of Multiphase Flow,* 43**,** 85-100.

KAUSHAL, D. R. & TOMITA, Y. 2002. Solids concentration profiles and pressure drop in pipeline flow of multisized particulate slurries. *International Journal of Multiphase Flow,* 28**,** 1697-1717.

KAUSHAL, D. R. & TOMITA, Y. 2007. Experimental investigation for near-wall lift of coarser particles in slurry pipeline using γ-ray densitometer. *Powder Technology,* 172**,** 177-187.

KHAN, M., YA, H. & PAO, W. 2019. Numerical investigation of the elbow angle effect on solid particle erosion for liquid-solid. *International Journal of Mechanical and Mechatronics Engineering,* 19**,** 1-13.

KOTZUR, B. A., BERRY, R. J., ZIGAN, S., GARCíA-TRIñANES, P. & BRADLEY, M. S. A. 2018. Particle attrition mechanisms, their characterisation, and application to horizontal lean phase pneumatic conveying systems: A review. *Powder Technology,* 334**,** 76-105.

KRUGGEL-EMDEN, H. & OSCHMANN, T. 2014. Numerical study of rope formation and dispersion of non-spherical particles during pneumatic conveying in a pipe bend. *Powder Technology,* 268**,** 219-236.

KUANG, S. B., LI, K., ZOU, R. P., PAN, R. H. & YU, A. B. 2013. Application of periodic boundary conditions to CFD-DEM simulation of gas–solid flow in pneumatic conveying. *Chemical Engineering Science,* 93**,** 214-228.

KUANG, S. B., LI, Z. Y. & YU, A. B. 2018. Review on modeling and simulation of blast furnace. *Steel Research International,* 89**,** 1700071-1/25.

KUANG, S. B. & YU, A. B. 2011. Micromechanic modeling and analysis of the flow regimes in horizontal pneumatic conveying. *AIChE Journal,* 57**,** 2708-2725.

KUANG, S. B., YU, A. B. & ZOU, Z. S. 2009. Computational study of flow regimes in vertical pneumatic conveying. *Industrial & Engineering Chemistry Research,* 48**,** 6846-6858.

KUANG, S. B., ZHOU, M. M. & YU, A. B. 2019a. CFD-DEM modelling and simulation of pneumatic conveying – A review. *Powder Technol.*, DOI: 10.1016/j.powtec.2019.02.011.

KUANG, S. B., ZHOU, M. M. & YU, A. B. 2019b. CFD-DEM modelling and simulation of pneumatic conveying – A review. *Powder Technol.,* 365**,** 186-207.

KUANG, S. B., ZOU, R. P., PAN, R. H. & YU, A. B. 2012. Gas solid flow and energy dissipation in inclined pneumatic conveying. *Industrial & Engineering Chemistry Research,* 51**,** 14289-14302.

KUMAR, U., MISHRA, R., SINGH, S. N. & SESHADRI, V. 2003. Effect of particle gradation on flow characteristics of ash disposal pipelines. *Powder Technology,* 132**,** 39-51.

LEVY, A. V. & CHIK, P. 1983. The effects of erodent composition and shape on the erosion of steel. *Wear,* 89**,** 151-162.

LEVY, A. V. & HICKEY, G. 1987. Liquid-solid particle slurry erosion of steels. 117**,** 129-146.

LI, L., LI, B. & LIU, Z. 2017. Modeling of spout-fluidized beds and investigation of drag closures using OpenFOAM. *Powder Technology,* 305**,** 364-376.

LI, Y., XU, Y. & THORNTON, C. 2005. A comparison of discrete element simulations and experiments for 'sandpiles' composed of spherical particles. *Powder Technology,* 160**,** 219-228.

LI, Y., ZHANG, H., LIN, Z., HE, Z., XIANG, J. & SU, X. 2019. Relationship between wear formation and large-particle motion in a pipe bend. *Royal Society Open Science,* 6.

LILLY, D. K. 1992. A proposed modification of the Germano subgrid‐scale closure method. *Physics of Fluids A: Fluid Dynamics,* 4**,** 633-635.

LIM, E. W. C. 2007. Voidage waves in hydraulic conveying through narrow pipes. *Chem. Eng. Sci.,* 62**,** 4529-4543.

LING, J., SKUDARNOV, P. V., LIN, C. X. & EBADIAN, M. A. 2003. Numerical investigations of liquid–solid slurry flows in a fully developed turbulent flow region. *International Journal of Heat and Fluid Flow,* 24**,** 389-398.

LOSPA, A. M., DUDU, C., RIPEANU, R. G. & DINITA, A. 2019. CFD Evaluation of sand erosion wear rate in pipe bends used in technological installations. *IOP Conference Series: Materials Science and Engineering,* 514.

LOTH, E. & DORGAN, A. J. 2009. An equation of motion for particles of finite Reynolds number and size. *Environmental Fluid Mechanics,* 9**,** 187-206.

MALLOUPPAS, G. & VAN WACHEM, B. 2013. Large Eddy Simulations of turbulent particle-laden channel flow. *International Journal of Multiphase Flow,* 54**,** 65-75.

MANSOURI, A., ARABNEJAD, H., SHIRAZI, S. A. & MCLAURY, B. S. 2015. A combined CFD/experimental methodology for erosion prediction. *Wear,* 332-333**,** 1090-1097.

MASSOUDI, M., RAJAGOPAL, K. R., EKMANN, J. M. & MATHUR, M. P. 1992. Remarks on the modeling of fluidized systems. *AIChE Journal,* 38**,** 471-472.

MATOUSEK, V. 1996. Internal structure of slurry flow in inclined pipe. Experiments and mechanistic modelling. *13th International Conference on Slurry Handling and Pipeline Transport – Hydrotransport.*

MATOUSEK, V. 2002. Pressure drops and flow patterns in sand-mixture pipes. *Experimental Thermal and Fluid Science* 26**,** 693-702.

MATOUŠEK, V. 1997. *Flow Mechanism of Sand-Water Mixtures.* PhD, University of Delft.

MATOUŠEK, V. 2005. Research developments in pipeline transport of settling slurries. *Powder Technology,* 156**,** 43-51.

MATOUŠEK, V. 2009. Pipe-wall friction in vertical sand-slurry flows. *Particulate Science and Technology,* 27.

MAZUMDER, Q. H., SHIRAZI, S. A. & MCLAURY, B. 2008. Experimental investigation of the location of maximum erosive wear damage in elbows. *Journal of Pressure Vessel Technology,* 130.

MENG, H. C. & LUDEMA, K. C. 1995. Wear models and predictive equations- their form and content. *Wear,* 181**,** 443–457.

MESSA, G. V. & MALAVASI, S. 2014a. Computational investigation of liquid-solid slurry flow through an expansion in a rectangular duct. *Journal of Hydrology and Hydromechanics,* 62**,** 234-240.

MESSA, G. V. & MALAVASI, S. 2014b. Numerical prediction of particle distribution of solid-liquid slurries in straight pipes and bends. *Engineering Applications of Computational Fluid Mechanics,* 8**,** 356-372.

MESSA, G. V. & MALAVASI, S. 2015. Improvements in the numerical prediction of fully-suspended slurry flow in horizontal pipes. *Powder Technology,* 270**,** 358-367.

MESSA, G. V., MALIN, M. & MALAVASI, S. 2014. Numerical prediction of fully-suspended slurry flow in horizontal pipes. *Powder Technology,* 256**,** 61-70.

MESSA, G. V. & MATOUŠEK, V. 2020. Analysis and discussion of two fluid modelling of pipe flow of fully suspended slurry. *Powder Technology,* 360**,** 747-768.

MIEDEMA, S. A. 2015. A head loss model for homogeneous slurry transport for medium sized particles. *Journal of Hydrology and Hydromechanics,* 63**,** 1-12.

MIEDEMA, S. A. & RAMSDELL, R. C. 2015. The limit deposit velocity model, a new approach. *Journal of Hydrology and Hydromechanics,* 63**,** 273-286.

MOUKALLED, F., MANGANI, L. & DARWISH, M. 2016. *The finite volume method in Computational Fluid Dynamics an advanced introduction with OpenFOAM and Matlab,* Springer.

NABIL, T., EL-SAWAF, I. & EL-NAHHAS, K. 2014. Sand-water slurry flow modelling in a horizontal pipeline *International Water Technology Journal,* 4.

NASR-EL-DIN, H., SHOOK, C. A. & COLWELL, J. 1987. The lateral variation of solids concentration in horizontal slurry pipeline flow. *International Journal of Multiphase Flow,* 13**,** 661-670.

OFEI, T. N. & ISMAIL, A. Y. 2016. Eulerian-Eulerian simulation of particle-liquid slurry flow in horizontal pipe. *Journal of Petroleum Engineering,* 2016**,** 1-10.

OH, J.-W., JUNG, J.-Y. & HONG, S. 2018. On-board measurement methodology for the liquid-solid slurry production of deep-seabed mining. *Ocean Engineering,* 149**,** 170-182.

OH, J.-W., JUNG, J.-Y., KIM, H.-W., HONG, S., SUNG, K.-Y. & BAE, D.-S. 2015. Gap size effect on the tribological characteristics of the roller for deep-sea mining robot. *Marine Georesources & Geotechnology,* 35**,** 120-126.

PAKZONKA, W., KENCHINGTON, J. M. & CHARLES, M. E. 1981. Hydroconveying of solids in horizontal pipes effects of solids concentraton and particle size on the deposit velocity. *The Canadian Journal of Chemical Engineering,* 59**,** 291-296.

PAPISTA, E., DIMITRAKIS, D. & YIANTSIOS, S. G. 2011. Direct numerical simulation of incipient sediment motion and hydraulic conveying. *Industrial and Engineering Chemistry Research,* 50**,** 630-638.

PARSI, M., NAJMI, K., NAJAFIFARD, F., HASSANI, S., MCLAURY, B. S. & SHIRAZI, S. A. 2014. A comprehensive review of solid particle erosion modeling for oil and gas

wells and pipelines applications. *Journal of Natural Gas Science and Engineering,* 21**,** 850-873.

PEI, J., LUI, A., ZHANG, Q., XIONG, T., JIANG, P. & WEI, W. 2018. Numerical investigation of the maximum erosion zone in elbows for liquid-particle flow. *Powder Technology,* 333**,** 47-59.

PEKER, S. M. & HELVACI, Ş. Ş. 2008. *Solid-liquid two phase flow,* Amsterdam, Elsevier.

PENG, W. & CAO, X. 2016. Numerical simulation of solid particle erosion in pipe bends for liquid–solid flow. *Powder Technology,* 294**,** 266-279.

PERETZ, M. F. & LEVY, A. 2019. Bends pressure drop in hydraulic conveying. *Advanced Powder Technology,* 30**,** 1484-1493.

Q. FANG , P.S. SIDKY & HOCKING, M. G. 1998. Microripple formation and removal mechanism of ceramic materials by solid-liquid slurry erosion. *Wear,* 93-101.

RAJI, A. O. & FAVIER, J. F. 2004. Model for the deformation in agricultural and food particulate materials under bulk compressive loading using discrete element method. II: Compression of oilseeds. *Journal of Food Engineering,* 64**,** 373-380.

RAVELET, F., BAKIR, F., KHELLADI, S. & REY, R. 2013. Experimental study of hydraulic transport of large particles in horizontal pipes. *Experimental Thermal and Fluid Science,* 45**,** 187-197.

REN, L., ZHAO, X. & ZHANG, S. 2017. Hydrodynamic investigation of slurry flows in horizontal narrow rectangular channels. *International Journal of Heat and Technology,* 35**,** 730-736.

RICE, H. P., FAIRWEATHER, M., PEAKALL, J., HUNTER, T. N., MAHMOUD, B. & BIGGS, S. R. 2015. Particle concentration measurement and flow regime identification in multiphase pipe flow using a generalised dual-frequency inversion method. *Procedia Engineering,* 102**,** 986-995.

SAFAEI, M. R., MAHIAN, O., GAROOSI, F., HOOMAN, K., KARIMIPOUR, A., KAZI, S. N. & GHAREHKHANI, S. 2014. Investigation of micro- and nanosized particle erosion in a 90 degrees pipe bend using a two-phase discrete phase model. *ScientificWorldJournal,* 2014**,** 740578.

SAKAI, M., MORI, Y., SUN, X. & TAKABATAKE, K. 2020a. Recent progress on mesh-free particle methods for simulations of multi-phase flows: A review. *KONA Powder and Particle Journal,* 37**,** 132-144.

SAKAI, M., MORI, Y., SUN, X. & TAKABATAKE, K. 2020b. Recent progress on mesh-free particle methods for simulations of multi-phase flows: A review. *KONA Powder and Particle Journal,* DOI: 10.14356/kona.2020017.

SENAPATI, P. K., MISHRA, B. K. & PARIDA, A. 2013. Analysis of friction mechanism and homogeneity of suspended load for high concentration fly ash & bottom ash mixture slurry using rheological and pipeline experimental data. *Powder Technology,* 250**,** 154-163.

SHARIFI, M. & YOUNG, B. 2013. Electrical Resistance Tomography (ERT) applications to chemical engineering. *Chemical Engineering Research and Design,* 91**,** 1625-1645.

SILVA, R., COTAS, C., GARCIA, F. A. P., FAIA, P. M. & RASTEIRO, M. G. 2015a. Particle distribution studies in highly concentrated solid-liquid flows in pipe using the mixture model. *Procedia Engineering,* 102**,** 1016-1025.

SILVA, R., GARCIA, F. A. P., FAIA, P. M. G. M. & RASTEIRO, M. G. 2015b. Settling suspensions flow modelling: A Review. *KONA Powder and Particle Journal,* 32**,** 41-56.

SINGH, J., KUMAR, S., SINGH, J. P., KUMAR, P. & MOHAPATRA, S. K. 2019a. CFD modeling of erosion wear in pipe bend for the flow of bottom ash suspension. *Particulate Science and Technology,* 37**,** 275-285.

SINGH, V., KUMAR, S. & MOHAPATRA, S. K. 2019b. Modeling of erosion wear of sand water slurry flow through pipe bend using CFD. *Journal of Applied Fluid Mechanics,* 12**,** 679-687.

SINHA, S. L., DEWANGAN, S. K. & SHARMA, A. 2015. A review on particulate slurry erosive wear of industrial materials: In context with pipeline transportation of mineral−slurry. *Particulate Science and Technology,* 35**,** 103-118.

SIVE, A. W. 1989. Hydraulic transportation - A Review. *Third International Conference on Bulk Materials, Storage, Handling and Transportation.* Newcastle.

SUN, B., FAN, J., WEN, D. & CHEN, Y. 2015. An experimental study of slurry erosion involving tensile stress for pressure pipe manifold. *Tribology International,* 82**,** 280-286.

SUN, R. & XIAO, H. 2015. Diffusion-based coarse graining in hybrid continuum–discrete solvers: Theoretical formulation and a priori tests. *International Journal of Multiphase Flow,* 77**,** 142-157.

SUN, R. & XIAO, H. 2016. SediFoam: A general-purpose, open-source CFD–DEM solver for particle-laden flow with emphasis on sediment transport. *Computers & Geosciences,* 89**,** 207-219.

TABAKOFF, W., KOTWAL, R. & HAMED, A. 1979. Erosion study of different materials affected by coal ash particles. *Wear,* 52**,** 161-173.

TING, X., XINZHUO, Z., MIEDEMA, S. A. & XIUHAN, C. 2019. Study of the characteristics of the flow regimes and dynamics of coarse particles in pipeline transportation. *Powder Technology,* 347**,** 148-158.

TODA, M., KOMORI, N., SAITO, S. & MAEDA, S. 1972. Hydraulic conveying of solids through horizontal and vertical pipes. *Journal of Chemical Engineering of Japan,* 5**,** 4-13.

TSUJI, Y., KAWAGUCHI, T. & TANAKA, T. 1993. Discrete particle simulation of two-dimensional fluidized bed. *Powder Technol.,* 77**,** 79-87.

TURIAN, R. M. & YUAN, T. F. 1977. Flow of Slurries in Pipelines. *Aiche Journal,* 23**,** 232-243.

UZI, A., BEIT HALEVY, G. & LEVY, A. 2020. CFD-DEM Modeling of soluble NaCl particles conveyed in brine. *Powder Technology,* 360**,** 1278-1294.

UZI, A., BEN AMI, Y. & LEVY, A. 2017. Erosion prediction of industrial conveying pipelines. *Powder Technology,* 309**,** 49-60.

UZI, A., KALMAN, H. & LEVY, A. 2016. A novel particle attrition model for conveying systems. *Powder Technology,* 298**,** 30-41.

UZI, A. & LEVY, A. 2018. Flow characteristics of coarse particles in horizontal hydraulic conveying. *Powder Technology,* 326**,** 302-321.

VAEZI, M. & KUMAR, A. 2015. Pipeline hydraulic transport of biomass materials: A review of experimental programs, empirical correlations, and economic assessments. *Biomass and Bioenergy,* 81**,** 70-82.

VITTAL, B. V. R. & TABAKOFF, W. 1984. Effect of the solid particle size in two phase flow around a plane cylinder.

VITTORIO MESSA, G. & MALAVASI, S. 2014. Computational investigation of liquid-solid slurry flow through an expansion in a rectangular duct. *Journal of Hydrology and Hydromechanics,* 62**,** 234-240.

VLASAK, P. & CHARA, Z. 2009. Conveying of solid particles in newtonian and non-newtonian carriers. *Particulate Science and Technology,* 27**,** 428-443.

VLASAK, P. & CHARA, Z. 2011. Effect of particle size distribution and concentration on flow behavior of dense slurries. *Particulate Science and Technology,* 29**,** 53-65.

VLASAK, P., CHARA, Z., KONFRST, J. & KRUPIČKA, J. 2015. Experimental investigation of coarse particle conveying in pipes. *EPJ Web of Conferences,* 92**,** 02111.

WANG, K., LI, X., WANG, Y. & HE, R. 2017a. Numerical investigation of the erosion behavior in elbows of petroleum pipelines. *Powder Technology,* 314**,** 490-499.

WANG, R.-Q., LAW, A. W.-K. & ADAMS, E. E. 2014. Large-Eddy Simulation (LES) of settling particle cloud dynamics. *International Journal of Multiphase Flow,* 67**,** 65-75.

WANG, S., LUO, K., YANG, S., HU, C. & FAN, J. 2017b. Parallel LES-DEM simulation of dense flows in fluidized beds. *Applied Thermal Engineering,* 111**,** 1523-1535.

WASP, E. J. & SLATTER, P. T. 2004. Deposition velocities for small particles in large pipes. *Proceedings of the 12th International Conference on the Transport and Sedimentation of Solid Particles.*

WELLINGER, K. & UETZ., H. S. 1955. Scouring and blasting wear under the influence of granular solids. *VDI-Forschungsheft,* 21B 449.

WEN, X., JIN, H., STEIN, O. T., FAN, J. & LUO, K. 2015. Large Eddy Simulation of piloted pulverized coal combustion using the velocity-scalar joint filtered density function model. *Fuel,* 158**,** 494-502.

WILSON, K. C. 1976. A unified physically-based analysis of solid–liquid pipeline flow. *Proc. 4th Int. Conf. on the Hydraulic Transport of Solids in Pipes.* Banff, Alberta, Canada.

WILSON, K. C., CLIFT, R. & SELLGREN, A. 2002. Operating points for pipelines carrying concentrated heterogeneous slurries. *Powder Technology,* 123**,** 19-24.

WOOD, R. J. K., JONES, T. F., GANESHALINGAM, J. & MILES, N. J. 2004. Comparison of predicted and experimental erosion estimates in slurry ducts. *Wear,* 256**,** 937-947.

WOOD, R. J. K., JONES, T. F., MILES, N. J. & GANESHALINGAM, J. 2001. Upstream swirl-induction for reduction of erosion damage from slurries in pipeline bends. *Wear,* 250**,** 770-778.

WU, H., LIANG, X. & DENG, Z. 2013. Numerical simulation on typical parts erosion of the oil pressure pipeline. *Thermal Science,* 17**,** 1349-1353.

XIE, D., WU, Y., ZHANG, Z., WANG, T., CHEN, P., CUI, Y., LI, C. & FENG, S. 2020. Numerical simulation of elbow erosion in liquid-solid two-phase flow. *IOP Conference Series: Materials Science and Engineering,* 740.

XU, B. H. & YU, A. B. 1997. Numerical simulation of the gas-solid flow in a fluidized bed by combining discrete particle method with computational fluid dynamics. *Chemical Engineering & Science,* 52**,** 2785-2809.

XU, L., ZHANG, Q., ZHENG, J. & ZHAO, Y. 2016. Numerical prediction of erosion in elbow based on CFD-DEM simulation. *Powder Technology,* 302**,** 236-246.

YANG, S., LUO, K., FAN, J. & CEN, K. 2014. Particle-scale investigation of the solid dispersion and residence properties in a 3-D spout-fluid bed. *AIChE Journal,* 60**,** 2788-2804.

YOON, C. H., KWON, O. K., KWON, K. S., KWON, S. K. & LEE, D. K. 2000. An experimental analysis on hydraulic lifting of solids through a small-scale vertical tube. *Geosystem Engineering,* 3**,** 42-48.

ZENG, D., ZHANG, E., DING, Y., YI, Y., XIAN, Q., YAO, G., ZHU, H. & SHI, T. 2018. Investigation of erosion behaviors of sulfur-particle-laden gas flow in an elbow via a CFD-DEM coupling method. *Powder Technology,* 329**,** 115-128.

ZENG, L., ZHANG, G. A. & GUO, X. P. 2014. Erosion–corrosion at different locations of X65 carbon steel elbow. *Corrosion Science,* 85**,** 318-330.

ZHANG, H., TAN, Y., YANG, D., TRIAS, F. X., JIANG, S., SHENG, Y. & OLIVA, A. 2012. Numerical investigation of the location of maximum erosive wear damage in elbow: Effect of slurry velocity, bend orientation and angle of elbow. *Powder Technology,* 217**,** 467-476.

ZHAO, Y., MA, H., XU, L. & ZHENG, J. 2017. An erosion model for the discrete element method. *Particuology,* 34**,** 81-88.

ZHENG, S. 2016. *Study of the erosion regularity on the vulnerable parts in gas-solid two phase flow of the gas flow line.* Doctor of phylosophy, Southwest Petroleum University.

ZHOU, J.-W., LIU, Y., LIU, S.-Y., DU, C.-L. & LI, J.-P. 2017. Effects of particle shape and swirling intensity on elbow erosion in dilute-phase pneumatic conveying. *Wear,* 380-381**,** 66-77.

ZHOU, M., KUANG, S., LUO, K., ZOU, R., WANG, S. & YU, A. 2020. Modeling and analysis of flow regimes in hydraulic conveying of coarse particles. *Powder Technology,* 373**,** 543-554.

ZHOU, M. M., WANG, S., KUANG, S. B., LUO, K., FAN, J. R. & YU, A. B. 2019. CFD-DEM modelling of hydraulic conveying of solid particles in a vertical pipe. *Powder Technology,* 354**,** 893-905.

ZHOU, Z. Y., KUANG, S. B., CHU, K. W. & YU, A. B. 2010. Discrete particle simulation of particle–fluid flow: model formulations and their applicability. *Journal of Fluid Mechanics,* 661**,** 482-510.

ZHU, H. P., ZHOU, Z. Y., YANG, R. Y. & YU, A. B. 2007. Discrete particle simulation of particulate systems: Theoretical developments. *Chemical Engineering & Science,* 62**,** 3378-3396.

ZHU, H. P., ZHOU, Z. Y., YANG, R. Y. & YU, A. B. 2008. Discrete particle simulation of particulate systems: A review of mayor applications and findings. *Chemical Engineering & Science,* 63**,** 5728-5770.

ZOUAOUI, S., DJEBOURI, H., MOHAMMEDI, K., KHELLADI, S. & AIT AIDER, A. 2016. Experimental study on the effects of big particles physical characteristics on the hydraulic transport inside a horizontal pipe. *Chinese Journal of Chemical Engineering,* 24**,** 317-322.

NOMENCLATURE

Nomenclature

B	Rinell hardness of the wall material, kg.mm
C_D	drag force coefficient
C_L	lift coefficient
C_v	feed solid concentration
d_p	particle diameter, m
E_F	Erosion wear, mm
$\mathbf{f}_{add,i}$	added mass force between particle i, N
$\mathbf{F}_{buoy,i}$	buoyancy force on particle i, N
$\mathbf{f}_{c,i}$	contact force between particle i, N
$\mathbf{f}_{cn,ij}$, $\mathbf{f}_{ct,ij}$	normal and tangential contact force between particle i and particle j, N
$\mathbf{f}_{d,i}$	drag force exerted on particle i, N
$\mathbf{f}_{fp,\mathrm{i}}$	fluid-solid interaction force on particle i , N
$\mathbf{F}_{pf}$	volumetric fluid-solid interaction force, N/m^3
$\mathbf{f}_{lift,i}$	lift force on particle i, N
$\mathbf{f}_{p,i}$	pressure gradient force on particle i, N
$\mathbf{f}_{.\tau,i}$	viscous force on particle i, N
$\mathbf{F}_{pf}$	volumetric fluid-solid interaction force, N/m^3

F_s	Particle shape factor
g	gravitational acceleration, m/s^2
I	dimensionless pressure drop, m/m
I_i	moment of inertia, kgm^2
K	turbulent kinetic energy
k_c	the number of particles in a considered computational cell
$k_{n,ij}$, $k_{t,ij}$	normal and tangential spring constant, N/m
m_i	mass of particle i, kg
n	number of particles overlapped with the cell considered
∇p	fluid pressure gradient, Pa
$\boldsymbol{r}$	vector from the mass center of the current particle to the contacting point, m
r/R	radial position
$\mathbf{R}_f$	stress tensor
$R_{,i}$	radius of particle i, m
$Re_{p,i}$	Reynolds number of particle i
Δt_{CFD}	time-step of liquid phase, s
Δt_R	Rayleigh time, s
Δt_p	solid time step, s

Δx	the characteristic grid size
$\mathbf{T}_{ij}$	total torque between particle *i* and particle *j*, N·m
$\mathbf{u}_{\mathrm{f}}$	fluid velocity, m/s
U_{f}	conveying speed, m/s
U_{l}	axial liquid velocity, m/s
U_{s}	axial solid velocity, m/s
U_{slip}	axial slip velocity, m/s
V_i	particle volume, m^3
$V_{i,part}$	total volume of elements of particle *i*, m^3
V_{cell}	total volume of elements of cell volume, m^3
$\mathbf{v}_i$	velocity of particle *i*, m/s
$\mathbf{v}_r$	relative velocity of particle *i* and particle *j*, m/s
w	Total mass flow rates, kg/s
Y	Young's modulus of particle, MPa
x, y, z	three components of orthogonal coordinate

Greek symbols

α	Impact angle, $^{\mathrm{o}}$
e	restitution coefficient

$\delta_{n,ij}$, $\delta_{t,ij}$	normal and tangential displacements between particle *i* and particle *j*, m
ε_f	void fraction
η	fluid viscosity, kg/(m·s)
μ	friction coefficient
ρ_f, ρ_p	fluid and particle density, kg/m^3
$\boldsymbol{\omega}_i$	angular velocity of particle *i*, rad/s
ω^*	fluid vorticity
Ω_p^*	particle *i* angular velocity, rad/s
$\gamma_{n,ij}$, $\gamma_{t,ij}$	damping coefficient in normal and tangential direction, kg/s
γ_w	specific weight of water, kN/m^3
$\boldsymbol{\tau}$	Reynolds stress, Pa
τ_p	period of pseudo-time
v	Poisson ratio of particle
Π_1	the mean particle-particle and particle forces per particle in the pipe section
Π2	the mean particle-fluid force per particle

Subscripts

c	contact force

d	drag force
g	gas phase (gas phase)
i	particle *i*
j	particle *j*
n	normal component of variable
p	particle phase
t	tangential component of variable

Acronyms

CFD	computational fluid dynamics
DEM	discrete element method
PISO	pressure implicit with splitting of operator